



HAL
open science

Control of electromechanical systems, application on electric power steering systems

Kazusa Yamamoto

► **To cite this version:**

Kazusa Yamamoto. Control of electromechanical systems, application on electric power steering systems. Automatic. Université Grenoble Alpes, 2017. English. NNT: 2017GREAT069. tel-01730404v1

HAL Id: tel-01730404

<https://theses.hal.science/tel-01730404v1>

Submitted on 13 Mar 2018 (v1), last revised 30 Apr 2018 (v2)

HAL is a multi-disciplinary open access archive for the deposit and dissemination of scientific research documents, whether they are published or not. The documents may come from teaching and research institutions in France or abroad, or from public or private research centers.

L'archive ouverte pluridisciplinaire **HAL**, est destinée au dépôt et à la diffusion de documents scientifiques de niveau recherche, publiés ou non, émanant des établissements d'enseignement et de recherche français ou étrangers, des laboratoires publics ou privés.

THÈSE

pour obtenir le grade de

DOCTEUR DE LA COMMUNAUTE
UNIVERSITE GRENOBLE ALPES

Spécialité : **Automatique-Productique**

Arrêté ministériel : 25 mai 2016

Présentée par

Kazusa YAMAMOTO

Thèse dirigée par **Damien KOENIG** et
codirigée par **Olivier SENAME**

préparée au sein du **GIPSA-Lab**
dans l'**Ecole Doctorale EEATS**

Control of Electromechanical Systems, Application to Electric Power Steering Systems

Thèse soutenue publiquement le **8 Novembre 2017**,
devant le jury composé de:

M. Michel BASSET

Professeur, Université de Haute Alsace, Président

M. Saïd MAMMAR

Professeur, Université d'Evry Val-d'Essonne, Rapporteur

M. Mohammed CHADLI

Professeur associé, HDR, Université de Picardie, Rapporteur

M. Pascal MOULAIRE

Ingénieur, Expert, JTEKT Europe, Examineur

M. Damien KOENIG

Professeur associé, HDR, Grenoble INP, Directeur de thèse

M. Olivier SENAME

Professeur, Grenoble INP, Co-Directeur de thèse



To my parents and my sister,

Remerciements

Je voudrais exprimer ma gratitude et mes sincères remerciements à mes directeurs de thèse, M. Damien Koenig et M. Olivier Sename, pour m'avoir pris sous leur responsabilité durant ces trois années de thèse. Je vous remercie pour tout ce que vous m'avez apporté, votre disponibilité, votre bonne humeur, vos encouragements ainsi que tous vos conseils sans lesquels cette thèse n'aurait pas connu une fin heureuse.

Je remercie chaleureusement les membres du Jury, M. Saïd Mammar et M. Mohammed Chadli pour avoir accepté d'être les rapporteurs de cette thèse, ainsi que pour tous leurs commentaires enrichissants. Je remercie également M. Michel Basset, président de mon jury, et M. Pascal Moulaire, mon encadrant à JTEKT, d'avoir accepté d'examiner mon travail.

Je tiens particulièrement à remercier les membres de l'équipe SLC, pour leur disponibilité, leur bonne humeur et leur support au sein de JTEKT. Ce fut un réel plaisir de travailler sur ce sujet intéressant à vos côtés. Je voudrais exprimer toute ma reconnaissance à Pascal, pour tout ce qu'il m'a apporté par son expertise et ses conseils d'un point de vue technique, mais aussi par sa positivité, ses encouragements et sa bonne humeur, ce qui a constitué un cadre de travail agréable durant cette thèse. Je remercie énormément Serge, un très grand pilote, pour toute sa patience, sa disponibilité et son professionnalisme à travailler dans la voiture et à réaliser bons nombres d'essais. Je remercie Luc pour les échanges sur le sujet qui ont permis d'avancer plus rapidement vis-à-vis des attentes industrielles. Sébastien et Pierre, je vous remercie pour votre aide concernant les modèles de simulation. Stéphane et Jon, je vous remercie également pour les outils et les scripts très pratiques. Yoann et Pilpil, je vous remercie pour votre support sur tout ce qui a porté sur l'implémentation, autant avec le soft embarqué que le ControlDesk. Ofaina et Jocelyn, je vous remercie pour tout votre support afin d'assurer la safety (bien que ce n'était pas forcément profitable à la partie fonctionnelle), avec un grand merci à Ofaina pour son énorme soutien dans les moments difficiles de la thèse. Enfin, je n'oublie pas, le service Mécanique et les Protos qui nous ont permis d'avoir les différents prototypes de DAE.

Je remercie toutes les personnes du département System, surtout à la team System design et l'ancien département Standard and Platforming pour leur accueil et leur bonne ambiance au travail, en particulier à Emilie pour son dynamisme et sa gentillesse en tout temps, à Thomas pour ses récits hors pair, au Marseillais pour son côté fun hispter et au trio de blagueurs et bavards Momo, Dim et Olivier. Je remercie l'équipe projet MFA2 pour l'intégration du SLC, spécifiquement Pierre, Anthony (x2) et Quentin. Un grand merci aux covoitureurs réguliers: El ponte, Sylvain, Pierrot ainsi qu'à Kev et Eli pour les trajets passés dans la rigolade et des discussions animées. Je remercie JTEKT Japan, en particulier le site de JJP Hanazono et l'équipe SD pour avoir permis la réalisation de cette thèse par son support financier et de son intérêt sur le sujet. Je remercie également JTEKT Europe, les assistantes et le management, particulièrement Lionel et Pascal pour m'avoir permis de réaliser dans de bonnes conditions cette thèse, notamment avec les déplacements au Gipsa. Je remercie Claire pour son aide dans la réalisation de mes présentations.

Je remercie tous les membres du D-AUTO, et spécialement l'équipe SLR, ainsi que l'ensemble du personnel du GIPSA-Lab, pour m'avoir permis de passer ces trois années dans un climat convivial. Insaf, Jean, Nassim, Donatien, Elodie, Ronak, Chhay, Phong, Hung un grand merci à vous ainsi qu'aux autres doctorants, je vous souhaite une très bonne poursuite de thèse, et que la force soit avec vous ! Raouia, Ahmad, Quan, Lara, Rachid, Aïda, et aux autres docteurs déjà partis, je vous remercie pour m'avoir permis de bien m'intégrer au labo et pour nous avoir partagés des années de votre expérience. Un merci particulier à Tan, collègue du bureau pendant ces trois ans, pour sa gentillesse ainsi que pour les nombreuses discussions. Un énorme merci à Nadia et Diego, pour leur gentillesse, leur hospitalité et pour les nombreux échanges à la fois techniques et culturelles. D'autre part, je remercie également les personnes que j'ai pu rencontrer et sympathiser durant mes années de thèse que ce soit dans le cadre de conférences ou au cours des rares sorties lyonnaises, en particulier à Joanna, Fabienne, Sara et Riku.

Je voudrais remercier les personnes qui m'ont marquées avec leur inspirante forte personnalité et leur grande gentillesse: Mcou, Ju, Laura, Yeb, Mél, Naïlou, Imen, Sarah, Loulou et Niko; ce qui m'a en partie donné la folie et le courage d'entreprendre une thèse afin d'approfondir mes compétences dans un domaine spécifique qui me plaît.

Enfin, je tiens à remercier mes parents, les Chkasons et le reste de ma famille au Japon pour tout leur soutien, sans oublier la ronronthérapie apportée par Owari, Spice et Gummy. Je voudrais finalement exprimer, ma grande reconnaissance à mon père pour son support inconditionnel et qui m'a permis d'arriver jusque là, ainsi que toute ma gratitude à ma sœur pour sa gentillesse, et qui a toujours été un modèle à poursuivre.

Merci infiniment

Notations

Mathematical notations

| | |
|-----------------------|---|
| \mathbb{R} | Real values set |
| \mathbb{C} | Complex values set |
| $\Re(\cdot)$ | Real part of a complex number |
| M^T | Transpose of matrix $M \in \mathbb{R}$ |
| M^* | Conjugate of matrix $M \in \mathbb{C}$ |
| M^+ | Pseudo inverse of Moore-Penrose of matrix M |
| $M = M^T$ | Real symmetric matrix M |
| $M \succ (\succeq) 0$ | M is symmetric and positive definite (semi definite) matrix |
| $M \prec (\preceq) 0$ | M is symmetric and negative definite (semi definite) matrix |
| (\star) | symmetric element of the opposite bloc in matrix |
| $\ \cdot\ _2$ | Norm 2 |
| $\ \cdot\ _\infty$ | Norm ∞ |

Acronyms related to control theory

| | |
|-----|--------------------------------|
| BMI | Bilinear Matrix Inequality |
| LMI | Linear Matrix Inequality |
| LTI | Linear Time Invariant |
| LPV | Linear Parameter Varying |
| LQG | Linear Quadratic Gaussian |
| LQR | Linear Quadratic Regulator |
| PIO | Proportional Integral Observer |

Acronyms related to vehicle

| | |
|------|------------------------------------|
| ADAS | Advanced Driver Assistance Systems |
| ASIL | Automotive Safety Integrity Level |
| CAN | Controller Area Network |
| ECU | Electronic Control Unit |
| EE | Electrical Electronic |
| EHPS | Electro-Hydraulic Power Steering |
| EPS | Electric Power Steering |
| HPS | Hydraulic Power Steering |
| QP | Quick Prototyping |
| SbW | Steer by Wire |
| SLOA | Sudden Loss Of Assist |
| TBLC | Torsion Bar Less Control |
| TSLC | Torque Sensor Less Control |

Contents

| | | |
|------------|--|-----------|
| I | Introduction | 1 |
| I.1 | General Introduction | 1 |
| I.2 | Thesis Structure | 4 |
| I.3 | Publications | 4 |
| II | An Overview of Power Steering Systems | 7 |
| II.1 | Introduction | 7 |
| II.2 | Steering Systems Overview | 7 |
| II.2.1 | Manual Steering Systems | 8 |
| II.2.2 | Hydraulic Power Steering Systems | 10 |
| II.2.3 | Electro-Hydraulic Power Steering System | 11 |
| II.2.4 | Electric Power Steering System | 11 |
| II.2.5 | Steer-by-Wire systems | 16 |
| II.3 | EPS Main Components Description | 17 |
| II.3.1 | Torque Sensor | 17 |
| II.3.2 | Electric Assistance Motor | 20 |
| II.4 | Conclusion | 22 |
| III | Electric Power Steering Modelling | 23 |
| III.1 | Introduction | 23 |
| III.2 | Electric Power Steering Dynamic Modelling | 24 |
| III.2.1 | P-EPS Model | 24 |
| III.2.2 | C-EPS Model | 26 |
| III.3 | Vehicle Dynamic Modelling | 29 |
| III.3.1 | Road reaction force | 32 |
| III.4 | Simulation Environment | 38 |
| III.5 | EPS on board, Vehicle Environment | 39 |
| III.5.1 | Mechanical Part | 39 |
| III.5.2 | Electronic Part (real time) | 40 |
| III.6 | Model validation from experiments | 42 |
| III.6.1 | Simulation of EPS Model - P-EPS | 43 |
| III.6.2 | Simulation of Rack Force Model - Parking | 44 |
| III.6.3 | Simulation of Rack Force Model - Transition Parking to Low Speed | 45 |
| III.6.4 | Simulation of Rack Force Model - Rolling | 48 |
| III.6.5 | Simulation of Vehicle Model | 49 |
| III.7 | Conclusion | 52 |

| | |
|--|-----------|
| IV Driver Torque Estimation | 53 |
| IV.1 Introduction | 53 |
| IV.2 State of the art | 54 |
| IV.2.1 Driver torque estimation with torque sensor signal | 54 |
| IV.2.2 Driver torque estimation without torque sensor signal | 55 |
| IV.3 Some theoretical background | 57 |
| IV.3.1 Signal Norms | 57 |
| IV.3.2 System Norms | 58 |
| IV.4 Proportional Integral Observer | 59 |
| IV.4.1 PIO definition | 59 |
| IV.4.2 Problem formulation | 60 |
| IV.4.3 Performance objectives | 63 |
| IV.4.4 Design Analysis | 67 |
| IV.5 \mathcal{H}_∞ filtering approach | 69 |
| IV.5.1 H_∞ filter definition | 70 |
| IV.5.2 Problem formulation | 71 |
| IV.5.3 Design analysis | 75 |
| IV.6 Simulation Results | 76 |
| IV.6.1 Simulation using a linear P-EPS Model | 77 |
| IV.6.2 Simulation using real data input | 81 |
| IV.7 Experimental Results | 85 |
| IV.7.1 Vehicle test at 15 kph | 85 |
| IV.7.2 Vehicle test at 30 kph | 87 |
| IV.8 Conclusion | 89 |
| | |
| V Control Design of Electric Power Steering Systems | 91 |
| V.1 Introduction | 91 |
| V.2 State of the art | 92 |
| V.2.1 Base Assist Design | 95 |
| V.2.2 Simple or Fixed-structure controller and low implementation cost | 96 |
| V.2.3 Non linear control scheme | 96 |
| V.2.4 Robust multi objective control design | 97 |
| V.3 EPS control design using driver torque estimation | 97 |
| V.3.1 A Torque SensorLess Control (TSLC) | 97 |
| V.3.2 A LQR Controller | 99 |
| V.3.3 A LPV Controller | 103 |
| V.4 EPS control design without driver torque estimation | 111 |
| V.4.1 Torsion-BarLess Control (TBLC) | 112 |
| V.4.2 H_∞ dynamic output feedback controller | 113 |
| V.5 Simulation Results | 116 |
| V.5.1 Simulation of the LQR observer-based controller | 117 |
| V.5.2 Simulation of the LPV observer-based state feedback controller | 119 |
| V.5.3 Simulation of H_∞ dynamic output feedback controller | 120 |
| V.6 Experimental Results | 121 |

| | |
|--|------------|
| V.6.1 Torque SensorLess Control | 121 |
| V.6.2 State-feedback Controllers based on Proportional Integral Observer . . . | 123 |
| V.6.3 Torsion Bar Less Control | 138 |
| V.7 Conclusion | 140 |
| VI Conclusions and Future Work | 143 |
| VI.1 General Conclusions | 143 |
| VI.2 Future Work | 144 |
| A Implementation Issues | 147 |
| A.1 Discretization | 147 |
| A.2 Signal characteristics | 148 |
| Bibliography | 149 |
| Résumé in French | 161 |

List of Figures

| | | |
|--------|---|----|
| I.1 | Steering System on Vehicle | 1 |
| I.2 | Outline of ADAS controls and steering system requirements [Matsuoka 2016] | 2 |
| I.3 | Fail operational EPS systems [JTEKT 2015] | 3 |
| | | |
| II.1 | Steering System Global Market Evolution [DaedalResearch 2016] | 8 |
| II.2 | Rack and Pinion steering system | 8 |
| II.3 | Manual Steering System | 8 |
| II.4 | Ratio influences on a prototype vehicle | 9 |
| II.5 | Recirculating-ball System | 10 |
| II.6 | Hydraulic Power Steering System | 11 |
| II.7 | Electro-Hydraulic Power Steering System | 11 |
| II.8 | EPS Main Components, P-EPS type | 12 |
| II.9 | Electric Power Steering System Diagram, C-EPS type | 13 |
| II.10 | Steering System Market Target Vehicle, [JTEKT 2015] | 13 |
| II.11 | Column Electric Power Steering System | 14 |
| II.12 | Pinion Electric Power Steering System | 14 |
| II.13 | Dual-Pinion Electric Power Steering System | 14 |
| II.14 | Rack direct Drive Electric Power Steering System | 15 |
| II.15 | Rack Parallel Electric Power Steering System | 15 |
| II.16 | Variable Gear Ratio Steering | 15 |
| II.17 | SbW systems | 16 |
| II.18 | Steering System Energy Consumption Comparison [Miyazaki 2008] | 17 |
| II.19 | Steering System Production Volume Evolution [Matsuoka 2016] | 17 |
| II.20 | JTEKT EPS Type Production Volume [Matsuoka 2016] | 17 |
| II.21 | Torque Sensor | 18 |
| II.22 | Torsion bar stiffness influences on a prototype vehicle at parking | 20 |
| II.23 | NT characteristics | 21 |
| | | |
| III.1 | P-EPS Dynamic Modeling | 24 |
| III.2 | C-EPS Dynamic Modeling | 26 |
| III.3 | C-EPS Simplified Mechanical Structure | 27 |
| III.4 | Bicycle Model | 29 |
| III.5 | Slip angle and Lateral tire force | 31 |
| III.6 | Lateral tire force VS Slip angle | 31 |
| III.7 | SAE tire force and moment axis system | 33 |
| III.8 | Tire/Road Interface on Steering Mechanism | 34 |
| III.9 | Self aligning torque characteristics | 35 |
| III.10 | Geometrical Interpretation of Pacejka model parameters | 36 |
| III.11 | Transition parking to low speed model | 37 |
| III.12 | C-EPS Full Simulation Environment | 38 |

| | |
|---|----|
| III.13 Real system, experimental environment structure | 39 |
| III.14 C-EPS on Clio X98 | 40 |
| III.15 Clio X98 on board electronic | 41 |
| III.16 Algorithm configuration in MicroAutoBox | 41 |
| III.17 JTEKT track | 42 |
| III.18 Rack force model validation from experiments | 43 |
| III.19 Frequency domain model validation $\frac{\theta_m}{u}$ | 43 |
| III.20 Frequency domain model validation $\frac{\theta_{SWA}}{u}$ | 44 |
| III.21 Rack Force Model at Parking | 44 |
| III.22 Driver Torque VS Steering Wheel Angle at Parking | 45 |
| III.23 Rack Force Model from Parking to 3 kph | 46 |
| III.24 Transition Conditions from Parking to 3 kph | 46 |
| III.25 Rack Force Model from Parking to 7kph | 47 |
| III.26 Transition Conditions from Parking to 7kph | 47 |
| III.27 Rack Force Tire Model Pacejka at 15 kph - Sinus manoeuvre | 48 |
| III.28 Rack Force Tire Model Pacejka at 30 kph - Sinus manoeuvre | 48 |
| III.29 Vehicle Model Structure | 49 |
| III.30 Rack Force Model at 30 kph - Snail test | 49 |
| III.31 Lateral Acceleration and Yaw rate at 30 kph - Snail test | 50 |
| III.32 Rack Force Model at 50 kph - Snail test | 51 |
| III.33 Lateral Acceleration and Yaw rate at 50 kph - Snail test | 51 |
| | |
| IV.1 Proposed Proportional Integral Observer Design | 60 |
| IV.2 Weighting function W_w^{-1} | 61 |
| IV.3 LMI regions in complex plane | 64 |
| IV.4 H_∞/H_2 performance evaluation according to α | 67 |
| IV.5 T_{zw} subject to different problem formulations | 68 |
| IV.6 T_{zn} subject to different problem formulations | 68 |
| IV.7 Block diagram of EPS sytem and PIO | 68 |
| IV.8 T_{dd} subject to different problem formulation | 69 |
| IV.9 H_∞ filter for fault estimation | 71 |
| IV.10 Standard H_∞ configuration | 71 |
| IV.11 Proposed H_∞ filtering approach for driver torque estimation | 72 |
| IV.12 Driver torque estimation filter under H_∞ general control configuration | 73 |
| IV.13 T_{zw} subject to different cut-off frequencies in $T(s)$ | 76 |
| IV.14 T_{zn} subject to different cut-off frequencies in $T(s)$ | 76 |
| IV.15 Simulation environment P-EPS system subject to road disturbance and mea- surements noise | 77 |
| IV.16 Driver torque estimation with road disturbance | 78 |
| IV.17 Driver torque estimation error with road disturbance | 78 |
| IV.18 Driver torque estimation with measurements noise | 79 |
| IV.19 Measurements noise affecting | 80 |
| IV.20 Driver torque estimation error with measurements noise | 80 |
| IV.21 Simulation configuration using real system measurements | 81 |

| | |
|---|-----|
| IV.22 P-EPS Test condition in parking - small SWA | 82 |
| IV.23 P-EPS Driver torque estimation in parking - small angle | 82 |
| IV.24 P-EPS Test conditions for lemniscate at 20 kph | 83 |
| IV.25 P-EPS Driver torque estimation 20 kph - lemniscate | 83 |
| IV.26 P-EPS Test conditions - nominal rolling | 84 |
| IV.27 P-EPS Driver torque estimation - nominal rolling | 84 |
| IV.28 Implementation configuration on real system Clio IV | 85 |
| IV.29 C-EPS Test conditions for lock-to-lock at 15 kph | 86 |
| IV.30 C-EPS driver torque estimation, no assistance at 15 kph | 86 |
| IV.31 C-EPS Test conditions for lock-to-lock at 15 kph | 87 |
| IV.32 C-EPS Test conditions for sinus at 30 kph | 87 |
| IV.33 C-EPS Driver Torque Estimation, with assistance at 30 kph | 88 |
| IV.34 C-EPS Road Information at 30 kph | 88 |
| | |
| V.1 Conventional Control Block | 93 |
| V.2 Advanced Steering Management Control Block (JTEKT) | 94 |
| V.3 Assist characteristics curves [JTEKT 2015] | 95 |
| V.4 Torque Target Generator in [Michelis 2011] JTEKT patent | 96 |
| V.5 Torque Sensorless Control diagram (JTEKT) | 98 |
| V.6 Torsion bar torque principle scheme | 98 |
| V.7 (a) $\frac{\dot{\theta}_c}{\tau_d}$, LQR varying Q_2 | 102 |
| V.8 (b) $\frac{u}{\tau_d}$, LQR varying Q_2 | 102 |
| V.9 (a) $\frac{\dot{\theta}_c}{\tau_d}$, LQR varying S | 102 |
| V.10 (b) $\frac{u}{\tau_d}$, LQR varying S | 102 |
| V.11 EPS LPV Models on a rectangular grid | 104 |
| V.12 EPS LPV System, Extended State-feedback Controller | 106 |
| V.13 LPV State-feedback Controller Design | 107 |
| V.14 LPV State-feedback Controller Design | 107 |
| V.15 LPV extended state-feedback, closed loop | 110 |
| V.16 (a) $\frac{\dot{\theta}_c}{\tau_d}$, PIO+LPV SF | 111 |
| V.17 (b) $\frac{u}{\tau_d}$, PIO+LPV SF | 111 |
| V.18 Torsion-BarLess Control diagram (JTEKT) | 112 |
| V.19 \mathcal{H}_∞ Control Scheme | 114 |
| V.20 General H_∞ control formulation | 115 |
| V.21 Controller Sensitivity | 116 |
| V.22 Sensitivity | 116 |
| V.23 EPS Characteristics - Steering feeling | 117 |
| V.24 (a) θ_c VS τ_d PIO+LQR 0kph | 117 |
| V.25 (b) θ_c VS F_r PIO+LQR 0kph | 117 |
| V.26 (a) θ_c VS τ_d PIO+LQR 15kph | 118 |
| V.27 (b) θ_c VS F_r PIO+LQR 15kph | 118 |
| V.28 (a) θ_c VS τ_d PIO+LQR 30kph | 118 |
| V.29 (b) θ_c VS F_r PIO+LQR 30kph | 118 |
| V.30 (a) θ_c VS τ_d PIO+LPV SF 15kph | 119 |

| | | |
|------|---|-----|
| V.31 | (b) θ_c VS F_r PIO+LPV SF 15kph | 119 |
| V.32 | (a) θ_c VS τ_d PIO+LPV SF 30kph | 120 |
| V.33 | (b) θ_c VS F_r PIO+LPV SF 30kph | 120 |
| V.34 | (a) θ_c VS τ_d H_∞ controller 30kph | 120 |
| V.35 | (b) θ_c VS F_r H_∞ controller 30kph | 120 |
| V.36 | TSLC - implementation on real system | 122 |
| V.37 | TSLC at 50 kph | 122 |
| V.38 | TSLC at 90 kph | 123 |
| V.39 | Rack Forces measured at different vehicle speed | 124 |
| V.40 | PIO+LQR controller - implementation on real system | 124 |
| V.41 | PIO+LQR at parking - Hysteresis θ_c VS τ_d | 125 |
| V.42 | PIO+LQR at parking - Evolution of involved torques | 126 |
| V.43 | PIO+LQR at 7 and 15 kph - Hysteresis θ_c VS τ_d | 127 |
| V.44 | PIO and LPV extended state feedback - implementation on real system | 128 |
| V.45 | PIO+LPV at 7 kph - Hysteresis θ_c VS τ_d | 129 |
| V.46 | PIO+LPV at 7 kph - Evolution of involved torques | 129 |
| V.47 | PIO+LPV at 7 kph - Resulting behaviour on the vehicle | 130 |
| V.48 | PIO+LPV at 15 kph - Hysteresis θ_c VS τ_d | 131 |
| V.49 | PIO+LPV at 15 kph - Evolution of involved torques | 131 |
| V.50 | PIO+LPV at 15 kph - Resulting behaviour on the vehicle | 132 |
| V.51 | PIO and LQR at low speeds - Hysteresis θ_c VS τ_d | 132 |
| V.52 | PIO+LPV at 30 kph - Hysteresis θ_c VS τ_d | 133 |
| V.53 | PIO+LPV at 30 kph - Evolution of involved torques | 134 |
| V.54 | PIO+LPV at 30 kph - Resulting behaviour on the vehicle | 134 |
| V.55 | PIO and LPV at 7 kph low μ - Hysteresis θ_c VS τ_d | 135 |
| V.56 | Sinus Manoeuvre low μ Rack Force and Steering Wheel Angle evolution | 136 |
| V.57 | Constant amplitude related to stick-slip test | 136 |
| V.58 | Steering Wheel Speed and Angle | 137 |
| V.59 | PIO and LPV at 15 kph high dynamics - Evolution of involved torque | 138 |
| V.60 | TBLC - implementation on real system | 138 |
| V.61 | TBLC at 30 kph | 139 |
| V.62 | TBLC at 50 kph | 140 |
| VI.1 | Fault Tolerant Control and Driver Torque Estimation Scheme | 145 |
| A.1 | Discretization with a Zero-Order Hold | 147 |
| A.2 | DAE de type pignon | 161 |
| A.3 | Système réel - structure de l'environnement expérimental | 163 |

List of Tables

| | | |
|-------|--|-----|
| II.1 | EPS motors requirements depending on system types | 20 |
| II.2 | Characteristics comparison of electric motors | 21 |
| II.3 | System performance requirement | 22 |
| III.1 | P-EPS system mechanical parameters | 25 |
| III.2 | C-EPS system mechanical parameters | 28 |
| III.3 | Bicycle model parameters | 30 |
| III.4 | Moment Parameters | 34 |
| III.5 | Pacejka Parameters | 36 |
| III.6 | Lugre Parameters | 37 |
| IV.1 | $\ T_{\tilde{z}w}\ _\infty$ and $\ T_{\tilde{z}n}\ _2$ subject to strategies H_∞ , H_2 and H_∞/H_2 | 67 |
| IV.2 | Influence of weighting function $T(s)$ on the H_∞ filter synthesis | 75 |
| V.1 | Set-up experimental conditions | 121 |
| V.2 | Synthesis table of the presented results | 141 |
| A.1 | Steering wheel angle characteristics | 148 |

Introduction

Contents

| | | |
|------------|-----------------------------|----------|
| I.1 | General Introduction | 1 |
| I.2 | Thesis Structure | 4 |
| I.3 | Publications | 4 |

I.1 General Introduction

This thesis has been carried out in a CIFRE (Conventions Industrielles de Formation par la REcherche) framework within a collaborative work between JTEKT Europe (a worldwide automotive supplier) and GIPSA-lab. In its industrial context, this study has been part of a customer project about Torque Sensor Less Control (TSLC), and also in a preliminary draft Torsion Bar Less Control (TBLC), both projects will be explained later on.

Nowadays, modern vehicles are equipped with more and more electronic systems that help the driving process while ensuring safety. Among them, Electric Power Steering (EPS) systems (see Fig I.1) have been widely expanded since its first release on automotive market was in 1988. Currently, most of passenger cars are equipped with EPS systems [Noguchi 2001], [Matsuoka 2016]. EPS aims at helping the driver to turn the vehicle wheels in the desired direction by reducing the required steering force.

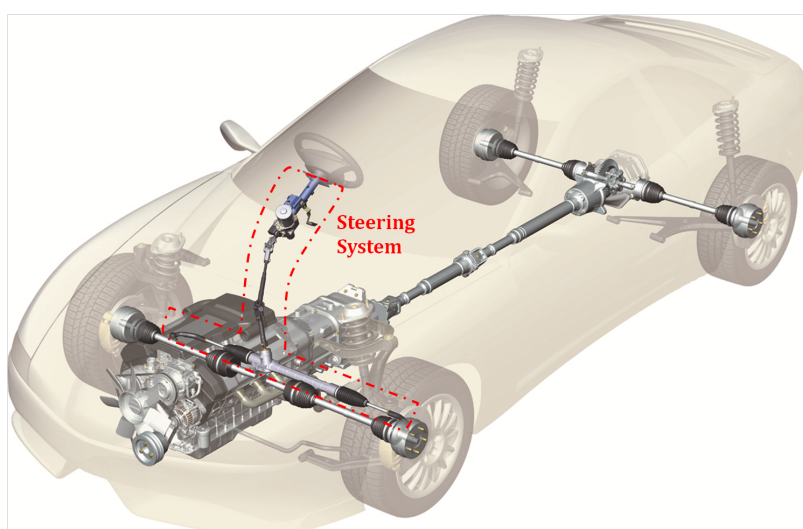


Figure I.1 – Steering System on Vehicle

Furthermore, automotive industry future trends seem to concentrate on autonomous driving systems for safety and environmental objectives. Hence, Advanced Driver Assistance Systems (ADAS) increasingly expand, since ADAS functions are developed to enhance the safety of vehicles and also driving comfort, such as Lane Keeping Assist (LKA), Lane Departure Warning (LDW), automatic parking, Traffic Jam Assist (TJA). An overview of ADAS expansion is shown in Fig I.2, together with the according steering characteristics.

Indeed, EPS is a key support for ADAS development and automated driving. Hence, steering systems requirements are evolving accordingly. Moreover, regarding ADAS democratisation (forecast in the coming year), EPS systems would become widespread. As it could be seen in Fig I.2, either EPS or SbW are expected steering systems to support those additional driving assistance functions. A major challenge for automotive manufacturer’s first rank suppliers is then a reduction of EPS cost production in order to meet growing markets demands (particularly those of emerging countries).

| Function name | ACC | AEB | LDW | LKA | TJA | TJA (with lane change function) | Automated steering | Automated steering /collision avoidance | |
|-----------------------------|------------------------|-----|-----|-----|-----------------------|---------------------------------|---|---|--------------------------------------|
| Control details | | | | | | | | | |
| Mass production (predicted) | Mass production | | | | 2015–2018 | | Around 2020 | Around 2025 | |
| Automation level | Driver responsibility | | | | Driver responsibility | | Driver responsibility → System responsibility | System responsibility | |
| Steering requirements | Override by the driver | | | | | | | Maintaining of basic functions in case of failure | Avoid interference with driver input |
| Steering system | EPS | | | SBW | | | EPS | SBW | |

ACC: Adaptive Cruise Control AEB: Automatic Emergency Braking LDW: Lane Departure Warning
 LKA: Lane Keeping Assist TJA: Traffic Jam Assist SBW: Steer by Wire

Figure I.2 – Outline of ADAS controls and steering system requirements [Matsuoka 2016]

In general, the amount of electronic systems has considerably increased in vehicles for recent years, to enhance performance (e.g engine electronics, transmission electronics) and functionalities (e.g chassis electronics, driver assistance). As it will be presented, EPS is an electromechanical systems composed with several sensors, electric (assistance) motor and ECU. Then, a safe operating vehicle driving condition is required whenever a failure or malfunction appears in the system. To this purpose, functional safety of EE systems in vehicles has been defined by the international standard ISO26262 since 2011 [Standard 2011]. Some safety goals need to be avoided by EPS systems, like self-steering (wheel rotates on its own, while no input is provided by the driver) or steering lock (driver is not able to rotate). Hence the following

steps are to be considered to cover failures in EPS systems:

- Step 1: Application of a backup control, providing a certain amount of assistance in such a way that the driver could stop the vehicle safely, only in case of possible failure coverage, for instance: the resolver (rotation angle sensor of the assist motor) or the torque sensor. EPS operation is maintained through activation of specific software.
- Step 2: Electronic hardware redundancy design, a downgraded EPS operation mode is achieved during failure as EPS electronic circuits and sensors are duplicated.
- Step 3: Electronic hardware and vehicle power supply redundancy design, this full duplication allows EPS to remain effective in case of any system failure.

The table in Fig I.3 summarizes the classification of fail-operational function inside JTEKT.

JFOPS (JTEKT Fail-Operational System)

| JFOPS | Concept | Method |
|---------------------------|--|--|
| JFOPS 4 | Complete fail-operational function | Complete redundancy of electronic hardware of the EPS system, including electric power supply of vehicle |
| JFOPS 3 | Fail-operational function | Redundancy of electronic hardware of the EPS system |
| JFOPS 2 And JFOPS 1 | Partial fail-operational function | Backup via software |
| JFOPS 0 | Stops the system in the event of failure | Conventional EPS |

Figure I.3 – Fail operational EPS systems [JTEKT 2015]

According to this short presentation and to achieve Step 1 (JFOPS 1/2) in case of torque sensor failure, a backup EPS controller has to be developed. Indeed, following car customer requirements, avoidance of Sudden Loss Of Assist (SLOA) could be judged as a safety goal of the vehicle. As recently, more and more large vehicles (high rack force involved) are equipped with EPS, a shut-down of EPS in case of electronics failure could result in unacceptable steering force for the driver and lead to an accident. To avoid such an event, a backup mode based on driver torque estimation has been developed.

Consequently, the main focus of this thesis is based on control development for EPS applications in the absence of torque sensor signal.

- At first, TSLC is studied as a software backup solution in case of hardware torque sensor failures. As a backup mode, the amount of assistance torque required is rather low compared to normal operation. Nevertheless, a fast development has been requested to match the application project schedule. Hence, a driver torque estimation has been developed to cover the loss of torque sensor signal as a quite conventional control structure that could be used to meet customer requirements.

- Then, TBLC is studied as an extension of the previous work. However, TBLC is targeted to operate on its own (as a nominal mode), which results in a higher expectation of assistance torque level. Furthermore, TBLC aims at facing the major challenge of reducing EPS cost production through a new EPS mechanical structure by removing torque sensor. Then, TBLC looks towards low cost vehicles market. Thus, EPS control approaches have been developed, on new EPS mechanical structure.

I.2 Thesis Structure

This thesis is organised in five chapters:

Chapter II: *An Overview of Power Steering Systems* provides a general framework on steering systems. In this chapter, an overall presentation on technologies used in power steering systems is carried out, especially on EPS since it is the application of this thesis.

Chapter III: *Electric Power Steering Modelling* considers EPS dynamics models and its interaction with tires, as the system is integrated on vehicle. Indeed, EPS establishes the connection between the road and the driver. Hence, a vehicle model and rack force model are also introduced to describe a realistic EPS behaviour. Finally, a development vehicle configuration is presented onto which experimental results have been performed.

Chapter IV: *Driver Torque Estimation* first provides a state of the art on such work performed on EPS and some backgrounds on observer design techniques. Then, two design approaches to estimate the driver torque are developed: a Proportional Integral Observer (PIO) and an H_∞ filter. Simulation and experimental results are shown to discuss the efficiency of the proposed observers.

Chapter V: *Control Design of Electric Power Steering Systems* presents EPS control objectives and a state of the art on common control design techniques. Next, two different type of control synthesis are developed: first, a gridded LPV (Linear Parameter Varying) state feedback controller where the whole state is estimated through the previous PIO. Then, a LTI (Linear Time Invariant) H_∞ controller based on restrained steering system information is designed. Simulation and vehicles test results are shown to assess the performance of the proposed control strategies.

Chapter VI: *Conclusions and Future Work* aims to summarize this thesis contribution and to discuss on further challenges that have arisen from this work, in particular concerning the development of new types of EPS systems involving a complete system design (mechanical structure, actuator sizing, sensor specification).

I.3 Publications

International conference papers

- C1 Kazusa Yamamoto, Damien Koenig, Olivier Sename, Pascal Moulaire. *A New Control Design for an Optimized Electric Power Steering System*, in preprints 20th IFAC World Congress, July 2017, Toulouse, France.

-
- C2** Kazusa Yamamoto, Damien Koenig, Olivier Sename, Pascal Moulaire. *H_∞ Filtering Design for Driver Torque Estimation in Electric Power Steering System*, in proceedings 13th International Symposium on Advanced Vehicle Control (AVEC), Sept 2016, Munich, Germany.
- C3** Kazusa Yamamoto, Damien Koenig, Olivier Sename, Pascal Moulaire. *Driver Torque Estimation in Electric Power Steering System using an H_∞/H_2 Proportional Integral Observer*, in proceedings 54th IEEE Annual Conference on Decision and Control (CDC), Dec 2015, Osaka, Japan.

Patent

- P1** Pascal Moulaire, Kazusa Yamamoto, Serge Gaudin, Yoann Baudin, Ofaina Taoffenua *Procédé de gestion de direction assistée avec reconstruction indirecte de l'information de couple volant*, ref. BR086617

An Overview of Power Steering Systems

Contents

| | |
|--|-----------|
| II.1 Introduction | 7 |
| II.2 Steering Systems Overview | 7 |
| II.2.1 Manual Steering Systems | 8 |
| II.2.2 Hydraulic Power Steering Systems | 10 |
| II.2.3 Electro-Hydraulic Power Steering System | 11 |
| II.2.4 Electric Power Steering System | 11 |
| II.2.5 Steer-by-Wire systems | 16 |
| II.3 EPS Main Components Description | 17 |
| II.3.1 Torque Sensor | 17 |
| II.3.2 Electric Assistance Motor | 20 |
| II.4 Conclusion | 22 |

II.1 Introduction

In this chapter, an overview of steering systems are presented in order to understand the evolution of this technology in the automotive market. First, steering systems structure and functionality are described. Then, the presentation is focused on different types of EPS systems. Finally, the main components of current EPS systems are presented (torque sensor and electric assistance motor) in order to get a better understanding on EPS sizing.

II.2 Steering Systems Overview

A steering system helps the driver to turn the vehicle wheels in the desired direction. In manual steering systems, only the driver is producing the torque needed to turn the vehicle wheels. However, a high amount of exertion is required by the driver (especially at low speed) which makes the driving process uneasy. According to automotive industry expansion, power-assisted steering systems (mainly Hydraulic Power Steering (HPS) and EPS) have been developed to provide an additional torque to the driver. Hence, the effort applied by the driver in the steering actions is reduced. Evolutions of steering systems demand over the years are shown in

Fig II.1 and discussed in [Noguchi 2001]. Manual steering market share is declining in favour of power steering systems while preference leans towards EPS compared to HPS.

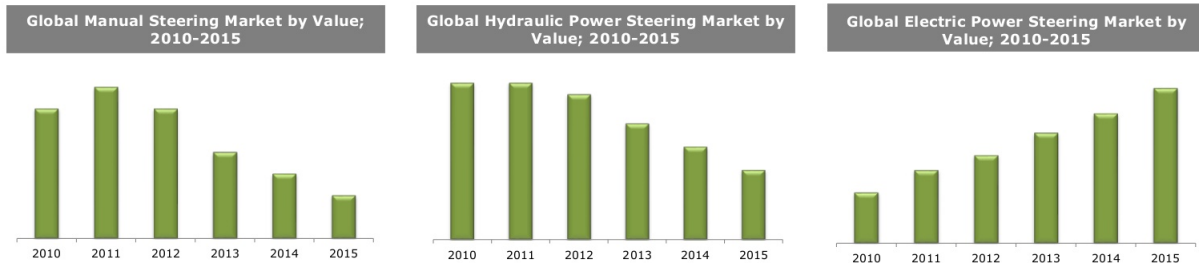


Figure II.1 – Steering System Global Market Evolution [DaedalResearch 2016]

In what follows, the structure and functioning of different steering systems are discussed.

II.2.1 Manual Steering Systems

As expressed in its designation, manual steering system involves only manual force in steering the wheels. This means that it relies only on physical effort and steering gear ratio to turn the front wheels. There is no additional force to support the driver's effort contrary to power steering.

A rack and pinion steering mechanisms are commonly used in vehicles, as illustrated in Fig II.2. In this type of systems, the steering shaft rotates the pinion gear which leads to rack motion. Consequently, the circular motion of the steering wheel is converted to a linear motion that steers the wheels, since a tie rod is connected to each end of the rack. Hence, the steering wheel rotation results in turning the wheels, a real rack and pinion type manual steering system is shown in Fig II.3.

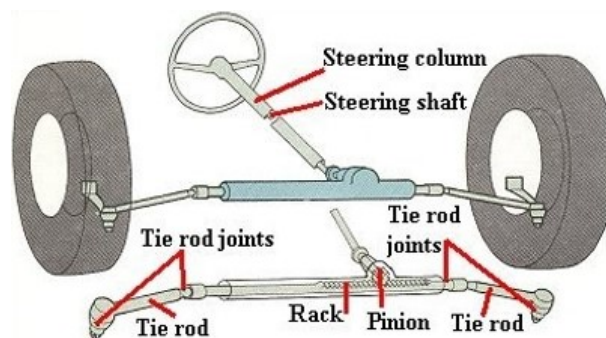
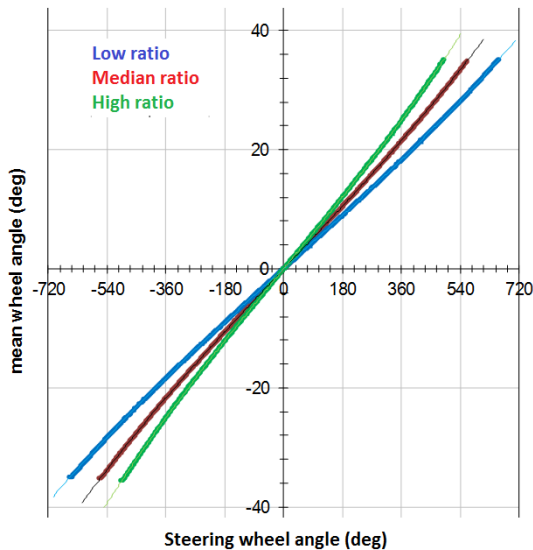


Figure II.2 – Rack and Pinion steering system

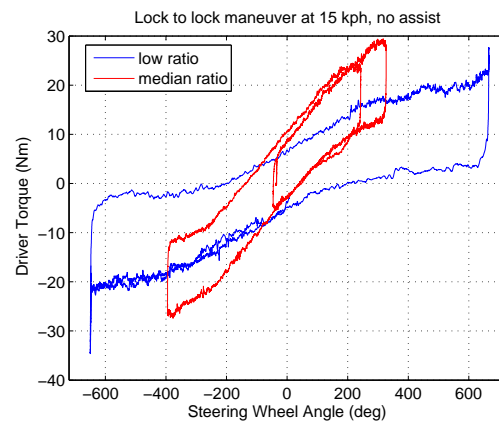


Figure II.3 – Manual Steering System

An important characteristic is the steering gear ratio corresponding to the ratio between the steering wheel and the vehicle front wheels, which acts as a reduction gear. Indeed, the gear assembly reduces the driver torque involved at the steering wheel through increasing the output torque (at pinion). Therefore, $x:y$ the steering ratio SR means that turning the steering wheel of an angle x deg leads to turn the front wheel of y deg, *i.e.*, $SR = \frac{\theta_{swa}^{fr}}{\alpha_t^{fr}}$ where the full range of steering wheel angle is θ_{swa}^{fr} and tire deflection is α_t^{fr} . Nevertheless, the steering ratio only is not sufficient to reduce the amount of applied driver torque while ensuring a good steering feel. In manual steering, the steering ratio depends mainly on the pinion ratio PR which defines the rack travel for one steering wheel turn $\theta_{swa}^{fr} = \frac{X_{rack}^{fr}}{PR} \times 360^\circ$ with X_{rack}^{fr} the full rack stroke. A lower pinion ratio results in a larger steering ratio. Then, it reduces the steering torque level but involves to turn more the steering wheel angle (in practice driving becomes slightly difficult as a wider steering angle is needed to take a curve). On the contrary, a higher ratio results in a lower steering ratio. Then, it leads to a higher steering torque level but with a smaller steering angle range.



(a) Steering angle VS Front wheel angle, influence of pinion ratio



(b) Ratio influences on a prototype vehicle

Figure II.4 – Ratio influences on a prototype vehicle

In Fig II.4, the effect induced by this pinion ratio is illustrated. In Fig II.4(a), three different pinion ratios (low, median and high) have been tested one by one on the same vehicle, then three plots are obtained showing the steering wheel angle function of the front wheels deflection, where the slope of each curve corresponds to the inverse of the steering ratio. As it could be seen, lowering the pinion ratio increases the steering wheel angle range. In Fig II.4(b), two different pinion ratio (low and median) picked up from the previous case have been tested successively on the same vehicle to realise a lock-to-lock manoeuvre. Then, two curves are obtained showing the steering wheel angle function of the driver torque. As it could be seen, the driver torque value is higher with a median ratio, however the steering wheel

angle range is smaller, therefore a quick response is obtained for tire cornering. According to Fig. II.4, the influence of the pinion ratio on steering performance regarding torque level and vehicle handling is emphasised. Though, manual steering involves heavy or low-geared steering, resulting in difficulty to steer large vehicles in parking or driving curves. Thus, power-assisted steering systems have been introduced to overcome those issues as described below.

Remark II.1

It is worth noting that there exists other types of manual steering systems. However, most of power steering systems are based on the previously detailed rack and pinion mechanism. Therefore, this is only a brief note to give global overview of steering types mechanics. Recirculating-ball type of steering system is often found on trucks or luxury cars, as it is adapted to large loads (reduce friction in the gear thanks to the balls) and large steering travels. The linkage that turns the front wheels is different to rack and pinion mechanism. The recirculating-ball steering mechanism (shown in Fig. II.5) is composed by a worm gear contained in a block with a threaded hole in it. Moreover, this block has gear teeth cut into the outside such that when the sector shaft is engaged, it moves the Pitman arm. Besides, the steering wheel connects to a shaft that rotates the worm gear, which is fixed inside the block. Hence, when the worm gear spins, it moves the block rather than twisting further into it. Then, the motion is transmitted through the gear to the Pitman arm which turns the wheels.

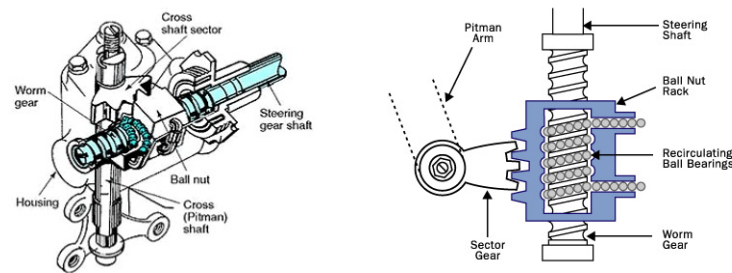


Figure II.5 – Recirculating-ball System

II.2.2 Hydraulic Power Steering Systems

HPS systems (Fig. II.6) were the first power-assisted steering to be commercialized on passenger car in the 50s (Chrysler Imperial). HPS are using a hydraulic system to multiply the force applied by the driver, hence some additional components composed the steering systems :

- a hydraulic control valve controlling the flow from the pump to the cylinder
- a hydraulic pump (for example, a rotary vane pump) sending fluid under pressure, with the flow delivered proportional to the engine speed
- a hydraulic cylinder is controlled in position and aims at applying a force to the steering gear that produces a rack displacement and wheels rotation. Here, hydraulic energy is converted to mechanical energy.
- a reservoir tank is containing hydraulic fluid

Actually, the hydraulic pump driven by the vehicle engine generates the hydraulic pressure (by increasing hydraulic fluid pressure). The induced hydraulic flow, controlled by a valve, goes through the hydraulic cylinder such that a suitable assistance is provided to the steering rack. Indeed, the steering wheel direction of rotation forces the fluid into one side or the other of the piston. Consequently, the piston moves the rack, tie rods and wheels in the desired direction. Some detailed studies regarding HPS could be found in [Wong 2001], [Rösth 2007].



Figure II.6 – Hydraulic Power Steering System

II.2.3 Electro-Hydraulic Power Steering System

EHPS is a hybrid system, as shown in Fig. II.7. This means, it uses the same hydraulic assist technology (same elements than an HPS), however the hydraulic pressure is generated differently. In this case, the hydraulic pump is driven by an electric motor, whereas in the previous case it was achieved by a drive belt at the engine (mechanically, so operating continuously until engine stops). So EHPS great advantage lies in energy saving, mostly in fuel economy (a detail study is realised in [Zhu 2010]).



Figure II.7 – Electro-Hydraulic Power Steering System

II.2.4 Electric Power Steering System

EPS systems have appeared since late 80s, and nowadays most vehicles are equipped with this technology. Indeed, this evolution could be explained regarding those following advantages [Miyazaki 2008]:

- a reduction of fuel consumption: the EPS weight is less than HPS since there include less components. Furthermore, EPS systems operate only when the driver turns the steering wheel whereas HPS systems are continuously running to maintain pressure in the hydraulic circuit, thus creating a load on the engine.
- a tunable system: EPS is an electromechanical system where the control law is implemented on an embedded software. Then, performance improvement could be easily done by modifying some tunable parameters, for instance the assistance curve.
- a modular system: EPS is composed of different subsystems, such packaging allows variable position of assist-motor unit on the steering system, resulting in different EPS types (featuring systems parameters).
- an environmentally-friendly system: EPS is less concerned with pollutant related to hydraulic oil, like oil disposal or oil leakage concerns. Besides, fuel consumption related to EPS systems involves reduction of CO_2 emissions.

In EPS systems, an assistance torque is provided by an electric motor, to reduce the amount of torque required from the driver to turn the wheels (especially in parking and low speed). The amount of supplied power is defined by the ECU according to a motor torque control policy, containing an assistance rule depending on the vehicle speed and torque sensor. Then, the torque transmitted to the pinion shaft is the sum of the driver and the assistance motor torque. Finally, the rack and pinion mechanisms imply the steering of the front wheels.

In Fig II.8, a view of the assembly of EPS principal components is shown. The torque sensor evaluates the steering torque applied by the driver and the electric motor generates an assistance torque amplified by the reduction gear. More details on those elements will be addressed later on.

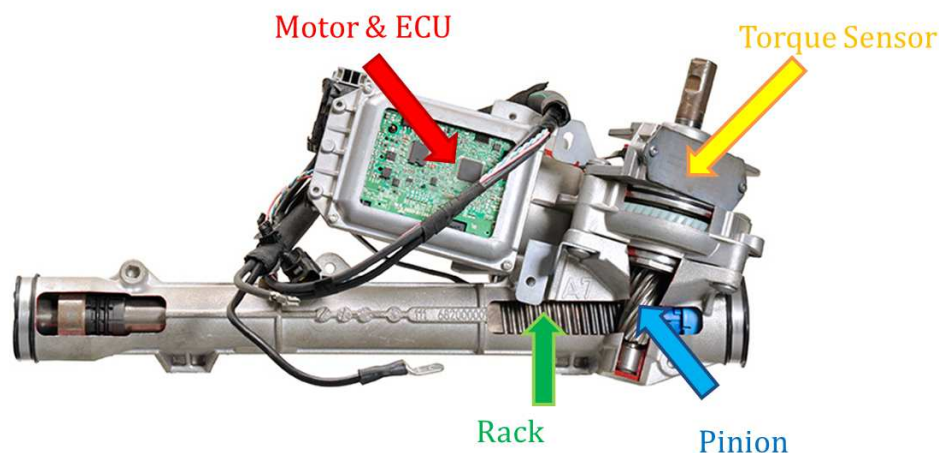


Figure II.8 – EPS Main Components, P-EPs type

Hence, the driver action on the steering wheel activates the assistance motor which supplies an additional torque to move the rack and to turn the vehicle wheels. A summary diagram is shown in Fig II.9. Indeed, as it could be observed on the rack and pinion mechanism illustrated

in Fig. II.8, the assist motor acts in accordance with the driver to rotate the pinion, where the rotary motion is transferred to a linear motion used to steer the vehicle front wheels.

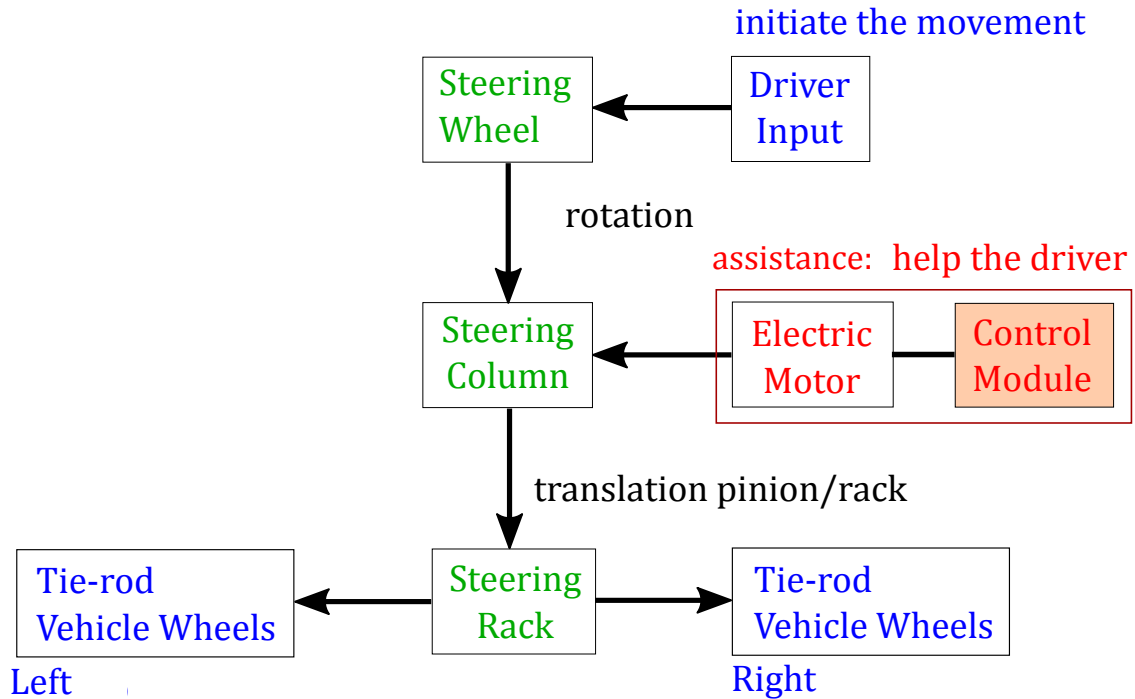


Figure II.9 – Electric Power Steering System Diagram, C-EPS type

As introduced previously, the modularity of EPS systems results in several types of product that have been developed for suitable vehicle types accordingly. Indeed, the needs regarding performance in light (car segment A and B) and large-size (remaining car segment) automobiles are not the same, a recommended compatibility between steering systems and vehicles is presented in Fig II.10.

| Vehicle | | UA/A | | | | | | B | | C | | D | | E | | F | | |
|-----------------|---------------|----------|------------|--|--|--|------------|---|--|---|--|---|--|---|--|---|--|--|
| | | SUV/P-UP | | | | | | | | | | | | | | | | |
| Electric assist | Column assist | C-EPS | [Blue bar] | | | | | | | | | | | | | | | |
| | Rack assist | P-EPS | [Blue bar] | | | | | | | | | | | | | | | |
| | | DP-EPS | | | | | [Blue bar] | | | | | | | | | | | |
| | | RP-EPS | | | | | [Blue bar] | | | | | | | | | | | |
| | | RD-EPS | | | | | [Blue bar] | | | | | | | | | | | |

Figure II.10 – Steering System Market Target Vehicle, [JTEKT 2015]

Thereafter, some features of different systems are presented.

II.2.4.1 Colum-assist

In a C-EPS (e.g on Renault Clio IV or Nissan Sentra), the power-assist unit is set on the steering column, so inside the cabin (see Fig. II.11).

It is appropriate for compact vehicles with a small space in the engine room and low rack force (up to 6kN). It was the first commercialized EPS system.

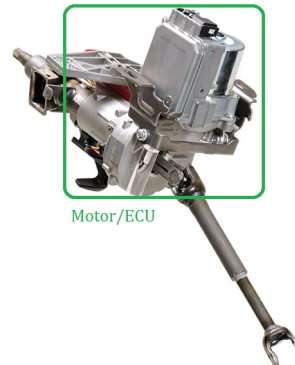


Figure II.11 – Column Electric Power Steering System

II.2.4.2 Rack-assist

In rack-assist, the power-assist unit is integrated either on rack (RD-EPS, RP-EPS) or pinion (P-EPS, DP-EPS), EPS is located in engine compartment. Therefore, it is adapted for medium to large-size vehicles with a high rack force (more than 8kN).

- Pinion type EPS: in a P-EPS (e.g on Peugeot 207), the assist unit is at the pinion shaft, see Fig II.12. Its small and compact design is adapted to engine compartment.

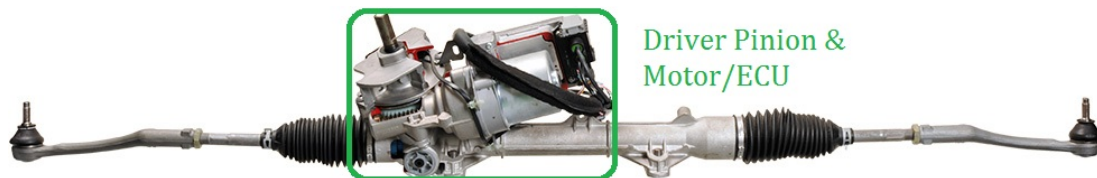


Figure II.12 – Pinion Electric Power Steering System

- Dual-Pinion type EPS: in a DP-EPS (e.g on Mercedes Class B or Peugeot 308), the assist unit is separated from the steering wheel axle giving flexibility in system installation, as shown in Fig II.13.

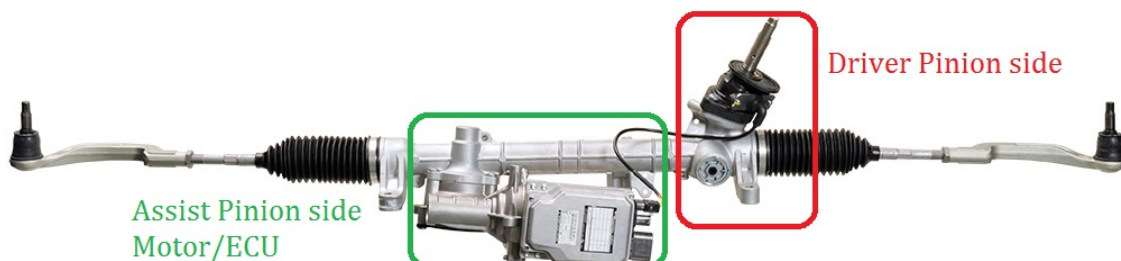


Figure II.13 – Dual-Pinion Electric Power Steering System

- Rack direct Drive type EPS

In a RD-EPS, the rack shaft is directly assisted, as illustrated in Fig II.14. A ball screw reduction mechanism has been adopted for high-power assistance with noise and vibration attenuation.



Figure II.14 – Rack direct Drive Electric Power Steering System

- Rack Parallel type EPS: in a RP-EPS (e.g on Ford Mustang), the assist unit is mounted in parallel to the steering rack, see Fig II.15. It provides an high assist steering performance and its structure gives an easy integration.



Figure II.15 – Rack Parallel Electric Power Steering System

II.2.4.3 Variable Gear Ratio Steering

VGR gives the capacity to adapt the vehicle’s steering ratio according to the vehicle speed or steering angle. Ideally, it would be expected that a small steering angle generates a large tire steering angle during low speed or parking manoeuvre (a quick ratio) to increase the vehicle handling, while a small steering motion generates a small tire steering at high speeds (a slow ratio) to improve stability.

- Mechanical VGR: through a specific mechanical design, as shown in Fig II.16, a steering rack can produce a variation of the steering ratio. Although it can only vary according to steering angle since the gear pattern is already established, this is sufficient to improve steering performance (uses in Mercedes SLK as direct-steer system).

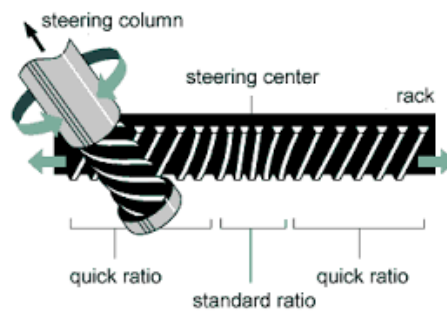


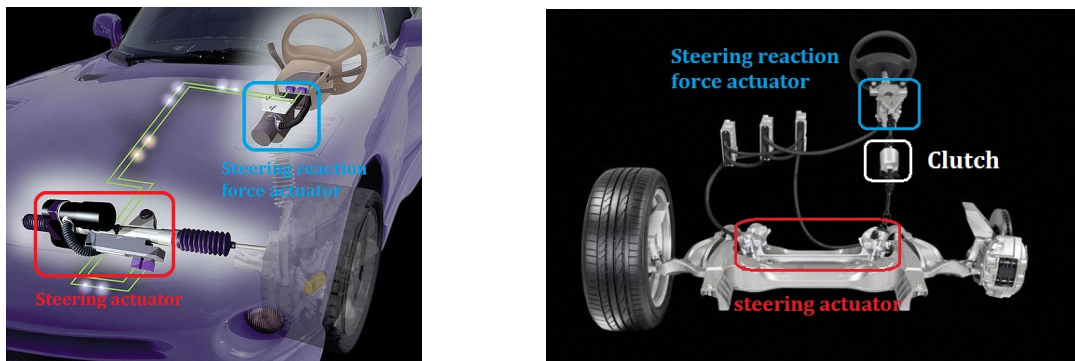
Figure II.16 – Variable Gear Ratio Steering

- **Electronical VGR:** an electronically controlled variable gear ratio (E-VGR), several design have been developed. BMW employs a planetary gearbox whereas Toyota implements a wave generator and a flexible gear. E-VGR could be extended to active steering system as the steering ratio varies depending in vehicle speed.

II.2.5 Steer-by-Wire systems

Steer-by-Wire (SbW) system aims at removing the mechanical link between the steering wheel and vehicle front wheels, as illustrated in Fig. II.17. SbW is an upcoming step for the future, especially for autonomous driving systems. Indeed, the removal of the mechanical link gives more freedom in automotive design: reduction of the vehicle weight, increasing engine compartment space thus facilitating its design, accommodation to new steering wheel like joysticks. The Infiniti Q50 (Nissan) was the first SbW system to be mass-produced in 2013.

SbW is composed by a steering reaction force actuator which creates a reaction force towards the driver to transmit the state of the vehicle and a steering actuator which steers the front wheels. A controller is designed to coordinate both actuators to improve vehicle handling and to give a good perception of the vehicle movement to the driver. Hence, SbW is an application of teleoperation systems where the driver interacts with the steering wheel part (master) which is connected by means of a controller (virtual steering column) to the steering rack part (remote slave) having an interaction with the road.



(a) SbW without clutch and one large actuator for steering (b) SbW with clutch and two small actuators for steering

Figure II.17 – SbW systems

Nevertheless, the challenges remain important in terms of safety and driver feeling. Indeed in SbW system, it is actually the motor which generates the resistance torque (artificial) back to the driver's hand. Therefore, a lack of feeling appears concerning steering kickback or small vibration which are also essential to know what is happening at the front wheels. In case of electronic faults (sensors or actuators), a fail-safe feature requires a backup system that still maintains the driving. For instance, a clutch could re-establish the mechanical linkage or a motor switching mechanism (redundancy of components) could cover and ensure steering capability [Mogi 2011]. Such systems are out of the scope of this thesis.

To conclude, this work will focus on EPS systems considering its advantages on manual, HPS (Fig. II.18) and following the steering market requirements (Fig. II.19).

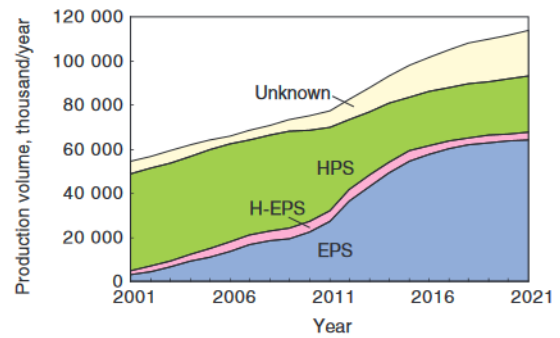
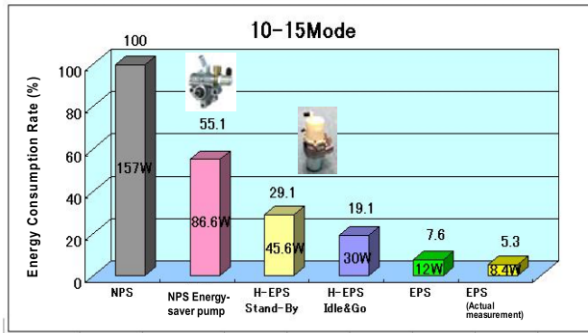


Figure II.18 – Steering System Energy Consumption Comparison [Miyazaki 2008]

Figure II.19 – Steering System Production Volume Evolution [Matsuoka 2016]

A back-up mode in case of torque sensor failure is more necessary for heavy vehicle equipped with a P-EPS or DP-EPS. Besides, regarding a development for lower production cost EPS, a C-EPS is preferred since light vehicles are equipped with it. Also, it was the most produced EPS type until now (Fig. II.20).

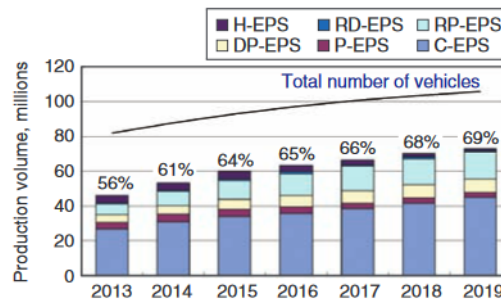


Figure II.20 – JTEKT EPS Type Production Volume [Matsuoka 2016]

II.3 EPS Main Components Description

Currently, torque sensor and electric assistance motor are found on all EPS systems types. Those components are essentials in EPS systems. Torque sensor is important since it measures an amount of steering torque on which current EPS control strategies are based on. On the other hand, electric assistance motor is the actuator that provides the assistance torque to the driver. Both components effects in EPS performance are discussed in this section.

II.3.1 Torque Sensor

The driver provides a torque at the steering wheel. Then in EPS systems, the torque sensor device measures the direction and the amount of applied torque. A torque sensor is composed

by an input shaft and an output (lower) shaft which are connected by a torsion bar. Hence, the sensor is mounted such as the column shaft is at input side and the pinion shaft at output side, as shown in Fig. II.21. When a torque is exerted by the driver, the torsion bar twists. Then, a relative movement between the shafts is observed. This distortion is detected by hall-type sensors which send a voltage signal to the ECU.

Hence, torque sensor signal will refer to the measurement of the steering force applied by the driver and captured at torsion bar level. A particular attention is paid to the fact that driver torque and torque sensor signal are equivalent in static condition only, as in dynamic condition torsion bar also captures the inertia effect of the steering wheel [Parmar 2004], [Marouf 2013].

Indeed, the magnetic flux density is modified due to the relative displacement of the magnet with respect to the magnetic yoke (ferromagnetic material). The yoke is a fixed part joints to the pinion shaft, whereas the magnet is a moving part joints to the torsion bar. A Hall effect sensor detects a voltage which is proportional to the magnetic flux density. Finally, the torque is computed using signals from main and sub cells, where the torque sensor signal is used in current EPS control strategy to provide assistance torque to the driver.

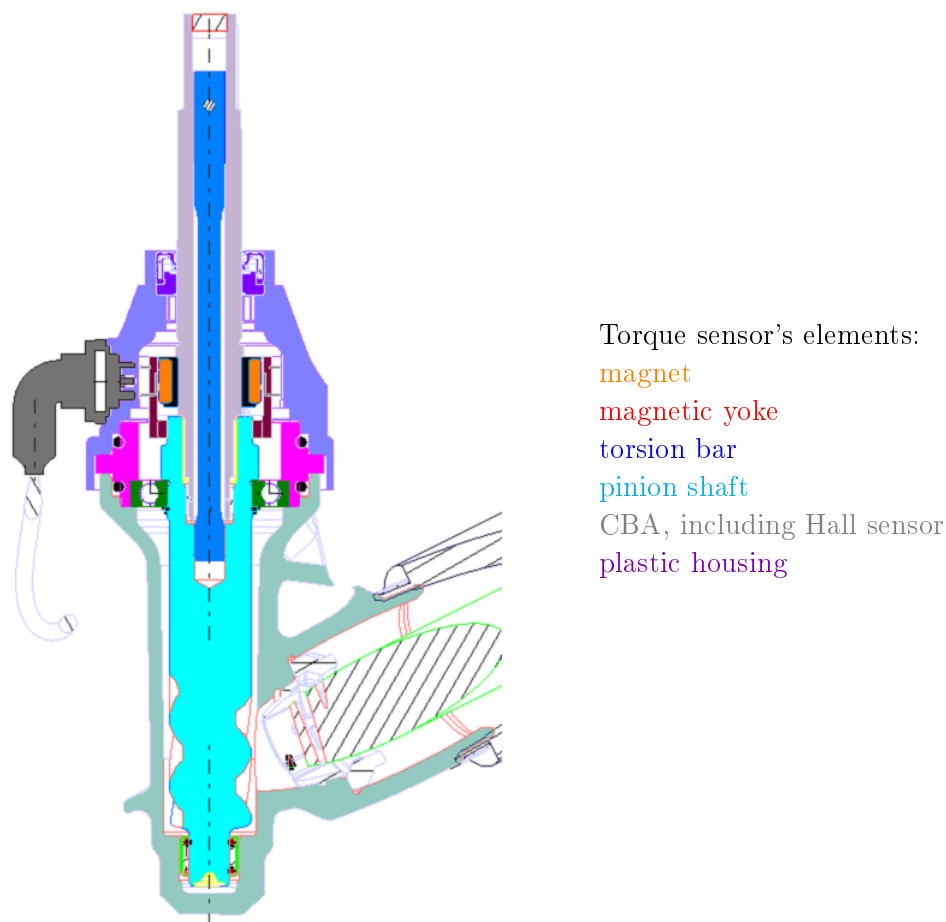


Figure II.21 – Torque Sensor

Moreover, torque sensor safety is required, to detect some defaults that appears in the cells,

i.e an erroneous output voltage which is lower than an error voltage threshold value would be considered as correct. An on-board diagnostics circuit is integrated to distinguish such case by forcing the output voltage to a defined value. Hence, a coverage is ensured in case of undervoltage or overvoltage or power outage or error in EEPROM. Nevertheless, some torque sensor failure case leads to shut-off the assistance as torque sensor signal is invalidated, e.g inconsistency on main and sub cells, even though one cell is faulty and the other correct (for more details on torque sensor failure mode see [Zhang 2016]).

Besides, torque sensor induces several constraints:

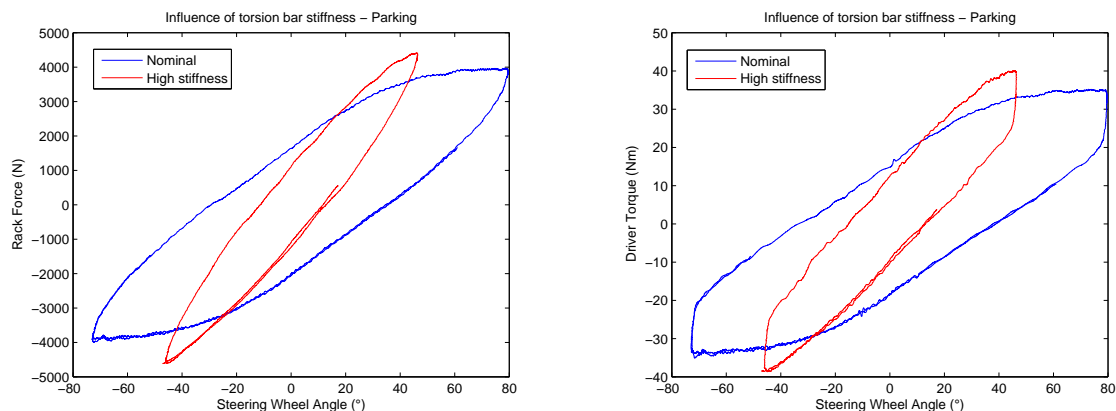
- a sensitivity regarding drifts in torque sensor's elements assembly (yoke, magnet...) which affects the output voltage
- extra steps, such as balancing (to determine measurement range) and calibration (to compensate dispersal and tolerance introduced during assembly), to obtain a valid torque signal
- an additional cost related to its components and assembly process

According to the above points, removing the torque sensor in EPS systems would lower the cost production.

Remark II.2

Torque sensor introduces an elasticity on EPS system due to torsion bar stiffness.

In Fig. II.22, the effect induced by the torsion bar stiffness is illustrated. In Fig. II.22 two different EPS systems namely a nominal EPS (mass-produced) and a prototype EPS (with a high torsion bar stiffness), have been tested successively on the same vehicle to realise a small steering wheel movement at parking. In Fig. II.22(a), the two curves show the steering wheel angle function of the rack force. A same amount of rack force is reached for both cases however with different steering wheel angle amplitude. In Fig. II.22(b) the two curves show the steering wheel angle function of the driver torque. Considering the nominal EPS, the same amount of driver torque is achieved for a steering wheel angle wider than on the prototype. This means that a high stiffness involves a fast response of the system, since less angle is required to initiate the motion. Nevertheless, it also results in a quick increases of the steering torque. Moreover, elasticity induced by the torsion bar stiffness acts as a natural filter. The road feedback (vibrations, kickback) is transmitted to the driver through the steering system, but the stiffness of the torsion bar attenuates those effects into the driver's hand. Therefore, a system without torsion bar provides a direct road feel.



(a) Steering angle VS Rack force
torsion bar influence

(b) Steering angle VS Driver torque
torsion bar influence

Figure II.22 – Torsion bar stiffness influences on a prototype vehicle at parking

II.3.2 Electric Assistance Motor

The electric motor has been used as an actuator in EPS systems, where the motor provides an assistance torque. EPS motor requirements, in terms of power, vary considering the type of EPS systems. Table II.1 compares some motor features impacts according to EPS types [Tanaka 2003].

| | Column-type | Pinion-type | Rack-type |
|--|-------------|-------------|-----------|
| Noise/vibration | high | medium | low |
| Environment resistance (temperature, water proof) | low | high | high |
| Motor power | low | medium | high |

Table II.1 – EPS motors requirements depending on system types

In fact, increasing EPS motors' power lead to larger motors with more noise, torque ripple, higher friction (so torque loss) and moments of inertia. Furthermore, those drawbacks are reflected at driver level and may degrade driving experience. Thus, EPS motors characteristics have evolved, from DC motor to brushless motors. Table II.2 compares these different characteristics.

| | Brush DC | Brushless DC | Brushless AC |
|-----------------------|--------------------|------------------|------------------|
| Controller | none, mechanically | square | sinusoidal |
| Structure | stator: magnet | stator: windings | stator: windings |
| | rotor: windings | rotor: magnet | rotor: magnet |
| Inertia | high | low | low |
| Rotation speed | low | high | high |
| Motor noise | high | low | low |
| Motor power | 500W-class | > 500W-class | > 500W-class |
| Rotor position sensor | - | mandatory | mandatory |

Table II.2 – Characteristics comparison of electric motors

Today, EPS systems are mostly equipped with brushless type, i.e permanent magnet synchronous motor (PMSM). Indeed, PMSMs are high-powered EPS motors, achieving low moment of inertia, low torque ripple, low cogging torque, low frictional loss torque while reducing noise characteristics. However, the motor controller is more complex than a DC as it necessitates a rotor position sensor (resolver), so PMSMs have the disadvantage to be more expensive [Tanaka 2000].

A common motor characteristic diagram describing the relationship between the motor rotational speed (rpm, revolution per minute) and torque (Nm) is called a NT characteristics. Considering EPS motors, NT characteristic needs to fulfil some system performance requirements which depend on the application (EPS type, vehicle type). In Fig. II.23, specifications of EPS motor performance are indicated by three points (description is done in Table II.3) and a NT characteristic satisfying these requirements is presented.

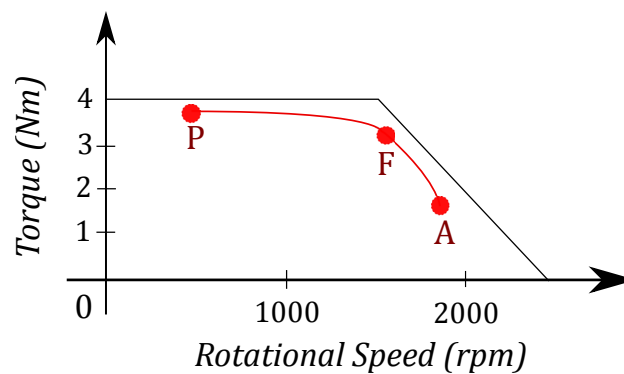


Figure II.23 – NT characteristics

| Operating point | Motor torque | Motor speed |
|-----------------|--------------|-------------|
| Parking (P) | τ_{max} | V_{min} |
| Fast (F) | τ_{int} | V_{int} |
| Avoidance (A) | τ_{min} | V_{max} |

Table II.3 – System performance requirement

Remark II.3

It is worth noting that in the considered application case, the motor control implemented in the electric assistance motor is provided by suppliers and could not be modified.

II.4 Conclusion

In this chapter, an overview of steering systems structure and functioning have been discussed. Regarding market evolution EPS systems emerge as the most appropriate solution considering customer expectations and requirements. Hence, a detailed presentation on different types of EPS systems and its main components has been done. Then, torque sensor is an expensive components in EPS systems, nevertheless essential regarding EPS control laws, even though failure could occur on such electrical component.

In next chapter, EPS systems modelling are presented as a basis to simulation environment, and also to design observer and control.

Electric Power Steering Modelling

Contents

| | |
|--|-----------|
| III.1 Introduction | 23 |
| III.2 Electric Power Steering Dynamic Modelling | 24 |
| III.2.1 P-EPS Model | 24 |
| III.2.2 C-EPS Model | 26 |
| III.3 Vehicle Dynamic Modelling | 29 |
| III.3.1 Road reaction force | 32 |
| III.4 Simulation Environment | 38 |
| III.5 EPS on board, Vehicle Environment | 39 |
| III.5.1 Mechanical Part | 39 |
| III.5.2 Electronic Part (real time) | 40 |
| III.6 Model validation from experiments | 42 |
| III.6.1 Simulation of EPS Model - P-EPS | 43 |
| III.6.2 Simulation of Rack Force Model - Parking | 44 |
| III.6.3 Simulation of Rack Force Model - Transition Parking to Low Speed | 45 |
| III.6.4 Simulation of Rack Force Model - Rolling | 48 |
| III.6.5 Simulation of Vehicle Model | 49 |
| III.7 Conclusion | 52 |

III.1 Introduction

This chapter aims at introducing EPS model together with a well defined simulation environment. At first, EPS models are defined according to mechanical equations. Then, a vehicle dynamic model including a road reaction force model is introduced to get a complete simulation environment used to validate the estimation and control strategy. Moreover, the real system configuration (a development mule) is presented, where experimental results are carried on. Finally, some simulation results using real input data are shown to validate the models presented in this chapter.

III.2 Electric Power Steering Dynamic Modelling

The mathematical model of the steering system is mostly defined using Newton's second law of motion. Regardless of EPS dynamical models complexity, three inputs have to be considered: the driver torque τ_d , the assist motor torque τ_m and the rack force F_r (tire/road contact forces). Hence, EPS model establishes the relation between these inputs acting respectively over the following three subsystems: steering wheel and column linkage, electric assist motor and gear box assembly, rack and pinion assembly.

Mechanically speaking, the steering systems can be represented by inertias or masses linked together via springs, dampers and friction elements. Depending on EPS components' decomposition level (consider not only steering wheel, assist motor, pinion and rack inertia but also intermediate shaft or worm gear), a C-EPS full order model of more than 8 degrees of freedom structure is achieved in [Badawy 1999], [Tamura 2012]. However, a reduced order model can be deduced by neglecting rigid elements (high stiffness springs) which contribute to high frequency modes [Badawy 1999]. Indeed, low frequency modes prevail on fundamental behaviour of the system. In practice, a driver's nominal input is roughly 2Hz and does not exceed 5Hz even in avoidance manoeuvre [Badawy 1999], [Marouf 2013] and the road information (tire/steering wheel transmission) concerns a frequency range of interest between [15 – 30]Hz [Sugitani 1997]. Hence, EPS global model within a frequency range of interest [0 – 30]Hz is sufficient. Several EPS models could be found in literature: [Saifia 2014], [Rongyun 2015] introduce EPS model including vehicle model to express the rack force. Otherwise, a model of the tie rod force is introduced as a linear spring dependent on vehicle speed [Zaremba 1995] where the model validity region is in rolling condition (around zero slip angle, tire force is varying almost linearly). Then, rack and tire connection is simplified to a constant tire stiffness model. Several studies are based on this linear reduced EPS model regarding simplicity [Mehrabi 2011], [Marouf 2012a], [Illán 2011], [Parmar 2004], [Zaremba 1997].

III.2.1 P-EPS Model

An illustration of P-EPS model (see II.2.4.2) composition is shown in Fig. III.1 where four main parts are distinguished: steering wheel, assist motor, pinion and rack.

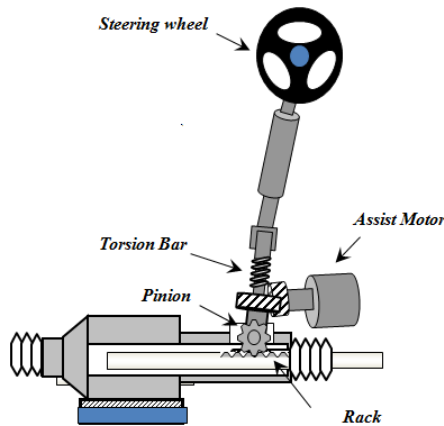


Figure III.1 – P-EPS Dynamic Modeling

The following equations are obtained from Newton's second law of motion where parameters are described in Table III.1:

- steering wheel dynamical equation:

$$J_c \ddot{\theta}_c = \tau_d - \left(D_{tb}(\dot{\theta}_c - \dot{\theta}_p) + K_{tb}(\theta_c - \theta_p) \right) - B_c \dot{\theta}_c - F_c \text{sgn}(\dot{\theta}_c) \quad (\text{III.1})$$

- assist motor shaft dynamical equation:

$$J_m \ddot{\theta}_m = \tau_m - \left(D_g(\dot{\theta}_m - R_m \dot{\theta}_p) + K_g(\theta_m - R_m \theta_p) \right) - B_m \dot{\theta}_m - F_m \text{sgn}(\dot{\theta}_m) \quad (\text{III.2})$$

- rack dynamical equation:

$$J_r \ddot{X}_r = \tau_{road} + \left(D_{pr}(R_p \dot{\theta}_p - \dot{X}_r) + K_{pr}(R_p \theta_p - X_r) \right) - \left(D_r \dot{X}_r + K_r X_r \right) - B_r \dot{X}_r \quad (\text{III.3})$$

- pinion shaft dynamical equation:

$$\begin{aligned} J_p \ddot{\theta}_p = & R_m \left(D_g(\dot{\theta}_m - G\dot{\theta}_p) + K_g(\theta_m - R_m \theta_p) \right) - R_p \left(D_{pr}(R_p \dot{\theta}_p - \dot{X}_r) + K_{pr}(R_p \theta_p - X_r) \right) \\ & + \left(D_{tb}(\dot{\theta}_c - \dot{\theta}_p) + K_{tb}(\theta_c - \theta_p) \right) \end{aligned} \quad (\text{III.4})$$

Therefore, a linear state-space representation of P-EPS model is expressed as:

$$\begin{cases} \dot{x} = Ax + Bu + Ed + Ww \\ y = Cx \end{cases} \quad (\text{III.5})$$

with $x = \left(\dot{\theta}_c \ \dot{\theta}_m \ \dot{\theta}_p \ \dot{X}_r \ \theta_c \ \theta_m \ \theta_p \ X_r \right)^T \in \mathbb{R}^8$ are the internal states, $d \in \mathbb{R}$ is the driver torque to be estimated, $w \in \mathbb{R}$ the road reaction torque is the unknown input, and $u \in \mathbb{R}$ the assist motor torque is the control signal.

The available measurements are $y = \left(\theta_c \ \theta_m \right)^T \in \mathbb{R}^2$ in this context. Indeed, an angle sensor is available on the vehicle to give the steering wheel angle, while the motor angle is given by the PMSM's resolver.

$$A = \begin{pmatrix} -\frac{B_c + D_{tb}}{J_c} & 0 & \frac{D_{tb}}{J_c} & 0 & -\frac{K_{tb}}{J_c} & 0 & \frac{K_{tb}}{J_c} & 0 \\ 0 & -\frac{B_m + D_g}{J_m} & \frac{D_g R_m}{J_m} & 0 & 0 & -\frac{K_g}{J_m} & \frac{K_g R_m}{J_m} & 0 \\ \frac{D_{tb}}{J_p} & \frac{D_g R_m}{J_p} & \frac{a_{33}}{J_p} & \frac{D_{pr} R_p}{J_p} & \frac{K_{tb}}{J_p} & \frac{K_g R_m}{J_p} & \frac{a_{35}}{J_p} & \frac{K_{pr} R_p}{J_p} \\ 0 & 0 & \frac{D_{pr} R_p}{J_r} & -\frac{D_{pr} + B_r + D_r}{J_r} & 0 & 0 & \frac{K_{pr} R_p}{J_r} & -\frac{K_{pr} + K_r}{J_r} \\ 1 & 0 & 0 & 0 & 0 & 0 & 0 & 0 \\ 0 & 1 & 0 & 0 & 0 & 0 & 0 & 0 \\ 0 & 0 & 1 & 0 & 0 & 0 & 0 & 0 \\ 0 & 0 & 0 & 1 & 0 & 0 & 0 & 0 \end{pmatrix}$$

where $a_{33} = -(B_p + D_{tb} + R_m^2 D_g + R_p^2 D_{pr})$, $a_{35} = -(K_{tb} + R_m^2 K_g + R_p^2 K_{pr})$.

$$\begin{aligned} B &= \left(0 \ \frac{1}{J_m} \ 0 \ 0 \ 0 \ 0 \ 0 \ 0 \right)^T, \quad E = \left(\frac{1}{J_c} \ 0 \ 0 \ 0 \ 0 \ 0 \ 0 \ 0 \right)^T, \\ W &= \left(0 \ 0 \ 0 \ \frac{1}{J_r} \ 0 \ 0 \ 0 \ 0 \right)^T \quad \text{and} \quad C = \begin{pmatrix} 0 & 0 & 0 & 0 & 1 & 0 & 0 & 0 \\ 0 & 0 & 0 & 0 & 0 & 1 & 0 & 0 \end{pmatrix} \end{aligned}$$

This P-EPS full model is used to design driver torque estimation, whereas in next section a C-EPS simplified model is introduced to design EPS control.

| Notation | Description | Unit |
|----------|----------------------------------|---------------|
| J_c | Steering column inertia | $kg.m^2$ |
| B_c | Steering column viscous friction | $N.m/(rad/s)$ |
| K_{tb} | Torsion bar stiffness | $N.m/rad$ |
| D_{tb} | Torsion bar damping | $N.m/(rad/s)$ |
| J_p | Pinion/gear inertia | $kg.m^2$ |
| K_{pr} | Pinion/rack stiffness | N/m |
| D_{pr} | Pinion/rack damping | $N/(m/s)$ |
| R_p | Pinion/rack reducer | m/rad |
| J_r | Rack and tie rods mass | kg |
| B_r | Rack viscous friction | $N/(m/s)$ |
| K_r | Rack stiffness | N/m |
| D_r | Rack damping | $N/(m/s)$ |
| R_m | Worm/gear reduction ratio | – |
| J_m | Motor inertia | $kg.m^2$ |
| B_m | Motor viscous friction | $N.m/(rad/s)$ |
| K_g | Worm/gear stiffness | $N.m/rad$ |
| D_g | Worm/gear damping | $N.m/(rad/s)$ |

Table III.1 – P-EPS system mechanical parameters

III.2.2 C-EPS Model

An illustration of C-EPS model (see II.2.4.1) is shown in Fig. III.2 where three main parts are distinguished: steering wheel, assist motor and rack.

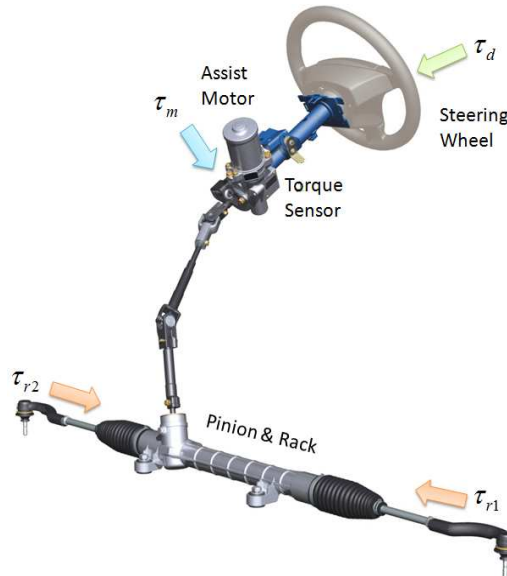


Figure III.2 – C-EPS Dynamic Modeling

Therefore, an EPS reduced order model is made of three main connected components: steering wheel angle and steering column (with driver torque input), assist motor and rack/pinion assembly (with motor torque input), rack/pinion assembly and tire (with road/tire reaction input). Furthermore, rack/pinion assembly and assist motor could be gathered in a common inertia subject to a high universal joint stiffness, as performed in [El-Shaer 2008] or [Marouf 2013], bringing rack equation to motor shaft. Then, a simplified mechanical EPS model is introduced composed by a steering wheel inertia and a global inertia as shown in Fig. III.3.

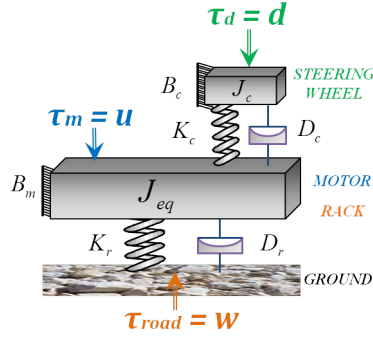


Figure III.3 – C-EPS Simplified Mechanical Structure

The following equation are obtained from Newton's second law of motion where parameters are described in Table III.2:

- applied at steering wheel:

$$J_c \ddot{\theta}_c = \tau_d - D_c \left(\dot{\theta}_c - \frac{\dot{\theta}_m}{R_m} \right) - K_c \left(\theta_c - \frac{\theta_m}{R_m} \right) - B_c \dot{\theta}_c - F_c \text{sgn}(\dot{\theta}_c) \quad (\text{III.6})$$

where the torque sensor signal is assimilated to $\tau_{TS} = K_c \left(\theta_c - \frac{\theta_m}{R_m} \right) + D_c \left(\dot{\theta}_c - \frac{\dot{\theta}_m}{R_m} \right)$

- applied at assist motor shaft:

$$J_{eq} \ddot{\theta}_m = \tau_m + \frac{D_c}{R_m} \left(\dot{\theta}_c - \frac{\dot{\theta}_m}{R_m} \right) + \frac{K_c}{R_m} \left(\theta_c - \frac{\theta_m}{R_m} \right) - B_m \dot{\theta}_m - K_r \frac{R_p^2}{R_m^2} \theta_m - D_r \frac{R_p^2}{R_m^2} \dot{\theta}_m - \frac{\tau_r}{R_m} - F_m \text{sgn}(\dot{\theta}_m) \quad (\text{III.7})$$

where $J_{eq} = J_m + \frac{R_p^2}{R_m^2} M_r$ ($B_{eq} = B_m + \frac{R_p^2}{R_m^2} D_r$) is the equivalent inertia (resp. viscous friction) and rack/pinion conversion is given by $X_r = R_p \theta_p$ whereas motor/pinion is $\theta_m = \theta_p R_m$

with the corresponding notation: τ_d is the torque applied by the driver, τ_m is the assist motor torque, τ_r is the road reaction torque, θ_c ($\dot{\theta}_c$) is the steering wheel angle (velocity), θ_m ($\dot{\theta}_m$) is the motor angle (velocity) and X_r is the rack position.

| Notation | Description | Unit |
|----------|----------------------------------|-------------------|
| J_c | Steering column inertia | kg m ² |
| B_c | Steering column viscous friction | N m/(rad/s) |
| K_c | Column stiffness | N m/rad |
| D_c | Column damping | N m/(rad/s) |
| F_c | Steering column friction | N m |
| R_p | Pinion/rack reducer | m/rad |
| M_r | Rack and tie rods mass | kg |
| B_r | Rack viscous friction | N/(m/s) |
| K_r | Rack stiffness | N/m |
| D_r | Rack damping | N/(m/s) |
| R_m | Motor reduction ratio | - |
| J_m | Motor inertia | kg m ² |
| B_m | Motor viscous friction | N m/(rad/s) |
| F_m | Motor friction | N m |

Table III.2 – C-EPS system mechanical parameters

Hence, a linear model is obtained defining the state vector $x = (\dot{\theta}_c \ \dot{\theta}_m \ \theta_c \ \theta_m)^T \in \mathbb{R}^4$, the control input $u = \tau_m \in \mathbb{R}$ as the assist torque motor, the exogenous input vector $\begin{pmatrix} d \\ w \end{pmatrix} = \begin{pmatrix} \tau_d \\ F_r \end{pmatrix} \in \mathbb{R}^2$ as the driver torque and the road reaction force, the measurement vector $y = \begin{pmatrix} \theta_c \\ \theta_m \end{pmatrix} \in \mathbb{R}^2$ as both angular position, a 4th order state-space model is deduced:

$$\begin{cases} \dot{x} = \begin{pmatrix} -\frac{B_c+D_c}{J_c} & \frac{D_c}{J_c R_m} & -\frac{K_c}{J_c} & \frac{K_c}{J_c R_m} \\ \frac{D_c}{J_{eq} R_m} & -\frac{B_{eq}}{J_{eq}} - \frac{D_c}{J_{eq} R_m^2} & \frac{K_c}{J_{eq} R_m} & -\frac{K_c+K_r R_p^2}{J_{eq} R_m^2} \\ 1 & 0 & 0 & 0 \\ 0 & 1 & 0 & 0 \end{pmatrix} x + \begin{pmatrix} 0 \\ \frac{1}{J_{eq}} \\ 0 \\ 0 \end{pmatrix} u + \begin{pmatrix} \frac{1}{J_c} \\ 0 \\ 0 \\ 0 \end{pmatrix} d + \begin{pmatrix} 0 \\ -\frac{R_p}{J_{eq} R_m} \\ 0 \\ 0 \end{pmatrix} w \\ y = \begin{pmatrix} 0 & 0 & 1 & 0 \\ 0 & 0 & 0 & 1 \end{pmatrix} x \end{cases} \quad (\text{III.8})$$

Therefore, (III.8) is expressed as:

$$\begin{cases} \dot{x} = Ax + Bu + Ed + Ww \\ y = Cx \end{cases} \quad (\text{III.9})$$

Although C-EPS model (III.8) is limited (since non-linear terms are neglected), a linear model in the desired operating bandwidth is sufficient. Thus, similarly to [El-Shaer 2008], the state-space representation (IV.4.2) is used for control design purposes. Nevertheless, according to model uncertainties, the controller shall be robust enough to achieve desired performance and stability on the real system.

III.3 Vehicle Dynamic Modelling

Vehicle motion can be characterized through 6 degrees of freedom (DOF): longitudinal, lateral and vertical translations plus roll, pitch and yaw rotations. In the literature, several vehicle models are considered: the quarter car model (vertical and longitudinal) or the vertical half vehicle model (extension of the previous model introducing pitch and roll motion) are often considered in suspensions framework, for more details see [Poussot-Vassal 2009].

Regarding steering systems studies, the lateral dynamics are mainly involved. A simplest vehicle model comprising lateral and yaw motions 2-DOF is obtained where roll, pitch, bounce and deceleration dynamics are neglected. Indeed, the level of vehicle's centre of gravity is assumed to be at the road surface, then roll and pitch angles of the vehicle are neglected. Consequently, each axle shares the same steering angles, i.e each wheel produces the same steering forces. A single track model is presented in Fig III.4, where the two front wheels and the two rear wheels are represented by single wheels. Table III.3 introduces parameters notations of the bicycle model, for further details refer to [Kiencke 2005].

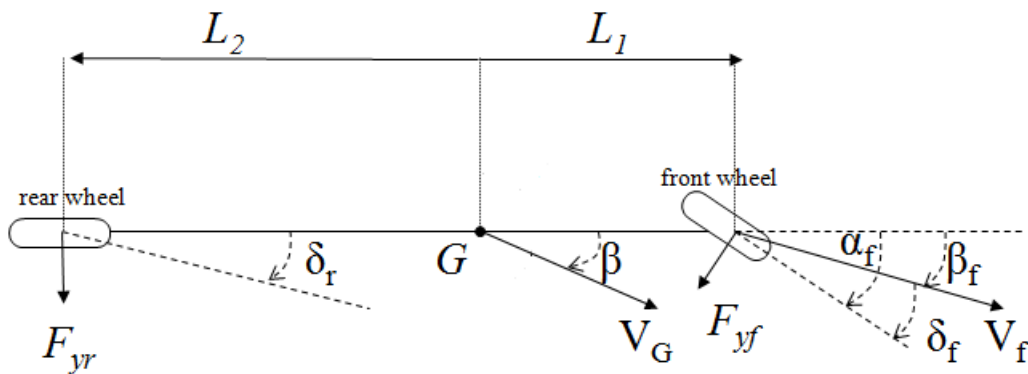


Figure III.4 – Bicycle Model

Remark III.1

The front wheel angle α_f is obtained from the steering wheel angle θ_c with the relation: $\alpha_f = \theta_c R_{ct}$ where R_{ct} is the average steering ratio which converts steering wheel angle to front wheel angle.

The vehicles considered in this thesis have no rear steering $\alpha_r = 0$.

| Notation | Description | Unit |
|------------|-----------------------------------|------|
| G | Center of Gravity (CoG) | - |
| F_{yf} | Front tire lateral force | N |
| F_{yr} | Rear tire lateral force | N |
| L_1 | Distance CoG and front axle | m |
| L_2 | Distance CoG and rear axle | m |
| V_G | Speed vector of CoG | m/s |
| V_x | Longitudinal speed of the vehicle | m/s |
| V_y | Lateral speed of the vehicle | m/s |
| α_f | Front wheel angle | rad |
| β | Vehicle sideslip angle | rad |
| β_f | Slip angle of the front axle | rad |
| β_r | Slip angle of the rear axle | rad |
| δ_f | Front wheel slip angle | rad |
| δ_r | Rear wheel slip angle | rad |

Table III.3 – Bicycle model parameters

Then, the equations of motion of the bicycle model, on the Y plane, is given by the sum of lateral forces $\sum F_y = Ma_y$ whereas on the Z-axis, the sum of torques provides the yaw dynamics $\sum \tau_z = I_\psi \ddot{\psi}$ [Rajamani 2012]:

$$\begin{cases} M(\dot{V}_y + V_x \dot{\psi}) = (F_{yf} \cos(\alpha_f) + F_{yr}) & (lateral) \\ I_\psi \ddot{\psi} = (L_1 F_{yf} \cos(\alpha_f) - L_2 F_{yr}) & (yaw) \end{cases} \quad (\text{III.10})$$

where $a_y = \dot{V}_y + V_x \dot{\psi}$ is the lateral acceleration, I_ψ is the yaw inertia ($kg.m^2$) and $\dot{\psi}$ is the yaw rate (rad/s). In (III.10) the disturbance moment and torque acting on vehicle (such as in [Ackermann 1996]) are ignored for simplicity (no crosswind, flat tires or lateral road slopes). Although (III.10) is a non-linear bicycle model (as lateral tire forces are non-linear), a linear form is introduced next.

The slip angle is the angle between the direction of motion and the wheel direction, see Fig III.5. These two directions are different whenever cornering, when the lateral tire force increases.

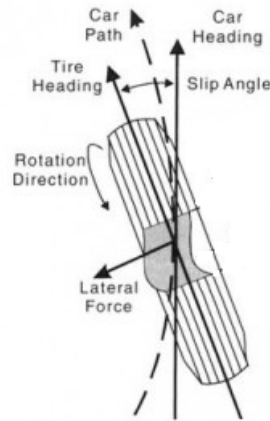


Figure III.5 – Slip angle and Lateral tire force

For small slip angles, the lateral forces at the wheels are approximated by a linear equation of the slip angle, as follows

$$\begin{cases} F_{yf} = C_{yf}\delta_f \\ F_{yr} = C_{yr}\delta_r \end{cases} \quad (III.11)$$

where C_{yf} (resp. C_{yr}) is the front (resp. rear) tire cornering stiffness (N/rad) represented by the slope in linear region of Fig III.6.

However, when the slip angle increases, this assumption does not hold as the tire contact patch is sliding. Then, the lateral force is a non-linear function of slip angle.

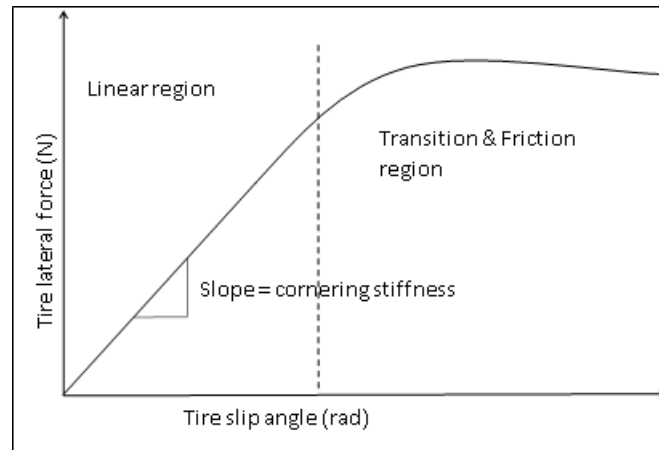


Figure III.6 – Lateral tire force VS Slip angle

From Fig III.4, the slip angles are expressed by:

$$\begin{cases} \delta_f = \alpha_f - \beta_f \\ \delta_r = -\beta_r \end{cases} \quad (III.12)$$

where sideslip angles are given by:

$$\begin{cases} \tan(\beta_f) = \frac{V_y + L_1\dot{\psi}}{V_x} \\ \tan(\beta_r) = \frac{V_y - L_2\dot{\psi}}{V_x} \end{cases} \quad (\text{III.13})$$

According to small angle assumption $\tan(\beta) \simeq \beta$ (during stable driving conditions β is actually no larger than 10°), applied to (III.13), we get:

$$\begin{cases} \delta_f = \alpha_f - \frac{V_y + L_1\dot{\psi}}{V_x} \\ \delta_r = -\frac{V_y - L_2\dot{\psi}}{V_x} \end{cases} \quad (\text{III.14})$$

Then, the expression of lateral tire forces in (III.15) is given by:

$$\begin{cases} F_{yf} = 2C_{yf} \left(\alpha_f - \frac{V_y + L_1\dot{\psi}}{V_x} \right) \\ F_{yr} = 2C_{yr} \left(-\frac{V_y - L_2\dot{\psi}}{V_x} \right) \end{cases} \quad (\text{III.15})$$

A factor 2 appears naturally, as two tires are involved.

Finally, the dynamical equations (III.10) are simplified subject to small angles assumption $\cos(\alpha_f) \simeq 1$ which lead to:

$$\begin{cases} M(\dot{V}_y + V_x\dot{\psi}) = 2C_{yf} \left(\alpha_f - \frac{V_y + L_1\dot{\psi}}{V_x} \right) - 2C_{yr} \left(\frac{V_y - L_2\dot{\psi}}{V_x} \right) \\ I_\psi\ddot{\psi} = 2L_1C_{yf} \left(\alpha_f - \frac{V_y + L_1\dot{\psi}}{V_x} \right) + 2L_2C_{yr} \left(\frac{V_y - L_2\dot{\psi}}{V_x} \right) \end{cases} \quad (\text{III.16})$$

A linear state-space representation of half-vehicle model is then:

$$\begin{cases} \begin{pmatrix} \dot{V}_y \\ \ddot{\psi} \end{pmatrix} = \begin{pmatrix} -\frac{2}{MV_x}(C_{yf} + C_{yr}) & -V_x - \frac{2}{MV_x}(L_1C_{yf} - L_2C_{yr}) \\ -\frac{2}{I_\psi V_x}(L_1C_{yf} - L_2C_{yr}) & -\frac{2}{I_\psi V_x}(L_1^2C_{yf} + L_2^2C_{yr}) \end{pmatrix} \begin{pmatrix} V_y \\ \dot{\psi} \end{pmatrix} + \begin{pmatrix} -\frac{2C_{yf}}{M} \\ -\frac{2L_1C_{yf}}{I_\psi} \end{pmatrix} \alpha_f \\ \begin{pmatrix} \dot{\psi} \\ a_y \end{pmatrix} = \begin{pmatrix} 0 & 1 \\ -\frac{2}{MV_x}(C_{yf} + C_{yr}) & -\frac{2}{MV_x}(L_1C_{yf} - L_2C_{yr}) \end{pmatrix} \begin{pmatrix} V_y \\ \dot{\psi} \end{pmatrix} + \begin{pmatrix} 0 \\ \frac{2C_{yf}}{M} \end{pmatrix} \alpha_f \end{cases} \quad (\text{III.17})$$

where the outputs are the lateral acceleration a_y and the yaw rate $\dot{\psi}$ (both measured on the test car) whereas the input is the front steer angle.

III.3.1 Road reaction force

The forces acting on the steering system come from the interaction tire/road, especially by the torsion of the tire. A general overview of the tire force and moment, measured at centre of contact, are shown in Fig III.7:

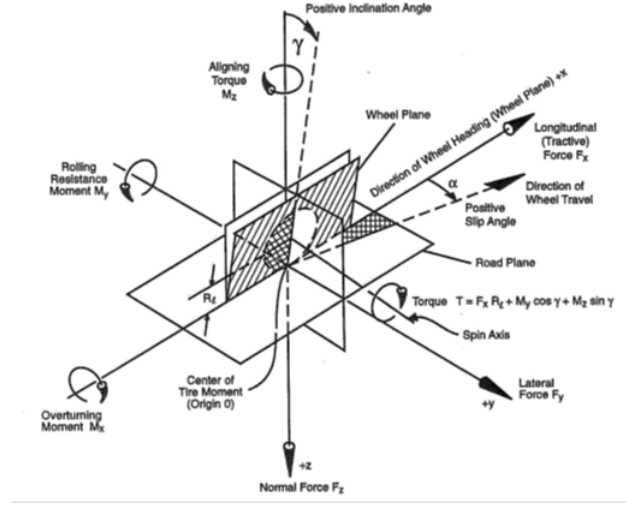


Figure III.7 – SAE tire force and moment axis system

III.3.1.1 Physical based modelling

The road reaction torque is the sum of several moments acting on the steer axis, then each effect is described below as presented in [Gillespie 1992].

- Vertical Moment

$$M_{v\lambda} = -(F_{zr} + F_{zl})\sin(\lambda)d\sin(\delta) \quad (\text{III.18})$$

Moment due to steering lateral inclination angle

$$M_{v\delta} = (F_{zl} - F_{zr})\sin(\nu)d\cos(\delta) \quad (\text{III.19})$$

Moment due to caster angle

$$M_v = M_{v\delta} + M_{v\lambda} \quad (\text{III.20})$$

where F_{zl} (resp. F_{zr}) is the vertical load on left (resp. right) wheels

- Lateral Moment

$$M_l = (F_{yl} + F_{yr})r\tan(\nu) \quad (\text{III.21})$$

where F_{yl} (resp. F_{yr}) is the lateral forces on left (resp. right) wheels

- Tractive Moment

$$M_t = (F_{xl} - F_{xr})d \quad (\text{III.22})$$

where F_{yl} (resp. F_{yr}) is the tractive forces on left (resp. right) wheels

- Self Aligning Torque

$$M_{at} = (M_{zl} + M_{zr})\cos\left(\sqrt{\lambda^2 + \nu^2}\right) \quad (\text{III.23})$$

where M_{zl} (resp. M_{zr}) is the aligning torque on left (resp. right) wheels

In Table III.4 parameters introduced to express the moments are described.

| Parameters | Description |
|------------|------------------------------|
| d | lateral offset at the ground |
| r | tire radius |
| λ | Lateral inclination angle |
| δ | Steer angle |
| ν | Caster angle |

Table III.4 – Moment Parameters

Actually, the moment M_g input to the steer axis is given by the forces and moments acting on the tires:

$$M_g = M_v + M_l + M_t + M_{at} \quad (\text{III.24})$$

Remark III.2

Tractive force is assumed to be equivalent at left and right side $F_{xl} = F_{xr}$ as the vehicle moves on the same surface $M_t = 0$

Hence, the tire/road interaction transmits the road movements to the driver through the steering system. As a result the rack force is the force to counter in order to turn the vehicle wheels.

$$F_r = \frac{M_g}{l_n} \quad (\text{III.25})$$

where l_n is the knuckle arm, the mechanism is illustrated in Fig. III.8.

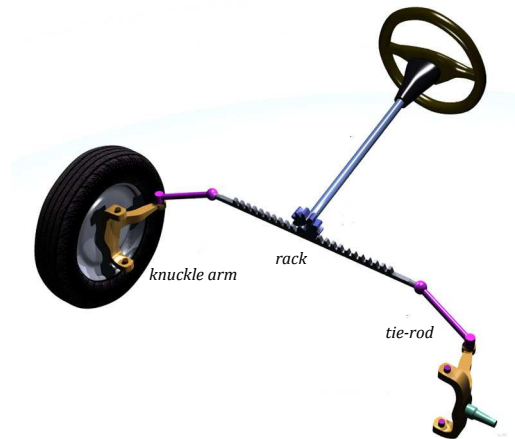


Figure III.8 – Tire/Road Interface on Steering Mechanism

Remark III.3

The rack force could also be decomposed in:

$$F_r = F_{tr}^R + F_{tr}^L \quad (\text{III.26})$$

where F_r is the total force applied on the rack, this means the sum of the force applied on

the tie-rods at left F_{tr}^L and right F_{tr}^R side. Nevertheless, it is usually assumed that there is a little difference between left and right tire response, so a common self aligning torque M_z .

The following terms will be referenced in this thesis, depending on the rack force effect:

- Steer out: steering out of centre, the self-aligning torque creates an opposite force at the rack side. Consequently, more torque is required to steer the wheels out of centre.
- Steer back: steering back to centre, the self-aligning torque tends to bring back the tire to centre position, so a natural force is added to the rack side. Consequently, less torque is required to steer the wheels back to centre.

III.3.1.2 Rack force model in rolling condition

The self-aligning torque increases linearly for small slip angle, in the same way as tire lateral force $T_z = C_z \alpha_f$. However, at large slip angle, the behaviour is not the same since the load fall until loss of grip, as shown in Fig III.9.

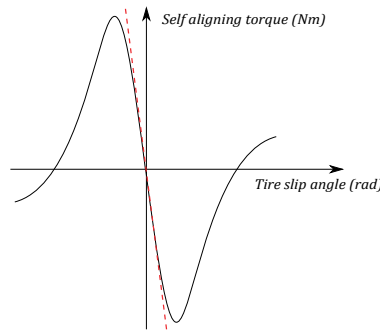


Figure III.9 – Self aligning torque characteristics

Regarding, simulation environment a Pacejka tire model (empirical model) [Brossard 2006], [Bakker 1987] has been considered to describe Y either as the self aligning torque M_z or lateral force F_y , and x as the slip angle δ .

$$\begin{cases} Y &= -D \sin[C \arctan(B\phi)] \\ \phi &= (1 - E)x + \frac{E}{B} \arctan(Bx) \end{cases} \Rightarrow Y = -D \sin[C \arctan(Bx - E(Bx - \arctan(Bx)))] \quad (III.27)$$

The four coefficients B, C, D, E in (III.27) of this magic formula are presented in Table III.5.

| Parameters | Description |
|------------|---|
| B | stiffness factor |
| C | shape factor |
| D | peak factor |
| E | curvature factor |
| BCD | stiffness (slip stiffness at zero slip) |

Table III.5 – Pacejka Parameters

However, the above equation is established under the assumption that the characteristics pass through the origin, which is actually not the case because of tire uniformity (ply steer, conicity). Hence, horizontal and vertical shifts should be considered as:

$$\begin{cases} Y = -D \sin[C \arctan(B\phi)] + S_v \\ \phi = (1 - E)(x + S_h) + \frac{E}{B} \arctan(B(x + S_h)) \end{cases} \quad (\text{III.28})$$

where S_h is the horizontal shift and S_v is the vertical shift. Figure III.10 shows that the above parameters could be determined, based on the characteristics curve of tire forces.

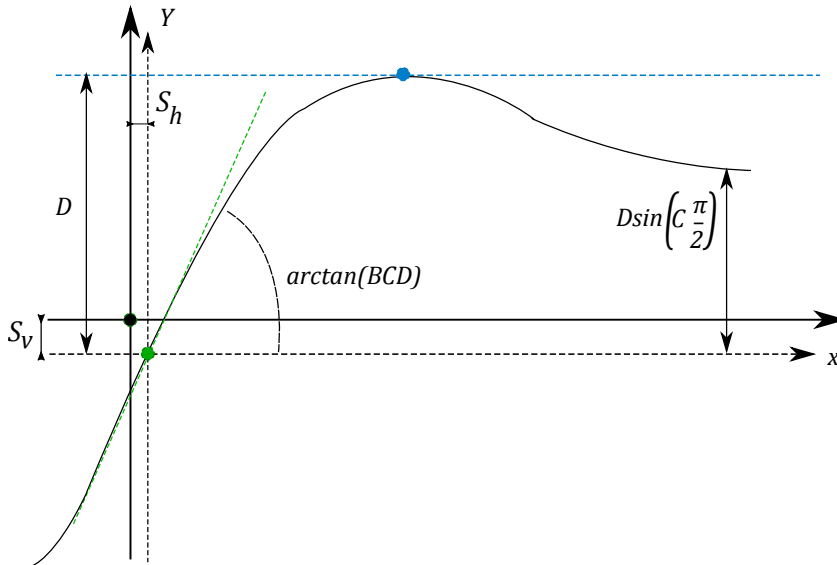


Figure III.10 – Geometrical Interpretation of Pacejka model parameters

III.3.1.3 Rack force model in parking

Although, rotational phenomenon is involving efforts on the tie-rods, rack displacement is in translation. Thus, force would be directly expressed rather than torque. The assistance torque required is maximum when the car is in parking condition, since the rack force is the most important when there is no vehicle motion. Indeed, the tire force is dominated by the stick friction in parking, whereas it is produced by the self-aligning torque in motion. Such a mode requires a more accurate friction model as the LuGre's one, such that the rack effort is calculated using the rack speed.

Then, consider the standard LuGre Model [Olsson 1998] given by:

$$\begin{aligned}
 F &= \sigma_0 z + \sigma_1 \frac{dz}{dt} + f(v) \\
 \frac{dz}{dt} &= v - \sigma_0 \frac{|v|}{g(v)} z \\
 g(v) &= \alpha_0 + \alpha_1 e^{-\left(\frac{v}{v_0}\right)^2} \\
 f(v) &= \alpha_2 v
 \end{aligned}
 \tag{III.29}$$

where z is the average Bristles deformation, F is the rack effort and v is the rack speed. Besides, to take into account the load variation (front axle crushing) in parking, the Coulomb force α_0 is chosen dependent on the load F_z and rack displacement x_r , i.e $\alpha_0 = \eta(x_r)F_z$.

| Parameters | Description |
|-----------------------|------------------------------|
| $g(v)$ | Stribeck effect |
| $f(v)$ | Viscous friction |
| σ_0 | Bristle stiffness |
| σ_1 | Bristle damping |
| α_2 | Viscous friction coefficient |
| $\alpha_1 + \alpha_0$ | Stiction force |
| α_0 | Coulomb friction force |
| v_0 | Stribeck velocity |

Table III.6 – Lugre Parameters

Remark III.4

Above, a constant σ_1 is considered, rather than a velocity dependent $\sigma_1(v)$ defined by:

$$\sigma_1(v) = \sigma_1 e^{-\left(\frac{v}{v_0}\right)^2}
 \tag{III.30}$$

Indeed, the damping characteristics changes (decreases) as velocity increases, because of more lubricant being forced into the interface.

III.3.1.4 Rack force in transition from parking to low speed

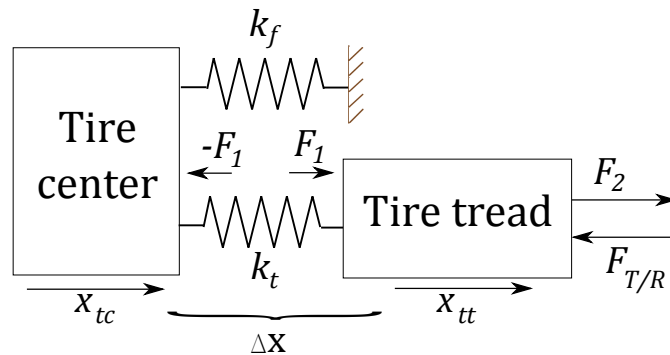


Figure III.11 – Transition parking to low speed model

$$\begin{aligned}
J_{wc}\ddot{x}_{wc} &= F_s y_s - F_r - K_f x_{wc} \\
J_{tt}\ddot{x}_{tt} &= k_t(x_{wc} - x_{tt}) + k_d V(x_{wc} - x_{tt}) - F_{T/R} \\
F_r &= k_t(x_{wc} - x_{tt})
\end{aligned} \tag{III.31}$$

In steady-state, the rack force F_r is expressed as:

$$F_r = \frac{F_{T/R}}{1 + \frac{k_d V}{k_t}} \tag{III.32}$$

Hence, in parking where $V = 0$ the force applied on the rack is the tire/road reaction force only (given by LuGre model), whereas in rolling condition $V \neq 0$ the additional force tends to decrease the friction force (indeed the rack force is generated by the self-aligning torque in motion).

III.4 Simulation Environment

Hence, the simulation environment illustrated in Fig III.12, is used in next chapters and is composed by the following elements:

- the EPS system model, either C-EPS (IV.4.2) or P-EPS (III.5)
- the vehicle model, essentially to obtain the road/tire interaction on EPS system (rack force) as described in section III.3. Indeed, the simulation of different vehicle conditions is achieved by referring to equations: LuGre model (III.29) for parking, for transition model (III.31) and Pacejka model (III.28) for nominal rolling
- the simplified electric assistance motor model, introducing high frequency dynamics

It is worth noting that the only input is the driver torque to remain in accordance with vehicle tests.

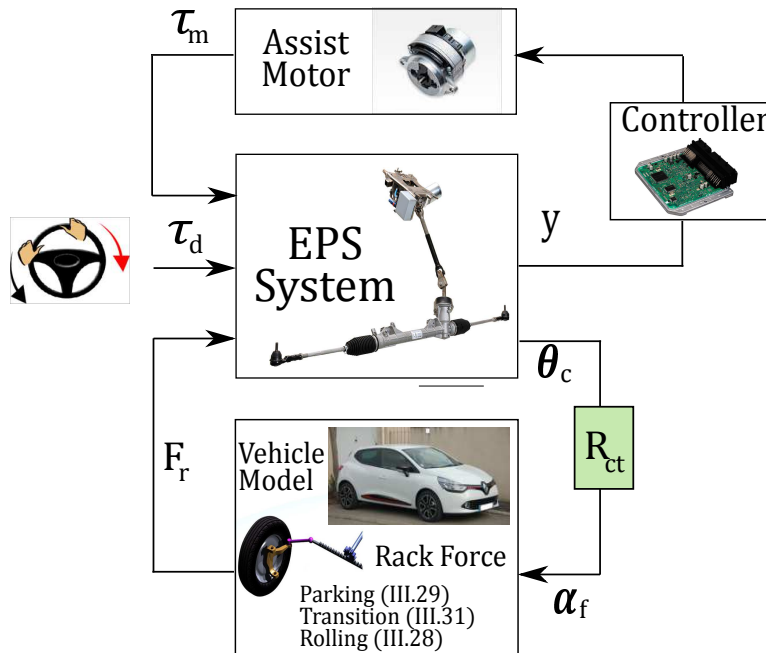


Figure III.12 – C-EPS Full Simulation Environment

III.5 EPS on board, Vehicle Environment

Experimental results have been carried out on a development mule (Clio X98) comprising several measurement devices (CAN interfaces) and an implementation software (MicroAutoBox). Hence, the real system could be decomposed in two parts: mechanical (EPS systems, steering wheel) and electronic (algorithm) communicating through CAN bus, as shown in Fig III.13.

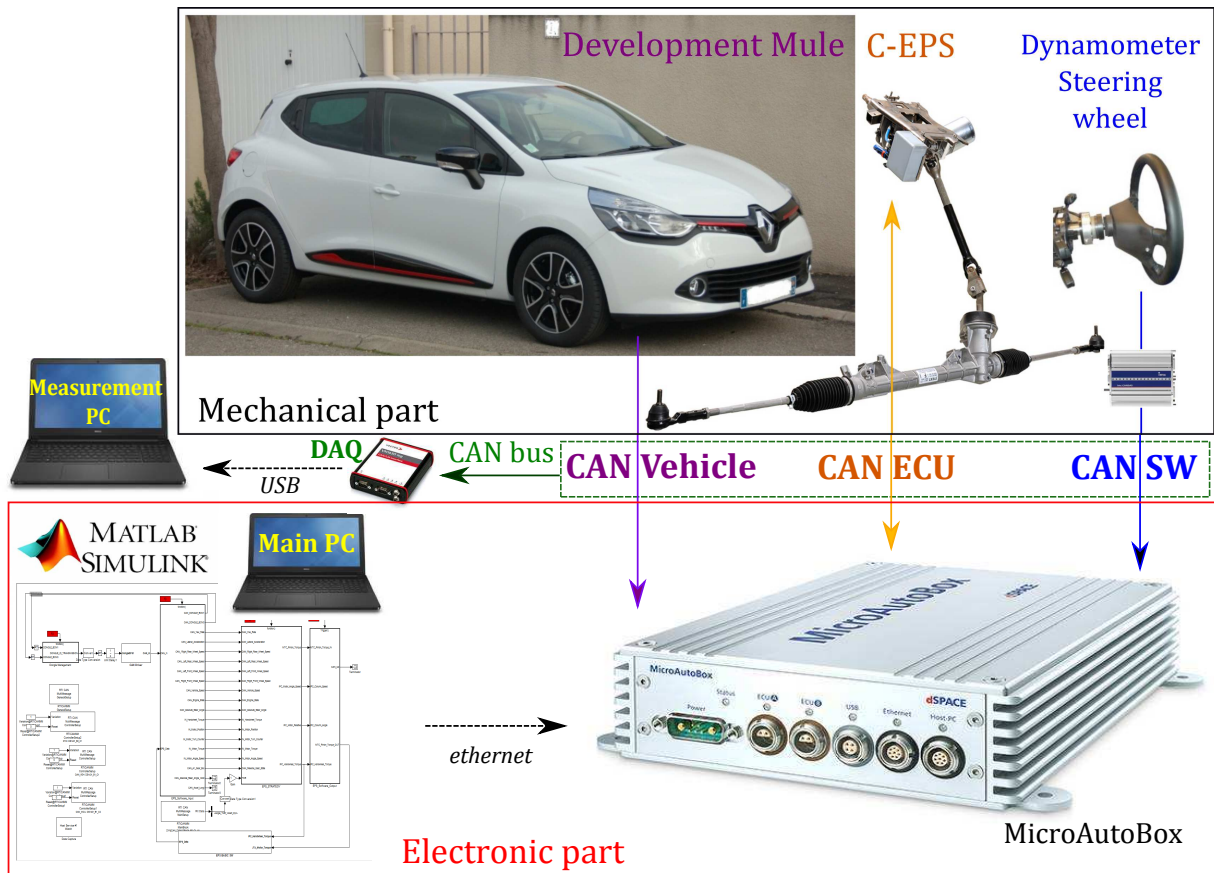


Figure III.13 – Real system, experimental environment structure

The whole experimental set-up is presented in the next sections.

III.5.1 Mechanical Part

The vehicle is equipped with a prototype C-EPS system: a nominal torsion bar stiffness, a low rack/pinion ratio and an electric assistance motor (PMSM) including a resolver. Furthermore, specific elements have been added on the vehicle such as a dynamometer steering wheel or even instrumented tie-rods.

Then, the list of sensors is decomposed in two parts:

- usual on board measurements: motor angle θ_m , torque sensor signal τ_{TS} , motor current I_m (EPS system sensor) and steering wheel angle θ_c , yaw rate $\dot{\psi}$, lateral acceleration a_y (vehicle system sensor)

- additional measurements required for validation: driver torque τ_d and rack force F_r (specific sensors are implemented on the test car)

An overview from driver's seat is shown in Fig III.14, besides some of the above elements could be distinguished (dynamometer steering wheel and C-EPS).

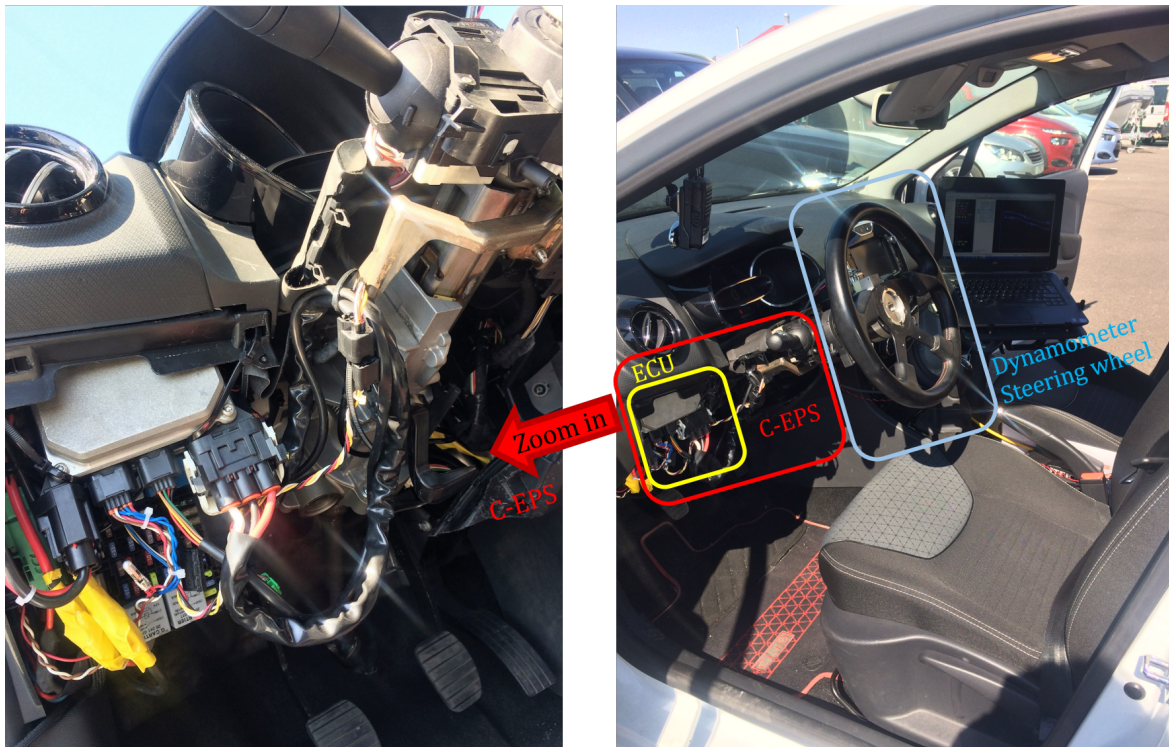


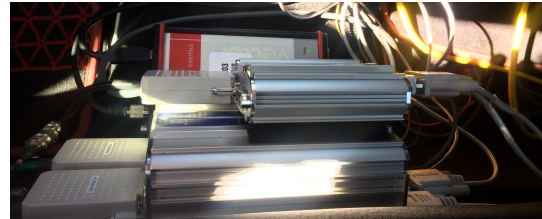
Figure III.14 – C-EPS on Clio X98

III.5.2 Electronic Part (real time)

Regarding implementation, a dSPACE rapid prototyping system have been used to develop and test observers and control strategies on the vehicle environment (further details are given in Appendix A). Indeed, models designed using Matlab/Simulink are implemented on the MicroAutoBox II DS1401/1511/1512 hardware. Moreover, the MicroAutoBox II combines high memory capacity and computing power, which means little implementation constraints unlike common embedded software. A laptop, connected to the MicroAutoBox via ethernet, allows on one hand to change and download different algorithms, and on the other hand to modify parameters of the applied strategy in real time. Concerning interfaces, three CAN bus are assigned: CAN Vehicle (lateral acceleration, yaw rate, vehicle speed), CAN ECU (motor angle, motor current, torque sensor signal) on which MicroAutoBox send EPS control signal and CAN SW (steering wheel angle) which needs a signal conditioner. Hardware devices installed on the vehicle are shown in Fig III.15.



(a) dSpace MicroAutobox



(b) CAN Interface

Figure III.15 – Clio X98 on board electronic

According to sensorless specification, I/O configuration is as follows: received data frames contain steering wheel angle, motor angle and vehicle speed, whereas sent data frame contains target motor torque, as illustrated in Fig III.16.

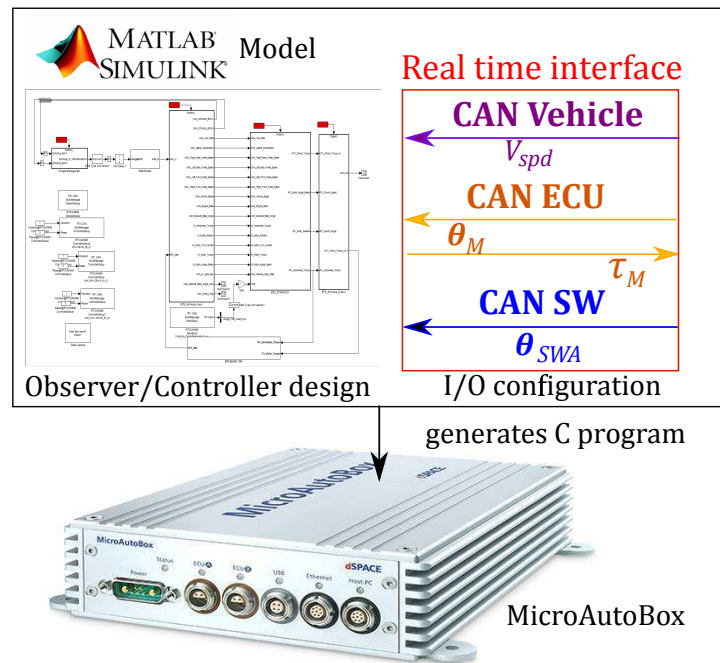


Figure III.16 – Algorithm configuration in MicroAutoBox

III.6 Model validation from experiments

A vehicle test engineer has performed evaluation of the development vehicle on a test track, shown in Fig III.17. A typical steering manoeuvre test could be mentioned, where the first two tests are carried out to evaluate vehicle handling whereas the last ones are intended for (vehicle and EPS) model validation.

- Test 1: sinus manoeuvre, the driver provides various steering wheel angle amplitudes in low frequency. A special case, where the driver travels the full rack stroke (up to maximal steering angle) is referred to lock-to-lock manoeuvre.
- Test 2: lemniscate shape pattern, the driver follows the drawing on the ground at a constant vehicle speed (also interpreted as a calibrated sinus according to steering wheel angle).
- Test 3: snail test, the driver turns the steering wheel (increases steering wheel angle) at a constant steering wheel speed until loss of grip.
- Test 4: swept sine, the driver does not hold the steering wheel, the input signal is the motor torque (control signal) configured as a sinus of constant amplitude with a varying frequency from 0.1 Hz to 60 Hz.



Figure III.17 – JTEKT track

In what follows, simulation results using input real data are presented. Regarding the P-EPS model, it was validated upon experimental data (obtained from a Peugeot 207) on a relevant frequency domain. Concerning the rack force (parking and transition), several tests have been realised on a development vehicle Clio IV, where the steering wheel angle and vehicle

speed are measured and used as model input, see Fig. III.18. Then, the measured rack force and corresponding model output are compared for validation purpose.

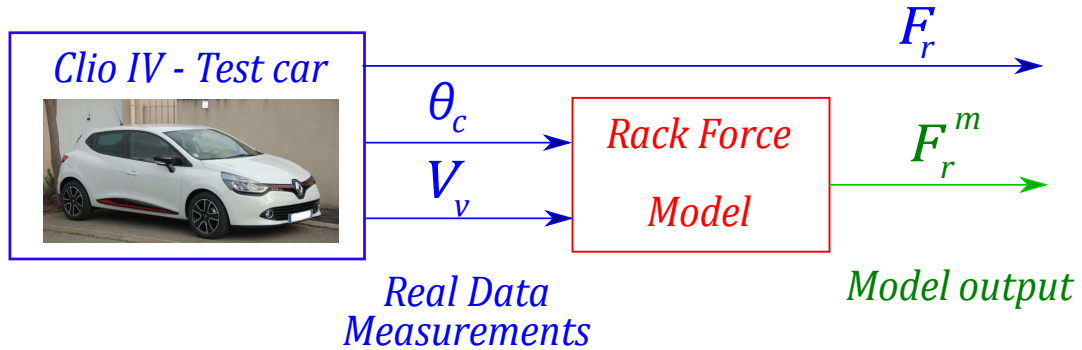


Figure III.18 – Rack force model validation from experiments

In the same way, the vehicle model including Pacejka tire model is validated subject to data obtained on the test car Clio IV in rolling condition.

III.6.1 Simulation of EPS Model - P-EPS

Test 4 has been realised on a development vehicle equipped with a P-EPS system to validate the proposed P-EPS model. On the figures below, the frequency response obtained using P-EPS model and from real data are presented: Fig. III.19 shows the frequency response from motor angle to motor torque while Fig. III.20 shows from steering wheel angle to motor torque. According to a comparison of the two plots on both figures, a good match between the model and the real system is observed up to 20 Hz. Indeed, the resonance frequencies are well captured by the model.

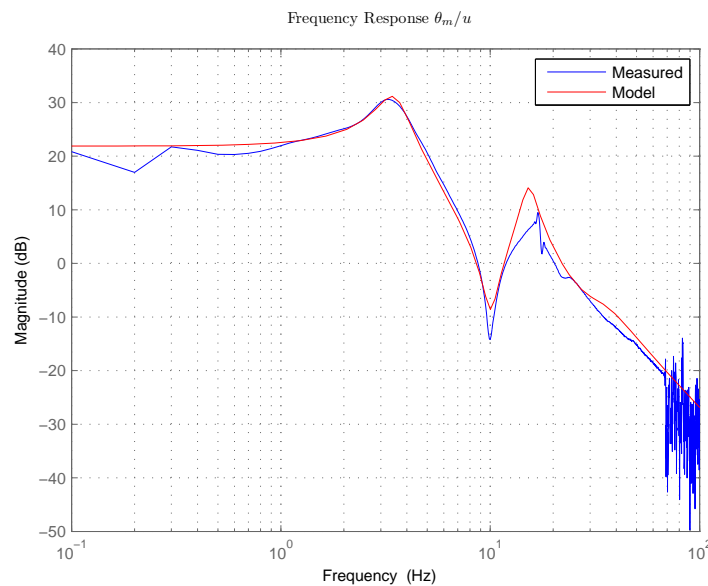


Figure III.19 – Frequency domain model validation $\frac{\theta_m}{u}$

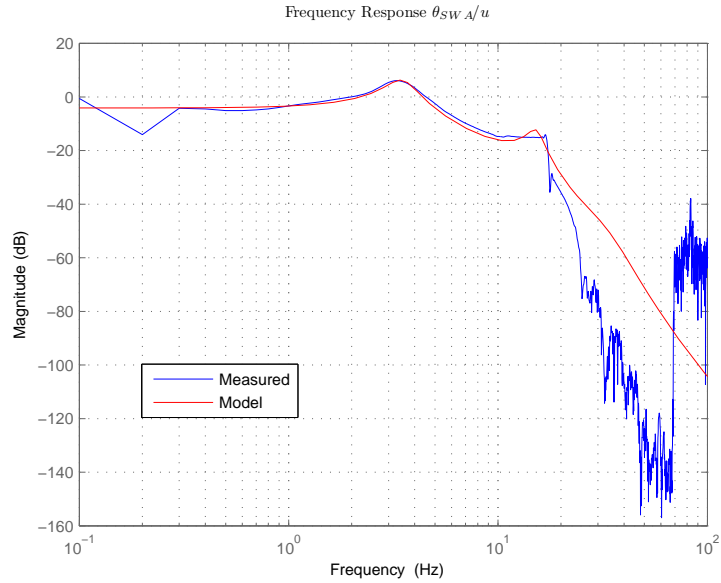


Figure III.20 – Frequency domain model validation $\frac{\theta_{SWA}}{u}$

III.6.2 Simulation of Rack Force Model - Parking

Test 1 (lock to lock) has been realised on a test car Clio IV in static condition (0 kph) to validate the rack force model at parking. Therefore, the figures below present the measured and the modelled rack force. In Fig. III.21, the steering wheel angle function of rack force is shown. The proposed parking model based on LuGre model fits well the real behaviour of the rack force, especially the shape of the hysteresis.

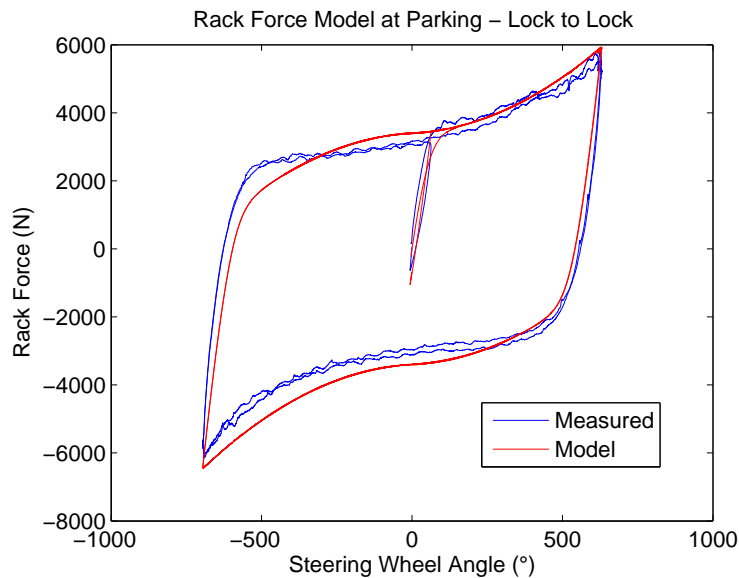


Figure III.21 – Rack Force Model at Parking

In Fig. III.22, the steering wheel angle function of driver torque is presented. It could be

noticed that the amount of driver torque in parking is very high as it reaches almost 20 Nm at the average steering wheel angle.

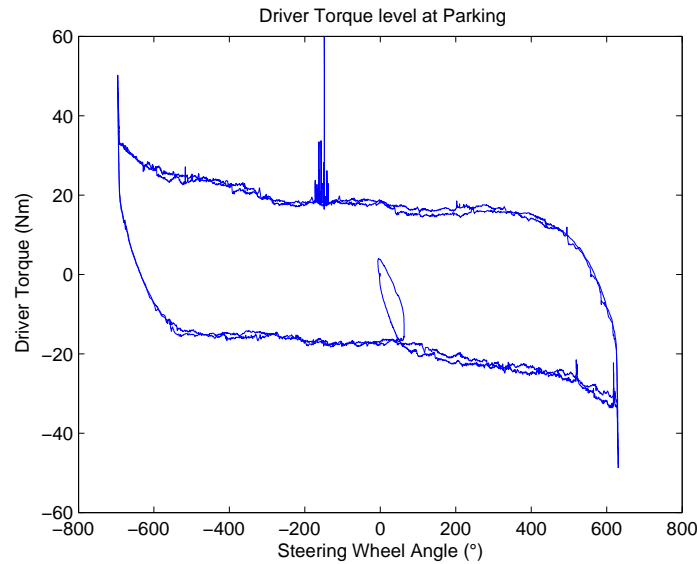


Figure III.22 – Driver Torque VS Steering Wheel Angle at Parking

III.6.3 Simulation of Rack Force Model - Transition Parking to Low Speed

Test 1 (lock to lock case) has been realised on a test car Clio IV such that measurement to validate the parking low speed transition rack force model is obtained. The results are presented for a transition from 0 kph to 3 kph and from 0 kph to 7 kph.

III.6.3.1 From Parking to 3 kph

In Fig. III.23, the steering wheel angle function of rack force is shown. The plot presents the evolution of rack force during a transition between parking and low speed (3 kph) under the conditions described in Fig. III.24. Indeed, three curves show the evolution of three variables function of time: the rack force (top), the vehicle speed (middle), the steering wheel angle (bottom). The transition occurs around 35s to 60s (between the red lines), as the steering wheel angle is kept at the same position while the vehicle speed increases until it reaches 3 kph. As it could be noticed, the rack force drops very quickly from parking to low speed, the maximum value varies from almost 6 kN to less than 2 kN (comparison made between the both end side of the red lines). Therefore, a transition model is necessary to correctly model this phenomenon and change in the hysteresis shape. A comparison of the transition rack force model with real data shows that this behaviour is well captured.

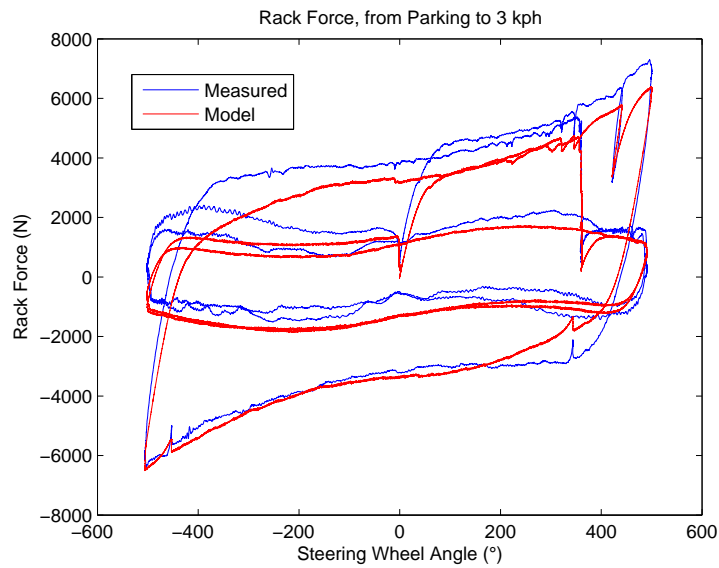


Figure III.23 – Rack Force Model from Parking to 3 kph

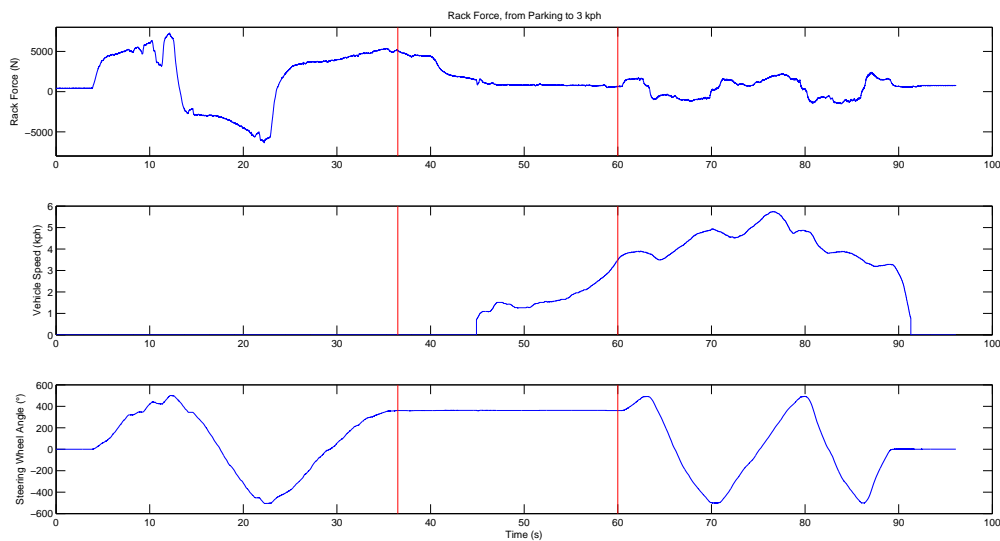


Figure III.24 – Transition Conditions from Parking to 3 kph

Remark III.5

Vehicle speed is detected only after a certain threshold (around 1 kph) and not as soon as the vehicle begins to move. Thus, the rack force begins to decrease while keeping a same steering wheel angle even though the vehicle speed is measured at 0 kph, see Fig. III.24.

III.6.3.2 From Parking to 7kph

In Fig. III.25, the steering wheel angle function of rack force is shown. The plot presents the evolution of rack force during a transition between parking and low speed (7 kph) under the

conditions described in Fig. III.26 (where the evolution of the rack force (top), the vehicle speed (middle), the steering wheel angle (bottom) function of time is shown). A similar behaviour than previously is observed during transition from parking to low speed (occurs around 30s), nevertheless the hysteresis shape between 3 kph and 7 kph is slightly different. Then, the proposed transition model adapts to this change which is confirmed by a comparison with real data as shown in Fig. III.25.

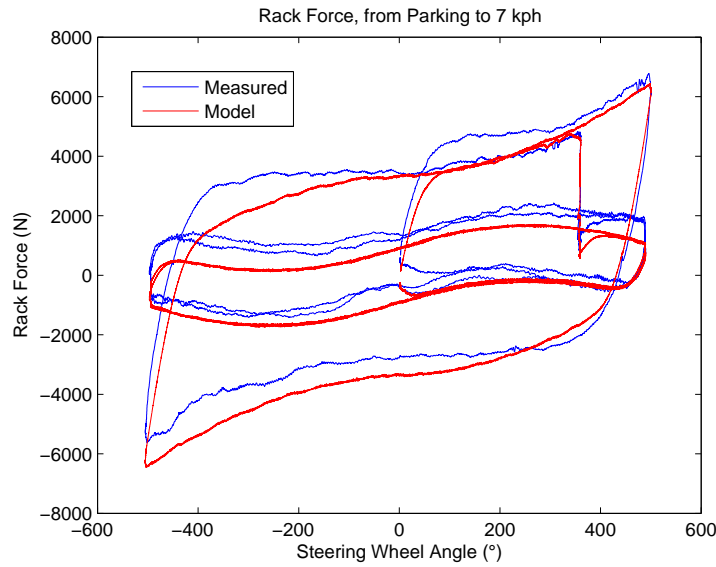


Figure III.25 – Rack Force Model from Parking to 7kph

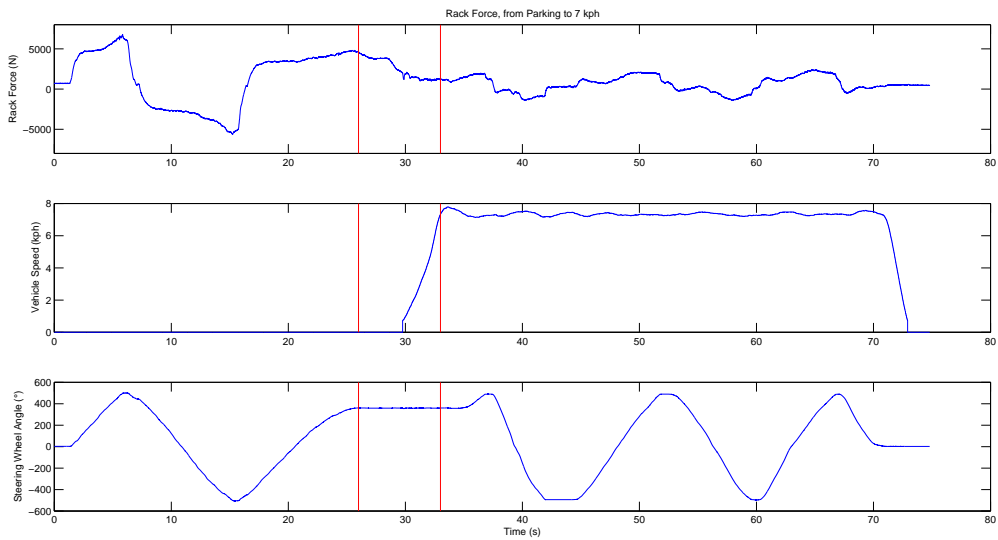


Figure III.26 – Transition Conditions from Parking to 7kph

III.6.4 Simulation of Rack Force Model - Rolling

Test 1 has been realised on a test car Clio IV at nominal speed to validate the rack force model in rolling. The results are presented according to two vehicle speed 15 kph and 30 kph, and figures display the measured and the modelled rack force.

In Fig. III.27 and III.28, the rack force is evolving depending on time. The proposed empirical Pacejka model fits well the real behaviour of the rack force at different vehicle speed. As it could be seen, the model outputs a sinusoidal rack force at same frequency and almost same amplitude as the measurements.

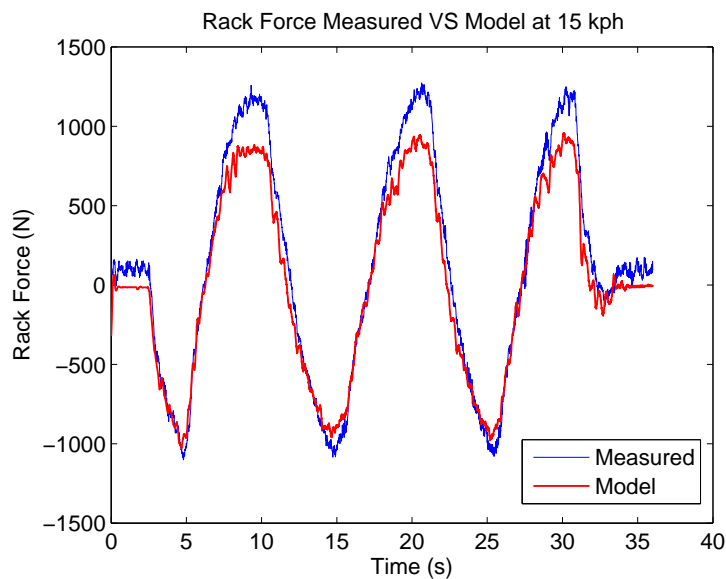


Figure III.27 – Rack Force Tire Model Pacejka at 15 kph - Sinus manoeuvre

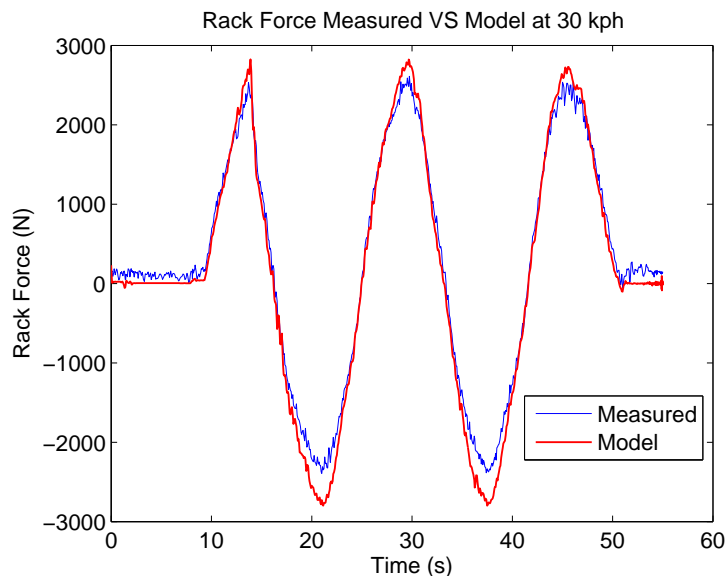


Figure III.28 – Rack Force Tire Model Pacejka at 30 kph - Sinus manoeuvre

III.6.5 Simulation of Vehicle Model

Test 3 has been realised on a test car Clio IV in nominal speed to validate the whole vehicle model (where the whole structure is recalled in Fig. III.29) including the Pacejka tire model. The results are presented considering two test cases for the vehicle speed 30 kph and 50 kph. The figures below display the measured and the modelled lateral acceleration and yaw rate (resp. rack force) regarding vehicle model (resp. Pacejka model).

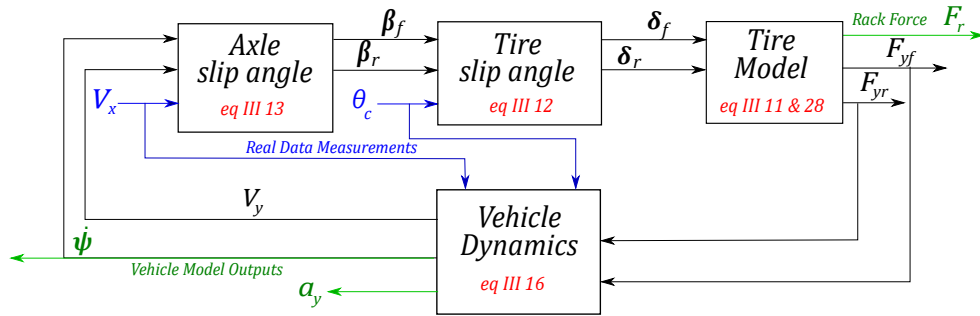


Figure III.29 – Vehicle Model Structure

III.6.5.1 Snail Test at 30 kph

Fig. III.30 shows the time evolution of the rack force, while Fig. III.31 illustrates the time evolution of the lateral acceleration (above) and the yaw rate (below). Regarding tests conditions, all the signals values are increasing until loss of grip, then the driver turns back the wheel and previous values are decreasing. A smooth transition from steer out to steer back is realised at 30 kph. Moreover, model outputs fit properly the real data. Indeed, the model is well defined to capture the real vehicle dynamical behaviour.

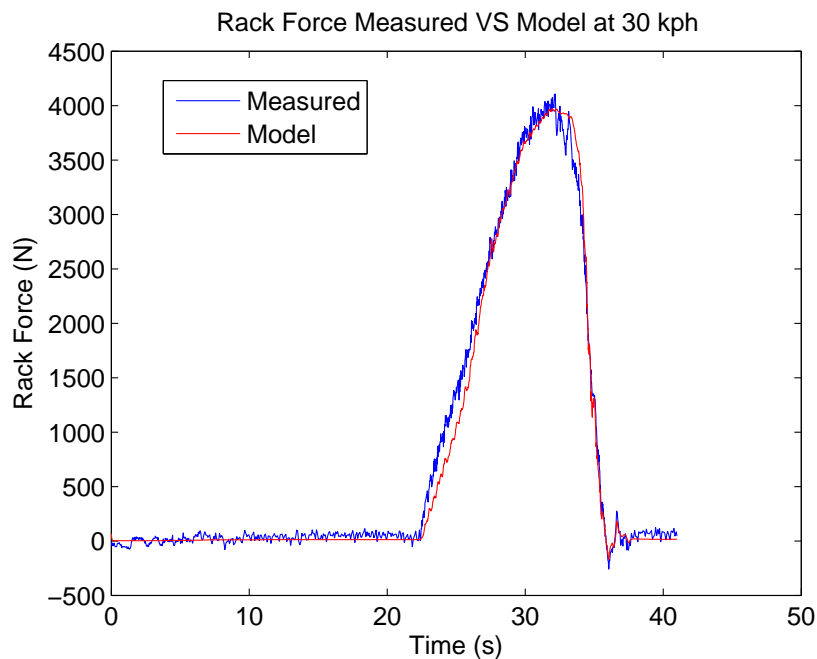


Figure III.30 – Rack Force Model at 30 kph - Snail test

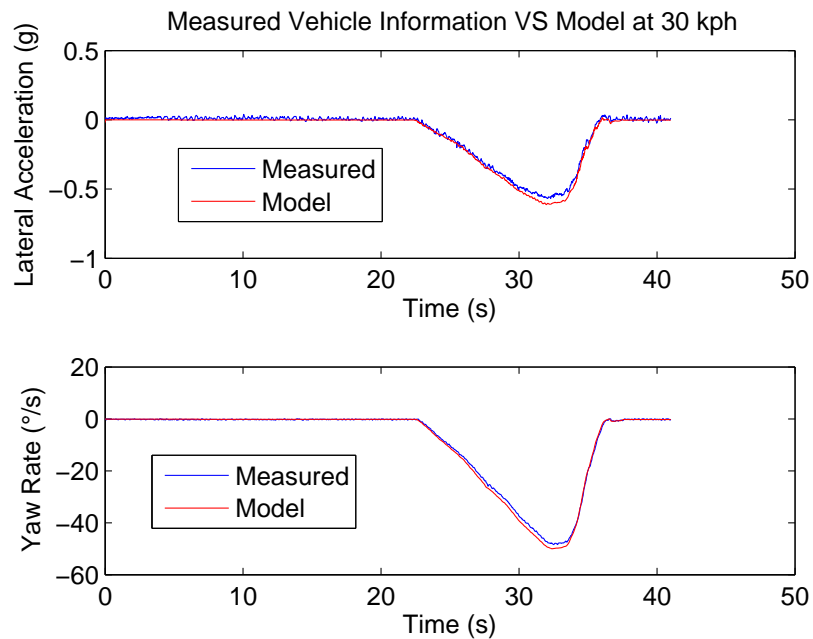


Figure III.31 – Lateral Acceleration and Yaw rate at 30 kph - Snail test

III.6.5.2 Snail Test at 50 kph

Fig. III.32 shows the time evolution of the rack force, while Fig. III.33 illustrates the time evolution of the lateral acceleration (above) and the yaw rate (below). All the signals are varying similarly to the previous condition. Nevertheless, the transition from steer out to steer back corresponds to an abrupt slope regarding vehicle parameters. However, the model fits properly the real data as shown in Fig. III.33. Regarding rack force Fig. III.32, the proposed model presents a non-linearity (due to loss of grip) as well as the real system.

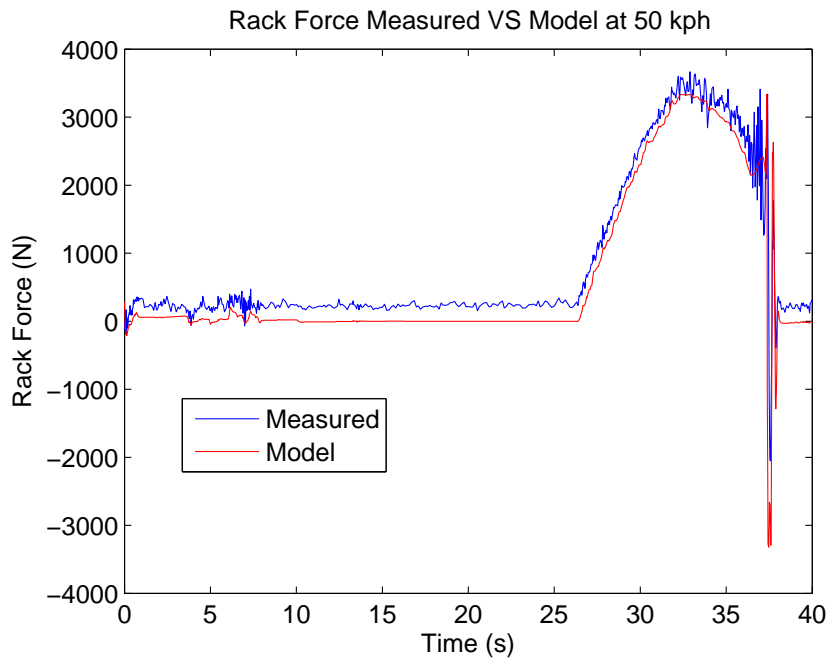


Figure III.32 – Rack Force Model at 50 kph - Snail test

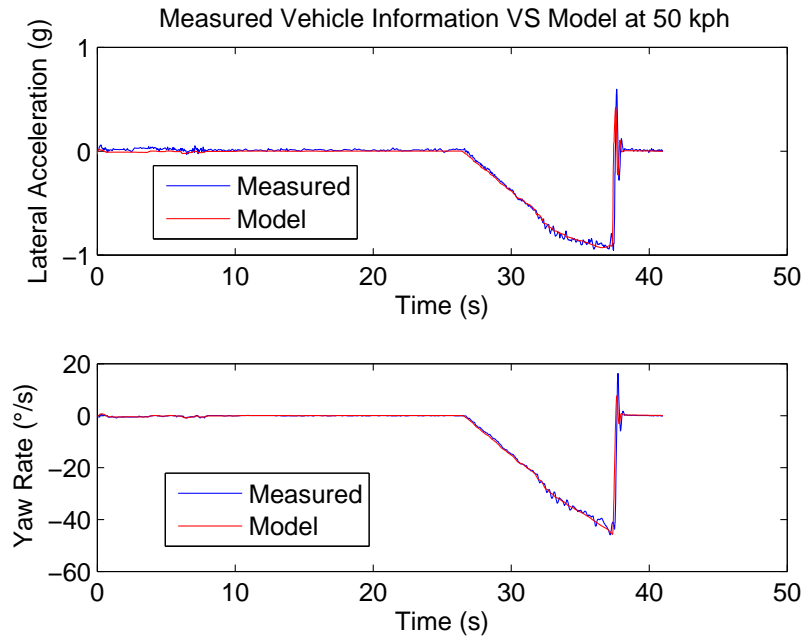


Figure III.33 – Lateral Acceleration and Yaw rate at 50 kph - Snail test

Considering those above comparisons, it is worth noting that the models validation from the experiments yield good results which will be used in the following chapter.

III.7 Conclusion

In this chapter, EPS models have been defined, that will be used in the following chapter. Then, a vehicle model (bicycle model) and rack force model have been introduced to represent a complete simulation environment. Indeed, EPS systems equip the vehicles, and the rack force according to driving conditions (parking, low speed or nominal speed) varies significantly, as it has been illustrated by the measurements on the test car. Moreover, model outputs and experimental data have been compared to assess the model accuracy. Finally, the experimental configuration on board (the mechanical and the electronic parts in the vehicle) has been described, since it is the test support for some strategies developed next. Then, chapter IV is about the design of driver torque estimation according to H_∞/H_2 proportional integral observer and H_∞ filter.

Remark III.6

Besides in perspective, more evolved but increased order EPS model could be developed through replacing the constant tire stiffness model, for instance by introducing a vehicle speed dependency (LPV, switched model) or by incorporating the vehicle dynamic, the structure shown in Fig. III.29.

Driver Torque Estimation

Contents

| | |
|--|-----------|
| IV.1 Introduction | 53 |
| IV.2 State of the art | 54 |
| IV.2.1 Driver torque estimation with torque sensor signal | 54 |
| IV.2.2 Driver torque estimation without torque sensor signal | 55 |
| IV.3 Some theoretical background | 57 |
| IV.3.1 Signal Norms | 57 |
| IV.3.2 System Norms | 58 |
| IV.4 Proportional Integral Observer | 59 |
| IV.4.1 PIO definition | 59 |
| IV.4.2 Problem formulation | 60 |
| IV.4.3 Performance objectives | 63 |
| IV.4.4 Design Analysis | 67 |
| IV.5 \mathcal{H}_∞ filtering approach | 69 |
| IV.5.1 H_∞ filter definition | 70 |
| IV.5.2 Problem formulation | 71 |
| IV.5.3 Design analysis | 75 |
| IV.6 Simulation Results | 76 |
| IV.6.1 Simulation using a linear P-EPS Model | 77 |
| IV.6.2 Simulation using real data input | 81 |
| IV.7 Experimental Results | 85 |
| IV.7.1 Vehicle test at 15 kph | 85 |
| IV.7.2 Vehicle test at 30 kph | 87 |
| IV.8 Conclusion | 89 |

IV.1 Introduction

In view of previous chapters and regarding current EPS control strategy, the torque sensor signal is essential in providing good steering performance and ensuring safety driving. Nevertheless, a torque sensor failure involves most of the time a SLOA which can be a safety relevant issue. Such a hazardous event is more and more handled by the vehicle manufacturers to be covered. Therefore, a back-up control is required to provide some assistance level to the

driver in order for the vehicle to stop in a safe manner, *i.e.*, whether get back home or garage. However the performance regarding steering feel is likely to be degraded, indeed the back-up mode aims at providing some assistance torque to facilitate the driving compared to a manual effort by the driver with no assistance at all. Then in this chapter, a torque sensor estimation is developed such that an on observer based back-up control enables to cover SLOA. Therefore, an assistance torque is ensured to be supplied, as the boost curve will depend on driving torque estimation and on vehicle speed during the back-up rolling conditions.

At first, a state of the art on the driver torque estimation in EPS system is carried out which is divided in two parts. Indeed, some studies are using the torque sensor signal (measurement of the torsion bar torque) and some are not. According to the thesis context, the latter framework is considered where the driver torque estimation is based on the steering wheel angle and the motor angle measurements. Before introducing methods to design the driver torque estimation, some norms definitions are recalled. Then, two approaches are presented: a proportional integral observer and a H_∞ filtering. Finally, some simulation and experimental results are presented to evaluate the obtained performance.

Some of the results given in this chapter have been presented in the following papers:

- C2** Kazusa Yamamoto, Damien Koenig, Olivier Sename, Pascal Moulaire. *H_∞ Filtering Design for Driver Torque Estimation in Electric Power Steering System*, in proceedings 13th International Symposium on Advanced Vehicle Control (AVEC), Sept 2016, Munich, Germany.
- C3** Kazusa Yamamoto, Damien Koenig, Olivier Sename, Pascal Moulaire. *Driver Torque Estimation in Electric Power Steering System using an H_∞/H_2 Proportional Integral Observer*, in proceedings 54th IEEE Annual Conference on Decision and Control (CDC), Dec 2015, Osaka, Japan.

IV.2 State of the art

In serial cars, the driver torque is actually not directly measured (such sensors are expensive and there are issues regarding their integration), instead a torque sensor signal is used which gives a representation of the steering torque involved in turning the wheels. As introduced in II.3.1, the torque sensor is implemented at torsion bar level. Therefore, torque sensor signal corresponds to torsion bar torque and is not a direct measurement of the applied driver torque. Several studies have already been carried out on driver torque estimation in EPS systems, where two different types of estimation methods emerge. These two approaches are presented as follows: those using torque sensor signal and those without. As seen below, the latter uses other vehicle and/or EPS available signals.

IV.2.1 Driver torque estimation with torque sensor signal

Regarding EPS model representation (state-space or transfer function) under the condition that torque sensor signal is measured, several driver torque estimation methods (extended state-space observer or based on EPS plant model) are presented in the following literature.

Considering steering wheel dynamic only, a single inertia model comprising steering wheel connected to torsion bar is introduced where the state vector is composed of the steering wheel angle and speed. In [Moreillon 2016] based on this simplified model, an extended state-space observer is designed by pole placement to estimate the driver torque and uses the torque sensor signal and the assist motor angle obtained from EPS available sensors.

A similar C-EPS model, as introduced in III.2.2 (IV.4.2), is composed of three states which are the difference between the angular positions of the steering wheel and pinion shaft, the steering wheel and the pinion shaft speed. Such a state simplification is feasible since torsion bar torque is assumed to be measured. Then, some works based on this representation have developed either linear or non-linear observer to estimate the driver torque, considering the torque sensor signal and the steering column speed as available measurements. In [Illán 2011], an extended state observer computing the driver and load torque is designed by pole placement, whereas in [Reichhartinger 2016] a sliding mode observer has been designed to estimate the driver torque.

Otherwise in [Yu 2017], an estimated driver torque taking as inputs the torque sensor signal and the following motor signals: current, angular position and velocity (where those input signals are scaled in the hand-wheel coordinate). This estimator has been proposed and could be adapted to any EPS mass model representation.

Besides, a driver torque estimation has been developed based on the plant model, in [Chabaan 2001a]. Therefore, a six order EPS model (including assist motor, steering column and rack dynamic) has been considered. The driver torque τ_d is expressed using the torque sensor signal τ_{ts} and the assist motor input current τ_m (control signal) using some relationships deduced from the EPS model, *i.e.*, $\tau_{ts} = G(s)\tau_d + H(s)\tau_m$. Then, both signals are required as measurements. However, the exact estimator expression which uses $G^{-1}(s)$ is not proper and unstable. In order to get a stable transfer function, some approximations have been made in a specified frequency range where the driver torque should be accurately computed *i.e.* $\hat{\tau}_d = \tilde{G}(s)(\tau_{ts} - H(s)\tau_m)$. The same driver torque estimator technique has been used in [Chitu 2013] but developed in discrete time.

IV.2.2 Driver torque estimation without torque sensor signal

Regarding system representation (either EPS model or vehicle model), several driver torque estimation methods (linear or non-linear) and to some extent, torsion torque estimation are proposed subject to different measurement signals from the system.

A relation between the torques acting on the motor shaft $\tau_{ts} = n\tau_{dm} - \tau_{road} - \tau_{rp}$ of an EPS system is considered involving disturbance torque on the motor shaft τ_{dm} with the gear ratio n , torsion bar torque τ_{ts} , road reaction torque τ_{road} , rack and pinion reaction torque τ_{rp} (similar to the sum of efforts applied on pinion shaft in III.2.1 eq.(III.4)). Some authors are interested in estimating the torsion torque $\hat{\tau}_{ts}$ applied to the motor shaft to cover torque sensor failure, *i.e.* the estimated signal is used for fault detection and fault tolerant control. In [Lawson 2008] and [Cholakal 2009a], the estimated torsion torque is computed based on motor load torque and road reaction torque estimations. A same road torque estimation $\hat{\tau}_{road}$ is proposed, based on vehicle dynamic (bicycle model) and linear tire model (similar expression than F_{yf} in III.3 eq.(III.15)) where inertial navigation system provides the necessary measurements (yaw rate,

vehicle velocities). Considering disturbance torque on the motor shaft $\hat{\tau}_{dm}$ a second order motor model is introduced where motor current is measured. In [Lawson 2008] a Luenberger observer is designed through pole placement, while in [Cholakal 2009a] a Kalman filter (the model is subject to unmodeled disturbances) and H_∞ filter (a disturbance vector is considered) are designed. Furthermore, in [Cholakal 2009b] an H_∞ Gaussian filter is synthesized based on a motor model affected by disturbance and white noise. Consequently, this approach requires some accurate sensors especially to estimate the road reaction torque, and also involved to design an observer to evaluate the disturbance torque on the motor shaft.

A similar C-EPS model, as introduced in III.2.2 (IV.4.2), including an electric dynamic of the motor is considered where [Marouf 2010] proposed a Sliding Mode Observer (SMO) to estimate both the driver torque and the road reaction force in an EPS system. However, regarding EPS simplified model and available measurements, the state-space representation of the system does not satisfy the observer matching condition. Therefore, additional inputs required to design the SMO are generated using High Order Sliding Mode Differentiator (HOSMD). In [Marouf 2012a, Marouf 2010], the SMO uses as inputs the steering wheel angle and the motor angle (absolute angular position of the motor) with additional outputs generated by HOSMD (at least both signals velocity). Furthermore, in [Marouf 2012b, Marouf 2013] a resolverless (as motor angle is not measured) SMO is proposed based on the measurements of motor currents and steering wheel angle where additional outputs are generated by HOSMDs (firstly motor angle and velocity, secondly steering wheel velocity). However, a PMSM dynamic model is included in EPS mechanical model increasing complexity and synthesis of the SMO.

A simplified six order DP-EPS mechanical model with an unknown input observer has been designed in [Mahmoud 2012] to estimate the EPS system states and driver torque, where the considered measurements are the steering wheel angle and assist torque. The observer gain is computed to minimise the error between the driver torque (unknown input) and its estimate. Also a six order P-EPS model is introduced in [Chabaan 2009] where the estimation principle is the one described in the previous section $\hat{\tau}_d = \tilde{G}(s)(\tau_{ts} - H(s)\tau_m)$ [Chabaan 2001a], nevertheless showing an improvement. Indeed, an additional estimator based on plant model has been introduced to get the torque sensor value $\tau_{ts} = G_1\theta_c + H_1\tau_m$ where G_1^{-1} is also approximated to obtain a stable and proper transfer function. This means that measured signals are the steering wheel angle and assist torque.

Besides, a driver torque estimation has been developed based on vehicle model. Then, some works based on this representation have synthesized either linear or non-linear observer to estimate the driver torque, considering the yaw rate, the steering wheel angle and speed as available measurements. In [Soualmi 2014], an unknown input proportional multi-integral Takagi-Sugeno observer is designed to estimate the states of the vehicle lateral motion and also the driver's torque. A similar development has been realised in [Sentouh 2011] through an unknown input proportional integral observer. Nevertheless, the aim of the above studies is focused on lateral control of vehicle which explains their choice to work with a vehicle model rather than an EPS model.

According to all these previous studies, one may say that driver torque estimation is still an open issue. The challenge here is to avoid the use of a torque sensor signal to estimate the driver

torque, while using vehicle and EPS system available measurements, i.e considering steering wheel angle and motor angle, as position sensors are affordable and widely implemented on vehicles.

The main objective is then to estimate the unmeasured driver torque input d , considering the unknown input w as a disturbance. This is taken into account on EPS representation in (IV.4.2) or (III.5). Such a problem is similar to the unknown input observer or sliding mode observer design as described in [Hui 2005]. However, according to EPS model and available measurements, the matching condition is not satisfied. Hence, additional outputs are required to overcome this issue which results into increased complexity in the synthesis design. Nevertheless, the estimation algorithm should be easily implementable under some software/hardware constraints, e.g ECU storage space. Then, the design of linear observer is preferred to the non-linear one. Moreover, a simple EPS mechanical model is expected to be kept which means not to increase the system states by including electric motor dynamics or vehicle model.

Therefore, two methodologies to estimate the driver torque while attenuating external disturbance are presented in the following section. A H_∞/H_2 Proportional Integral Observer (PIO) is proposed to minimize the effect of road disturbances (resp. sensor noise) according to \mathcal{H}_∞ -norm (resp. \mathcal{H}_2 -norm) while providing a fast convergence of the estimation through pole placement. Then, a \mathcal{H}_∞ filtering approach is suggested to estimate the driver torque under road disturbance attenuation and measurements noise. Contrary to PIO which requires the driver torque to be slowly time varying, this second design only requires to specify the frequency range of interest on which the driver torque is to be estimated. Before getting in the design synthesis, some definitions on norms are recalled in the following section.

IV.3 Some theoretical background

Some few reminders about signal and system norms are introduced in this section. The following definitions and criteria are used in the following chapters for the synthesis of the proposed estimation strategies.

The following state space representation is considered for given matrices $A \in \mathbb{R}^{n \times n}$, $B \in \mathbb{R}^{n \times n_w}$, $C \in \mathbb{R}^{n_z \times n}$ and $D \in \mathbb{R}^{n_z \times n_w}$:

$$\begin{cases} \dot{x}(t) &= Ax(t) + Bw(t) \\ z(t) &= Cx(t) + Dw(t) \end{cases} \quad (\text{IV.1})$$

where $x(t) \in \mathbb{R}^n$ is the state, $w(t) \in \mathbb{R}^{n_w}$ is the input and $z(t) \in \mathbb{R}^{n_z}$ is the output. The reader interested by more details may have a look at [Scherer 2000, Doyle 1992].

IV.3.1 Signal Norms

Definition IV.1 (2-norm)

The 2-norm, is given by:

$$\|x(t)\|_2 = \sqrt{\int_0^\infty x^*(t)x(t)dt} \quad (\text{IV.2})$$

The square of 2-norm is interpreted as the total energy expended, for a signal $x(t)$ of finite energy during a time $t \geq 0$.

Definition IV.2 (∞ -norm)

The ∞ -norm is given by:

$$\|x(t)\|_{\infty} = \sup_t |x(t)| \quad (\text{IV.3})$$

$$\|X\|_{\infty} = \sup_{\omega} \|X(j\omega)\| = \sup_{\text{Re}(s) \geq 0} \|X(s)\| \quad (\text{IV.4})$$

IV.3.2 System Norms

Definition IV.3 (\mathcal{H}_{∞} -norm)

The \mathcal{H}_{∞} -norm of a proper LTI system defined as on (IV.1) from input $w(t)$ to output $z(t)$ is the induced energy-to-energy gain defined as:

$$\begin{aligned} \|G(j\omega)\|_{\infty} &= \sup_{\omega \in \mathbb{R}} \bar{\sigma}(G(j\omega)) \\ &= \sup_{w(t) \in \mathcal{L}2} \frac{\|z\|_2}{\|w\|_2} \end{aligned} \quad (\text{IV.5})$$

Remark IV.1

As explained in [Sename 2016], \mathcal{H}_{∞} represents the maximal gain of the frequency response of the system. As it measures the maximum amplification that the system can deliver on the whole frequency set, it is even called the worst case attenuation level. For SISO (resp. MIMO) systems, it represents the maximal peak value on the Bode magnitude (resp. singular value). \mathcal{H}_{∞} -norm is only defined by numerical solutions, i.e, LMI resolution.

Definition IV.4 (\mathcal{H}_2 -norm)

The \mathcal{H}_2 -norm of a proper LTI system defined as in (IV.1) from input $w(t)$ to output $z(t)$ is the energy of the impulse response $g(t)$ defined as:

$$\begin{aligned} \|G(j\omega)\|_2 &= \sqrt{\int_{-\infty}^{\infty} g^*(t)g(t)dt} \\ &= \sqrt{\frac{1}{2\pi} \int_{-\infty}^{\infty} \text{Tr}[G^*(j\omega)G(j\omega)]d\omega} \\ &= \sup_{w(s) \in \mathcal{H}2} \frac{\|z(s)\|_{\infty}}{\|w(s)\|_2} \end{aligned} \quad (\text{IV.6})$$

It is finite if and only if $G(s)$ is strictly proper (in (IV.1), $D = 0$).

Remark IV.2

As explained in [Sename 2016], the \mathcal{H}_2 -norm loosely represents the area located below the Bode diagram for SISO systems, whereas it is the impulse-to-energy gain of $z(t)$ in response to a white noise input $w(t)$ for MIMO systems. \mathcal{H}_2 -norm can either be obtained analytically (controllability and observability Grammians) or numerically (LMIs resolution).

Therefore, some objective formulation could be given following:

- \mathcal{H}_∞ performance aims at minimizing the maximum magnitude, bounding the output energy while ensuring robustness to model uncertainty. Hence, \mathcal{H}_∞ is a disturbance attenuation, formulated in the worst-case performance analysis.
- \mathcal{H}_2 performance is rather considered to minimize the average magnitude of the error system, and is suited to manage stochastic aspects, *e.g.*, measurement noise.
- $\mathcal{H}_\infty/\mathcal{H}_2$ problem formulation has been introduced to deal with different objectives regarding the external signal characteristics, such as noises and disturbances.

IV.4 Proportional Integral Observer

IV.4.1 PIO definition

PIO is a generalization of Luenberger observer where an additional term is introduced to the initial observer equation chosen to be proportional to the integral of the estimation error. PIO has been introduced in [Wojciechowski 1978] for SISO linear system, then [Kaczorek 1979] and [Shafai 1985] extends it to MIMO linear systems improving the estimation robustness towards variations in system parameters and disturbance. Besides, PIO design has been developed on descriptor systems in [Koenig 2002] or applied on switched system in [Nouailletas 2008]. Therefore, a PIO is effective in estimating plant perturbations, faults and input disturbances that can be modelled by an additional term. Indeed, PIO could be designed also for fault detection and estimation as carried out in [Farhat 2015] or for state and disturbance vector estimation as done in [Sentouh 2011]. Furthermore, an adaptive PIO structure has been proposed in [Shafai 2002] to estimate system states, parameters and disturbances, a modified advanced PIO has been developed in [Bakhshande 2015] to improve estimation performance and robustness. Hence, several PIO design methods for different types of systems subject to different purposes have been studied.

Let considered the following state-space model for given matrices $A \in \mathbb{R}^{n \times n}$, $B \in \mathbb{R}^{n \times n_u}$, $E \in \mathbb{R}^{n \times n_d}$ and $C \in \mathbb{R}^{n_y \times n}$:

$$\begin{cases} \dot{x} &= Ax + Bu + Ed \\ y &= Cx \end{cases} \quad (\text{IV.7})$$

where $x \in \mathbb{R}^n$ is the state, $d \in \mathbb{R}^{n_d}$ is the disturbance, $u \in \mathbb{R}^{n_u}$ is the control signal and $y \in \mathbb{R}^{n_y}$ is the measurements.

Let considered the following state (proportional) observer to estimate the state variables x using the control input u and the measured output y :

$$\dot{\hat{x}} = A\hat{x} + Bu + L(y - C\hat{x}) \quad (\text{IV.8})$$

where $\hat{x} \in \mathbb{R}^n$ is the estimated state variables.

Then the estimation error $e = x - \hat{x}$ dynamic is then obtained as follows:

$$\dot{e} = (A - LC)e + Ed \quad (\text{IV.9})$$

Hence, in the case there is no disturbance, *i.e.* $d = 0$, the observer estimates accurately the state, subject that $(A - LC)$ is a Hurwitz matrix. However, in the case there is a constant

disturbance i.e $d \neq 0$, a constant steady-state error between the estimated and actual state appears.

A Proportional Integral Observer (PIO) allows to remove this estimation error as proposed below:

$$\begin{cases} \dot{\hat{x}} &= A\hat{x} + Bu + L_p(y - C\hat{x}) + E\hat{d} \\ \dot{\hat{d}} &= L_i(y - C\hat{x}) \end{cases} \quad (\text{IV.10})$$

where $\hat{d} \in \mathbb{R}^{n_d}$ is the estimated disturbance, $L_p \in \mathbb{R}^{n_x \times n_y}$ and $L_i \in \mathbb{R}^{n_d \times n_y}$ are the PIO gain. This is presented below in the context of EPS systems.

IV.4.2 Problem formulation

Now, in order to develop a PIO on the EPS system, the assumption that the driver torque is slowly time-varying (i.e $\tau_d \simeq 0$) is required, and is now considered as an additional variable of the state-space EPS model. Let us recall the state-space representation of EPS model introduced in the previous chapter, either a P-EPS system III.2.1 (III.5) or C-EPS system III.2.2 . Then, (IV.11) holds for both case:

$$\begin{cases} \dot{x} &= Ax + Bu + Ed + Ww \\ y &= Cx + Nn \end{cases} \quad (\text{IV.11})$$

where $x \in \mathbb{R}^{n_x}$ is the EPS system states, $d \in \mathbb{R}$ is the driver torque (unmeasured input to be estimated), $w \in \mathbb{R}$ is the road disturbance (unknown input), $u \in \mathbb{R}$ is the control input, $y \in \mathbb{R}^2$ is the measurements (steering wheel angle and motor angle), $n \in \mathbb{R}^2$ is the measurement noise.

Remark IV.3

Proposed PIO design could fit to any EPS system types and mechanical modelling size, according to previously presented model in case of a C-EPS $n_x = 4$ whereas for a P-EPS $n_x = 8$.

In order to design a PI observer for EPS system (IV.11), the proposed method is to ask for a multi-objective criterion to ensure the minimization of the road and measurement noise effect. The inclusion of such performance requirement is done following the scheme in Fig. IV.1 where a weighting function W_w is considered to specify the frequency range onto which the road disturbance is attenuated. Then, the augmented representation of EPS system inputs are the road disturbance \bar{w} specified on a frequency range defined by W_w , the control signal u and the driver torque d to be estimated, whereas the PIO inputs are the measured plant outputs y affected by sensor noise n and the control signal u . Then, PIO output is the estimated driver torque \hat{d} and the augmented state variables \hat{x}_a .

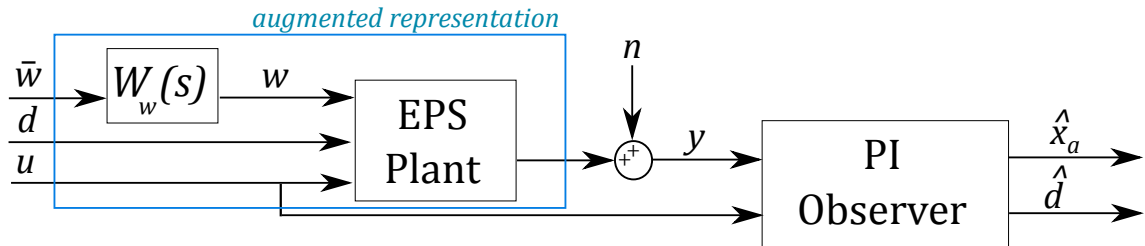


Figure IV.1 – Proposed Proportional Integral Observer Design

The weighting function $W_w(s)$ introduced to specify the frequency range of interest on which the disturbance w should be attenuated, is given in a state-space formulation by:

$$w = W_w(s)\bar{w} \Leftrightarrow \begin{cases} \dot{x}_w &= A_w x_w + B_w \bar{w} \\ w &= C_w x_w + D_w \bar{w} \end{cases} \quad (\text{IV.12})$$

where $W_w(s)^{-1}$ frequency response is shown Fig. IV.2 and is defined by:

$$W_w(s)^{-1} = \frac{s + \omega_b \varepsilon}{\frac{s}{M_s} + \omega_b} \quad (\text{IV.13})$$

- ω_b is the minimum bandwidth frequency such that $W_w^{-1}(j\omega_b) = 0dB$
- M_s is the maximum peak magnitude such that $W_w^{-1}(\infty) = M_s$
- ε is the maximum steady-state error such that $W_w^{-1}(0) = \varepsilon$

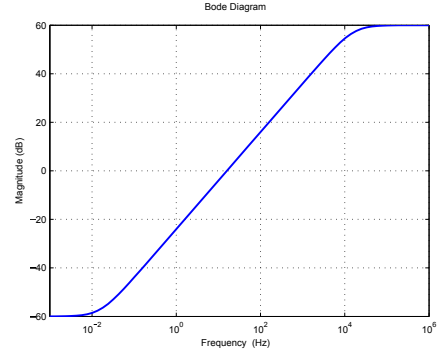


Figure IV.2 – Weighting function W_w^{-1}

Remark IV.4

It must be emphasised that the road reaction force also acts in low frequencies. It is then considered as a disturbance to be rejected on driver torque estimation process.

Therefore, the augmented representation combining (IV.11) and (IV.12) is given by:

$$\begin{cases} \begin{pmatrix} \dot{x} \\ \dot{x}_w \end{pmatrix} &= \begin{pmatrix} A & WC_w \\ 0 & A_w \end{pmatrix} \begin{pmatrix} x \\ x_w \end{pmatrix} + \begin{pmatrix} B \\ 0 \end{pmatrix} u + \begin{pmatrix} E \\ 0 \end{pmatrix} d + \begin{pmatrix} WD_w \\ B_w \end{pmatrix} \bar{w} \\ y &= (C \ 0) \begin{pmatrix} x \\ x_w \end{pmatrix} + Nn \end{cases} \quad (\text{IV.14})$$

and (IV.14) is expressed in the form:

$$\begin{cases} \dot{x}_a &= A_a x_a + B_a u + E_a d + W_a \bar{w} \\ y &= C_a x_a + Nn \end{cases} \quad (\text{IV.15})$$

where $x_a \in \mathbb{R}^{n_x+1}$ represents the augmented states.

Then, to apply a PIO on the augmented representation (IV.15), the following assumption $\dot{d} \simeq 0$ is done, such that the driver torque d becomes a state of the extended system defined as:

$$\begin{cases} \begin{pmatrix} \dot{x}_a \\ \dot{d} \end{pmatrix} &= \begin{pmatrix} A_a & E_a \\ 0 & 0 \end{pmatrix} \begin{pmatrix} x_a \\ d \end{pmatrix} + \begin{pmatrix} B_a \\ 0 \end{pmatrix} u + \begin{pmatrix} W_a \\ 0 \end{pmatrix} \bar{w} \\ y &= (C_a \ 0) \begin{pmatrix} x_a \\ d \end{pmatrix} + Nn \end{cases} \quad (\text{IV.16})$$

A simplified notation of (IV.16) is given by:

$$\begin{cases} \dot{x}_{ad} &= A_{ad}x_{ad} + B_{ad}u + W_{ad}\bar{w} \\ y &= C_{ad}x_{ad} + Nn \end{cases} \quad (\text{IV.17})$$

where $x_{ad} = \begin{pmatrix} x_a^T & d^T \end{pmatrix}^T \in \mathbb{R}^{n_x+2}$ is the extended state.

Hence, the state-space representation of PIO according to the system (IV.16) is expressed as:

$$\begin{pmatrix} \dot{\hat{x}}_a \\ \dot{\hat{d}} \end{pmatrix} = \begin{pmatrix} A_a - L_p C_a & E_a \\ -L_i C_a & 0 \end{pmatrix} \begin{pmatrix} \hat{x}_a \\ \hat{d} \end{pmatrix} + \begin{pmatrix} L_p \\ L_i \end{pmatrix} y \quad (\text{IV.18})$$

where $\hat{x}_a \in \mathbb{R}^{n_x+1}$ is the estimated of the augmented state and $\hat{d} \in \mathbb{R}$ is the estimated driver torque.

The estimation error is introduced such that $e_{ad} = \begin{pmatrix} \tilde{x}_a^T & \tilde{d}^T \end{pmatrix}^T$ with $\tilde{x}_a = x_a - \hat{x}_a$, $\tilde{d} = (d - \hat{d})$ where the estimation error dynamic is deduced from (IV.17) and (IV.18) is:

$$\begin{cases} \dot{e}_{ad} &= \begin{pmatrix} A_a - L_p C_a & E_a \\ -L_i C_a & 0 \end{pmatrix} e_{ad} + \begin{pmatrix} W_a \\ 0 \end{pmatrix} \bar{w} + \begin{pmatrix} L_p \\ L_i \end{pmatrix} Nn \\ \tilde{d} &= \begin{pmatrix} 0 & 1 \end{pmatrix} e_{ad} \end{cases} \quad (\text{IV.19})$$

Then, (IV.19) is expressed by:

$$\begin{cases} \dot{e}_{ad} &= (A_{ad} - L_a C_{ad})e_{ad} + W_{ad}\bar{w} + L_a Nn \\ \tilde{z} &= D_{ad}e_{ad} \end{cases} \quad (\text{IV.20})$$

where $L_a = \begin{pmatrix} L_p & L_i \end{pmatrix}^T \in \mathbb{R}^{n_x+2}$ is the observer gain to be determined.

From (IV.20), $(A_{ad} - L_a C_{ad})$ is a Hurwitz matrix if and only if the pair (A_{ad}, C_{ad}) is detectable, or equivalently:

$$\text{rank} \begin{bmatrix} pI - A & -WC_w & -E \\ 0 & pI - A_w & 0 \\ 0 & 0 & pI \\ C & 0 & 0 \end{bmatrix} = n_x + n_w + n_d \quad (\text{IV.21})$$

$\forall p \in \mathbb{C}$ such that $\text{Re}(p) \geq 0$. Here n_x and $n_w = 1$ denotes the number of states x in (IV.11) and x_w in (IV.12) while $n_d = 1$ denotes the driver torque (estimated). Since a stable weighting function is chosen for (IV.12), (IV.21) comes to:

$$\text{rank} \begin{bmatrix} pI - A & -E \\ 0 & pI \\ C & 0 \end{bmatrix} = n_x + n_d \quad (\text{IV.22})$$

for all p such that $\text{Re}(p) \geq 0$. For the considered extended model (IV.11) of the EPS system regarding d as an additional state under $\dot{d} \simeq 0$, the condition (IV.22) is satisfied since the pair

$\left(\begin{bmatrix} A & E \\ 0 & 0 \end{bmatrix}, \begin{bmatrix} C & 0 \\ 0 & 0 \end{bmatrix} \right)$ is observable.

Thus, the observer described in (IV.18) exists. It is worth noting that, when no disturbance/noise act, the estimation error will then be asymptotically stable.

The main objective is to estimate the driver torque subject to road disturbances and measurements noise, and to ensure stability of the proposed observer estimation error. For this purpose, a pole placement method using LMI regions has been considered in the design procedure to handle the convergence rate and stability requirements. Furthermore, the design of the observer aims at minimizing the effect of road disturbances (respectively sensor noise) subject to H_∞ -norm (resp. H_2 -norm) on the driver torque estimation error. Thus, the performance objective is focused only on the minimization of the driver torque estimation error \tilde{d} rather than including also the internal augmented states error \tilde{x}_a .

Therefore, the sensitivity functions deduced from (IV.20) are given by:

$$T_{\tilde{z}\tilde{w}}(s) = D_{ad} (sI - (A_{ad} - L_a C_{ad}))^{-1} W_{ad} \quad (\text{IV.23})$$

$$T_{\tilde{z}n}(s) = D_{ad} (sI - (A_{ad} - L_a C_{ad}))^{-1} L_a N \quad (\text{IV.24})$$

where $T_{\tilde{z}\tilde{w}}$ is the transfer function between the driver torque estimation error and road disturbances, $T_{\tilde{z}n}$ is the transfer function between the driver torque estimation error and measurements noise

IV.4.3 Performance objectives

In this section, several design objectives have been proposed considering performance of PIO estimation.

IV.4.3.1 Pole placement

In this section, a pole placement condition is defined according to the LMI conditions developed in [Chilali 1996].

Definition IV.5 (LMI regions)

Any subset \mathcal{D} of the complex plane is defined as a LMI region if there exists a symmetric matrix $M = M^T$ and a matrix L such that the characteristic function of \mathcal{D} is negative definite

$$\mathcal{D} = \{z \in \mathbb{C} : f_{\mathcal{D}}(z) < 0\} \quad (\text{IV.25})$$

with $f_{\mathcal{D}}(z) = L + zM + \bar{z}M^T$.

An example of LMI region could be given by half plane $Re(z) < -\alpha$, $f_{\mathcal{D}}(z) = z + \bar{z} + 2\alpha$. Let introduce a LMI region such that \mathcal{D}_+ is defined as:

$$\mathcal{D}_+ = \{z = x + jy \in \mathbb{C} : x < -\lambda_{min} < 0\} \quad (\text{IV.26})$$

where the corresponding domain is illustrated on Fig. IV.3

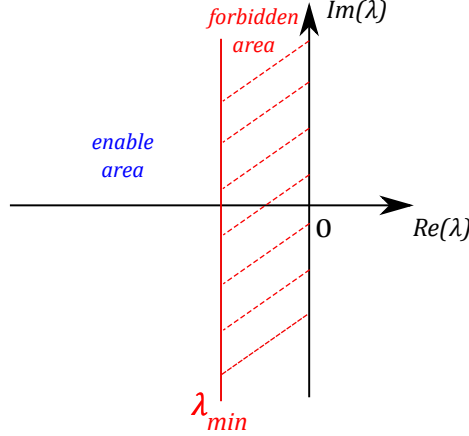


Figure IV.3 – LMI regions in complex plane

Then, a matrix A has all its eigenvalues in the region defined in \mathcal{D}_+ , if there exists a single symmetric positive matrix $P = P^T > 0$ such that

$$A^T P + PA + 2\lambda_{min} < 0 \quad (\text{IV.27})$$

In the PIO case study, the closed-loop estimation error dynamics is defined by the eigenvalues of $(A_{ad} - L_a C_{ad})$. Setting only an upper bound λ_{min} on the real part of the observer poles ensures stability and allows to define convergence speed of the estimate.

$$A_{ad}^T P + PA_{ad} - C_{ad}^T Y^T - Y C_{ad} + 2\lambda_{min} P < 0 \quad (\text{IV.28})$$

where $Y = PL_a$ with P a positive definite matrix and the observer gain L_a is deduced as $L_a = P^{-1}Y$ after solving the LMI equations. Using L_a defined in (IV.28) as the observer gain in (IV.20) guarantees that all the poles are in the left-half plane region, i.e. $Re(\lambda) < \lambda_{min}$.

IV.4.3.2 H_∞ performance

As stated in the beginning of the chapter, the road reaction disturbance w should be highly attenuated. In practice, it is sufficient to minimize the disturbance effects on the frequency domain of interest subject to the considered application. The weighting function described in (IV.13) is a filter, where the design parameters are the minimal bandwidth ω_b , the static error ε and the maximum of the sensibility function M_s . Furthermore, the road disturbance has to be rejected efficiently in low frequencies (up to 30Hz), as it is the frequency range for driver's torque input.

The minimization of the disturbances \bar{w} on the driver torque estimation error \tilde{d} is handled using H_∞ -norm, determined by bounding the closed-loop transfer function from \bar{w} to \tilde{d} , $T_{\tilde{d}\bar{w}}$.

Theorem IV.1

The problem formulation is given as: minimize γ_∞ such that $\|T_{\tilde{d}\bar{w}}\|_\infty \leq \gamma_\infty$. Hence, the H_∞ constraint is verified if there exists a symmetric positive matrix $P = P^T > 0$ such that the LMI is satisfied:

$$\begin{pmatrix} A_{ad}^T P + PA_{ad} - C_{ad}^T Y^T - Y C_{ad} + D_{ad}^T D_{ad} & P W_{ad} \\ * & -\gamma_\infty^2 \end{pmatrix} < 0 \quad (\text{IV.29})$$

where $Y = PL_a$, the observer gain L_a is deduced as $L_a = P^{-1}Y$ after solving the LMI.

IV.4.3.3 Generalized H_2 performance

The minimization of the effect of measurements noise n on the driver torque estimation error \tilde{d} is handled using generalized H_2 -norm, defined in [Scherer 2000] on the transfer function from \tilde{z} to n , $T_{\tilde{z}n}$.

Theorem IV.2

The problem formulation is given as: minimize γ_2 such that $\|T_{\tilde{z}n}\|_2 \leq \gamma_2$. Hence, the generalized H_2 constraint is verified if there exists a symmetric positive matrix $P = P^T > 0$ such that the LMI is satisfied:

$$\begin{pmatrix} A_{ad}^T P + P A_{ad} - C_{ad}^T Y^T - Y C_{ad} & -Y N \\ * & -I \end{pmatrix} < 0 \quad (IV.30)$$

$$\begin{pmatrix} P & D_{ad}^T \\ * & \gamma_2^2 \end{pmatrix} > 0$$

where $Y = PL_a$, the observer gain L_a is deduced as $L_a = P^{-1}Y$ after solving the LMI.

Remark IV.5

It is worth noting that, a weighting function could also be introduced to specify the frequency range on which measurements noise (high frequency signal) should be attenuated, in order to improve attenuation of measurements noise on the estimation error.

IV.4.3.4 A proposed mixed H_∞/H_2 synthesis

Finally, this part presents a PIO synthesis with a combination of $\mathcal{H}_2/\mathcal{H}_\infty$ performance and pole assignment specifications, using a LMI solution.

Theorem IV.3

Consider the system model (IV.14) under the assumption $\dot{d} \simeq 0$ and the PIO described in (IV.18), the mixed H_∞/H_2 problem consists of finding an observer gain L_a that places the closed-loop poles in the left-half plane while minimizing the H_∞ and H_2 performance, objectives as follows:

$$T_\infty = \left\| \frac{\tilde{z}}{w} \right\|_\infty < \gamma_\infty \quad \text{and} \quad T_2 = \left\| \frac{\tilde{z}}{n} \right\|_2 < \gamma_2 \quad (IV.31)$$

Such an observer gain L_a exists if there exists $P = P^T > 0$ and a matrix Y such that the

following LMIs are satisfied:

$$\begin{aligned}
 & A_{ad}^T P + P A_{ad} - C_{ad}^T Y^T - Y C_{ad} + 2\lambda_{min} P < 0 \\
 & \begin{pmatrix} A_{ad}^T P + P A_{ad} - C_{ad}^T Y^T - Y C_{ad} + D_{ad}^T D_{ad} & P W_{ad} \\ * & -\gamma_\infty^2 \end{pmatrix} < 0 \\
 & \begin{pmatrix} A_{ad}^T P + P A_{ad} - C_{ad}^T Y^T - Y C_{ad} & -Y N \\ * & -I \end{pmatrix} < 0 \\
 & \begin{pmatrix} P & D_{ad}^T \\ * & \gamma_2^2 \end{pmatrix} > 0
 \end{aligned} \tag{IV.32}$$

where $Y = P L_a$. Then, the observer gain L_a is deduced as $L_a = P^{-1} Y$.

However, it is not possible to minimize simultaneously both H_∞ and H_2 criteria. Therefore, a linear combination of γ_∞ and γ_2 is considered to solve the problem:

$$\min \alpha \gamma_\infty + (1 - \alpha) \gamma_2 \tag{IV.33}$$

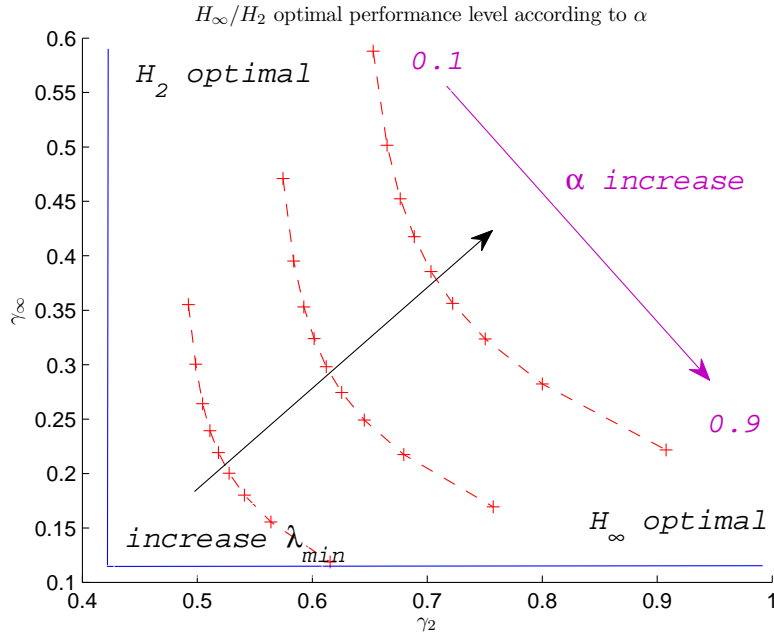
where $\alpha \in [0; 1]$, γ_∞ and γ_2 are positive scalars.

Then, the observer described in (IV.18) with the gain $L_a = P^{-1} Y$ obtained subject to previous LMIs, is an H_∞/H_2 PIO with pole placement.

Remark IV.6

Here, a common Lyapunov matrix P has been used to ensure convexity to the multi-objective problem [Chilali 1996].

In Fig. IV.4, a Pareto-like optimal (trade-off) curve between H_∞ and H_2 performance level (γ_∞ and γ_2) illustrates the compromise that is involved in the multi-objective optimization. Indeed, Pareto optimality corresponds in the mixed approach at the fact that γ_∞ (H_∞ performance level) can not be reduced without increasing γ_2 (H_2 performance level). Fig. IV.4 displays on x-axis γ_∞ and on y-axis γ_2 obtained by resolving the H_∞/H_2 optimal problem subject to various value on α computed on the range $[0.1 : 0.9]$ with a step of 0.1. Considering α close to 1 corresponds to almost solve the LMIs (IV.32) under $\gamma_{opt} = \gamma_\infty$ therefore γ_∞ has decreased while γ_2 has increased. Inversely, α close to 0 corresponds to almost solving the LMIs (IV.32) under $\gamma_{opt} = \gamma_2$ therefore γ_2 has decreased while γ_∞ has increased. Besides, regarding choice upon LMI regions, the global performance on H_∞/H_2 is modified since a fast response results in additional constraint. Following this point, three curves are presented according to three different values on λ_{min} (-40, -50, -60) where a larger real part choice involves to increase γ_∞ and γ_2 .


 Figure IV.4 – H_∞/H_2 performance evaluation according to α

IV.4.4 Design Analysis

In this part, some synthesis results obtained using the previous design objectives are presented. A comparison between the different approaches H_∞ , H_2 , mixed $\mathcal{H}_2/\mathcal{H}_\infty$ is done to highlight the efficiency of the multi-objective formulation $\mathcal{H}_2/\mathcal{H}_\infty$.

From (IV.20) the effective attenuation subject to minimization of H_∞ -norm is shown in Fig. IV.5 using the Bode diagram of the transfer function from disturbance w to the driver torque estimation error \tilde{z} :

$$|T_{\tilde{z}w}| < |W_w^{-1}| \gamma_\infty \quad (\text{IV.34})$$

Indeed, the synthesis has been realised on the augmented representation (IV.14), such that:

$$|T_{\tilde{z}\bar{w}}| < \gamma_\infty \quad \text{with} \quad w = W_w \bar{w} \quad (\text{IV.35})$$

In Table IV.1 the norms of $\|T_{\tilde{z}w}\|_\infty$ and $\|T_{\tilde{z}n}\|_2$ are computed according to the resolution of the three minimization problems H_∞ , H_2 and H_∞/H_2 .

| | H_2 | H_∞ | H_∞/H_2 |
|-------------------------------|----------------|----------------|----------------|
| $\ T_{\tilde{z}w}\ _\infty$ | $6.5382e^{-3}$ | $2.8892e^{-7}$ | $4.5015e^{-3}$ |
| $\ T_{\tilde{z}\theta_c}\ _2$ | 1.974 | 9.6728 | 0.6459 |
| $\ T_{\tilde{z}\theta_m}\ _2$ | 0.5917 | 0.3028 | $7.2380e^{-2}$ |

 Table IV.1 – $\|T_{\tilde{z}w}\|_\infty$ and $\|T_{\tilde{z}n}\|_2$ subject to strategies H_∞ , H_2 and H_∞/H_2

Fig. IV.5 shows the resulting attenuation of the road disturbance on the estimation error subject to the minimization problems H_∞ , H_2 and H_∞/H_2 . Although all approaches meet the requirement, PIO design under H_∞ performance provides the best result.

Fig. IV.6 shows the resulting attenuation of the measurements noise on the estimation error subject to the minimization problems H_∞ , H_2 and H_∞/H_2 . Left side illustrates the attenuation of the driver torque estimation error \tilde{z} subject to sensor noise on the steering wheel angle $y_1 = \theta_c + \beta_1 n$ and subject to sensor noise on the motor angle $y_2 = \theta_m + \beta_2 n$ on the right side. PIO design under mixed $\mathcal{H}_2/\mathcal{H}_\infty$ performance provides the best result.

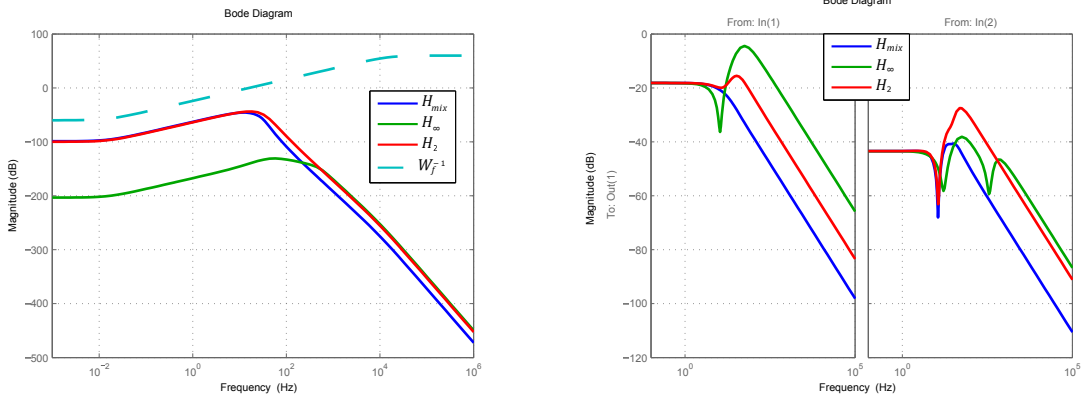


Figure IV.5 – T_{zw} subject to different problem formulations Figure IV.6 – T_{zn} subject to different problem formulations

Besides, the estimation performance is evaluated through the transfer function $T_{\hat{d}d}(s)$. Considering the EPS system (IV.11) and associate PIO (IV.18) as illustrated in Fig. IV.7,

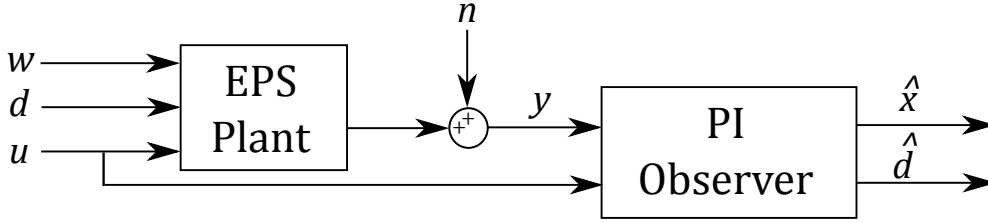


Figure IV.7 – Block diagram of EPS system and PIO

Then, the state-space equation is written as:

$$\begin{cases} \begin{pmatrix} \dot{x} \\ \dot{\hat{x}}_{ad} \end{pmatrix} = \begin{pmatrix} A & 0 \\ L_a C & A_{ad} - L_a C_{ad} \end{pmatrix} \begin{pmatrix} x \\ \hat{x}_{ad} \end{pmatrix} + \begin{pmatrix} B \\ B_a \end{pmatrix} u + \begin{pmatrix} E \\ 0 \end{pmatrix} d + \begin{pmatrix} W \\ 0 \end{pmatrix} w \\ \hat{d} = \begin{pmatrix} 0 & D_{ad} \end{pmatrix} \begin{pmatrix} x \\ \hat{x}_{ad} \end{pmatrix} \end{cases} \quad (\text{IV.36})$$

Thus, the transfer function from the driver torque estimation to the input driver torque $T_{\hat{d}d} =$

$T_{\hat{d}_y} T_{yd}$ is obtained according to:

$$\begin{cases} T_{yd} = C(sI - A)^{-1} E \\ T_{\hat{d}_y} = D_{ad}(sI - (A_{ad} - L_a C_{ad}))^{-1} L_a \end{cases} \quad (\text{IV.37})$$

$$\Rightarrow T_{\hat{d}d} = D_{ad}(sI - (A_{ad} - L_a C_{ad}))^{-1} L_a \cdot C(sI - A)^{-1} E \quad (\text{IV.38})$$

Fig. IV.8 shows the resulting bandwidth of the observer subject to the minimization problems H_∞ , H_2 and H_∞/H_2 . Although the design under $\mathcal{H}_2/\mathcal{H}_\infty$ presents the lowest cut-off frequency which is around 10 Hz, the estimation performed through this approach is still sufficient since the driver makes manoeuvres at low frequency.

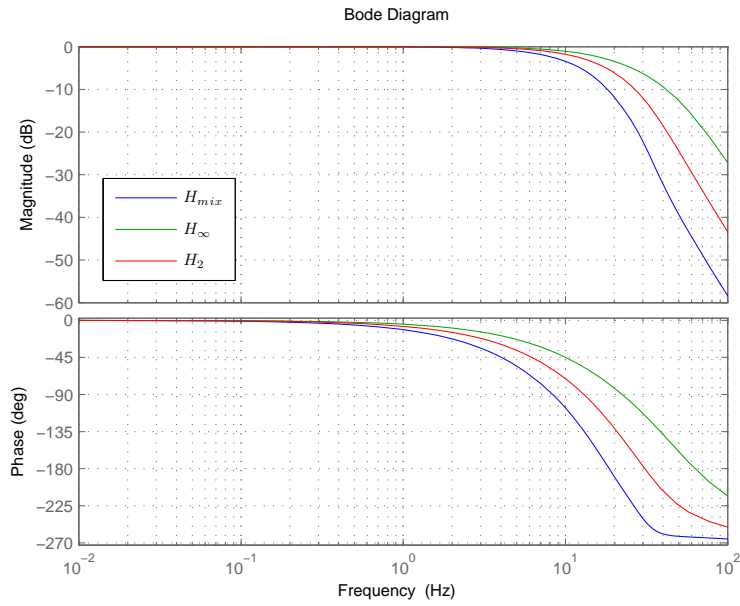


Figure IV.8 – $T_{\hat{d}d}$ subject to different problem formulation

Therefore, the mixed $\mathcal{H}_2/\mathcal{H}_\infty$ problem formulation presents the best compromise to get a PIO where the driver torque estimation is less affected by road disturbance and measurements noise. Nevertheless, the assumption $\dot{d} \simeq 0$ might be quite strong. Then, a H_∞ filtering approach is developed in the next section, where the driver torque is considered as an unknown input to be estimated.

IV.5 \mathcal{H}_∞ filtering approach

The main objective of this section is to estimate the unmeasured input d subject to the road disturbance w and sensor noises n affecting the system presented in (IV.11), using a H_∞ filtering approach. Therefore, the driver torque is considered as an unknown input to be estimated, in the framework of H_∞ synthesis formulation. In the following, the known input u is not considered, but can be easily included in the filter equations. H_∞ filter approach does not require knowledges on spectral densities on the noise processes contrary to Kalman

filter. Moreover, H_∞ synthesis provides robustness to disturbances and model uncertainties, demonstrated in robust H_∞ filtering in [Souza 1995]. Besides, H_∞ filtering has been applied to state estimation in [Yang 2005], [Hung 2003], and also to fault detection and isolation in [Marcos 2000]. This part has been developed in the latter context.

IV.5.1 H_∞ filter definition

Consider a linear time invariant system:

$$\begin{cases} \dot{x} &= Ax + Bw \\ y &= Cx + Dw \\ z &= Lx \end{cases} \quad (\text{IV.39})$$

where $x \in \mathbb{R}^n$ is the state, $w \in \mathbb{R}^{n_w}$ is the disturbance, $y \in \mathbb{R}^{n_y}$ is the measurements, $z \in \mathbb{R}^{n_z}$ is the output to be estimated (linear combination of states).

Then, the H_∞ filter structure for the system (IV.39) is:

$$\begin{cases} \dot{x}_f &= A_f x_f + B_f y \\ \hat{z} &= C_f x_f + D_f y \end{cases} \quad (\text{IV.40})$$

where $x_f \in \mathbb{R}^n$ is the filter state and $\hat{z} \in \mathbb{R}$ is the estimated of z .

The estimation error is defined by $e = z - \hat{z}$, the augmented system formed from the system (IV.39) and H_∞ filter (IV.40) :

$$\begin{cases} \begin{pmatrix} \dot{x} \\ \dot{x}_f \end{pmatrix} &= \begin{pmatrix} A & 0 \\ B_f C & A_f \end{pmatrix} \begin{pmatrix} x \\ x_f \end{pmatrix} + \begin{pmatrix} B \\ B_f D \end{pmatrix} w \\ e &= (C_1 - D_f C_2 \quad C_f) \begin{pmatrix} x \\ x_f \end{pmatrix} - D_f D w \end{cases} \quad (\text{IV.41})$$

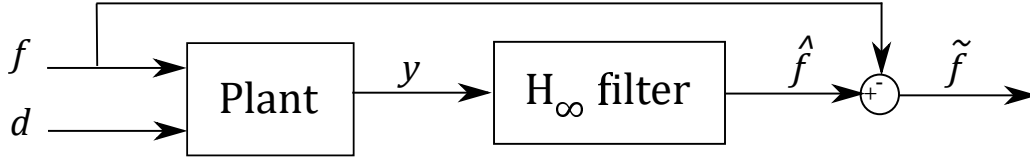
The H_∞ filtering problem associated to the system (IV.39) is to find a filter in the form (IV.40) such that the corresponding error dynamic is asymptotically stable and satisfied $\|T_{zw}\|_\infty < \gamma$. Then, the H_∞ problem could be solved using LMIs [Li 1997]. As a short illustration, other approaches to H_∞ filtering have been developed using transfer function such as interpolation [Fu 1991] or polynomial [Grimble 1990].

Besides, H_∞ filtering has been applied to fault detection in [Kim 2006] and fault estimation in [Farhat 2016], [Sheng 2016]. Those studies present several design methods.

Let consider a general system subject to disturbances d and faults f described as:

$$\begin{cases} \dot{x} &= Ax + E_d d + E_f f \\ y &= Cx + F_d d + F_f f \end{cases} \quad (\text{IV.42})$$

Then, the fault detection problem is stated as follows: design a dynamic output filter $F(s)$ as shown in Fig. IV.9 such that the transfer between the estimation error $\tilde{f} = f - \hat{f}$ and the exogenous inputs $w = \begin{pmatrix} d^T & f^T \end{pmatrix}^T$ satisfy the H_∞ criteria $\|T_{\tilde{f}w}\|_\infty < \gamma$.


 Figure IV.9 – H_∞ filter for fault estimation

Indeed, the fault f is estimated whereas the effect of disturbances d are minimized.

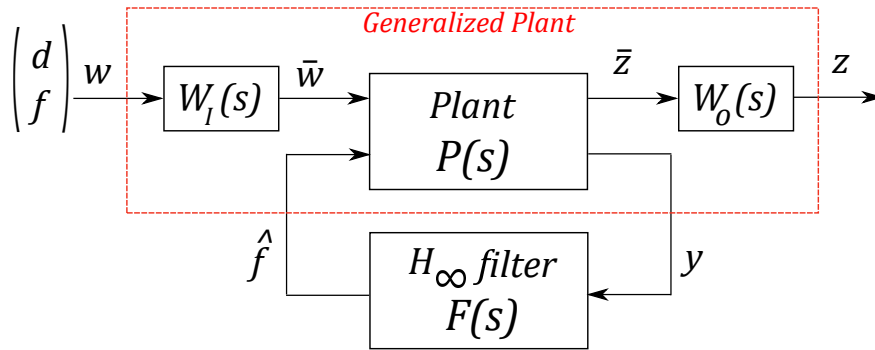
The filter $F(s)$ is expressed as:

$$\begin{cases} \dot{x}_F = A_F x_F + B_F y \\ \hat{f} = C_F x_F + D_F y \end{cases} \quad (\text{IV.43})$$

Then, the system could be written under standard H_∞ control configuration, according to the following transposition: $z = f - \hat{f}$ as the controlled output, $w = \begin{pmatrix} d^T & f^T \end{pmatrix}^T$ as the vector of exogenous inputs, y as the filter input and $u = \hat{f}$ as the output. Hence, the plant $P(s)$ is described by:

$$\begin{cases} \dot{x} = Ax + \begin{pmatrix} E_d & E_f \end{pmatrix} \begin{pmatrix} d \\ f \end{pmatrix} + 0\hat{f} \\ z = 0x + \begin{pmatrix} 0 & 1 \end{pmatrix} \begin{pmatrix} d \\ f \end{pmatrix} - 1\hat{f} \\ y = Cx + \begin{pmatrix} F_d & F_f \end{pmatrix} \begin{pmatrix} d \\ f \end{pmatrix} + 0\hat{f} \end{cases} \Rightarrow \begin{cases} \dot{x} = Ax + B_w w + B_u u \\ z = C_z x + D_{wz} w + D_{uz} u \\ y = C_y x + D_{wy} w + D_{uy} u \end{cases} \quad (\text{IV.44})$$

Moreover, weighting functions $W_I(s)$ and $W_O(s)$ could be introduced into the design to specify the frequency range of interest in order to limit conservatism induced by H_∞ norm. Then, Fig. IV.10 presents the generalized plant configuration, including these design parameters.


 Figure IV.10 – Standard H_∞ configuration

In next part, H_∞ filtering approach has been applied to estimate the driver torque considered as an unknown input.

IV.5.2 Problem formulation

A H_∞ filtering approach could be designed to estimate the driver torque subject to disturbances and measurements noise. Then, the proposed scheme in Fig. IV.11 shows a H_∞ filter for

driver torque estimation and the generalized plant which is obtained by introducing weighting functions $W_d(s)$ and $W_w(s)$ on the initial EPS system (Plant), a P-EPS model as described in III.2.1 (III.5). Besides, the H_∞ filter inputs are the steering wheel angle and the motor angle (same measurements as PIO case), output is the driver torque estimation \hat{d} .

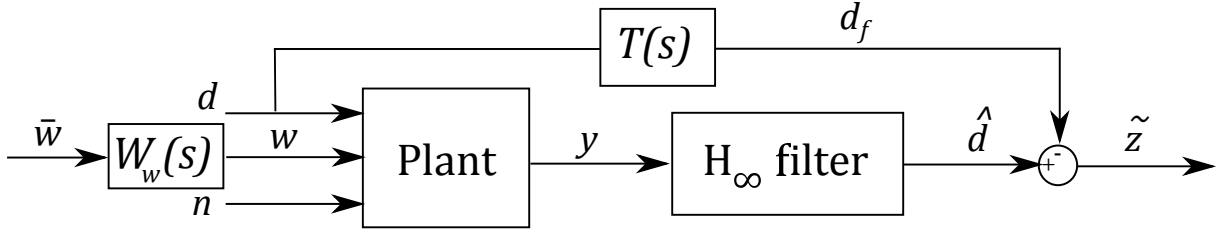


Figure IV.11 – Proposed H_∞ filtering approach for driver torque estimation

As presented before for the design of PI observer, some weighting functions are considered in H_∞ filtering synthesis. Furthermore, in this approach the assumption over driver torque dynamic $\dot{d} \simeq 0$ introduced into the previous section is not required. Nevertheless, the estimation is changed into a filtered version of the unknown input, *i.e* driver torque, to decrease the conservatism introduced by the H_∞ techniques. Then, a low pass filter is applied on the driver torque such that $d_f = T(s)d$ and a state-space representation is given in (IV.45). This allows to specify the frequency range on which estimation performance is expected. In practice, the driver torque average range is up to 2 Hz and does not exceed 5 Hz even in emergency case (avoidance manoeuvre).

$$\begin{cases} \dot{x}_t = A_t x_t + B_t d \\ d_f = C_t x_t + D_t d \end{cases} \quad (\text{IV.45})$$

Moreover a weighting function is introduced for the road disturbance such that $w = W_w(s)\bar{w}$ in order to specify the frequency range and amplitude of disturbance attenuation, in the same way as in PIO case (IV.13) and Fig. IV.2.

$$\begin{cases} \dot{x}_w = A_w x_w + B_w \bar{w} \\ w = C_w x_w + D_w \bar{w} \end{cases} \quad (\text{IV.46})$$

In this application framework, n_t represents the number of states in (IV.45) which depends on the low pass filter $T(s)$ order n_t (in this case $n_t = 1$ or 2), and $n_w = 1$ represents the number of states in (IV.46). The generalized plant over P-EPS system III.2.1 (III.5) subject to measurement noise, is defined with the augmented state vector $x_a = \begin{pmatrix} x^T & x_t^T & x_w^T \end{pmatrix}^T \in \mathbb{R}^{n_x+n_w+n_t}$ (note that here $n_x + n_w = 9$) and the exogenous input vector $w_a = \begin{pmatrix} d^T & \bar{w}^T & n^T \end{pmatrix}^T \in \mathbb{R}^4$ whereas $\tilde{z} = d_f - \hat{d} \in \mathbb{R}$ is the estimation error to be minimized. Thus, the following formulation:

$$\begin{cases} \dot{x}_a = \begin{pmatrix} A & 0 & WC_w \\ 0 & A_t & 0 \\ 0 & 0 & A_w \end{pmatrix} x_a + \begin{pmatrix} E & WD_w & 0 \\ B_t & 0 & 0 \\ 0 & B_w & 0 \end{pmatrix} w_a + \begin{pmatrix} 0 & 0 & 0 \end{pmatrix} \hat{d} \\ \tilde{z} = \begin{pmatrix} 0 & C_t & 0 \end{pmatrix} x_a + \begin{pmatrix} D_t & 0 & 0 \end{pmatrix} w_a - 1 \cdot \hat{d} \\ y = \begin{pmatrix} C & 0 & 0 \end{pmatrix} x_a + \begin{pmatrix} 0 & 0 & N \end{pmatrix} w_a + 0 \cdot \hat{d} \end{cases} \quad (\text{IV.47})$$

Then, the synthesis of H_∞ filter is done, according to the general control configuration as illustrated in Fig. IV.12.

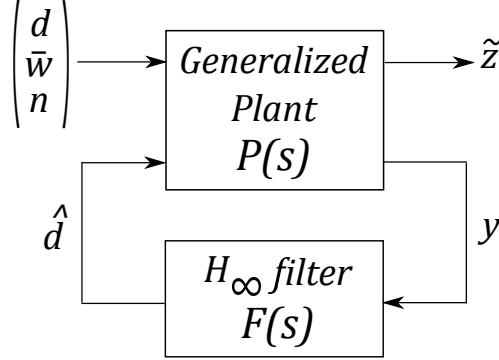


Figure IV.12 – Driver torque estimation filter under H_∞ general control configuration

Indeed, $P(s)$ based on (IV.47) could also be expressed in the following form:

$$\begin{cases} \dot{x}_a = A_a x_a + B_w w_a + B_u \hat{d} \\ \tilde{z} = C_z x_a + D_{zw} w_a + D_{zu} \hat{d} \\ y = C_y x_a + D_{yw} w_a + D_{yu} \hat{d} \end{cases} \quad (\text{IV.48})$$

$$\begin{pmatrix} \tilde{z} \\ y \end{pmatrix} = P(s) \begin{pmatrix} w_a \\ \hat{d} \end{pmatrix} \quad \text{where} \quad P(s) = \begin{pmatrix} A_a & B_w & B_u \\ C_z & D_{zw} & D_{zu} \\ C_y & D_{yw} & D_{yu} \end{pmatrix} \quad (\text{IV.49})$$

with $x_a \in \mathbb{R}^{9+nt}$ the augmented states, $w_a \in \mathbb{R}^4$ the exogenous inputs, $y \in \mathbb{R}^2$ the measurements, $\tilde{z} \in \mathbb{R}$ the estimation error and $\hat{d} \in \mathbb{R}$ the estimated signal.

The H_∞ filter $F(s)$ is given by:

$$\begin{cases} \dot{x}_f = A_f x_f + B_f y \\ \hat{d} = C_f x_f + D_f y \end{cases} \quad (\text{IV.50})$$

where $x_f \in \mathbb{R}^{9+nt}$ is the filter states (same number of states than the augmented plant $P(s)$).

Then, the problem is to design the standard H_∞ filter $F(s)$ that minimizes the H_∞ -norm of the overall system from w_a to \tilde{z} . Therefore, the closed loop system is given by:

$$\begin{cases} \dot{x}_{ag} = \begin{pmatrix} A & 0 & WC_w & 0 \\ 0 & A_t & 0 & 0 \\ 0 & 0 & A_w & 0 \\ B_f C & 0 & 0 & A_f \end{pmatrix} x_{ag} + \begin{pmatrix} E & WD_w & 0 \\ B_t & 0 & 0 \\ 0 & B_w & 0 \\ 0 & 0 & B_f N \end{pmatrix} w_a \\ \tilde{z} = \begin{pmatrix} -D_f C & C_t & 0 & -C_f \end{pmatrix} x_{ag} + \begin{pmatrix} D_t & 0 & -D_f N \end{pmatrix} w_a \end{cases} \quad (\text{IV.51})$$

where $x_{ag} = \begin{pmatrix} x_a^T & x_f^T \end{pmatrix}^T$ and $\tilde{z} = d_f - \hat{d}$.

A simplified notation of (IV.51) is introduced with $B_{ag} = \begin{pmatrix} E_{ag} & W_{ag} & N_{ag} \end{pmatrix}$:

$$\begin{cases} \dot{x}_{ag} = A_{ag}x_{ag} + B_{ag}w_a \\ \tilde{z} = C_{ag}x_{ag} + D_{ag}w_a \end{cases} \quad (\text{IV.52})$$

Therefore, the estimation of the filtered driver torque, considering a system in the form (IV.52), within H_∞ formulation is to find a filter $F(s)$, i.e. determine matrices A_f, B_f, C_f and D_f , such that $\|T_{\tilde{z}w_a}(s)\|_\infty \leq \gamma_\infty$.

Proposition IV.1 (H_∞ synthesis)

Consider the standard H_∞ problem formulation of Fig. IV.12, and the representation in (IV.52).

If there exists a symmetric positive definite matrix $X = X^T > 0$ to the LMI:

$$\begin{pmatrix} A_{ag}^T X + X A_{ag} & X B_{ag} & C_{ag}^T \\ * & -\gamma I & D_{ag}^T \\ * & * & -\gamma I \end{pmatrix} < 0 \quad (\text{IV.53})$$

$$\begin{aligned} A_{ag} &= \begin{pmatrix} A_a + B_u D_f C_y & B_u C_f \\ B_f C_y & A_f \end{pmatrix}, & B_{ag} &= \begin{pmatrix} B_w + B_u D_f D_{yw} \\ B_f D_{yw} \end{pmatrix}, \\ C_{ag} &= \begin{pmatrix} C_z + D_{zu} D_f C_y & D_{zu} C_f \end{pmatrix} & D_{ag} &= D_{zw} + D_{zu} D_f C_y. \end{aligned}$$

Then, H_∞ filter $F(s)$ satisfies $\|T_{\tilde{z}w_a}(s)\|_\infty \leq \gamma$.

Nevertheless, the matrix inequalities presented in the previous theorem are Bilinear Matrix Inequalities (BMIs). As Lyapunov function X and filter matrices A_f, B_f, C_f, D_f are unknown terms does not depend affinely but are multiplied. A Linear Matrix Inequality (LMI) can be obtained using the elimination lemma (see [Gahinet 1994], [Farhat 2016] for a detailed proof).

Proposition IV.2 (H_∞ synthesis through elimination lemma)

Consider the system $P(s)$ defined in (IV.48) and the H_∞ filter $F(s)$ in (IV.50).

If there exists $\gamma > 0$ and symmetric positive matrices $R = R^T > 0$ and $S = S^T > 0$ satisfying the following LMIs :

$$\begin{pmatrix} N_R & 0 \\ 0 & I_{n_{w_a}} \end{pmatrix}^T \begin{pmatrix} A_a R + R A_a^T & R C_z^T & B_w \\ * & -\gamma I_{n_z} & D_{zw} \\ * & * & -\gamma I_{n_{w_a}} \end{pmatrix} \begin{pmatrix} N_R & 0 \\ 0 & I_{n_{w_a}} \end{pmatrix} < 0 \quad (\text{IV.54})$$

$$\begin{pmatrix} N_S & 0 \\ 0 & I_{n_z} \end{pmatrix}^T \begin{pmatrix} A_a^T S + S A_a & S B_w & C_z^T \\ * & -\gamma I_{n_{w_a}} & D_{zw}^T \\ * & * & -\gamma I_{n_z} \end{pmatrix} \begin{pmatrix} N_S & 0 \\ 0 & I_{n_z} \end{pmatrix} < 0 \quad (\text{IV.55})$$

$$\begin{pmatrix} R & I_n \\ I_n & S \end{pmatrix} \geq 0 \quad (\text{IV.56})$$

with $N_R = \text{Ker} \begin{pmatrix} B_u^T \\ D_{zw}^T \end{pmatrix}$, $N_S = \text{Ker} \begin{pmatrix} C_y \\ D_{yw} \end{pmatrix}$.

Then, a positive definite matrix $X = X^T > 0$ is obtained as:

$$\begin{pmatrix} S & I_n \\ N^T & 0 \end{pmatrix} = X \begin{pmatrix} I_n & R \\ 0 & M^T \end{pmatrix}, \quad MN^T = I_n - RS \quad (\text{IV.57})$$

Hence, now that X is known, its value is provided in (IV.53). Then, (IV.53) becomes a LMI under unknown matrices A_f, B_f, C_f, D_f , solving the LMI gives the parameter of the filter F .

IV.5.3 Design analysis

A compromise between estimation performance and disturbance rejection has to be found through the design parameters of the H_∞ filter. Indeed, the ideal case is to get $T(s) = 1$ which means to estimate the driver torque regardless of his frequency range. Table IV.2 shows the influence of the choice of the weighting function $T(s)$ on H_∞ filter synthesis where some variations on the cut-off frequency and order of $T(s)$ have been performed. Then, the estimation performance has been assessed through the steady state gain $T_{\hat{d}d}(\omega = 0)$ (that should be close to 1) and the maximal disturbance rejection $\min_{\gamma_\infty} \|T_{\hat{z}w_a}\|_\infty \leq \gamma_\infty$ (i.e value of γ_∞ is expected to be as small as possible).

| $T(s)$ 1 st order | | | |
|------------------------------|------|------|------|
| w_n | 5Hz | 10Hz | 25Hz |
| γ_∞ | 0.15 | 0.27 | 0.51 |
| steady state gain | 0.91 | 0.75 | 0.49 |
| $T(s)$ 2 nd order | | | |
| $\zeta = 0.7$ and w_n | 5Hz | 10Hz | 25Hz |
| γ_∞ | 0.12 | 0.12 | 0.34 |
| steady state gain | 0.98 | 0.98 | 0.69 |

Table IV.2 – Influence of weighting function $T(s)$ on the H_∞ filter synthesis

As seen in Table IV.2, increasing the bandwidth of $T(s)$ leads to a degradation of estimation, (as γ_∞ gets closer to 1). The previous overview shows that a second order filter $T(s)$ is convenient, however this choice increases the size of the synthesized H_∞ filter. From (IV.52), the transfer matrix $T_{\hat{z}w_a} = [T_{\hat{z}d}; T_{\hat{z}\bar{w}}; T_{\hat{z}n}]$ of the sensitivity functions is given by:

$$T_{\hat{z}d}(s) = C_{ag}(sI - A_{ag})^{-1}E_{ag} + D_t \quad (\text{IV.58})$$

$$T_{\hat{z}\bar{w}}(s) = C_{ag}(sI - A_{ag})^{-1}W_{ag} \quad (\text{IV.59})$$

$$T_{\hat{z}n}(s) = C_{ag}(sI - A_{ag})^{-1}N_{ag} + D_f N \quad (\text{IV.60})$$

Fig. IV.13 shows the resulting attenuation of the road disturbance on the estimation error ($T_{\tilde{z}w}$) subject to three different cut-off frequencies in $T(s)$ which are 25 Hz (blue), 10 Hz (green) and 5 Hz (red). Although all approaches meet well the requirement, defining $T(s)$ with a higher cut-off frequency (25 Hz) degrades attenuation level compared to the results obtained regarding $T(s)$ with lower cut-off frequency (5 Hz or 10 Hz).

Fig. IV.14 shows the resulting attenuation of the measurements noise on the estimation error ($T_{\tilde{z}d}$) subject to three different cut-off frequencies in $T(s)$ which are 25 Hz (blue), 10 Hz (green) and 5 Hz (red). Left side illustrates the attenuation of the driver torque estimation error \tilde{z} subject to sensor noise on the steering wheel angle $y_1 = \theta_c + \beta_1 n$ and the right side subject to sensor noise on the motor angle $y_2 = \theta_m + \beta_2 n$. A synthesis under $T(s)$ with a high cut-off frequency (25 Hz) leads to an estimation error which is sensitive to measurements noise (at high frequency the magnitude on the bode diagram does not decrease), whereas a $T(s)$ with a low cut-off frequency (5 Hz or 10 Hz) provides a good attenuation of the measurements noise on the estimation error.

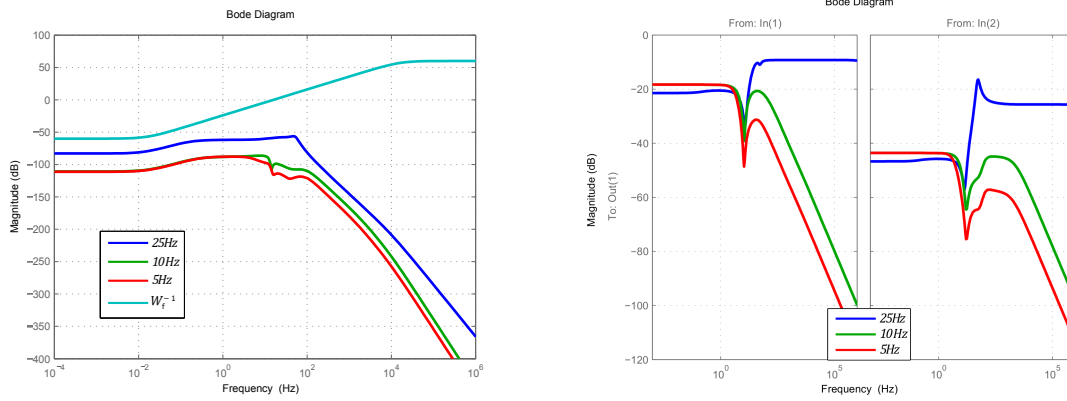


Figure IV.13 – $T_{\tilde{z}w}$ subject to different cut-off frequencies in $T(s)$ Figure IV.14 – $T_{\tilde{z}d}$ subject to different cut-off frequencies in $T(s)$

These results enable analysis allows to conclude that the optimization problem becomes harder to solve when a greater frequency range is considered. As both remaining syntheses show similar performances, the one designed considering $T(s)$ with a cut-off frequency of 10 Hz is preferred under a low pass filter of first order in order for the number of states to be kept small. Then, in the next section, simulation results are presented where a comparison between mixed $\mathcal{H}_2/\mathcal{H}_\infty$ PIO and H_∞ filter is done.

IV.6 Simulation Results

In this section, simulation results are presented to evaluate the performance of the proposed driver torque estimation techniques ($\mathcal{H}_2/\mathcal{H}_\infty$ PIO and H_∞ filter). At first, a linear P-EPS model (III.5) is considered with either measurements noise or road disturbance. Then, PIO is assessed using real data measured on vehicle (Peugeot 207 equipped with a P-EPS system) which are the steering wheel angle and motor angle.

IV.6.1 Simulation using a linear P-EPS Model

According to a unique scenario of a driver torque input of 5 Nm at 0.5 Hz, two cases are presented below: on the one hand a road disturbance such that $w = 2kN$ is considered, and on the other hand a white noise affects the output of the P-EPS model. Simulation environment is described in Fig. IV.15 where P-EPS system inputs are the driver torque d and road disturbance w (in this case the control signal u is not taken in account) while outputs y are the steering wheel angle and motor angle affected by sensors noise n . Measured signals are supplied in $\mathcal{H}_2/\mathcal{H}_\infty$ PIO and H_∞ filter which are estimating the driver torque \hat{d} and \hat{d}_∞ . Then, the obtained results are compared with the actual driver torque.

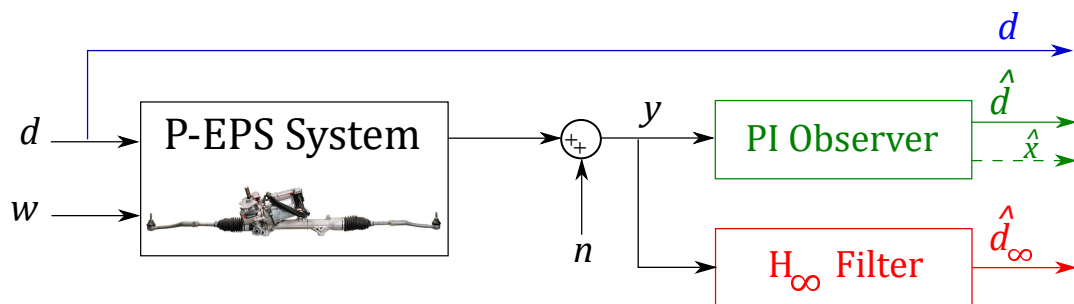


Figure IV.15 – Simulation environment P-EPS system subject to road disturbance and measurements noise

IV.6.1.1 P-EPS Model with road disturbance

In this case, a road disturbance appears after 1s while the driver makes a sinusoidal manoeuvre of amplitude 5 Nm at 0.5 Hz. A comparison between the applied driver torque (blue) and the estimated driver torque using either $\mathcal{H}_2/\mathcal{H}_\infty$ PIO (green) or H_∞ filter (red) is illustrated in Fig. IV.16. Indeed, a good driver torque estimation is performed.

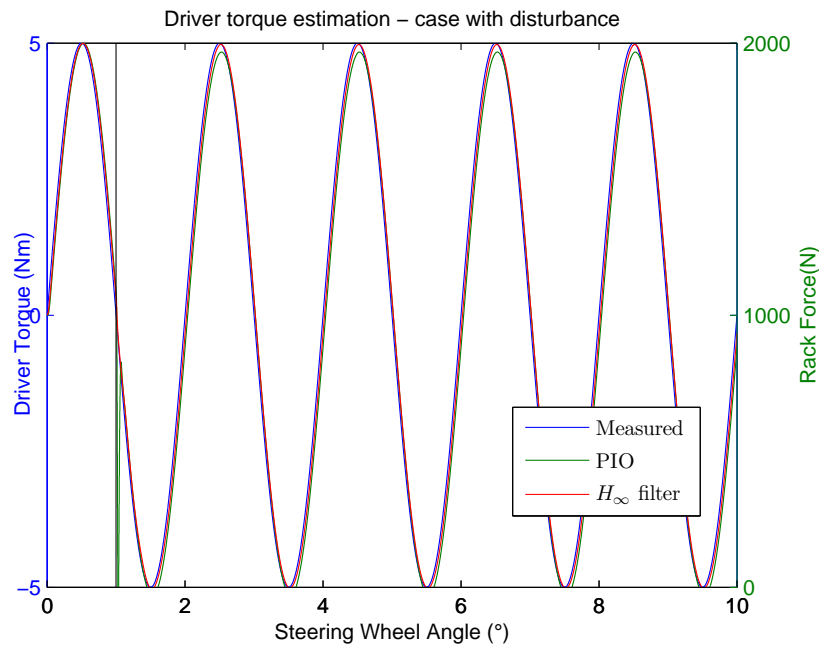


Figure IV.16 – Driver torque estimation with road disturbance

Moreover, in Fig. IV.17 the driver torque estimation error using either $\mathcal{H}_2/\mathcal{H}_\infty$ PIO (green) or H_∞ filter (red) is shown. Even though a road disturbance appears, a good convergence to the driver torque is achieved, as the estimation error amplitude is low (less than 0.5 Nm). Indeed, regarding previous sections on design analysis road disturbance is well attenuated.

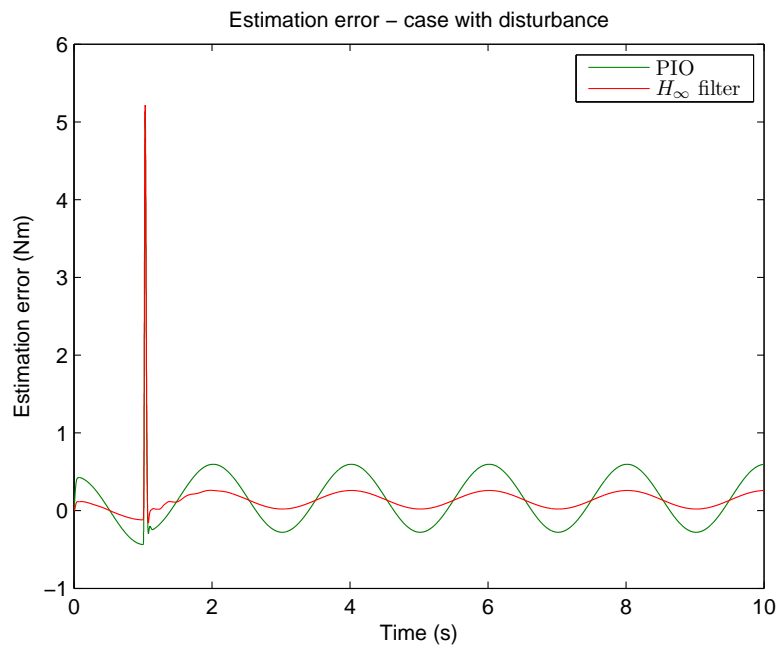


Figure IV.17 – Driver torque estimation error with road disturbance

A quantitative error analysis could be introduced using Root Mean Square Error (RMSE)

$$RMSE = \sqrt{\frac{\sum_{i=1}^n (d - \hat{d})^2}{n}} \quad (IV.61)$$

and Normalized Root Mean Square Error (NRMSE) over the range of the measured data.

$$NRMSE = \frac{RMSE}{d_{max} - d_{min}} \quad (IV.62)$$

Through these simulation results, the H_∞ filter presents a slightly better driver torque estimation (since H_∞ filter presents a wide-range of observer bandwidth) and road disturbance rejection rather than using the $\mathcal{H}_2/\mathcal{H}_\infty$ PIO. Indeed, PIO RMSE = 0.4596Nm (resp. NRMSE = 3.82%) whereas H_∞ filter RMSE = 0.2234Nm (resp. NRMSE = 2.23%) which confirms a little qualitative difference.

IV.6.1.2 P-EPS Model with measurements noise

In this case, the driver makes a sinusoidal manoeuvre of amplitude 5 Nm at 0.5 Hz. Nevertheless, measurements are disturbed by white noise with a small amplitude. A comparison between the applied driver torque (blue) and the estimated driver torque using either $\mathcal{H}_2/\mathcal{H}_\infty$ PIO (green) or H_∞ filter (red) is illustrated in Fig. IV.18. A good driver torque estimation is performed, as PIO RMSE = 0.3483Nm (resp. NRMSE = 3.48%) and H_∞ filter RMSE = 0.2265Nm (resp. NRMSE = 2.22%) remain small values.

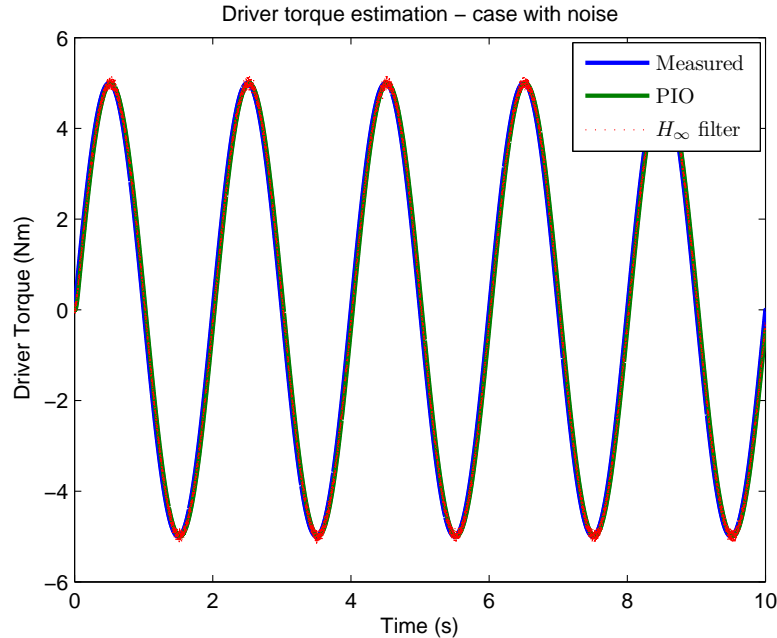


Figure IV.18 – Driver torque estimation with measurements noise

where measurements noise affecting the steering wheel angle and motor angle are presented in Fig. IV.19.

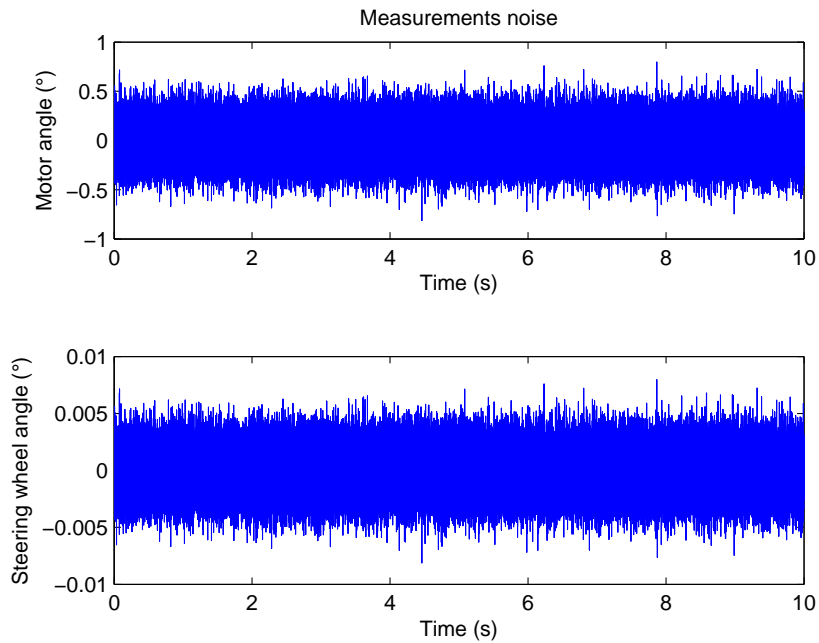


Figure IV.19 – Measurements noise affecting

Moreover, in Fig. IV.20 the driver torque estimation error using either $\mathcal{H}_2/\mathcal{H}_\infty$ PIO (green) or H_∞ filter (red) is shown. Even though measurements present some sensor noise, a good convergence to the driver torque is achieved, as the estimation error amplitude is low (less than 0.5 Nm).

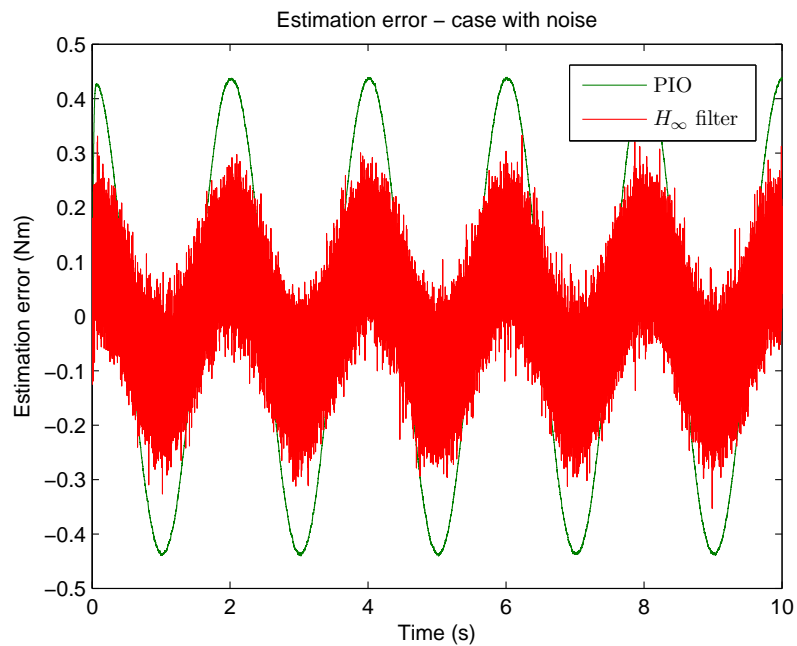


Figure IV.20 – Driver torque estimation error with measurements noise

Through these simulation results, the $\mathcal{H}_2/\mathcal{H}_\infty$ PIO presents a better attenuation of measurements noise on the driver torque estimation rather than using the H_∞ filter. Indeed, the PIO is designed subject to $\mathcal{H}_2/\mathcal{H}_\infty$ performance criteria whereas H_∞ filter is not synthesized to fulfil a multi-objective problem. Furthermore, considering previous section on H_∞ filter design analysis, measurements noise might poorly be attenuated subject to design choice on $T(s)$ like in this simulation. Regarding these two simulation cases, $\mathcal{H}_2/\mathcal{H}_\infty$ PIO shows a better compromise between road disturbances and measurements noise attenuation while ensuring a good driver torque estimation results (convergence rate and low amplitude of the estimation error). Therefore, $\mathcal{H}_2/\mathcal{H}_\infty$ PIO is preferred to the H_∞ filter. In the following part, where simulation results using real measurements are presented, only $\mathcal{H}_2/\mathcal{H}_\infty$ PIO case is illustrated.

IV.6.2 Simulation using real data input

Real data from steering angle sensor and motor resolver have been gathered on a Peugeot 207 equipped with a nominal P-EPS system with no assistance $u = 0$. Moreover, a driver torque sensor has been added on the vehicle in order to compare the estimated value and the real torque applied by the driver. Therefore, vehicle is equipped with a dynamometer steering wheel which has a slightly greater inertia than standard steering wheel.

Fig. IV.21 shows the simulation configuration using input real data, which are the steering wheel angle and the motor angle, in order to verify $\mathcal{H}_2/\mathcal{H}_\infty$ PIO performance.

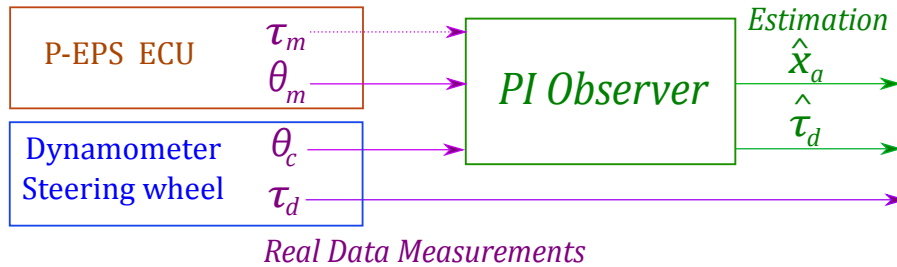


Figure IV.21 – Simulation configuration using real system measurements

In what follows, several cases are illustrated subject to measurements obtained at parking and rolling. Considering the latter case, data have been gathered under different test conditions: on a lemniscate (where the driver realises a specific manoeuvre) and also on an open road (where the driver follows the road).

Data on parking, the driver turns the steering wheel on a small rotational range. In Fig. IV.22(a) steering wheel angle and Fig. IV.22(b) rack force involved during this test case are shown. It is worth noting that the tire force evolves linearly, as small steering wheel angle is entered.

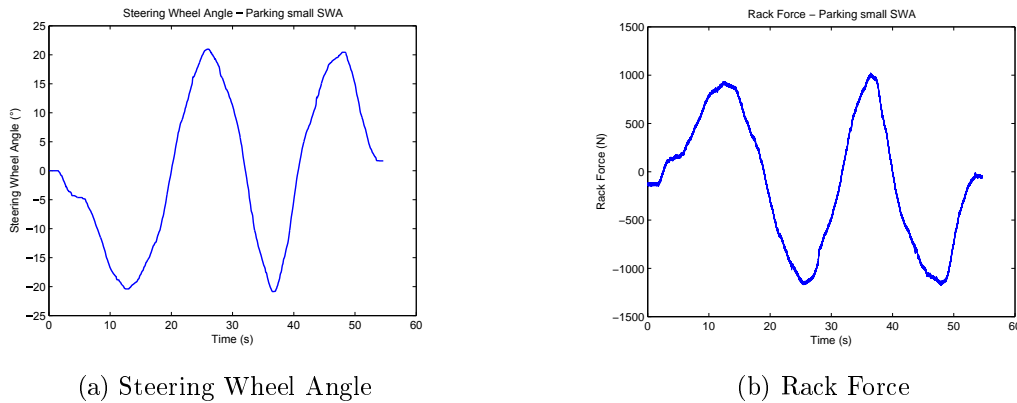


Figure IV.22 – P-EPS Test condition in parking - small SWA

In Fig. IV.23 a comparison between measured (blue) and estimated (green) driver torque is presented. As it could be seen, a good driver torque estimation is obtained with $RMSE = 0.9503$ Nm and a $NRMSE = 4.34\%$.

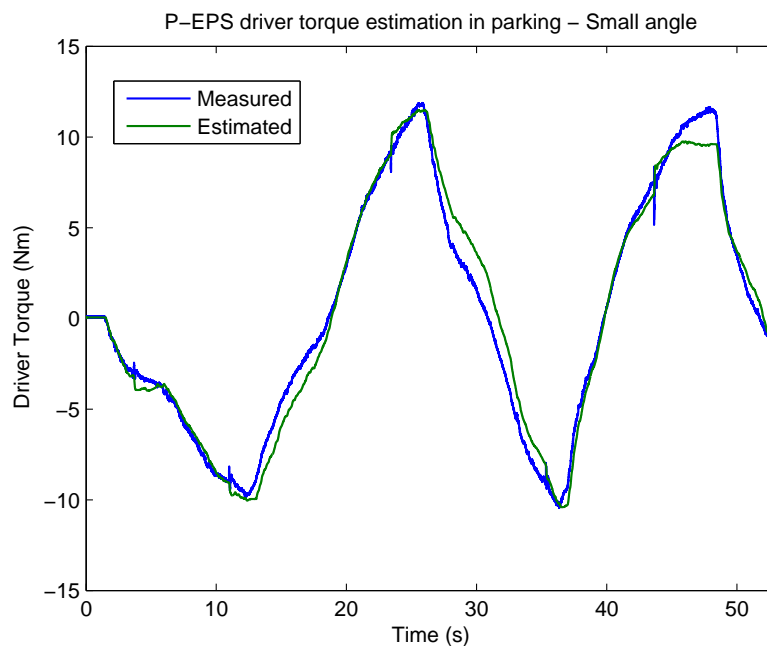


Figure IV.23 – P-EPS Driver torque estimation in parking - small angle

Data on lemniscate, the driver realises a calibrated sinus manoeuvre at a constant speed of 20 kph. Besides, the steering wheel angle range is wider than the previous parking test. In Fig. IV.24(a) steering wheel angle and Fig. IV.24(b) vehicle trajectory of the test are presented. It is worth noting that the vehicle trajectory corresponds well to the lemniscate drawn on the test track since the driver follows this line, while steering wheel angle represents a sinus.

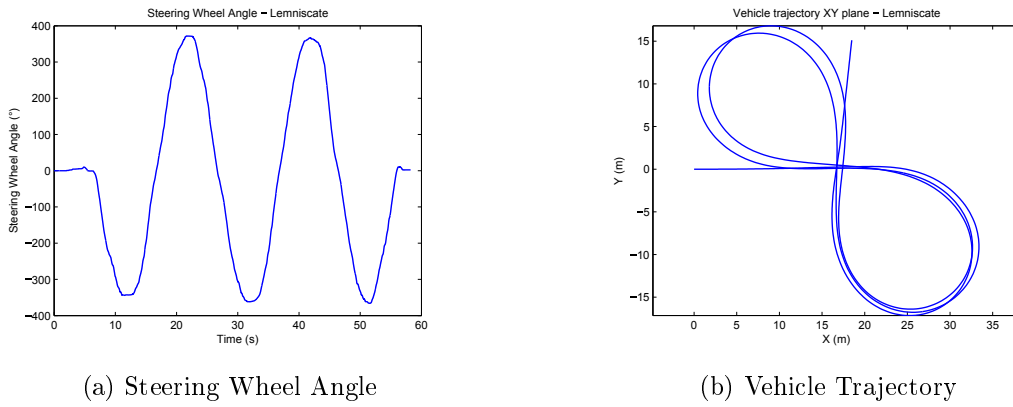


Figure IV.24 – P-EPS Test conditions for lemniscate at 20 kph

In Fig. IV.25 a comparison between measured (blue) and estimated (green) driver torque is shown. As it could be noticed, a good driver torque estimation is obtained with a NRMSE = 8.07%. Even though, estimation is slightly worsen in steer back compared to steer out.

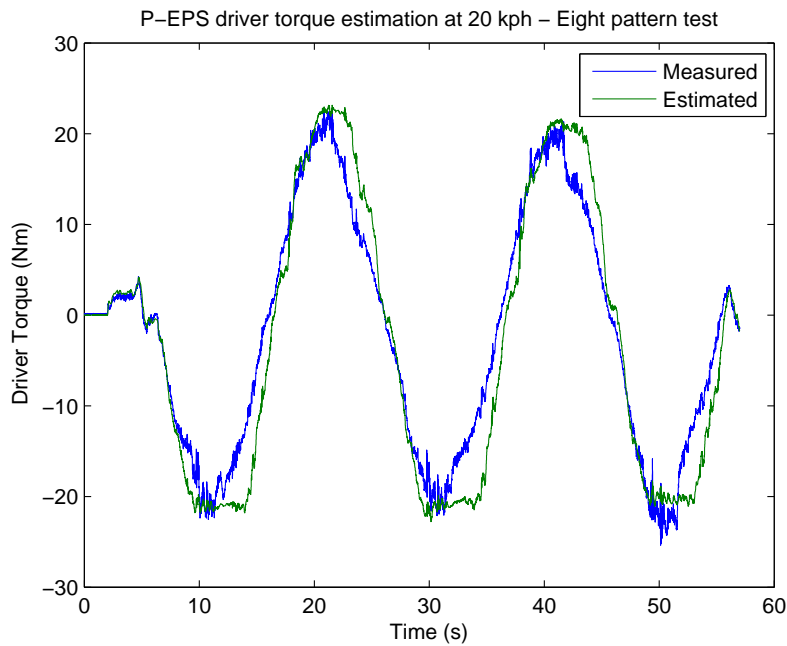


Figure IV.25 – P-EPS Driver torque estimation 20 kph - lemniscate

Data under nominal rolling condition, the driver evolves on an open road where curves and straight lines are established. As presented in Fig. IV.26, the steering wheel angle and vehicle speed are varying as an appropriate driving is required under this condition.

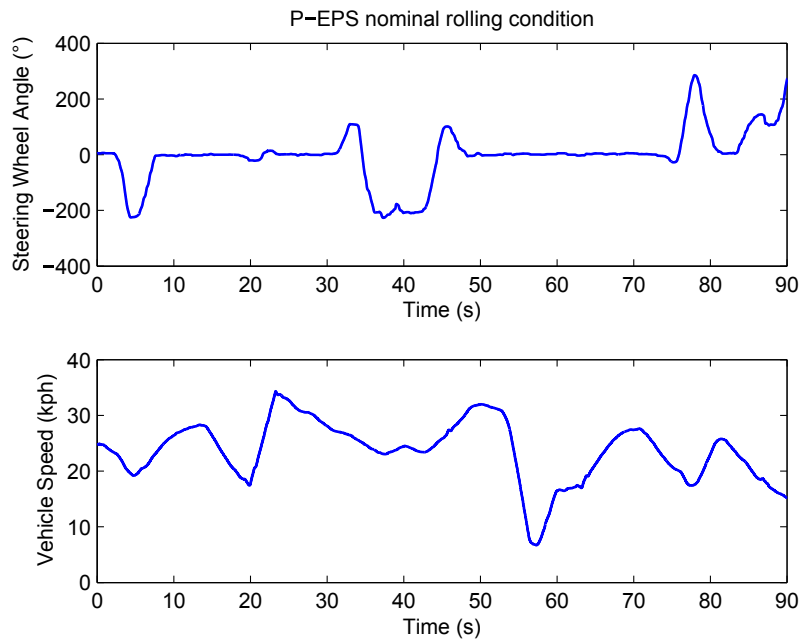


Figure IV.26 – P-EPS Test conditions - nominal rolling

In Fig. IV.27 a comparison between measured (blue) and estimated (green) driver torque is presented, and even under this varying condition a good driver torque estimation is obtained with a NRMSE = 6.45%.

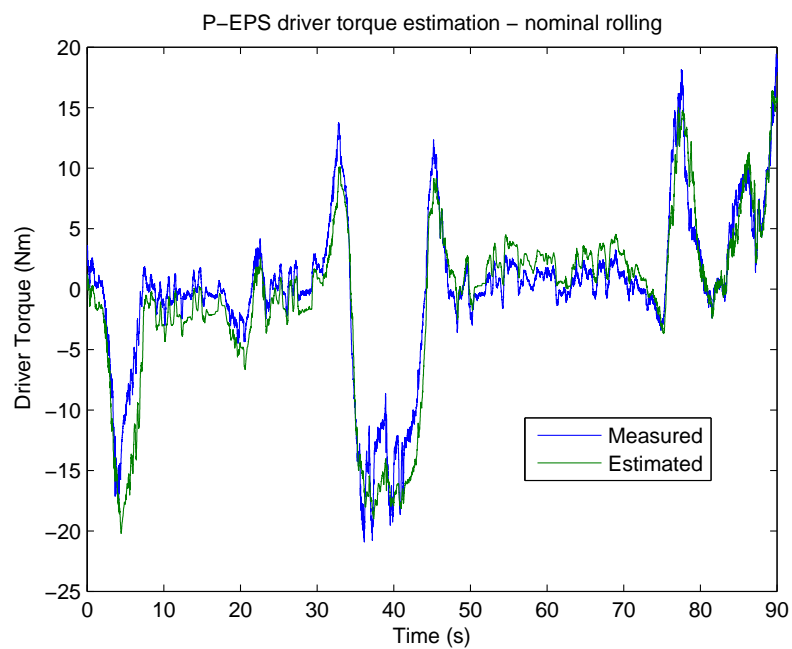


Figure IV.27 – P-EPS Driver torque estimation - nominal rolling

According to these simulation results, it is worth noting that $\mathcal{H}_2/\mathcal{H}_\infty$ PIO performs a good driver torque estimation under several driving conditions (steering wheel rotational range, vehicle speed). Hence, a $\mathcal{H}_2/\mathcal{H}_\infty$ PIO is implemented on vehicle.

IV.7 Experimental Results

A $\mathcal{H}_2/\mathcal{H}_\infty$ PIO has been implemented on the real system using Quick Prototyping (QP), on the test car which is a Clio IV equipped with a standard C-EPS system (nominal torsion bar stiffness) and a prototype pinion gear (a low pinion/rack ratio). Fig. IV.28 illustrates the implementation configuration. Hence, the design procedure under $\mathcal{H}_2/\mathcal{H}_\infty$ performance with pole placement has been applied on the corresponding C-EPS model. In this section, experimental results are presented to evaluate the performance of the proposed driver torque estimation obtained in real time on the real system. A sinus manoeuvre is realised, at first at low speed 15 kph with no assistance torque $u = 0$ and then at nominal speed 30 kph with assistance torque $u \neq 0$.

Fig. IV.28 shows the configuration on real system where a discretized $\mathcal{H}_2/\mathcal{H}_\infty$ PIO has been implemented in the MicroAutobox, CAN ECU (resp. CAN SW) send data frame containing motor angle (resp. steering wheel angle) which are the observer inputs. A measurement computer receives the estimated $\hat{\tau}_d$ and real τ_d driver torque during the whole test time.

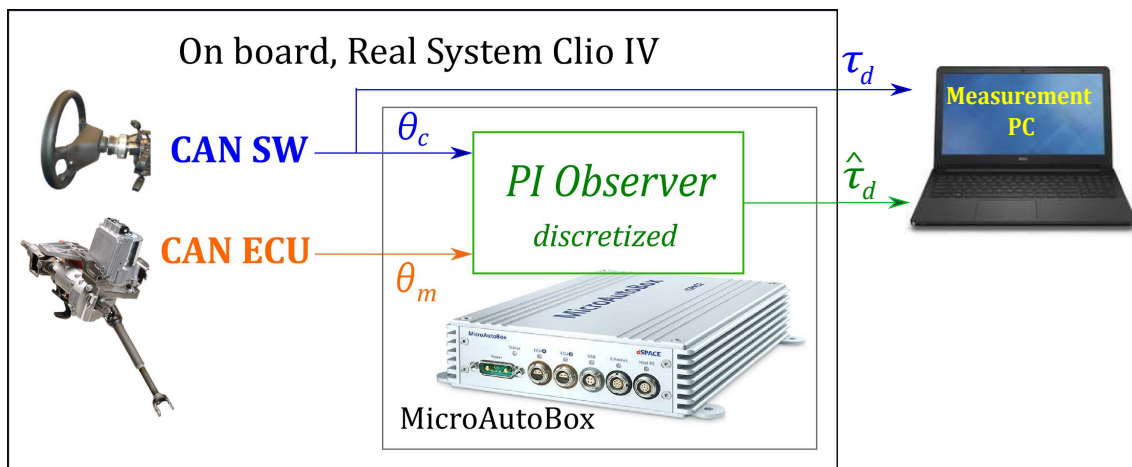


Figure IV.28 – Implementation configuration on real system Clio IV

IV.7.1 Vehicle test at 15 kph

The driver realises a lock-to-lock manoeuvre at a constant speed of 15 kph. In Fig. IV.29(a) steering wheel angle and Fig. IV.29(a) vehicle trajectory involved during this test are presented. Indeed, the steering wheel angle describes a triangular-like shape which results in sequences of circular trajectory on the test track, since steer out and steer back realises each half curvilinear trajectory.

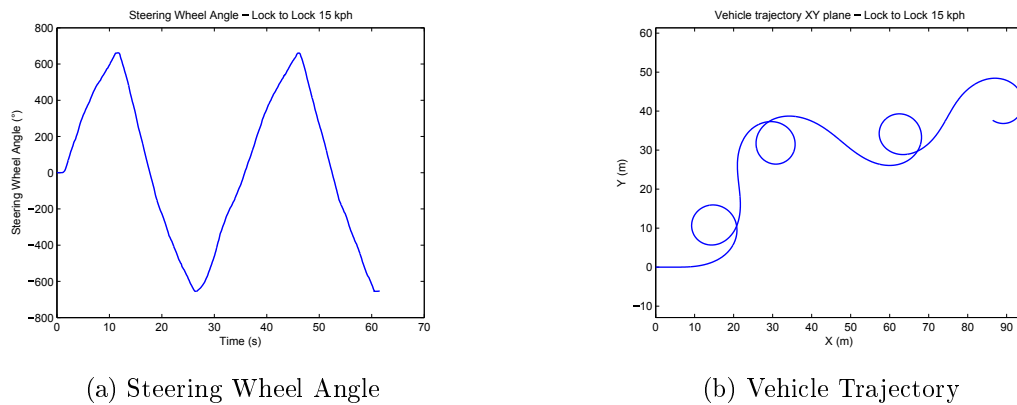


Figure IV.29 – C-EPS Test conditions for lock-to-lock at 15 kph

In Fig. IV.30, a comparison between measured driver torque (blue) and implemented estimation result (green) is shown. As it could be seen, a good driver torque estimation is obtained with a NRMSE = 4.69%. Nevertheless, at mechanical rack stop (where the driver torque highly increases) the estimation is less good. Indeed, as there is no assistance torque on this low ratio configuration, the driver encounters more rapidly the mechanical stop when making a lock-to-lock sinus manoeuvre. This means that the torsion-bar stiffness increases and is not anymore equal to its nominal value, hence the driver torque estimation is slightly different compared to the measured driver torque.

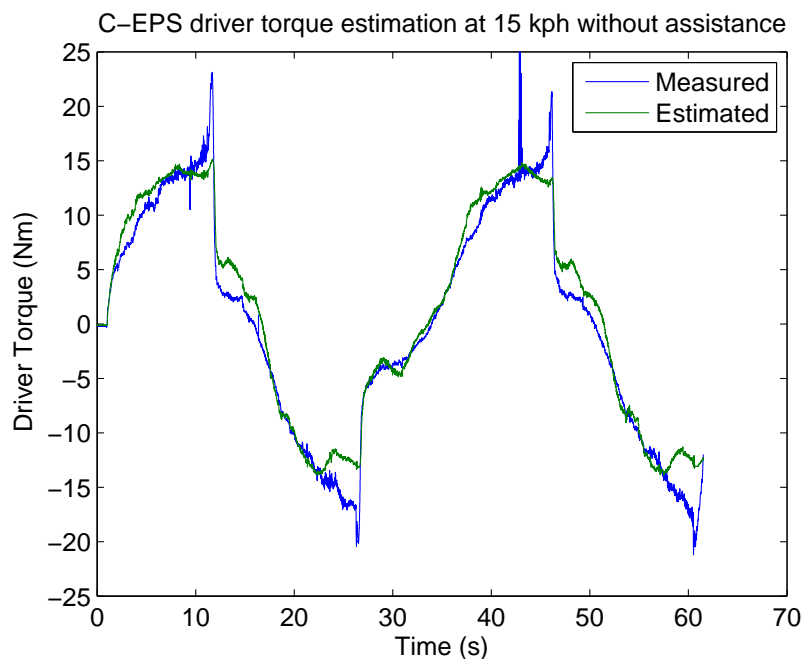


Figure IV.30 – C-EPS driver torque estimation, no assistance at 15 kph

In Fig. IV.31(a) the rack force applied during this test on the left (green) and right (blue) tie-rod is shown, while in Fig. IV.31(b) the total rack force is shown (sum of both load). It

could be noticed that the force applied on each tie-rod is rather the same, so the symmetric assumption is verified.

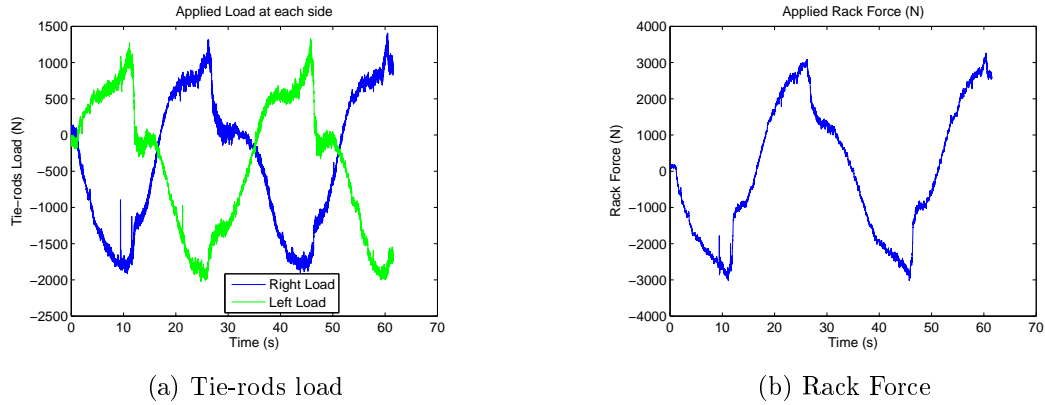


Figure IV.31 – C-EPS Test conditions for lock-to-lock at 15 kph

IV.7.2 Vehicle test at 30 kph

The driver realises a sinus manoeuvre at 30 kph. In Fig. IV.32(a) steering wheel angle and Fig. IV.32(b) vehicle trajectory involved during this test are presented. Similarly to the previous case, the steering wheel angle describes a sinus which results in sequences of circular trajectory realised on the test track.

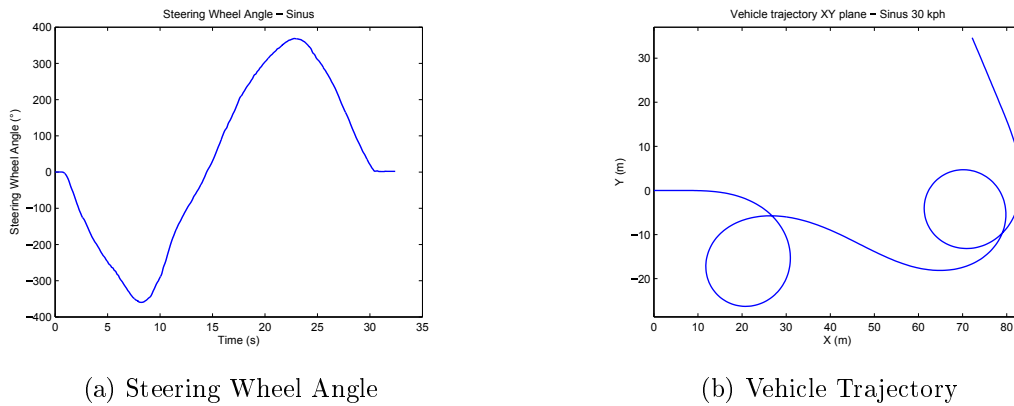


Figure IV.32 – C-EPS Test conditions for sinus at 30 kph

In Fig. IV.33 a comparison between measured driver torque (blue) and implemented estimation result (green) is shown. Contrary to the previous case, the driver performs a lower steering wheel angle range and gets some assistance torque. As it could be seen, a good driver torque estimation is obtained with a $NRMSE = 6.94\%$. However, the estimation is better when the driver turns the steering wheel at the right side rather than at the left side.

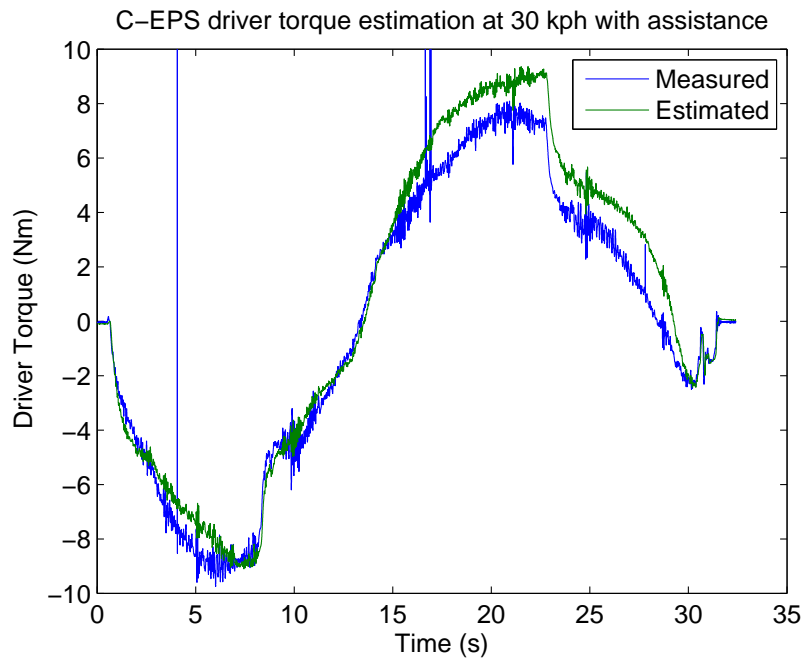


Figure IV.33 – C-EPS Driver Torque Estimation, with assistance at 30 kph

In Fig. IV.34(a) the rack force applied during this test on the left (green) and right (blue) tie-rod is shown, while in Fig. IV.34(b) the total rack force is shown (sum of both load). It could be seen that the force applied on each tie-rod does not show the same behaviour, so this asymmetry introduces a small error in the driver torque estimated value.

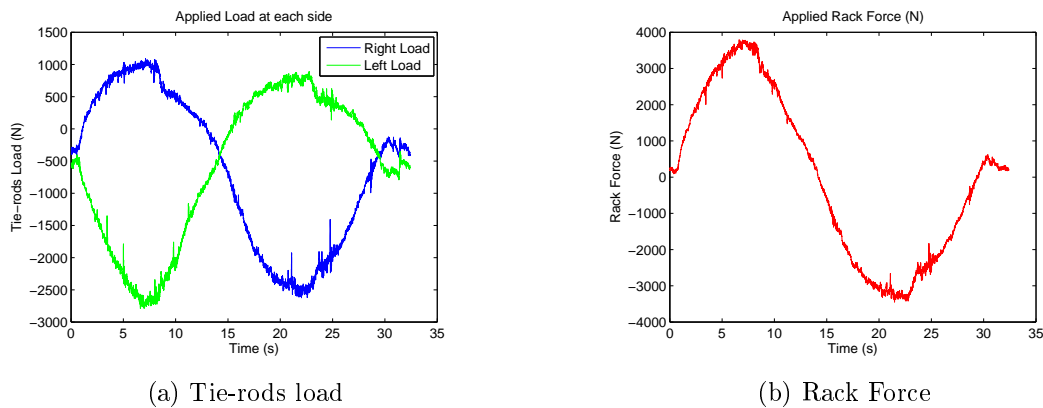


Figure IV.34 – C-EPS Road Information at 30 kph

Regarding these results, it is worth noting that the implemented $\mathcal{H}_2/\mathcal{H}_\infty$ PIO performs a good driver torque estimation, even though real system presents some non-linear behaviour that are not taken into account on the problem design formulated at the beginning of this chapter.

Remark IV.7

To go further, a driver torque model could be introduced to cover a wider functional range

of estimation. It means for example to design a proportional double integral observer [Koenig 2005].

IV.8 Conclusion

In this chapter, different methods have been developed to estimate the driver torque:

- a PIO subject to multi-objective $\mathcal{H}_\infty/\mathcal{H}_2$ design with pole placement, under the assumption that the driver torque is slowly varying in time $\dot{d} = 0$
- a H_∞ filtering approach, with the driver torque is estimated at low frequency

Several simulations have been done using both techniques to assess their performances. According to these results, the $\mathcal{H}_\infty/\mathcal{H}_2$ PIO design is selected and is tested using input real data. Then, an observer synthesized following this design procedure has been implemented on a development vehicle. Finally, it is worth saying that a relatively good driver torque estimation has been obtained under these different testing conditions. Therefore, this observer could be used in the next chapter in a control strategy based on driver torque estimation.

Besides in perspective, a switched multiple integral observer could be developed in order to improve the driver torque estimation (such method increases the implementation complexity on a real system). Indeed, as introduced in III.3.1 the road reaction force is changed according to vehicle speed (especially between stand still and motion), then a switched EPS model could be proposed. Moreover, the driver torque dynamic could be modelled to achieve a better estimation on a wider functional range and ensure better robustness to disturbances.

Control Design of Electric Power Steering Systems

Contents

| | |
|--|------------|
| V.1 Introduction | 91 |
| V.2 State of the art | 92 |
| V.2.1 Base Assist Design | 95 |
| V.2.2 Simple or Fixed-structure controller and low implementation cost | 96 |
| V.2.3 Non linear control scheme | 96 |
| V.2.4 Robust multi objective control design | 97 |
| V.3 EPS control design using driver torque estimation | 97 |
| V.3.1 A Torque SensorLess Control (TSLC) | 97 |
| V.3.2 A LQR Controller | 99 |
| V.3.3 A LPV Controller | 103 |
| V.4 EPS control design without driver torque estimation | 111 |
| V.4.1 Torsion-BarLess Control (TBLC) | 112 |
| V.4.2 H_∞ dynamic output feedback controller | 113 |
| V.5 Simulation Results | 116 |
| V.5.1 Simulation of the LQR observer-based controller | 117 |
| V.5.2 Simulation of the LPV observer-based state feedback controller | 119 |
| V.5.3 Simulation of H_∞ dynamic output feedback controller | 120 |
| V.6 Experimental Results | 121 |
| V.6.1 Torque SensorLess Control | 121 |
| V.6.2 State-feedback Controllers based on Proportional Integral Observer | 123 |
| V.6.3 Torsion Bar Less Control | 138 |
| V.7 Conclusion | 140 |

V.1 Introduction

In the previous chapter, a driver torque estimation has been developed to deal with torque sensor failure. In this chapter, EPS control methods without relying on torque sensor signal are developed, regarding different target applications: either a back-up mode to avoid Sudden Loss Of Assist (SLOA) or a nominal mode for lower production cost EPS systems (using less

sensor data such that at least torque sensor cost is saved). Concerning the latter issue, EPS control is designed on a simplified C-EPS system, since this type appears to be well suited to meet customers expectations.

At first, the objectives of EPS control are discussed. Then, a state of the art on EPS control, including industrial and academic approaches, is presented. Thereafter, two different control approaches are proposed: either an (observer based) state feedback controller, in section V.3, or a dynamic output feedback one, in section V.4. Besides, a back-up control strategy for an industrial purpose is described. Then, a LQR and a state-feedback LPV controller have been designed subject to steering performance and driver feeling. Nevertheless, these methods are based on a previously designed observer IV.4 which requires steering wheel angle and motor angle measurements (refers to section IV.4.2). Therefore, an algorithm based only on vehicle and steering wheel data have been developed within an industrial framework to reduce the measurements required to provide assistance torque (i.e saving sensors to decrease EPS cost production). With this in mind, a H_∞ dynamic output feedback controller based on steering wheel data have also been studied. Finally, some simulation results (in V.5) and experimental results (in V.6) are presented to evaluate the obtained performance (a comparison of steering effort with no assistance case has been done). Besides, several strategies have been implemented on real vehicles where different tests have been realised subject to control objectives.

This chapter has lead to the following contributions which include a patent:

- C1** Kazusa Yamamoto, Damien Koenig, Olivier Sename, Pascal Moulaire. *A New Control Design for an Optimized Electric Power Steering System*, in preprints 20th IFAC World Congress, July 2017, Toulouse, France.
- P1** Pascal Moulaire, Kazusa Yamamoto, Serge Gaudin, Yoann Baudin, Ofaina Taofifenua *Procédé de gestion de direction assistée avec reconstruction indirecte de l'information de couple volant*, ref. BR086617

V.2 State of the art

In EPS systems an electric motor provides some additional torque in accordance with the steering torque applied by the driver to turn the steering wheel. Therefore, a control law is implemented in the ECU to compute the assistance torque adapted to driving conditions. Moreover, the EPS system ensures the driver feeling function of the road reaction force. Thus, EPS control deals with some subjective performance criteria like feeling or comfort which are not systematically measurable neither easy to define. In this section, the guidelines to meet desired performance in EPS systems, together with a state of the art on several methods to design EPS controller are presented.

The objectives that are expected to be satisfied in the control design of EPS systems are as follows:

- provide a suitable assistance torque to give the good steering performance to the driver. Indeed, at low speed driving (e.g parking manoeuvre) it is expected that a high assistance torque is provided, since the amount of tire/road reaction force is high. Then, at high speed driving, a lower assistance torque is required to get a heavier steering feel for safe driving,

- guarantee closed-loop stability,
- ensure an adapted road-feedback to the driver, so that the driver feels the reaction force of the vehicle motion due to road conditions, while attenuating undesirable road information (shimmy, resonant frequency of suspension or EPS mechanical components) [Endo 2004],
- get robustness to model uncertainties regarding non-linearities related to Coulomb friction or the mechanical parameter variations, and also according to operating point (road surface, driving conditions, vehicle weight...),
- have a low complexity regarding implementation issue (ECU storage...), indeed a switched control expands implementation cost.

In this section, a state of the art on EPS control (including industrial, which presents different structure of EPS control according to considered industrial objectives, and academic approach) proposes an overview on design methods that allows to meet these performance criteria. Industrial approach is referred to different structure of EPS control regarding considered industrial objectives (customers expectations).

EPS system suppliers have proposed several technical solutions to provide assistance to the driver while ensuring steering and road feedback to the driver. Mitsubishi Electric Corporation conventional EPS controller is shown in red in Fig. V.1, on which steering manoeuvrability and steering wheel returnability have been improved through a steering angle feedback control in [Kurishige 2002b, Satake 2003]. Delphi's similar conventional strategy, proposed in [Badawy 1999], is also shown in blue in Fig. V.1. Finally, the JTEKT conventional controller structure is a combination of both strategy.

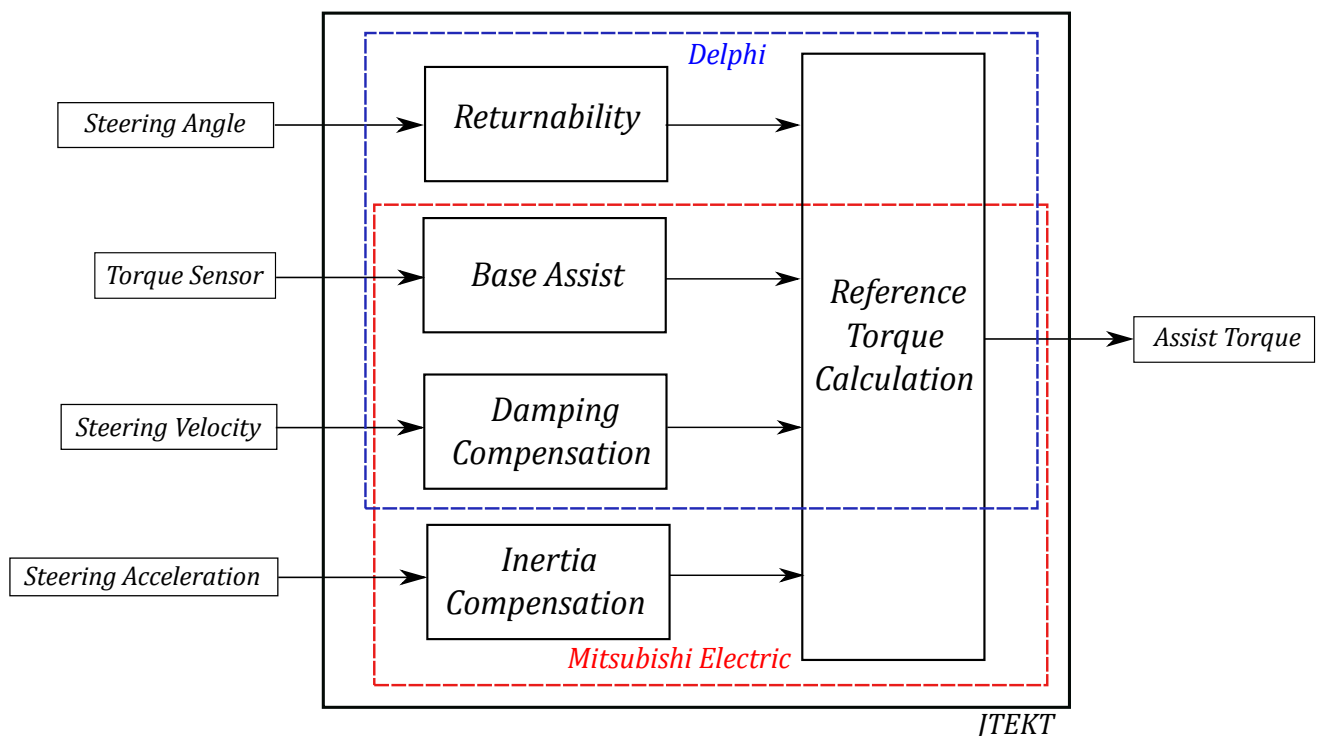


Figure V.1 – Conventional Control Block

Main functionalities of conventional EPS control blocks are explained below, more details in parameter design and tuning are given in [Hu 2008].

- *Returnability* (return to the zero position) aims to bring back the steering wheel to the centre. Indeed, inherent friction in the road wheel and steering system, prevents the steering wheel to return to centre position at low vehicle speed, especially when the driver releases the wheel.
- *Base Assist* generates an assistance torque depending on vehicle speed and input steering torque (torque sensor signal) to ensure the appropriate reduction of driver effort to turn the steering wheel. A fine tuned base assist map is needed to provide a suitable driving performance.
- *Damping Compensation* aims to mitigate the oscillations and overshoots during steering at high vehicle speed (stability improvement). Indeed, the aligning torque is large at high speed and an overshoot in steering wheel could lead to unexpected yaw motion of the vehicle.
- *Inertia Compensation* aims to improve the dynamical performance of the steering system which is deteriorated by the steering mechanism inertia. Otherwise, a heavy steering feel results when the driver turns quickly the steering wheel.

NSK company has proposed in [Kozaki 1999] another EPS control scheme, a similar one developed by JTEKT is shown in Fig. V.2.

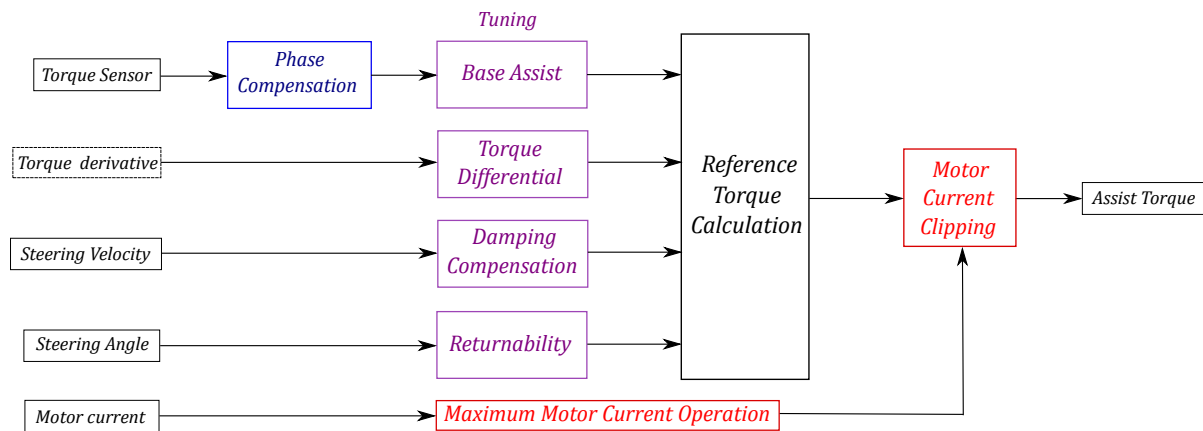


Figure V.2 – Advanced Steering Management Control Block (JTEKT)

This control diagram uses additional functions which are described below.

- *Phase compensation* (software) has been introduced to increase the phase margin while keeping the same gain.
- *Torque differential* improves system stability and disturbance rejection.

This new control scheme allows to get better performance, increases the steering assistance level, partial friction and inertia compensation and reduces ripple and sticking effect.

Other subfunctions could also be implemented such as active return, as long as the core of this steering assistance strategy is kept: base assist and torque differential.

Remark V.1

A safety relevant block Motor current clipping is illustrated in red in Fig. V.2. Its objective is to limit the maximum motor current to protect the ECU and the motor from overheating, or to clip the motor torque target to cover failure in assist torque computation to avoid self-steer, blocking. Even though functional safety is essential in mass-produced EPS systems, this chapter only deals with the design of the controller subject to nominal performances.

Addressing industrial concerns, EPS controllers are developed as a combination of algorithms with different objectives to fulfil. In what follows, at first some works about *base assist* design are reviewed regarding its importance in EPS control to define the steering performance. Then, some various academical works are briefly presented subject to control methods applied on EPS systems.

V.2.1 Base Assist Design

The previous part has presented the main requirements to achieve a good EPS control where each algorithm block is concerned with a specified functionality. Among them, the *base assist* is considered as the most important element, since it shapes mainly the assist level and also the steering feel. Hence, several studies have dealt with the design of base assist: in [Zhang 2009], [Canudas De Wit 2005], [Xue-Ping 2009] where assistance curves characteristics are analysed, and in [Ono 2016] where a focus is done on steering feel design. Mainly, the assistance characteristic is using as inputs the torque sensor and vehicle speed. Fig. V.3 illustrates a commonly used characteristic curve. It could be noticed that the driver needs more assistance torque at low speed, conversely less at high speed, also the assistance torque acts in the same direction as the torque sensor signal, in order to perform an additional torque.

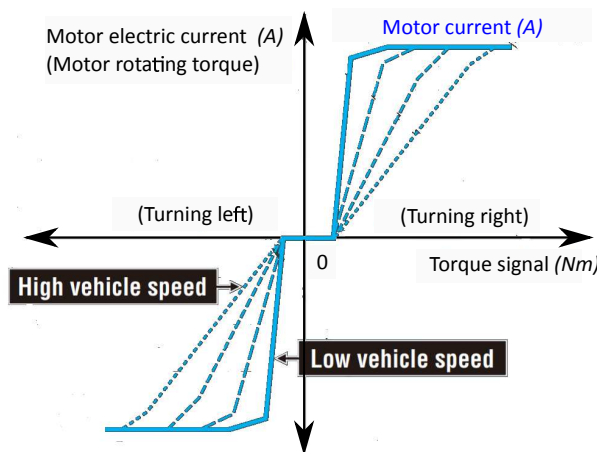


Figure V.3 – Assist characteristics curves [JTEKT 2015]

In JTEKT patent [Michelis 2011], a reference steering assistance torque is computed through weighting several measurements which are obtained using vehicle data (yaw rate, lateral acceleration, steering wheel angle) and EPS data (torque sensor, assist motor current). The algorithm structure is shown in Fig V.4. The idea is to take into account the vehicle lateral

acceleration that affects the steering feel and driver's comfort. This desired torque target generator allows to improve global performance of assistance.

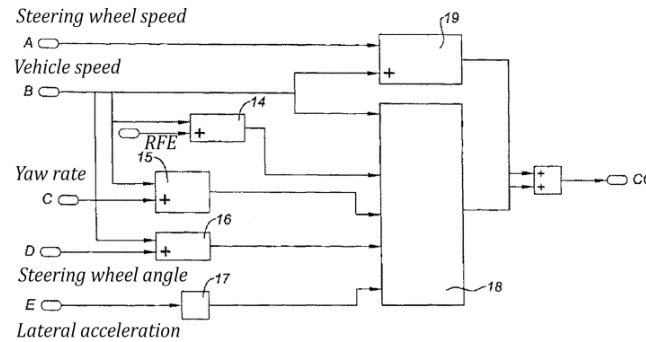


Figure V.4 – Torque Target Generator in [Michelis 2011] JTEKT patent

V.2.2 Simple or Fixed-structure controller and low implementation cost

[Kim 2002] developed an EPS control logic to reduce the driver's steering torque (PI), to provide various steering feels (reference steering torque), and to improve return to centre performance (PID). In [Seo 2012], a PI type dynamic inversion method is suggested to enforce stability and to reduce the unexpected change of steering wheel angle due to the road torque. In [Dong 2010] an active disturbance rejection controller is presented where the control objectives are to reduce the steering torque exerted by the driver considering external disturbances and system uncertainties. [Sugitani 1997] is focused on supplying road information to the driver using a \mathcal{H}_∞ controller where the weighting functions are designed regarding the frequency characteristics of rack force transmission. In [Zaremba 1997], [El-Shaer 2008] high-order lead-lag compensators are implemented. In [Zaremba 1998], a synthesis based on a \mathcal{H}_2 -norm minimization under fixed-structure controller is presented. Indeed, constrained optimization ensures requirements of steering torque assistance, feeling and response.

V.2.3 Non linear control scheme

In [Qiao 2007], [Zhang 2007], [Saifia 2014] and [Li 2009b], fuzzy control methods are applied to EPS systems to improve driver feeling. In [Saifia 2014], the Takagi-Sugeno (T-S) fuzzy method is introduced to represent the nonlinear behaviour of EPS systems (mainly caused by friction and road disturbances). Then, a controller is designed to ensure closed-loop system stability in presence of actuator saturation and external disturbances. The control saturation design is achieved through two different methods: constrained and saturated control input. In [Li 2009b], a robust fuzzy control method based on T-S model, is investigated to reduce torque ripples at high steering manoeuvre, and to get a good steering feel. In [Chen 2008a] a sliding mode controller (SMC) is proposed to improve the steering wheel's return to centre using steering column rotational dynamic. Moreover, a trigger rule has been introduced to switch between assist (boost curve) and return control. In [Wilhelm 2015], a control method for friction compensation is presented to achieve the same behaviour as a frictionless EPS system.

V.2.4 Robust multi objective control design

In [Chabaan 2001b], a \mathcal{H}_∞ robust controller is designed for a C-EPS system subject to multiple objectives: assist torque generation, road information feedback to the driver and robustness. Then, the proposed approach is made of a feedforward and feedback controllers, together with a driver torque estimation. In [Marouf 2011, Marouf 2012a, Marouf 2012b, Marouf 2013], a reference model is designed based on an ideal EPS system which ensures to generate assistance torque, supply road information and attenuate vibrations. The motor angle is chosen as the reference signal as it depends on driver torque, on road reaction force and on the assistance torque. A sliding mode controller is designed to respond to the variations of all these inputs to track the desired motor angle. Besides, a sliding mode observer is developed to estimate the inputs of the reference model regarding implementation issue. In [El-Shaer 2009, El-Shaer 2010], a fixed structure EPS controller under robust multi-objective \mathcal{H}_∞/H_2 performance is developed. The driver feeling objective is satisfied following H_2 performance while H_∞ performance is accounted for road disturbance mitigation. Furthermore, robust stability is ensured through passivity of the EPS feedback system.

According to this state of the art and to the industrial objective I.1, EPS control design is still a challenging problem, since it needs to account for several performance requirements while being a highly non-linear system. Indeed, the control should meet many objectives as explained before: generate assistance torque, ensure closed-loop stability, supply road information to the driver while attenuating undesired vibrations, or improve steering wheel returnability. Moreover, robustness towards parameters uncertainties and modelling errors is expected. Finally, most of these works require the torque sensor signal as available measurement, in addition to steering wheel angle, motor angle, motor current...

In what follows, some EPS control designs without using the measured torque sensor signal are presented subject to two different approaches, the first one based on a steering torque estimation, while the second one does not. According to the application (back-up or lower cost EPS nominal strategy) in EPS control objectives, the driver feeling is less emphasised in regards to steering effort level.

V.3 EPS control design using driver torque estimation

In this section, a back-up control for an industrial purpose is presented. Then nominal control strategies (LQR and LPV methods) which aim to be applied on lower cost EPS systems, are developed. Furthermore, a motor torque proportional to the driver could be kept in addition to ensure that an assistance is provided to the driver (similar effect as the *base assist*). Indeed, the steering torque is estimated within this part.

V.3.1 A Torque SensorLess Control (TSLC)

Torque SensorLess Control aims at providing some assistance torque to the driver in case of torque sensor failure. In this case, an internal signal is sent to the ECU whether there is a torque sensor failure. Therefore, TSLC is a back-up control which has been developed to avoid

SLOA, and thus to improve safety and driving comfort. In this section, a quick overview on TSLC concept is shown.

In the literature, some works on fault tolerant control in EPS systems have been carried out. An illustration in [Cholakkal 2009b] and [Lawson 2008] (supported by innovation research program NSERC and NCE-Auto21), a fault tolerant control has been developed considering a torque sensor failure. Under a fault tolerant scheme, such that the estimated value replaces the sensor signal when the fault residual exceeds a defined threshold. In [Cholakkal 2009a], a \mathcal{H}_∞ robust control is designed only on EPS system, so that the motor model and controller are excluded in this synthesis. Therefore, this approach could be considered in future EPS systems as a way to detect the torque sensor failure or even as a redundancy signal for safety.

TSLC general framework is depicted in Fig. V.5, where the torsion bar torque is estimated through the relationship $\hat{\tau}_{ts} = R(V_v)(\dot{\theta}_{sw} - \dot{\theta}_m) + K(V_v)(\theta_{sw} - \theta_m)$ shown in Fig. V.6.

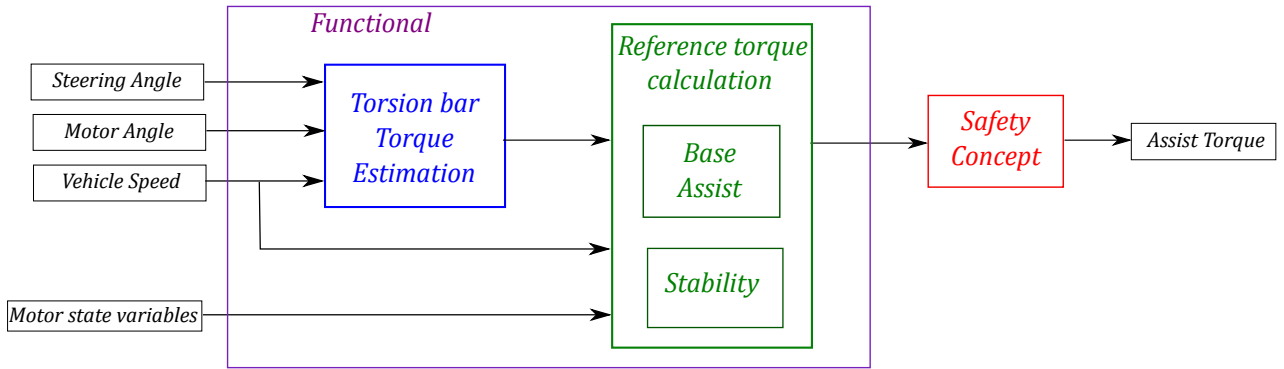


Figure V.5 – Torque Sensorless Control diagram (JTEKT)

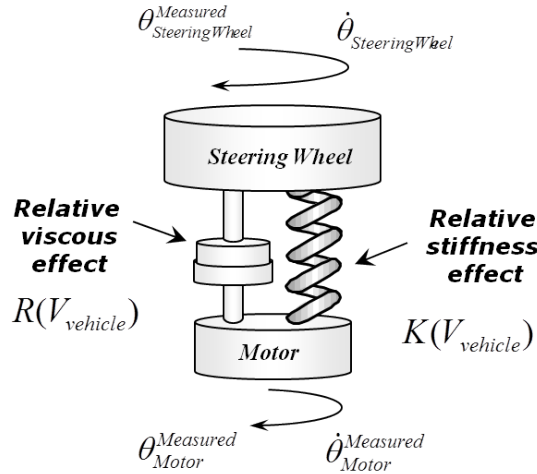


Figure V.6 – Torsion bar torque principle scheme

It could be noted that the TSLC functional principle in Fig. V.5 is similar in its structure to the controller presented in [Kurishige 2001, Kurishige 2002a], since an assist map generates and manages the assistance torque whereas stability is ensured based on the motor dynamic (rather than on steering wheel velocity as in Kurishige et al). Moreover, a safety concept had to be developed on TSLC to handle steering wheel angle safety accuracy which involves to

cover undetected accuracy of $\pm 8^\circ$. Indeed, self-steering or steering-lock must be avoided even in back-up mode. The performances obtained using TSLC are illustrated in the experimental results section.

The next section is considering nominal performance objectives to face the challenge of EPS cost reduction by saving the cost related to the torque sensor. Furthermore, the configuration of the EPS mechanical structure under such a target involves to adapt some EPS systems parameter, such as pinion gear. As introduced in II.2.1, this allows to obtain a system with less steering effort. Consequently, steering assistance level is emphasised rather than road feeling which could be supplied according to change in torsion bar stiffness, a recall of II.3.1.

V.3.2 A LQR Controller

Many LQR controller design methods applied on EPS system could be found in literature with some studies that also developed observers to estimate the whole states (LQG), an overview is given as an introduction.

In [Ciarla 2013], an optimal LQR control is designed to reject steering column oscillations generated by the column stiffness. Hence, the torsion angle and its derivative are penalized. In [Chitu 2013, Chitu 2011], a LQR control design is proposed to improve driver steering feel. Besides, the study does not use the torque sensor signal, as in [Parmar 2004]. Hence, in the previous work [Parmar 2002] an optimal-stochastic LQG controller is designed, where weighting matrices in the LQR are chosen regarding the effort applied by the driver. This could be expressed through the steering column torque and the power expanded to move the rack. Besides, in [Shi 2009] a control structure with feedforward (base assist) and LQG feedback is developed to ensure refined steering performance and robustness. The cost function in the LQR approach by [Shi 2009] is defined to minimize the error between target and actual current which corresponds to the steering performance. In the same way, [Mehrabani 2011] investigates a modified LQG controller to track the target assistance motor while attenuating external disturbances. In [Wenchang 2011], an extended EPS model including a vehicle model (a bicycle model with two degree of freedom) is introduced on which a LQR controller is designed defining the cost function to minimize a combination of steering wheel angle, yaw rate and sideslip angle. Consequently, the control improves the steering characteristics and handling stability.

In this section, a LQR controller based on the augmented model (IV.15) of previous chapter is used. Let us recall that this augmented model considers driver torque and road disturbance as additional state variables. Furthermore, no additional sensor is necessary (torque sensor is not required), since the augmented states are estimated following earlier PIO design in IV.4.2.

V.3.2.1 Background on LQR Controller

The objective of an optimal control is to minimize a cost function which penalizes both states and input behaviours [Solomon 1992]:.

Consider the system

$$\begin{cases} \dot{x} &= Ax + Bu \\ y &= Cx + Du \end{cases} \quad (\text{V.1})$$

where the pair (A, B) is stabilizable.

An infinite horizon time invariant problem is defined as:

$$\min_u J(u) = \int_0^{\infty} (x^T Q x + u^T R u) dt \quad (\text{V.2})$$

where $Q = Q^T > 0$ and $R = R^T > 0$ are design parameters respectively the state and cost penalties. The optimal state feedback controller minimizing the quadratic criteria J is obtained as:

$$u^* = -Kx \quad \text{with} \quad K = R^{-1}B^T P \quad (\text{V.3})$$

where P is solution to Algebraic Riccati Equation (ARE)

$$A^T P + PA - PBR^{-1}B^T P + Q = 0 \quad (\text{V.4})$$

Considering (V.1), if one is interested in minimizing the output y then $\|y\|^2$ introduces a cross term. The following cost functional is to be minimized:

$$\min_u J(u) = \int_0^{\infty} (x^T Q x + u^T R u + 2x^T S u) dt \quad (\text{V.5})$$

Let introduce the following constraints:

$$R > 0 \quad \text{and} \quad Q - SR^{-1}S^T \geq 0 \quad (\text{V.6})$$

and rewrite the cost functional as:

$$\min_u J(u) = \int_0^{\infty} (x^T (Q - SR^{-1}S^T)x + \mu^T R \mu) dt \quad (\text{V.7})$$

where $\mu = u + R^{-1}S^T x$, substituting in original state equation (V.1):

$$\dot{x} = (A - BR^{-1}S^T)x + B\mu \quad (\text{V.8})$$

Then, the redefined LQR problem yields an optimal control law $\mu = -R^{-1}B^T P x$ where P is stabilizing solution to ARE:

$$(A - BR^{-1}S^T)^T P + P(A - BR^{-1}S^T) - PBR^{-1}B^T P + (Q - SR^{-1}S^T) = 0 \quad (\text{V.9})$$

The optimal control law for the original system is then:

$$u^* = -R^{-1}(B^T P + S^T)x \quad (\text{V.10})$$

V.3.2.2 A LQR Design for the EPS system

The objective is to apply the LQR approach to the augmented EPS plant (IV.15) under the assumption that $\dot{d} = \varepsilon d$ with $\varepsilon \in [-0.01; 0[$ (to verify that (A, B) is stabilizable):

$$EPS \text{ Plant (IV.15)} : \begin{cases} \dot{x}_{ad} &= A_{ad}x_{ad} + B_{ad}u + W_{ad}\bar{w} \\ y &= C_{ad}x_{ad} + Nn \end{cases}$$

where $x_{ad} = \begin{bmatrix} x_a^T & d \end{bmatrix}^T \in \mathbb{R}^6$, where $x_a = \begin{pmatrix} \dot{\theta}_c & \dot{\theta}_m & \theta_c & \theta_m & d & x_f \end{pmatrix}^T$ are the augmented states, the control input $u = \tau_m \in \mathbb{R}$ as the assist torque motor, the exogenous input $\bar{w} \in \mathbb{R}$ as the road reaction force, the measurement vector $y = x_{ad}$ assuming that all the states are available.

In EPS systems, the assistance torque depends on the amount of driver torque, then the weight of assistance torque error is chosen to minimize the error of assistance torque target and the motor torque $z = u - K_a d$. Indeed, the simplest way to define a torque target is to choose it proportional to the driver torque $K_a d$. Moreover, since the steering wheel velocity affects the stability of the system (steering wheel damping, safety of the driver), therefore a weight on this variable $\dot{\theta}_c$ is also introduced such that:

$$\min_u J(u) = \int_0^\infty \left(z^T Q z + u^T R u + \dot{\theta}_c^T Q_2 \dot{\theta}_c \right) dt \quad (\text{V.11})$$

$$\min_u J(u) = \int_0^\infty \left((u - K_a d)^T Q (u - K_a d) + u^T R u + \dot{\theta}_c^T Q_2 \dot{\theta}_c \right) dt \quad (\text{V.12})$$

Hence, in a general formulation:

$$\min_u J(u) = \int_0^\infty \left(u^T R u + 2d^T S u + d^T Q_1 d + \dot{\theta}_c^T Q_2 \dot{\theta}_c \right) dt \quad (\text{V.13})$$

An appropriate selection of these parameters ensures a suitable level of assistance torque provided to the driver, $Q_2 = 0.2$, $Q_1 = 5$, $R = 0.1$, $S = -0.35$, taking into account the input torque limitation of the assistance motor.

Then, the observer-based controller is given by:

$$\begin{cases} \dot{\hat{x}}_{ad} &= (A_{ad} - B_{ad}K_{lqr} - L_a C_{ad}) \hat{x}_{ad} + L_a y \\ u &= -K_{lqr} \hat{x}_{ad} \end{cases} \quad (\text{V.14})$$

where the PIO (IV.18) introduced in the previous chapter is recalled as follows:

$$PIO \text{ (IV.18)} : \begin{cases} \dot{\hat{x}}_a &= A_a \hat{x}_a + E_a \hat{d} + L_p (y - C_a \hat{x}_a) + B_a u \\ \hat{d} &= L_i (y - C_a \hat{x}_a) \end{cases}$$

V.3.2.3 Design Analysis

In this section, the performance of the LQR design are assessed.

Fig. V.7 shows the open loop transfer function from driver torque τ_d to steering wheel speed $\dot{\theta}_c$, and also the closed loop obtained for two different values of design matrix $Q_2 = 0.1$,

$Q_2 = 2$. Fig. V.8 shows the closed loop transfer function from driver torque τ_d to control signal u for the previous values of design matrix Q_2 . Then, LQR controller increases well the response of the transfer $\frac{\dot{\theta}_c}{\tau_d}$, i.e a better steering wheel response is obtained with a small value of Q_2 . Moreover, the transfer $\frac{u}{\tau_d}$ illustrates that a small Q_2 results in a wider bandwidth of the closed-loop system, this means that a better assistance torque is provided to the driver.

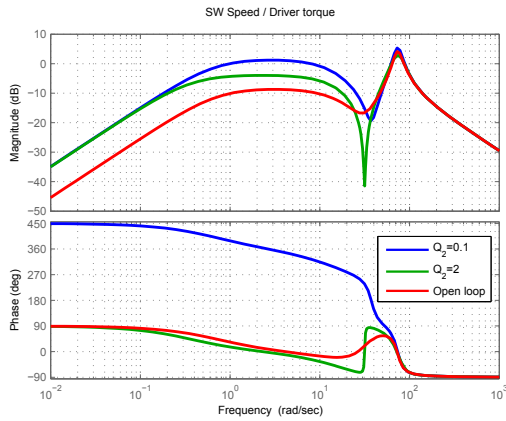


Figure V.7 – (a) $\frac{\dot{\theta}_c}{\tau_d}$, LQR varying Q_2

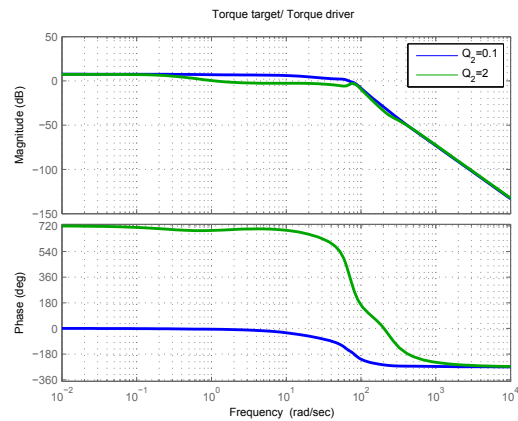


Figure V.8 – (b) $\frac{u}{\tau_d}$, LQR varying Q_2

Fig. V.9 shows the open loop transfer function from the driver torque τ_d to steering wheel speed $\dot{\theta}_c$, and also the closed loop obtained for three different values of design matrix $S = 0.12$, $S = 0.24$ and $S = 0.36$. Fig. V.10 shows the closed loop transfer function from driver torque τ_d to control signal u the previous values of design matrix S . Then, LQR controller increases well the response of the transfer $\frac{\dot{\theta}_c}{\tau_d}$, i.e a better steering wheel response is obtained with a greater value of S . Moreover, the transfer $\frac{u}{\tau_d}$ illustrates that a higher S results in a wider bandwidth of the closed-loop system, this means that a better assistance torque is provided to the driver. Indeed, this design parameter S is related to the steering assistance level, then a high value results into high assist motor torque, i.e less steering effort is required by the driver.

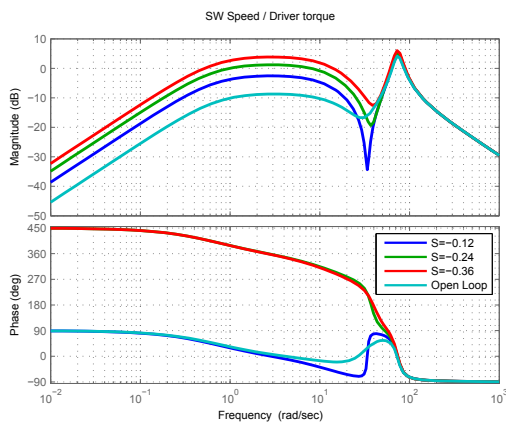


Figure V.9 – (a) $\frac{\dot{\theta}_c}{\tau_d}$, LQR varying S

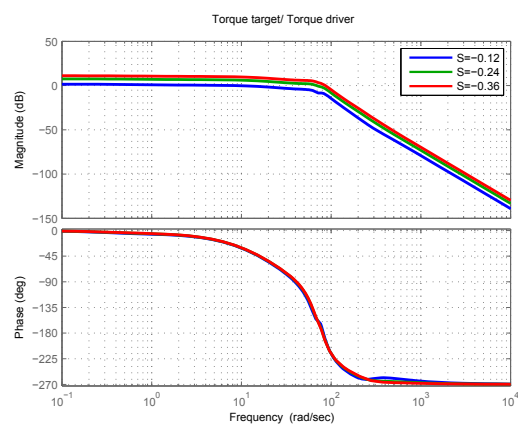


Figure V.10 – (b) $\frac{u}{\tau_d}$, LQR varying S

The performances obtained using PIO+LQR are illustrated in the next section V.5 and 6. Even though, LQR control provides high steering support to the driver, feeling is limited regarding the lack of a characteristic curve as a constant assistance gain is applied whatever the vehicle speed or the steering functional point. Thus, in the next part, a LPV controller is proposed.

V.3.3 A LPV Controller

In literature, few studies on LPV control methods have been developed on EPS systems, a review is given as an introduction.

In [Rongyun 2015] a LPV/ \mathcal{H}_∞ control has been developed to ensure steering performance, driver's feel and robustness. Thus, a LPV system has been introduced with three varying parameters: the column stiffness, the assist motor magnetic reluctance and the worm/gear reduction ratio. Nevertheless, in the general EPS model representation, these mechanical parameters are assumed to be constant, even though a slight parameter variation subsists. Then, a LPV systems as described in [Yamamoto 2011], with two varying parameters: the torque sensor and the vehicle speed, seems more intuitive compared to the previously proposed parameters choices. A gain scheduling control for this LPV system has been designed to obtain an HPS like steering feeling.

In this section, a gridded LPV EPS system is introduced on which an extended state feedback controller is synthesized. Similarly, no additional sensors are necessary (torque sensor is not required), since EPS systems states and driver torque are estimated following previously designed PIO in IV.4.2.

V.3.3.1 Brief introduction to LPV systems

A brief background on LPV systems is presented here, with a special focus to state feedback control. The interested reader may found more details in these systems and other control approaches in [Wu 1996, Apkarian 1995].

Representation of LPV systems

Consider the following LPV state-space model:

$$\begin{cases} \dot{x} &= A(\rho)x + B(\rho)u \\ y &= C(\rho)x + D(\rho)u \end{cases} \quad (\text{V.15})$$

where $x \in \mathbb{R}^n$ is the state, $u \in \mathbb{R}^{n_u}$ is the control signal and $y \in \mathbb{R}^{n_y}$ is the measurements, and ρ is a vector of time-varying parameters assumed to be known (either measured or estimated) and bounded, defined in the convex set \mathcal{P}_ρ .

$$\mathcal{P}_\rho = \{\rho = (\rho_1, \rho_2, \dots, \rho_N) \quad \text{with } \rho_i \in [\underline{\rho}_i \quad \bar{\rho}_i], \quad \forall i\} \quad (\text{V.16})$$

Remark V.2

Under requirements of rate-bounded parameter variations $\dot{\rho}$ is defined in the compact space $\mathcal{P}_{\dot{\rho}}$ such that $\dot{\rho}_i \in [\underline{\nu}_i \quad \bar{\nu}_i], \quad \forall i$. This corresponds to the case of slow varying parameters.

A large variety of LPV systems exist, among them several classes of LPV models are presented, based on the dependence on the varying parameters ρ , as illustrated below for some well known cases.

Affine System In such case, the system matrices are affine in the parameter:

$$A(\rho) = A_0 + A_1\rho_1 + \dots + A_N\rho_N \Rightarrow A(\rho) = A_0 + \sum_{i=1}^N A_i\rho_i \quad (\text{V.17})$$

Polynomial System In such case, the system matrices present polynomial parameter dependence:

$$A(\rho) = A_0 + A_1\rho + A_2\rho^2 + \dots + A_S\rho^S \Rightarrow A(\rho) = \sum_{i=0}^S A_i\rho^i \quad (\text{V.18})$$

Polytopic System A polytopic system is represented as:

$$\Sigma(\rho) = \sum_{k=1}^Z \alpha_k(\rho) \begin{pmatrix} A_k & B_k \\ C_k & D_k \end{pmatrix} \quad (\text{V.19})$$

where $\sum_{k=1}^Z \alpha_k(\rho) = 1$, $\alpha_k(\rho) \geq 0 \forall k$ and $\begin{pmatrix} A_k & B_k \\ C_k & D_k \end{pmatrix}$ are the LTI systems at each vertex k .

Indeed, under the assumption that the parameters are bounded, the vector of parameters ρ evolves inside a polytope represented by $Z = 2^N$ vertices ω_i such that $\rho = \sum_{i=1}^Z \alpha_i\omega_i$ is a convex combination of the vertices.

Gridded Systems In a grid-based approach, the LPV model of the system corresponds to a collection of linearizations on a gridded domain of parameter values. As seen later, regarding EPS systems, relevant parameter variables could be defined by vehicle speed VS and steering torque ST (in general corresponding to torque sensor or estimated driver torque). Then, a gridded LPV EPS systems is illustrated in Fig. V.11, where a LTI system is defined at each gridded point depending on parameter vector ρ .

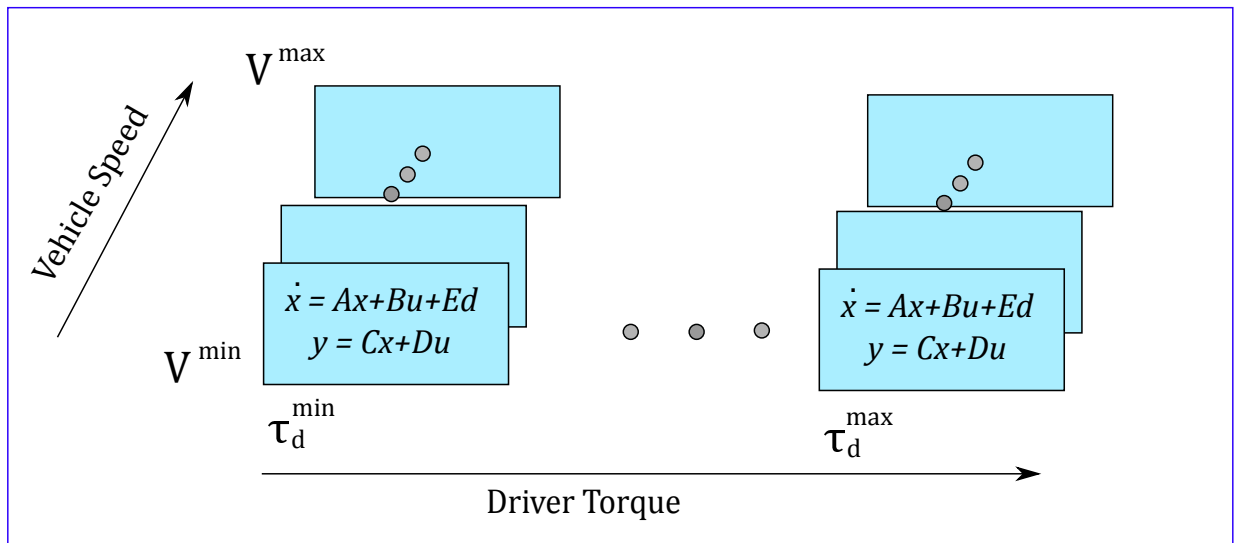


Figure V.11 – EPS LPV Models on a rectangular grid

Stability for the LPV systems

Stability analysis of LPV systems is a complex task since the state space matrices are time-varying contrary to LTI systems. Indeed, the system may be stable for frozen parameter values whereas unstable for varying parameters (this is similar for switching systems). Moreover, the notions of stability are no more equivalent regarding asymptotic and exponential stability. First, the notion of quadratic stability, through quadratic Lyapunov function $V(x) = x^T P x$ is often used in term of design for its simplicity [Wu 1995], [Blanchini 2000].

Consider a LPV system $\dot{x} = A(\rho)x$, the quadratic stability is defined as:

Definition V.1 (Quadratic stability)

$\dot{x} = A(\rho)x$ is quadratically stable if there exists a quadratic Lyapunov function $V(x) = x^T P x > 0$ such that a positive definite matrix $P = P^T > 0$ satisfies:

$$A(\rho)^T P + P A(\rho) < 0, \forall \rho \in \mathcal{P}_\rho \quad (\text{V.20})$$

Remark V.3

This approach may be conservative since stability is checked for a common Lyapunov function subject to any variation of the parameters.

Robust stability allows to consider parameter varying Lyapunov function.

Definition V.2 (Robust stability)

$\dot{x} = A(\rho)x$ is robustly stable if there exists a quadratic Lyapunov function $V(x) = x^T P(\rho)x > 0$ such that a positive definite matrix $P(\rho) = P(\rho)^T > 0$ satisfies:

$$A(\rho)^T P(\rho) + P(\rho) A(\rho) + \dot{\rho} \frac{\partial P}{\partial \rho} < 0, \forall \rho \in \mathcal{P}_\rho \quad (\text{V.21})$$

under consideration of bounded parameters and rate-bounded parameter variations

Remark V.4

A parametrization of $P(\rho)$ can be chosen to handle the effect of derivation in the above condition, for example either an affine parametrization $P(\rho) = P_0 + \sum_{i=1}^N P_i \rho_i$ or a polynomial parametrization $P(\rho) = P_0 + \sum_{i=1}^N P_i \rho^i$. The gridding approach could be used instead.

V.3.3.2 A LPV state feedback design for EPS system

It is straightforward that, based on the previous knowledge, steering torque and vehicle speed are the main parameters that characterize EPS systems. Therefore, considering both signals to define the vector of parameters ρ of a EPS LPV system seems appropriate.

In this work, a gridded LPV system is proposed where the steering characteristics is included in the nominal LTI EPS system. Besides, in the section presenting the base assist design, a polynomial expression of the curve is preferred to obtain good performance. Then, a grid based approach is chosen in order to simplify LPV control design.

As the steering characteristic generates the assistance target torque, it could be expressed subject to the applied steering torque: $\tau_m = K(\rho)\rho$ where $\rho = \tau_{st}$. In the synthesis, it is

assumed that the steering torque is measured and expressed following $\tau_{st} = C_{st}x$ (i.e the torsion bar torque), as illustrated in Fig. V.12.

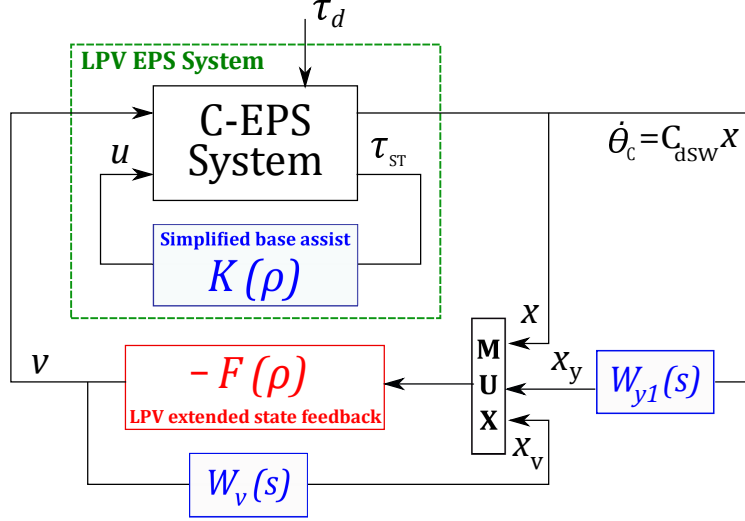


Figure V.12 – EPS LPV System, Extended State-feedback Controller

Then, the EPS LPV system is in the form:

$$\dot{x} = Ax + BK(\rho)\tau_{st} + Bv + Ed \quad (\text{V.22})$$

where $x \in \mathbb{R}^4$ is the EPS system states, $d \in \mathbb{R}$ is the driver torque and $u \in \mathbb{R}$ is the control input. Thus the LPV state-space model:

$$\dot{x} = A(\rho)x + Bv + Ed \quad (\text{V.23})$$

where $A(\rho) = A + BK(\rho)C_{st}$. Besides, ρ is bounded as steering torque and vehicle speed values are bounded. The parameters trajectories are then defined in a known compact set. Furthermore, $\dot{\rho}$ is rate-bounded as vehicle acceleration and derivative of steering torque are also bounded.

The design objective is to stabilize the plant through a wide operational range with a good performance considering actuator constraints. For this purpose:

- actuator constraints are defined through the weighting functions $W_u(s)$

$$\frac{e_v}{v} = W_v(s) \Rightarrow \begin{cases} \dot{x}_v &= A_v x_v + B_v v \\ e_v &= C_v x_v + D_v v \end{cases} \quad (\text{V.24})$$

- and performance is specified according to steering wheel velocity with the weighting functions $W_{y1}(s)$ with $y_1 = \dot{\theta}_c$

$$\frac{e_y}{\dot{\theta}_c} = W_{y1}(s) \Rightarrow \begin{cases} \dot{x}_y &= A_y x_y + B_y \dot{\theta}_c \\ e_y &= C_y x_y + D_y \dot{\theta}_c \end{cases} \quad (\text{V.25})$$

In Fig. V.13, the extended plant including the weighting functions to achieve the design objectives is shown.

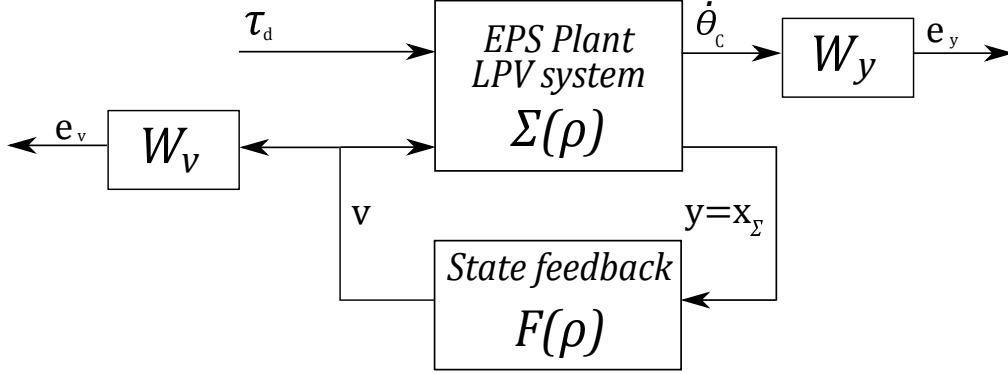


Figure V.13 – LPV State-feedback Controller Design

Then, the augmented plant is defined as:

$$\begin{cases} \begin{pmatrix} \dot{x} \\ \dot{x}_v \\ \dot{x}_y \end{pmatrix} = \begin{pmatrix} A + BK(\rho)C_{st} & 0 & 0 \\ 0 & A_v & 0 \\ B_y C_{dSW} & 0 & A_y \end{pmatrix} \begin{pmatrix} x \\ x_v \\ x_y \end{pmatrix} + \begin{pmatrix} B \\ B_v \\ 0 \end{pmatrix} u + \begin{pmatrix} E \\ 0 \\ 0 \end{pmatrix} d \\ \begin{pmatrix} e_v \\ e_y \end{pmatrix} = \begin{pmatrix} 0 & C_v & 0 \\ D_y C_{dSW} & 0 & C_y \end{pmatrix} \begin{pmatrix} x \\ x_v \\ x_y \end{pmatrix} + \begin{pmatrix} D_v \\ 0 \end{pmatrix} v \end{cases} \quad (\text{V.26})$$

where $C_{dSW} = [1 \ 0 \ 0 \ 0]$ i.e $\dot{\theta}_c = C_{dSW}x$, and $C_{st} = [0 \ 0 \ K_c \ -\frac{K_c}{R_m}]$ i.e $\tau_{st} = C_{st}x$ (refer to section III.2.2).

And the generalized plant expressed in the standard H_∞ control framework is illustrated in Fig. V.14:

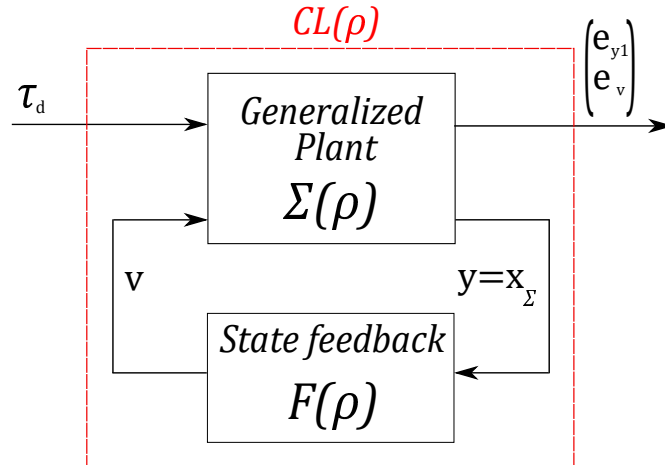


Figure V.14 – LPV State-feedback Controller Design

Then, the parameter dependent LPV state-feedback is designed on this extended representation, where the induced \mathcal{L}_2 norm from d to controlled output $z = (e_v \ e_y)^T$ is such that

$$\|T_{zd}(s)\|_\infty < \gamma.$$

Considering a generalized LPV state-space representation:

$$\begin{cases} \dot{x} = A(\rho)x + B_d(\rho)d + B_u(\rho)u \\ z = C_z(\rho)x + D_{zd}(\rho)d + D_{zu}(\rho)u \end{cases} \quad (\text{V.27})$$

which corresponds to (V.26), note that except for $A(\rho)$ the remain matrices are LTI in this study case.

Regarding the set of time-varying parameters ρ that is rate-bounded :

- ρ is measurable or at least estimated, and $\rho \in X$ with $X_\rho = \{\rho \in \mathbb{R}^s, \rho_{min}^k \leq \rho^k \leq \rho_{max}^k, k = 1 \dots s\}$ a compact set that represents the range of ρ .
- $\dot{\rho}$ the derivative of ρ is bounded i.e $|\dot{\rho}^k| < \nu^k$, and $X_{\dot{\rho}} = \{\dot{\rho} \in \mathbb{R}^s, \dot{\rho}_{min}^k \leq \dot{\rho}^k \leq \dot{\rho}_{max}^k, k = 1 \dots s\}$

According to [Wu 1995], the following theorem ensures the existence of a LPV state-feedback controller $u = -F(\rho)x$ which guarantees closed loop stability and induced L_2 -norm from d to z less than $\gamma > 0$.

Theorem V.1

Consider the LPV model (V.27) with parameters trajectories ρ defined on the set X_ρ , and rate-bounded such that $\dot{\rho}$ is defined on the set $X_{\dot{\rho}}$.

There exists a LPV parameter-dependent state-feedback controller which guarantees closed loop stability and an upper bound $\gamma > 0$ on the \mathcal{L}_2 -gain of the closed loop system from d to z for any $\rho \in X_\rho$, if and only if there exists a symmetric positive definite matrix $P(\rho) = P(\rho)^T > 0$ and a matrix $Y(\rho)$ for all $\rho \in \mathcal{P}$ such that:

$$\begin{pmatrix} A(\rho)P(\rho) + P(\rho)A(\rho)^T + B_u(\rho)Y(\rho) + Y(\rho)^T B_u(\rho)^T \pm \nu_k \frac{\partial P}{\partial \rho_k} & * & * \\ B_w(\rho)^T & -\gamma I & * \\ C_z(\rho)P(\rho) + D_{zu}(\rho)Y(\rho) & D_{zd}(\rho) & -\gamma I \end{pmatrix} < 0 \quad (\text{V.28})$$

where $\rho \in X_\rho$ and $\nu^k = \dot{\rho}_{max}^k \in X_{\dot{\rho}}$.

Finally, the parameter dependent state feedback is given by: $F(\rho) = -Y(\rho)P(\rho)^{-1}$.

In order to solve the LMI problem (V.28) and find the LPV state-feedback controller, a basis is chosen to express the matrix $P(\rho)$ and $Y(\rho)$ (to predefine the functional dependence in ρ). Here, subject to the functional dependence of the EPS LPV model on ρ , a polynomial form has been chosen, which is similar to the shape of steering characteristic curve, such design choice has been applied in [Abbas 2014].

$$P(\rho) = P_0 + \rho P_1 + \rho^2 P_2 \quad (\text{V.29})$$

$$Y(\rho) = Y_0 + \rho Y_1 + \rho^2 Y_2 \quad (\text{V.30})$$

Besides, the LMIs (V.28) require the solutions matrices $P(\rho)$ and $Y(\rho)$ to satisfy an infinite number of constraints over all trajectories of ρ in the set. Thus to relax the problem, a gridding approach has been proposed such that the LMIs are solved at the grid points defined by ρ^k .

In [Hjartarson 2015] the LPV toolbox *LPVTools* to deal with LPV controller design is proposed where LPV systems are defined as a state-space array. However, the controller $F(\rho)$ presented in the next part is obtained by computing over the gridded points, the LMIs (V.28) using YALMIP interface and SeDuMi solver.

V.3.3.3 Analysis of the closed loop observer based LPV state feedback controller

Regarding implementation issue and cost reduction framework, the varying parameter corresponding to the steering torque is not measured, moreover all the states of EPS system are also not available. However, this could be solved considering the PIO developed in the previous chapter IV.4.2 such that the driver torque is the varying parameter $\rho = \hat{d}$, and then

$$\begin{aligned}\tau_m &= K(\rho)\hat{d} \\ y_1 &= C_1\hat{x} \\ v &= -\begin{pmatrix} F_x(\rho) & F_v(\rho) & F_y(\rho) \end{pmatrix} \begin{pmatrix} \hat{x}^T & x_v^T & x_y^T \end{pmatrix}^T\end{aligned}$$

Let recall, the previously introduced state-space representation of C-EPS system and PIO:

$$EPS \text{ Plant (IV.11)} : \begin{cases} \dot{x} &= Ax + Bu + Ed + Ww \\ y &= Cx + Nn \end{cases}$$

$$PIO \text{ (IV.18)} : \begin{cases} \dot{\hat{x}}_a &= A_a\hat{x}_a + E_a\hat{d} + L_p(y - C_a\hat{x}_a) + B_a u \\ \dot{\hat{d}} &= L_i(y - C_a\hat{x}_a) \end{cases}$$

Then, the LPV extended state feedback controller is expressed as below, where additional states have been defined through designed weighting functions:

$$LPV \text{ state feedback} : u = K(\rho)\hat{d} - \begin{pmatrix} F_x(\rho) & F_v(\rho) & F_y(\rho) \end{pmatrix} \begin{pmatrix} \hat{x} \\ x_v \\ x_y \end{pmatrix}$$

$$Extended \text{ state} : \begin{pmatrix} \dot{x}_v \\ \dot{x}_y \end{pmatrix} = \begin{pmatrix} A_v & 0 \\ 0 & A_y \end{pmatrix} \begin{pmatrix} x_v \\ x_y \end{pmatrix} + \begin{pmatrix} B_v \\ 0 \end{pmatrix} v + \begin{pmatrix} 0 \\ B_y \end{pmatrix} y_1$$

Then, Fig. V.15 shows the closed-loop observer based controller.

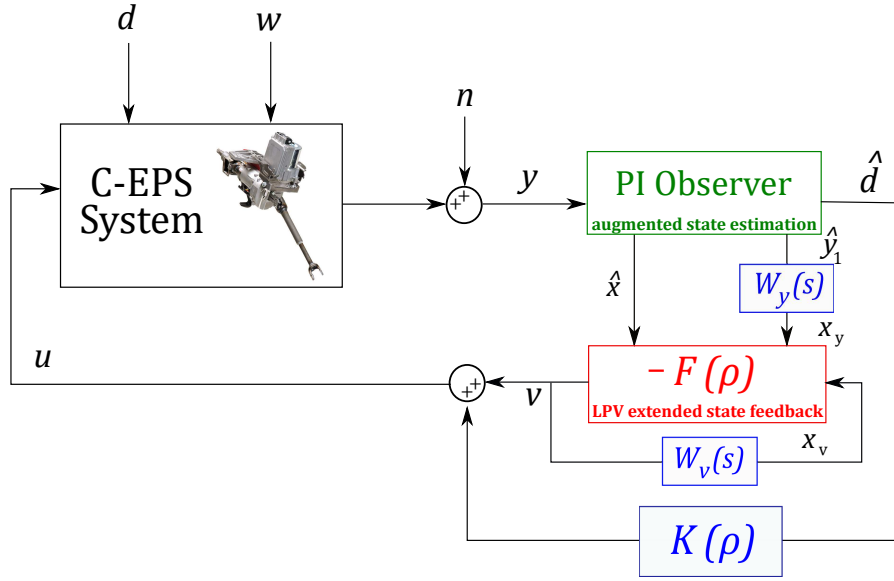


Figure V.15 – LPV extended state-feedback, closed loop

According to Fig. V.15, the closed loop system is given by:

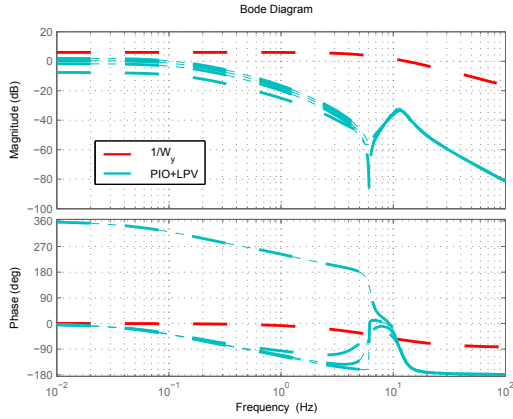
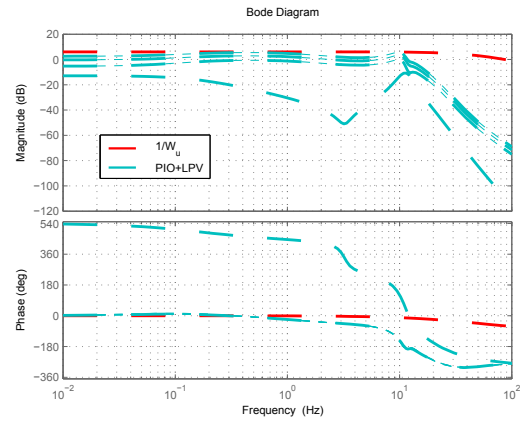
$$\left\{ \begin{array}{l} \begin{pmatrix} \dot{x} \\ \dot{x}_v \\ \dot{x}_y \\ \dot{\hat{x}} \\ \dot{\hat{d}} \\ \dot{x}_w \end{pmatrix} = \begin{pmatrix} A & -BF_v(\rho) & -BF_y(\rho) & -BF_x(\rho) & BK(\rho) & WC_w \\ 0 & A_u - B_u F_v(\rho) & -B_u F_y(\rho) & -B_u F_x(\rho) & 0 & 0 \\ 0 & 0 & A_y & B_y C_1 & 0 & 0 \\ L_p C & -BF_u(\rho) & -BF_y(\rho) & A - L_p C - BF_x(\rho) & E + BK(\rho) & 0 \\ L_i C & 0 & 0 & -L_i C & 0 & 0 \\ 0 & 0 & 0 & 0 & 0 & A_w \end{pmatrix} \begin{pmatrix} x \\ x_v \\ x_y \\ \hat{x} \\ \hat{d} \\ x_w \end{pmatrix} \\ \\ + \begin{pmatrix} E \\ 0 \\ 0 \\ 0 \\ 0 \\ 0 \end{pmatrix} d + \begin{pmatrix} WD_w \\ 0 \\ 0 \\ 0 \\ 0 \\ B_w \end{pmatrix} \bar{w} + \begin{pmatrix} 0 \\ 0 \\ 0 \\ L_p N \\ L_i N \\ 0 \end{pmatrix} n \\ \\ u = \begin{pmatrix} 0 & -F_v(\rho) & -F_y(\rho) & -F_x(\rho) & K(\rho) & 0 \end{pmatrix} \begin{pmatrix} x \\ x_v \\ x_y \\ \hat{x} \\ \hat{d} \\ x_f \end{pmatrix} \end{array} \right. \quad (V.31)$$

The closed-loop performance for frozen parameters, where the gridded points are defined by ρ and with a very simplified symmetric assistance curve $K(\rho)$

$$\rho = [-10 \quad -5 \quad -1 \quad 0 \quad 1 \quad 5 \quad 10] Nm$$

$$K(\rho) = [1.5 \quad 2 \quad 1 \quad 0 \quad 1 \quad 2 \quad 1.5]$$

are shown on the figure below. Fig. V.16 presents the transfer function from driver torque τ_d to steering wheel speed $\dot{\theta}_c$ and the weighting function W_y^{-1} , while Fig. V.17 presents the transfer function from driver torque τ_d to control signal u and the weighting function W_v^{-1} . In both cases, the closed-loop systems meet the requirements defined in the design and guarantee the H_∞ performance. Moreover, regarding Fig. V.17 the transfer $\frac{u}{\tau_d}$ ($\rho = 0$) shows that the motor torque provides an assistance torque (the amount is varying depending on operating point ρ) that acts in the same way as the driver torque.


Figure V.16 – (a) $\frac{\dot{\theta}_c}{\tau_d}$, PIO+LPV SF

Figure V.17 – (b) $\frac{u}{\tau_d}$, PIO+LPV SF

The performances using PIO+LPV are illustrated in simulation. Then, the above design has been implemented on the real system with the experimental results shown in section V.6.

V.4 EPS control design without driver torque estimation

In the previously presented studies, the steering torque is either measured (torque sensor) or estimated in order to define (through a *base assist*) the amount of steering assistance required such that the steering effort felt by the driver is ensured to be reduced in accordance with a good transmission of road information. However, the steering torque estimation involves less cost than using a torque sensor but needs the steering wheel angle and the motor angle as measurements (two different sensor signals). Very few studies have been realised on other way than based on the steering torque to produce an appropriate assistance torque to the driver. Nevertheless, industrials have been interested in this field [Varunjikar 2016, Champagne 2014, Champagne 2016] which also requires few measurements available on the vehicle. Considering the torque sensor degradation, the amount of assistance could be computed based on a steering load estimation. However, the steering rack loads acting on EPS varies according to road surface condition (low μ), driving manoeuvre, hence the assist torque needs to be adjusted according to those conditions. Therefore, the trade-off between feeling and assistance level is made difficult as there is a lack on direct driver's intention.

In this section, the control structure presents the advantage to use a minimum number of sensor data, e.g only the steering wheel angle is assumed to be measured in addition to vehicle

data. Indeed, such strategy presents some benefits which are: to reduce EPS production cost since the motor angle sensor integrated in EPS systems is no more required, and also to reach a wider range of vehicles regarding a back-up mode then gain more customers. Hence, considering the lower cost EPS system requirements, a nominal control for an industrial purpose is presented and also a H_∞ dynamic output feedback controller has been developed.

V.4.1 Torsion-BarLess Control (TBLC)

Torsion-BarLess Control is applied on a EPS system with a simplified mechanical structure, as torque sensor and torsion bar are suppressed (indeed, this strategy does not require to estimate the steering torque). TBLC aims at providing a nominal performance concerning assistance torque and steering feel. TBLC is expected to provide an assistance amount based only on vehicle data (lateral acceleration, vehicle speed) and steering wheel data (position and speed) such that a minimum number of sensor data is required. Indeed, this strategy is expected to reach low-cost EPS systems market.

TBLC general concept is depicted in Fig. V.18 where μ name the road surface adhesion (low μ is for slippery, icy road while high μ is for concrete, asphalt road):

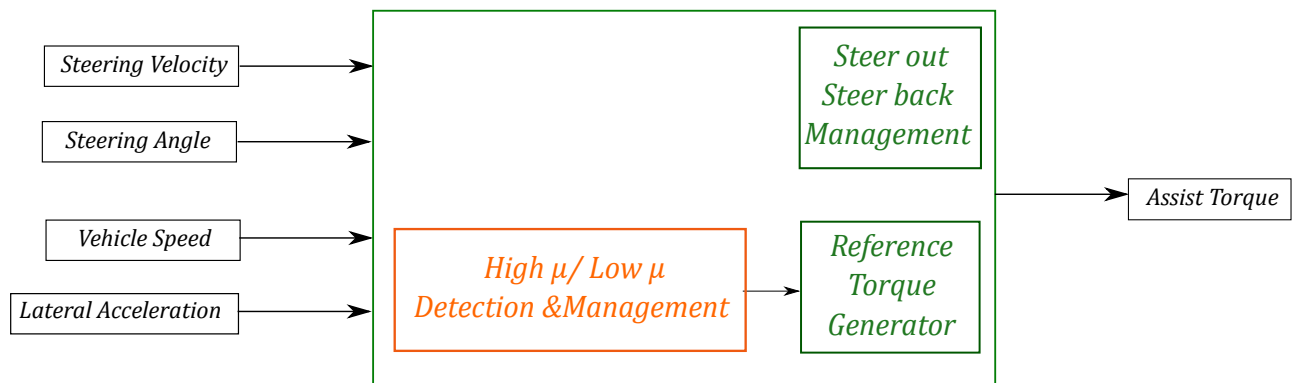


Figure V.18 – Torsion-BarLess Control diagram (JTEKT)

As shown in Fig. V.18, TBLC principle is based on a motor target torque generator which depends on road conditions and also on steering manoeuvre (as explained in III.3.1 steer out requires more assistance torque than steer back in rolling condition, as in the latter case the self-aligning torque is acting in the same way which makes the steering easier).

- a motor target torque generator similar to the one described in [Michelis 2011] computes an appropriate assistance torque to support the driver (a combination of various weighting sideways acceleration). However, as the torque sensor is not measured, a rack force model is introduced to compute the force that the driver needs to counter.
- a steer out, steer back management block (a detection on which condition based on steering wheel angle and velocity) has been developed in order to weight (an adjusting coefficient) the assistance torque involved. Indeed, steer back requires less assistance torque, as the vehicle dynamic (self-aligning torque) tends towards the same motion than the driver, whereas it is the inverse in steer out. Thus, if the same assistance torque was provided regardless of the case, it would result in a bad driving feel.

- a high μ , low μ detection and management block needs also to be introduced to handle the variation in assistance torque due to road conditions. Indeed, on low friction road surface (like snow or ice) the road reaction force applied on the rack is weaker than on high friction road (like asphalt). Thus, if a same assistance torque was provided regardless of the case, it would result in an over-assistance on ice surface which might involve an undesirable loss of grip.

The performances obtained using TBLC are illustrated in the experimental results section.

V.4.2 H_∞ dynamic output feedback controller

In literature, some robust control theory have been applied on EPS systems, and H_∞ controller have been designed, an overview is given as an introduction.

In [Chen 2005], a two controllers structure is proposed including a motion controller (\mathcal{H}_2 optimal controller) to attenuate the road disturbance and a motor controller (PI) to reach fast response. The first controller is related to the driver's feeling while the second is addressed for sufficient assistance torque. The same architecture is used in [Li 2009a] nevertheless, a robust \mathcal{H}_∞ mixed sensitivity controller is designed using weighting functions to attenuate the road disturbance at high frequency. A comparative synthesis is done in [Chen 2008b].

In this section, a H_∞ dynamic output feedback controller is designed considering the steering wheel angle as available output while in the previous studies torque sensor signal was considered as output.

V.4.2.1 Controller synthesis

According to the restricted assumption that only the steering wheel angle is measured (corresponding to $y = \theta_c$ in this section). A conventional EPS control strategy based on a characteristic curve to generate assistance torque is not used. Indeed, another approach based on angle is proposed in this framework. Then, no observer design is needed and the steering torque remains unknown. Consequently, the first step is to verify that the proposed controller is still able to provide convenient steering assistance (i.e to support the driver in his manoeuvre), and is not interested in driver feeling. Moreover to simplify the problem, the road disturbance is not considered as an external input, but expressed through parameter uncertainty. The transfer function of the C-EPS system is given by:

$$y = G_{yd}(s)\tau_d + G_{yu}(s)\tau_m \quad (\text{V.32})$$

corresponding to the state-space representation in (IV.4.2)

$$\begin{cases} \dot{x} &= Ax + Bu + Ed \\ y &= Cx \end{cases} \quad (\text{V.33})$$

where $x = \begin{pmatrix} \dot{\theta}_c & \dot{\theta}_m & \theta_c & \theta_m \end{pmatrix}^T \in \mathbb{R}^4$ the state vector, $u = \tau_m \in \mathbb{R}$ the control signal, $d = \tau_d \in \mathbb{R}$ the driver torque and $y = \theta_c \in \mathbb{R}$ the measured steering wheel angle.

Some works in EPS systems developed controllers tracking a reference angle target: in [Coudon 2007] a simple reference model where an ideal front wheel angle is generated, whereas in [Marouf 2012a] a reference model is designed to obtain an ideal motor angle.

Similarly, a H_∞ controller synthesis is proposed according to angle control on EPS system, as illustrated in Fig. V.19. The following transfer functions $T_d(s)$, $W_z(s)$ and $W_u(s)$ have been introduced only for synthesis purpose (not concerned with implementation issue) to get the controller $K(s)$, with EPS plant represented by $G_{yd}(s)$ and $G_{yu}(s)$.

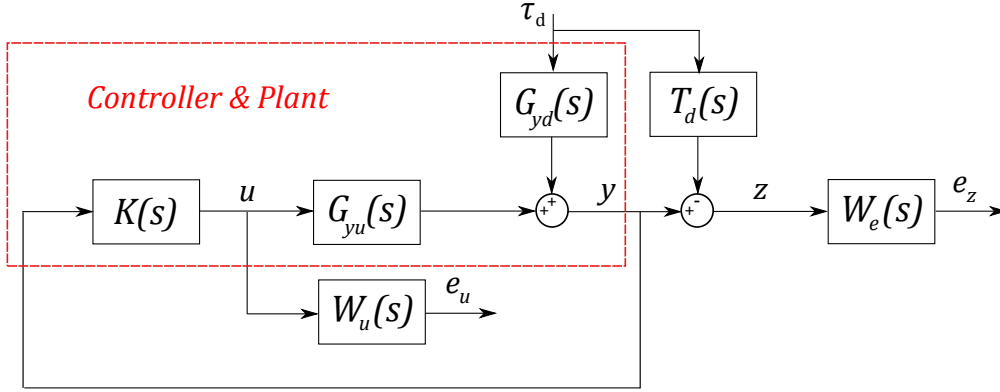


Figure V.19 – \mathcal{H}_∞ Control Scheme

The design parameters are:

- Matching function, defining the performance level, according to the transfer function from the driver input to the steering wheel angle

$$\tau_d = T_d(s)y_r \quad (\text{V.34})$$

- Weighting functions for tracking error and actuator constraints:

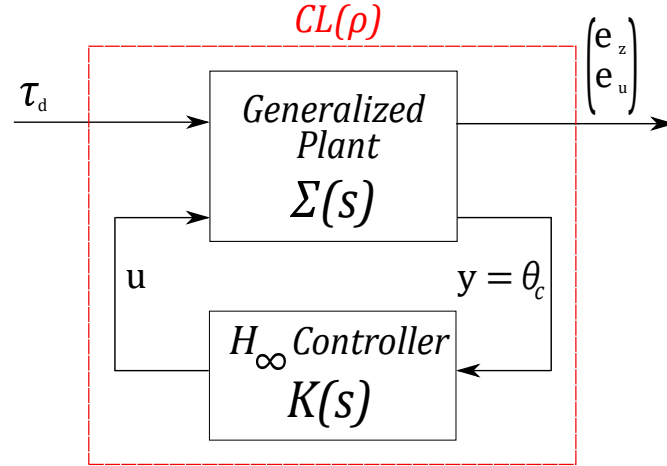
The driver characteristics are the following: acting frequency up to $5Hz$ and maximum driver torque expected is $10Nm$ (corresponds usually to the torque sensor saturation value).

$$\frac{1}{W_e} = \frac{s + \omega_b \varepsilon}{\frac{s}{M_s} + \omega_b} \quad (\text{V.35})$$

The actuator characteristics is such that the bandwidth is from $30Hz$ to $50Hz$ and motor torque maximum is $5Nm$.

$$\frac{1}{W_u} = \frac{\varepsilon_1 s + \omega_{bc}}{s + \frac{\omega_{bc}}{M_u}} \quad (\text{V.36})$$

Fig. V.19 is usually transformed into the standard H_∞ control configuration of Fig. V.20 in order to design the H_∞ controller $K(s)$.

Figure V.20 – General H_∞ control formulation

Then the state space representation of the generalized plant P :

$$\begin{cases} \dot{x} &= Ax + B_d d + B_u u \\ z &= C_z x + D_{dz} d + D_{uz} u \\ y &= C_y x + D_{dy} d + D_{uy} u \end{cases} \quad (\text{V.37})$$

where $z = (e_z \ e_u)^T$ is the controlled outputs and $d = \tau_d$ is the driver torque (external input).

The dynamic output feedback controller is defined as $K(s)$:

$$\begin{cases} \dot{x}_k &= A_k x_k + B_k y \\ u &= C_k x_k + D_k y \end{cases} \quad (\text{V.38})$$

Therefore, the closed-loop system is:

$$\begin{cases} \begin{pmatrix} \dot{x} \\ \dot{x}_k \end{pmatrix} &= \begin{pmatrix} A + B_u D_k C_y & B_u C_k \\ B_k C_y & A_k \end{pmatrix} \begin{pmatrix} x \\ x_k \end{pmatrix} + \begin{pmatrix} B_d + B_u D_k D_{dy} \\ B_k D_{dy} \end{pmatrix} d \\ z &= \begin{pmatrix} C_z + D_{uz} D_k C_y & D_{uz} C_k \end{pmatrix} \begin{pmatrix} x \\ x_k \end{pmatrix} + \begin{pmatrix} B_d + B_u D_k D_{dy} \end{pmatrix} y \end{cases} \quad (\text{V.39})$$

Then, the objective is to find $K(s)$, the matrices A_k , B_k , C_k and D_k subject to the \mathcal{H}_∞ norm of the closed loop system is as small as possible: $\min. \gamma_\infty$ such that $\|T_{zd}(s)\|_\infty < \gamma_\infty$. The controller could be obtained by solving using a LMI approach of the H_∞ control problem (Bounded Real Lemma) [Gahinet 1994].

V.4.2.2 Design analysis

The closed-loop performance illustrated on Fig. V.22 presents the transfer function from driver torque τ_d to tracking error e_y and the weighting function W_e^{-1} , while Fig. V.21 presents the transfer function from driver torque τ_d to control signal u and the weighting function W_u^{-1} . In both cases, the closed-loop systems meet the requirements defined in the design and guarantee the H_∞ performance. Moreover, the transfer $\frac{u}{\tau_d}$ in Fig. V.21 ensures that the motor torque

provides an assistance torque (the phase starts at 0° with a gain greater than 1) to help the driver. Besides, Fig. V.22 shows that the tracking error is very low (less than $-40dB$), then the reference steering wheel angle is reached.

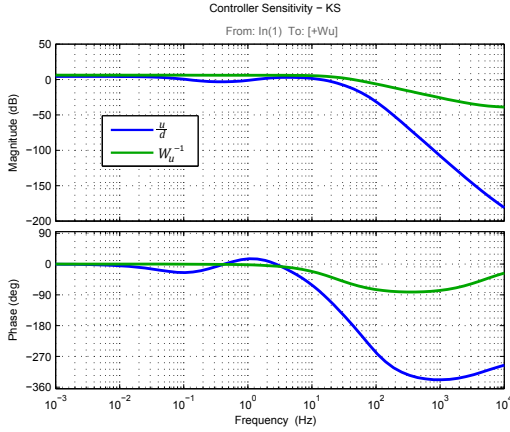


Figure V.21 – Controller Sensitivity

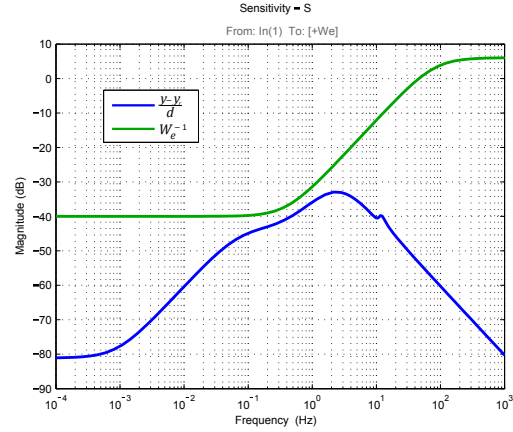


Figure V.22 – Sensitivity

V.5 Simulation Results

In this section, some simulation results according to simulation environment of Fig. III.12 are presented. Therefore, it includes EPS system, actuator dynamic and non-linear road reaction force model. Indeed, simulation allows to verify controller performances before implementation, mainly steering level and stability.

Regarding an EPS controller, its performances are assessed through the driver steering feel and comfort. However, these characteristics are subjective since drivers' profile (skill, sensitivity) are varied. Thus, there are no well-defined measurements to quantify it. Several works have been carried out to define the relationship between steering feel (rating) and vehicle handling (measurements) in [Rothhämel 2010, Rothhämel 2011]. Similarly in [Dang 2014, Dang 2015], the correlations between subjective and objective evaluations considering on centre steering feel (a small steering wheel angle range) have been studied. Nevertheless, these elements remain only guidelines to meet a satisfactory steering characteristics. Hence, steering feel issues are evaluated subject to the plot of the driver torque τ_d against the steering wheel angle θ_c as illustrated in [Morita 2009] and in [Yili 2009] where the Lissajous curve of steering torque and steering angle show the driver feeling (steering ability results in smoothness on the plot, and an appropriate steering effort could be also judged). A similar steering characteristic as in [Yamamoto 2011] is illustrated on Fig. V.23 (for rolling conditions).

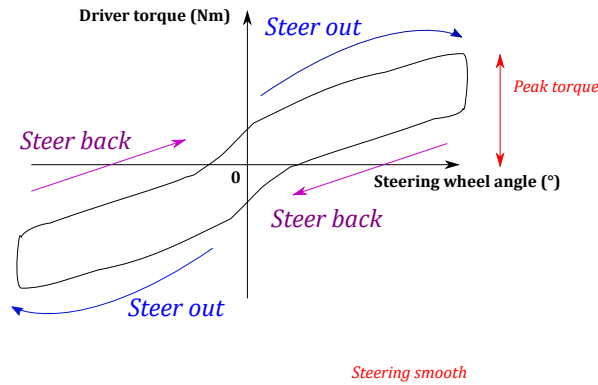


Figure V.23 – EPS Characteristics - Steering feeling

V.5.1 Simulation of the LQR observer-based controller

Simulation using the $\mathcal{H}_2/\mathcal{H}_\infty$ PIO and LQR controller (see V.3.2) have been realised. Moreover, a simple EPS control law $u = k\tau_d$ (dash green) is plotted as a comparison in order to evaluate the assistance level.

A sinusoidal driver input at 8 Nm and 0.1 Hz in parking have been realised. Performance is shown according to Fig. V.24 through the steering wheel angle function of driver torque plot. The rack force involved in parking is given on Fig. V.25 corresponding to almost 33 Nm at pinion side to counter. Indeed, a good amount of assistance torque is provided since 8 Nm is sufficient to realise a lock-to-lock manoeuvre in parking.

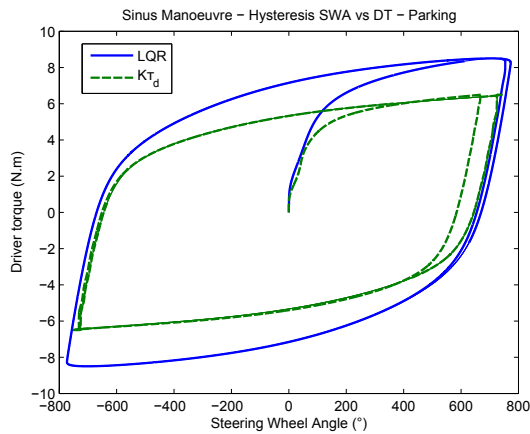


Figure V.24 – (a) θ_c VS τ_d
PIO+LQR 0kph

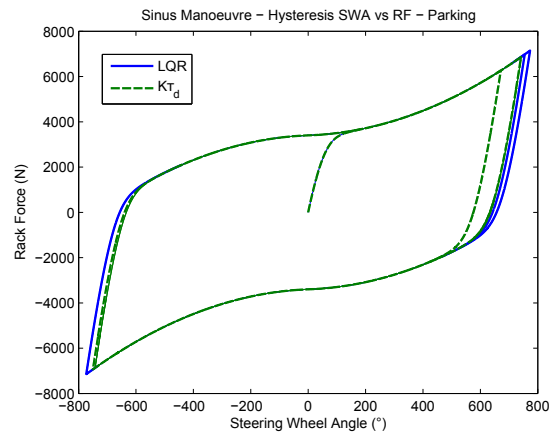


Figure V.25 – (b) θ_c VS F_r
PIO+LQR 0kph

A sinusoidal driver input at 3 Nm and 0.05 Hz at 15 kph have been realised. Performance is shown according to Fig. V.26 through the steering wheel angle function of driver torque plot. The rack force involved at 15 kph is given on Fig. V.27 corresponding to almost 11 Nm at pinion side to counter. According to the simulation, the driver needs only 3 Nm to turn the steering wheel almost up to 450° , this means that the vehicle is easy to handle.

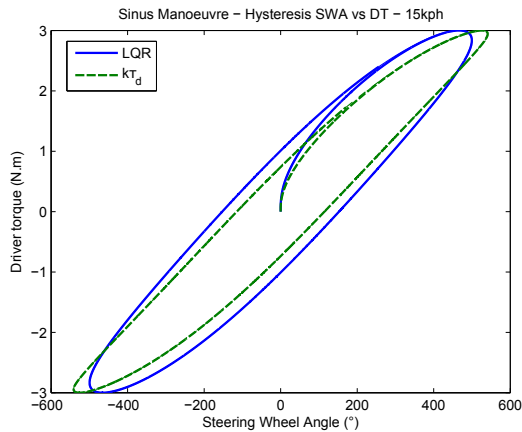


Figure V.26 – (a) θ_c VS τ_d
PIO+LQR 15kph

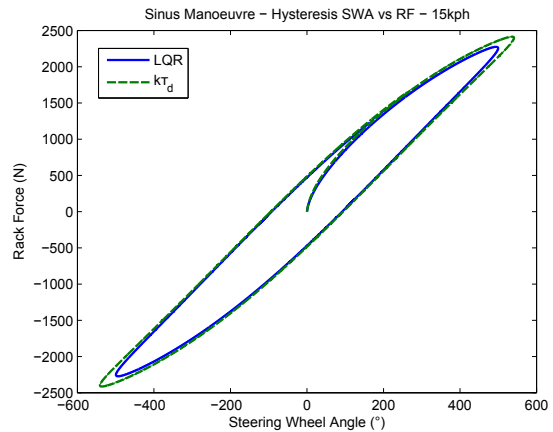


Figure V.27 – (b) θ_c VS F_r
PIO+LQR 15kph

A sinusoidal driver input at 5 Nm and 0.1 Hz at 30 kph have been realised. Performance is shown according to Fig. V.28 through the steering wheel angle function of driver torque plot. The rack force involved at 30 kph is given on Fig. V.29 corresponding to almost 20 Nm at pinion side to counter, it could be noticed that beyond 300°, the rack force is decreasing which indicates gradually a loss of grip.

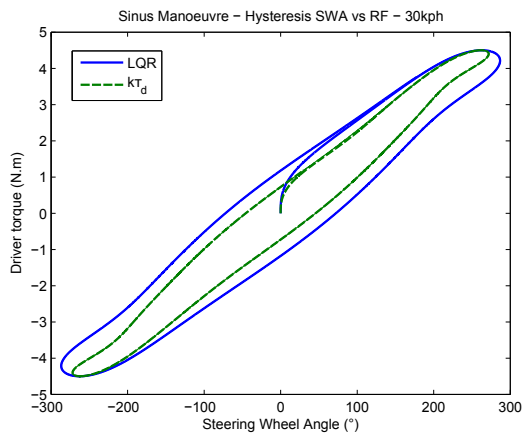


Figure V.28 – (a) θ_c VS τ_d
PIO+LQR 30kph

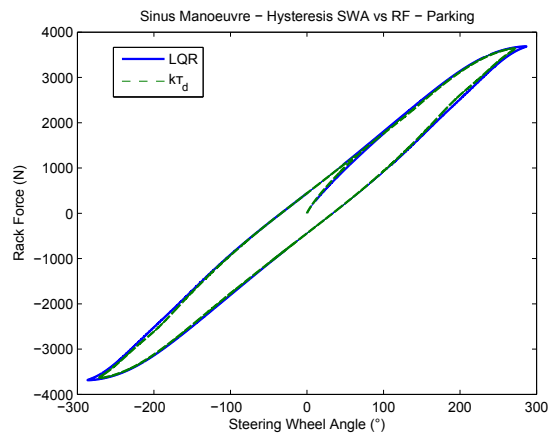


Figure V.29 – (b) θ_c VS F_r
PIO+LQR 30kph

These simulation results show that the proposed LQR controller based on a PIO provides a good steering performance and feeling in overall, as the obtained curves are close compared to the simple EPS control law. Moreover, the driver torque required to steer the wheel remains less than 10 Nm (even less than 5 Nm in rolling conditions) and the hysteresis shape is smooth.

V.5.2 Simulation of the LPV observer-based state feedback controller

Simulation using the $\mathcal{H}_2/\mathcal{H}_\infty$ PIO and LPV controller (see Fig. V.15) have been realised. Moreover, a JTEKT controller with a reduced assistance (dot magenta), which is different from the previous simple control law $u = k\tau_d$, is plotted as a comparison in order to evaluate the overall vehicle handling (steering and feeling).

A sinusoidal driver input at 5 Nm and 0.05 Hz at 15 kph has been realised. Performance is shown according to Fig. V.30 through the steering wheel angle function of driver torque plot. The rack force involved at 15 kph is given on Fig. V.30 corresponding to almost 10 Nm at pinion side to counter. According to the simulation, the driver torque level is convenient as it requires almost 5 Nm to turn the steering wheel once. Besides, the on-centre steering characteristic is more similar to Fig. V.23 than Fig. V.26.

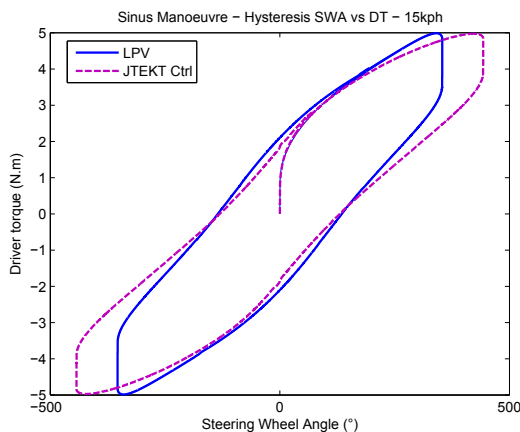


Figure V.30 – (a) θ_c VS τ_d
PIO+LPV SF 15kph

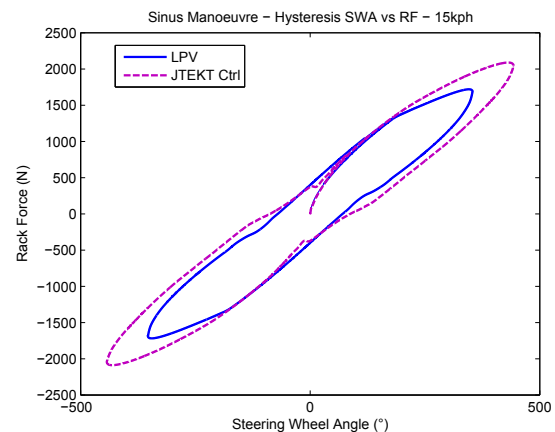


Figure V.31 – (b) θ_c VS F_r
PIO+LPV SF 15kph

A sinusoidal driver input at 8 Nm and 0.1 Hz at 30 kph have been realised. Performance is shown according to Fig. V.32 through the steering wheel angle function of driver torque plot. The rack force involved at 30 kph is given on Fig. V.32 corresponding to almost 15 Nm at pinion side to counter. The driver torque is higher at 30 kph than at 15 kph, nevertheless assistance level remains rather good, less than 8 Nm.

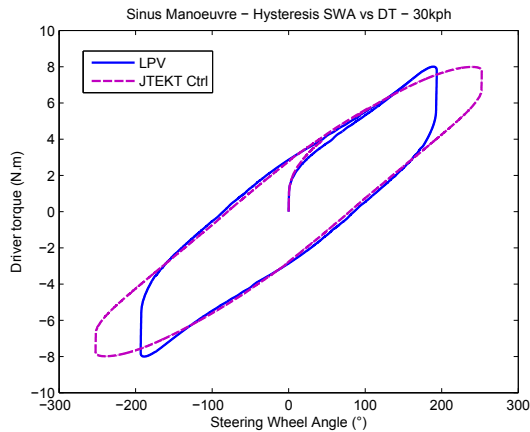


Figure V.32 – (a) θ_c VS τ_d
PIO+LPV SF 30kph

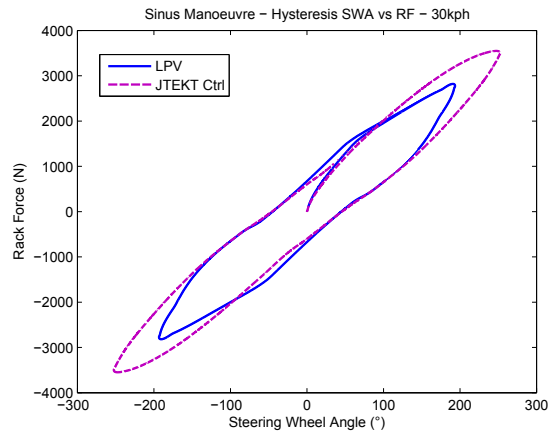


Figure V.33 – (b) θ_c VS F_r
PIO+LPV SF 30kph

These simulation results show that the proposed LPV controller based on PIO achieves a good driver feeling and assistance as the hysteresis shapes are close compared with JTEKT controller. Moreover, the assistance motor part provides half the torque required to turn the vehicle wheels which could be improved.

V.5.3 Simulation of H_∞ dynamic output feedback controller

Simulation using the H_∞ dynamic output feedback controller has been realised. Contrary to previous strategies this one is not based on any driver torque information. Then, the simulation aims at verifying that a steering support is provided to the driver, therefore a comparison with no assistance case $u = 0$ (red) has been realised in order to evaluate the assistance level.

A sinusoidal driver input at 6 Nm and 0.1 Hz at 30 kph have been realised. Fig. V.34 shows the steering wheel angle function of driver torque plot, while Fig. V.35 shows the steering wheel angle function of rack force involved at 30 kph, in both case (H_∞ controller and no assist).

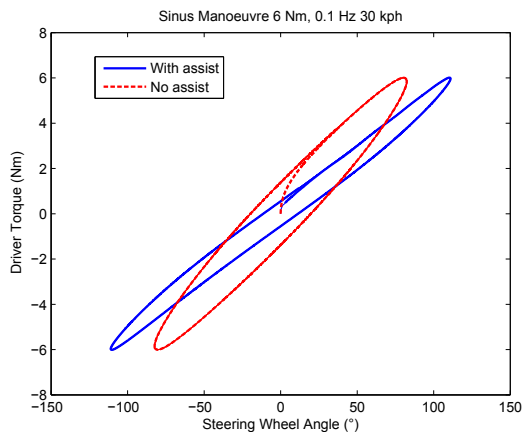


Figure V.34 – (a) θ_c VS τ_d
 H_∞ controller 30kph

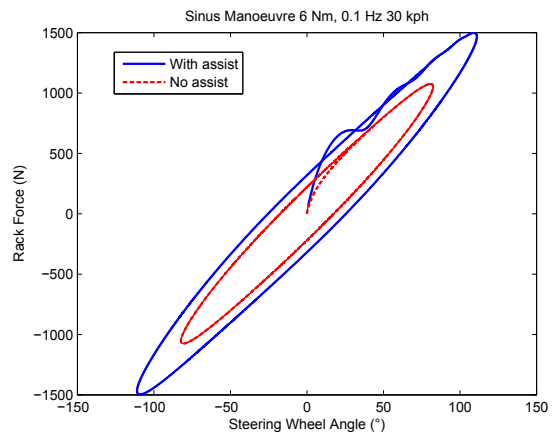


Figure V.35 – (b) θ_c VS F_r
 H_∞ controller 30kph

The result shows that the proposed method enables to provide some steering support and reduce the hysteresis.

V.6 Experimental Results

Several strategies have been implemented and tested on real systems depending on application objectives. Indeed, the proposed TSLC has been implemented on a DP-EPS test car (B-class, a heavy vehicle) according to its target, i.e a back-up control. Some tests results at high speed are shown, since SLOA at high velocity is more surprising and dangerous (severe safety issue). Therefore, TSLC steering feel under these conditions have been evaluated.

Besides, the strategies developed in order to reach a reduced EPS systems cost production, have been implemented on another test car (Clio IV, a light vehicle) equipped with one of the following prototype C-EPS. *Proto 1* is composed of a nominal torsion bar stiffness and a prototype pinion gear (a low pinion/rack ratio), while *Proto 2* is composed of a nominal pinion gear and a mono-bloc pinion shaft (no torsion bar). Indeed, both EPS conceptions reduce the cost as torque sensor is removed, and even more for *Proto 2* according to additional components savings. The PIO based controllers (LQR and LPV) have been implemented with *Proto 1* setting as the driver torque is still estimated in this concept, whereas the TBLC is implemented with *Proto 2* setting. Indeed, *Proto 2* from its mechanical structure involves to review the EPS model whereas *Proto 1* keeps the same structure as a standard EPS system (only a parameter modification in the model). Thus, this combination between *Protos* and control strategies has been tested. The on board vehicle environment has been introduced in the chapter III.5. Some tests results at low and nominal speed are shown, since the steering effort is mostly required at these velocities (too heavy in case there is no assistance). Therefore, steering assistance level and driver feeling under these conditions has been evaluated.

The experimental configuration is summarized in the table V.1 below.

| Test car | Mechanics | Control | Test conditions |
|----------|----------------------|----------------------|----------------------------|
| B-Class | DP-EPS | TSLC | 50, 90 kph (high speed) |
| Clio IV | C-EPS <i>Proto 1</i> | PIO based controller | 7, 15 kph (low speed) |
| | C-EPS <i>Proto 2</i> | TBLC | 30, 50 kph (nominal speed) |

Table V.1 – Set-up experimental conditions

V.6.1 Torque SensorLess Control

TSLC has been implemented on a B-Class equipped with a mass-produced DP-EPS system using an embedded software. Indeed, back-up mode is more targeted on heavy vehicle like sedan, as the gap to steer the wheel between loss of assistance and with assistance is large. Fig. V.36 presents the implementation of TSLC as described in V.3.1. The measurements θ_c (steering wheel angle), V_v (vehicle speed) and θ_m (from which the motor acceleration is deduced) are used in TSLC. A dynamometer steering wheel has been mounted on the vehicle which enables to measure the driver torque τ_d and an accurate steering wheel angle for performance analysis purpose.

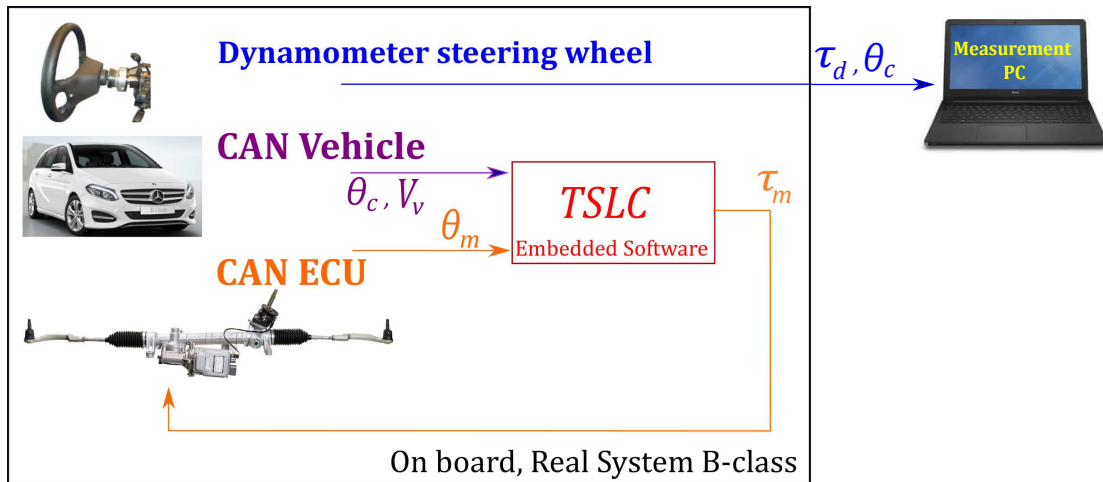


Figure V.36 – TSLC - implementation on real system

In this part, two tests results are presented under a sinusoidal manoeuvre at 50 kph and 90 kph with almost the same steering wheel angle amplitude.

Fig. V.37 (resp. V.38) illustrates the performance of TSLC obtained at 50 kph (resp. 90kph). Indeed, in both figures a comparison between the back-up mode TSLC (blue) and no assistance at all (red) is shown. Even though, in TSLC the steering torque level is rather high (especially in 90 kph compared to 50 kph), it remains better than driving without any assistance. Besides, it is typical in EPS system design that the assist level decreases as the vehicle speed increases in order to ensure a good steering feel (this is tunable through the base assist). Indeed, the difference of steering torque level under TSLC mode, could be observed by comparing both figures.

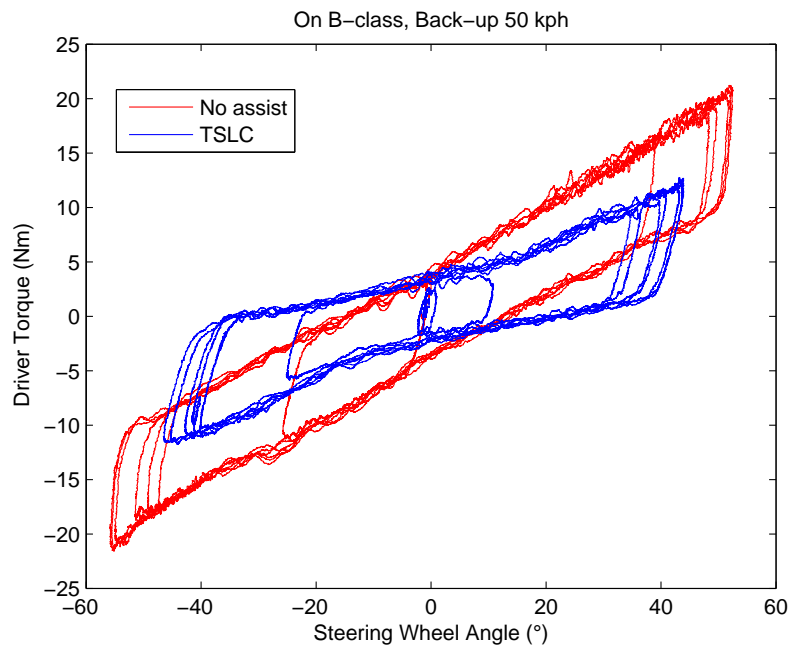


Figure V.37 – TSLC at 50 kph

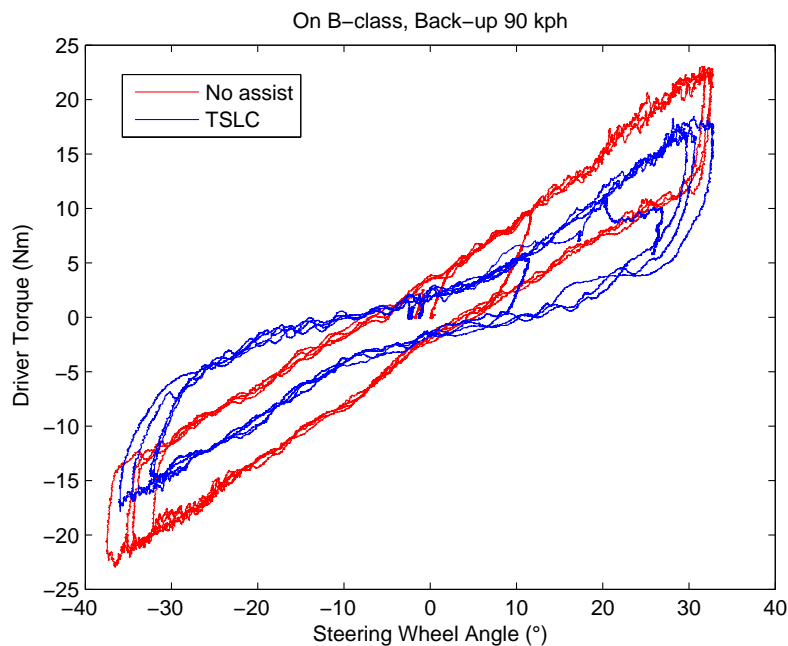


Figure V.38 – TSLC at 90 kph

TSLC keeps providing assistance to the driver even in case of torque sensor failure. Although the measured driver torque level is high, it is less than driving without any assistance: at 50 kph the steering effort achieves 12 Nm with TSLC whereas it achieves 21 Nm without assistance and at 90 kph the steering effort achieves 18 Nm with TSLC whereas it achieves 23 Nm without assistance. Considering TSLC as a back-up mode, the obtained results are sufficient enough.

Remark V.5

TSLC includes safety concept that restricts functional performance. Therefore, the steering torque level reached in TSLC during these tests is rather high, as the assistance torque is limited for safety reasons. Indeed, a trade-off between functional and safety have been realised to apply TSLC strategy.

V.6.2 State-feedback Controllers based on Proportional Integral Observer

Proportional Integral Observer and Controllers (LPV and LQR) have been implemented using Quick Prototyping (QP), on a test car Clio IV equipped with a prototype C-EPS system (nominal torsion bar stiffness) and a prototype pinion gear (a low pinion/rack ratio). At first, vehicle handling (driver torque level) has been assessed through sinusoidal manoeuvres in low frequency at different vehicle speed. Therefore, the driver torque against the steering wheel angle curve is shown subject to each test results. Indeed, driving conditions change according to vehicle speed as the road reaction transmitted to EPS evolves, see Fig V.39. Then, the steering performance under these different conditions is evaluated.

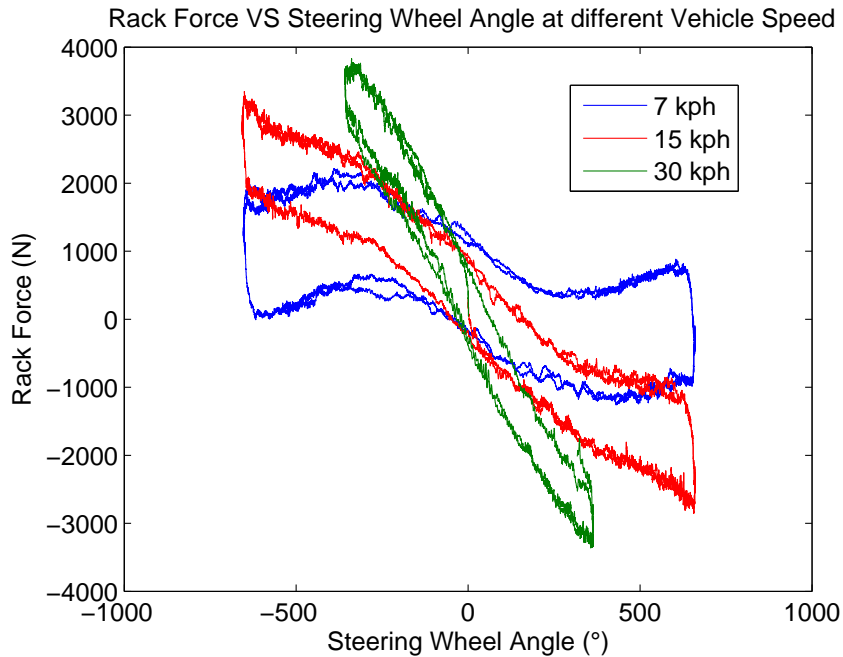


Figure V.39 – Rack Forces measured at different vehicle speed

In what follows, experimental results carried out using PIO and LQR controller are shown first, then some other results using PIO and LPV controller are presented.

V.6.2.1 LQR Controller

Referring to section V.3.2, the designed PIO and LQR controller has been discretized at sampling frequency of 1kHz and implemented on the MicroAutobox following the scheme given by Fig V.40. The measurements θ_c (steering wheel angle) and θ_m are used in the PI observer which estimates the augmented states required in the LQR controller. Besides, some additional sensors are mounted on the vehicle to measure the driver torque τ_d , the assistance motor current I_m and the forces applied on the rack F_r for performance analysis purpose.

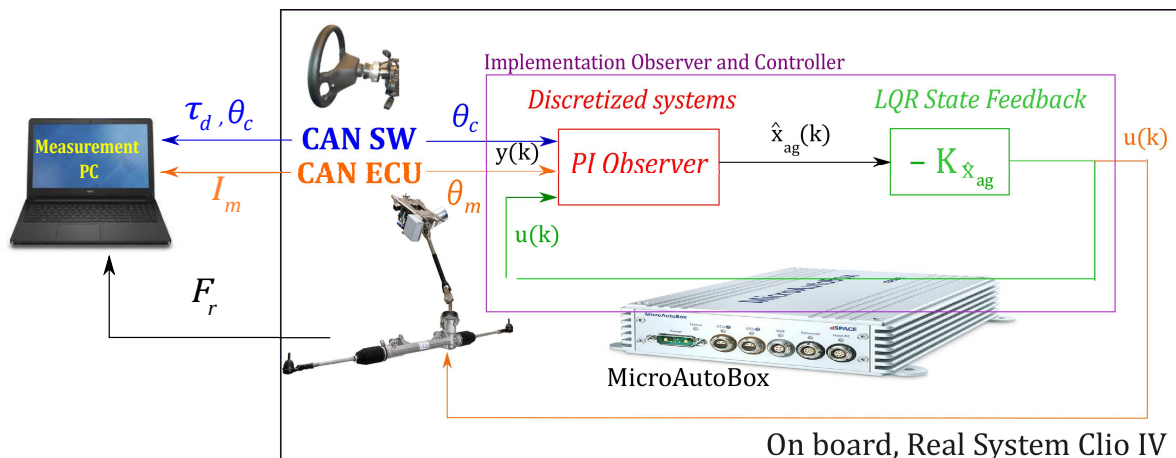


Figure V.40 – PIO+LQR controller - implementation on real system

In this part, several tests results are presented under parking and low speed (7 kph and 15 kph) under lock-to-lock manoeuvre (remind that the driver inputs a sinus on the steering wheel with the maximal angular amplitude).

Vehicle test at Parking - Lock-to-lock

At parking, the road reaction force differs widely from rolling conditions. Moreover, in a parking manoeuvre the assistance torque is to be as large as possible, and no road feedback is expected. Especially, a steady steering effort on centre, while steering out or back, is a required behaviour.

In Fig V.41, the steering wheel angle function of driver torque is plotted to assess the achieved performance. Two lock-to-lock test results are shown: in one case the driver has no assistance (red) whereas in the second the proposed LQR controller is applied (blue). Indeed, the driver needs to provide around 20 Nm in case there is no assistance while with assistance the driver input is around 5 Nm in average (therefore much less steering effort is required). Furthermore, the hysteresis shape remains similar and the difference in amplitude indicates that the steering performance obtained is acceptable.

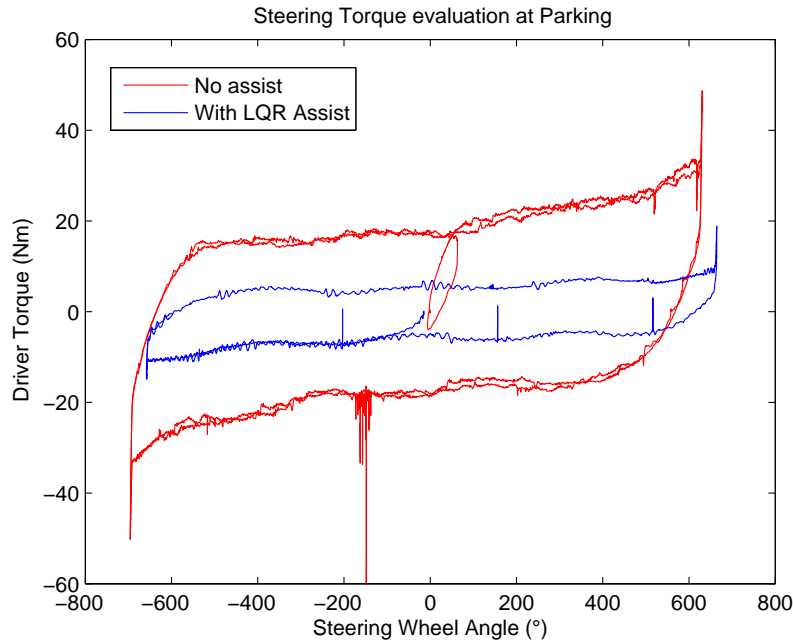


Figure V.41 – PIO+LQR at parking - Hysteresis θ_c VS τ_d

In Fig V.42, the three EPS inputs (rack force (blue), driver torque (red) and assistance torque (green)) are measured during the previous tests. The signals are formulated at pinion level and their evolution according to time is shown in the test case including assistance.

Hence, the sum of applied torques at the pinion side at equilibrium could be represented by:

$$\tau_d + R_m \tau_m - F_r R_p - F_f R_p = 0 \quad (\text{V.40})$$

where the pinion assistance torque $R_m \tau_m$ supports the driver torque τ_d to counter the rack force F_r and the friction force acting on the rack F_f in order to turn the vehicle front wheels.

Regarding (V.40) it is worth noting that a high assistance torque results directly in reducing the driver torque to steer the wheels. Therefore, the steering effort could also be evaluated considering driver and assist motor torque evolutions.

Indeed as illustrated in Fig V.42, the amount of rack force that the driver needs to overcome in order to turn the vehicle wheels is very high. However, the driver torque and the assistance torque act in the same direction, and the sum of torques result in tire motion. Moreover, the driver torque is weaker than the assistance torque which means that the steering effort is almost provided by the assist motor (counters almost all the road reaction force). Besides, the assistance torque curve is almost twice the driver torque one, which approximates the most simple way to ensure assistance, *i.e* to provide a proportional amount $K_a\tau_d$. Therefore, an acceptable steering performance is obtained at parking.

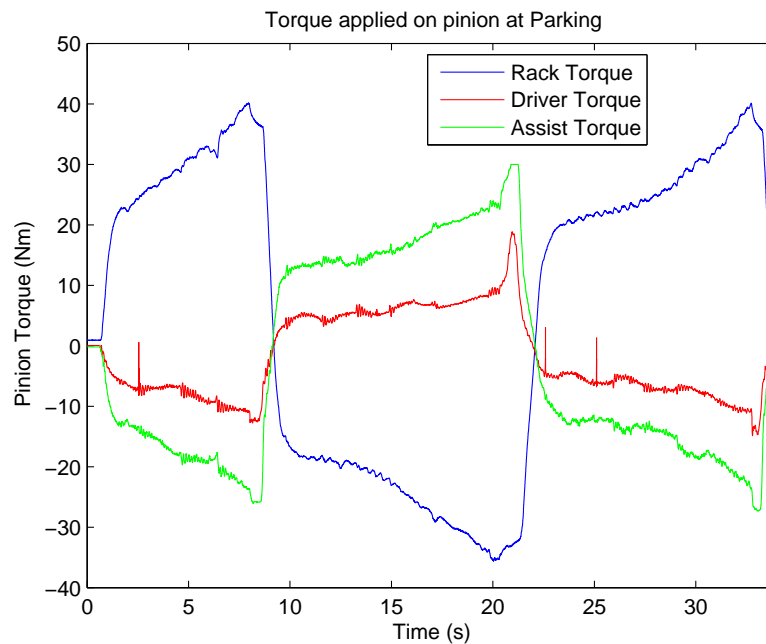


Figure V.42 – PIO+LQR at parking - Evolution of involved torques

Vehicle test at low speed - Lock-to-lock

In Fig V.43, steering wheel angle function of driver torque is plotted. Two tests results are shown, from a same manoeuvre but at different vehicle speed: one at 7 kph (blue) and the other one at 15 kph (green). It could be noticed that the driver torque is very low, less than 5 Nm.

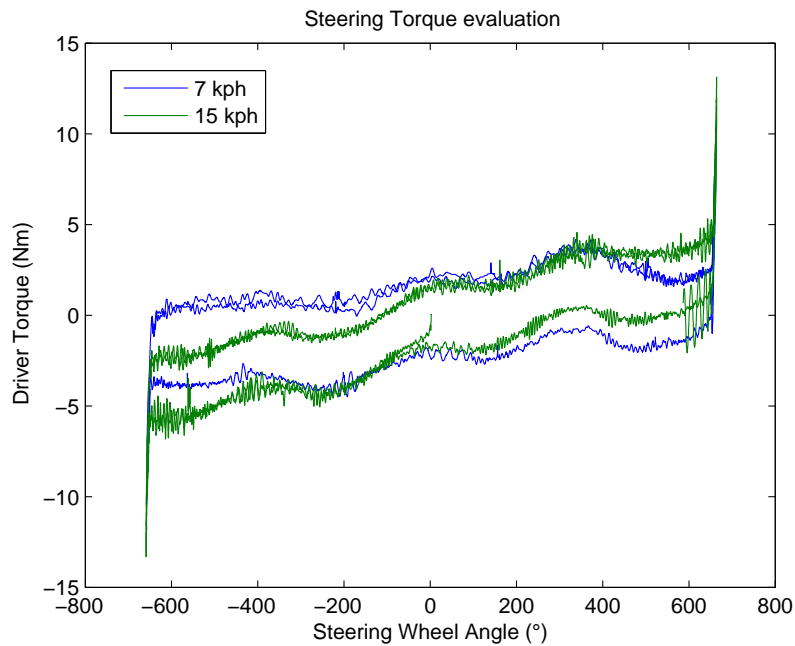


Figure V.43 – PIO+LQR at 7 and 15 kph - Hysteresis θ_c VS τ_d

Nevertheless, the driver feeling is degraded at 7 kph, as the torque level drops during steering out at high steering angle (from 400° to 650° the driver torque decreases from 4Nm to 2Nm). Moreover, the driver needs to provide some inverted torque (around -2Nm) when steering back. Thus, the hysteresis is not smooth enough to provide a good steering feel, although the steering level is satisfying. Also, torque ripple appears at high steering wheel angle at 15 kph, which degrades the driver feeling and steering comfort (around -600° the torque ripple amplitude is nearly $\pm 0.7\text{Nm}$). Regarding nominal steering performance objective, a better result is expected.

Indeed, the designed LQR controller is well suited for parking. Consequently, a too high steering assistance is provided in rolling conditions, as the road reaction force behaves too differently between parking (Fig. III.21 in III.6.2) and rolling (Fig. V.39). Therefore, a LPV controller has been implemented to improve the driver feeling.

V.6.2.2 LPV Controller

Referring to section V.3.3, the designed PIO and LPV extended state feedback have been discretized at sampling frequency of 1kHz and implemented on the MicroAutobox following the scheme given by Fig V.44. The measurements θ_c (steering wheel angle) and θ_m are used in the PI observer which estimates the augmented states required in the LPV controller. Besides, some additional sensors are mounted on the vehicle to measure the driver torque τ_d , the assistance motor current I_m and the forces applied on the rack F_r for performance analysis purpose.

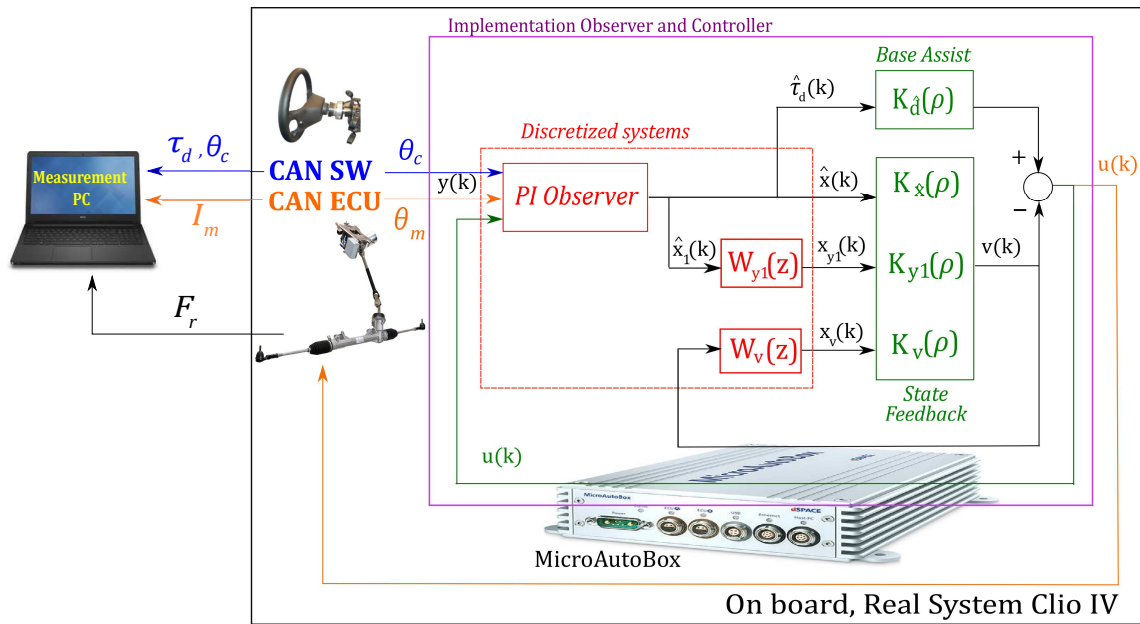


Figure V.44 – PIO and LPV extended state feedback - implementation on real system

In this part, several tests results are presented under different vehicle speeds (7 kph, 15 kph and 30 kph) subject to a sinusoidal driver input. Furthermore, some in-depth tests have been carried out such as higher steering dynamics, stick-slip or even rolling on low friction course.

Remark V.6

Besides, a synthesis in discrete time could have been performed, nevertheless in this considered case, the bandwidth of the system is very small compared to the sampling frequency.

Vehicle test at 7 kph - Sinus manoeuvre

When started in first gear a corresponding vehicle speed is around 7 kph, so carrying out vehicle test at this velocity is representative of assistance level required at very low speed. Hence, sinusoidal and lemniscate pattern manoeuvres have been realized on the dynamic pad of JTEKT test ground.

In Fig V.45, steering wheel angle function of driver torque is plotted, indeed it gives the performance achieved. Two tests results are shown, even though both results from sinusoidal test, steering wheel amplitude is different: a free sinus is realised by the driver (blue) while a calibrated sinus on the lemniscate is realised (purple). In both case, the steering torque remains low, less than 5Nm, which means that the driver is well assisted in its manoeuvre. However, compared with Fig. V.43 the steering effort is a bit heavier but the steering feel is better as the hysteresis is smoother.

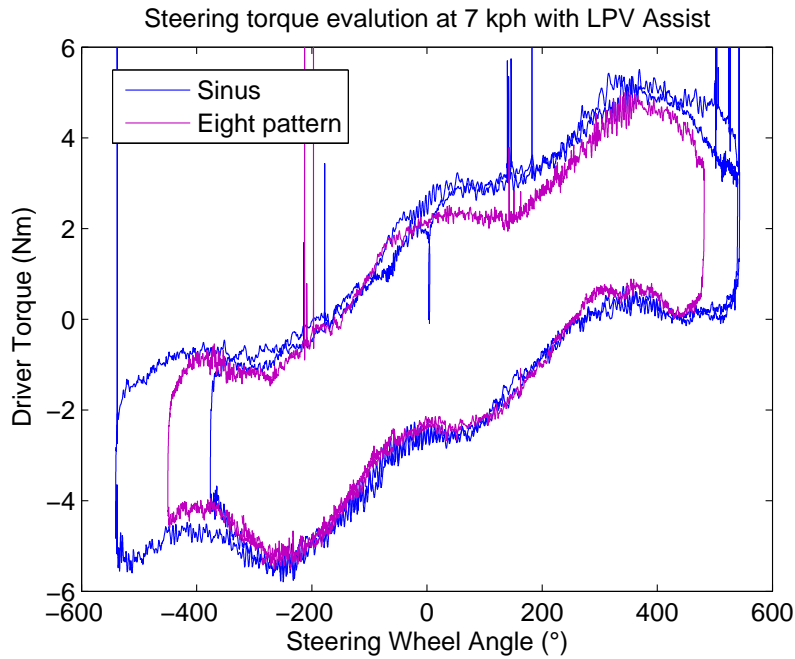


Figure V.45 – PIO+LPV at 7 kph - Hysteresis θ_c VS τ_d

In Fig. V.46(a) and V.46(b), the three EPS inputs (rack force (blue), driver torque (red) and assistance torque (green)) are measured during the previous tests. The three signals are converted at pinion side and their evolution according to time is shown for both manoeuvre, in the left: free sinus and in the right: calibrated sinus. The driver torque and the assistance torque act in the same direction, and the sum of torques allows to counter the road reaction torque. The driver torque and the assistance torque is almost equivalent which means that the steering effort is half provided by the assist motor. Therefore, an acceptable steering performance and feeling is obtained at 7 kph.

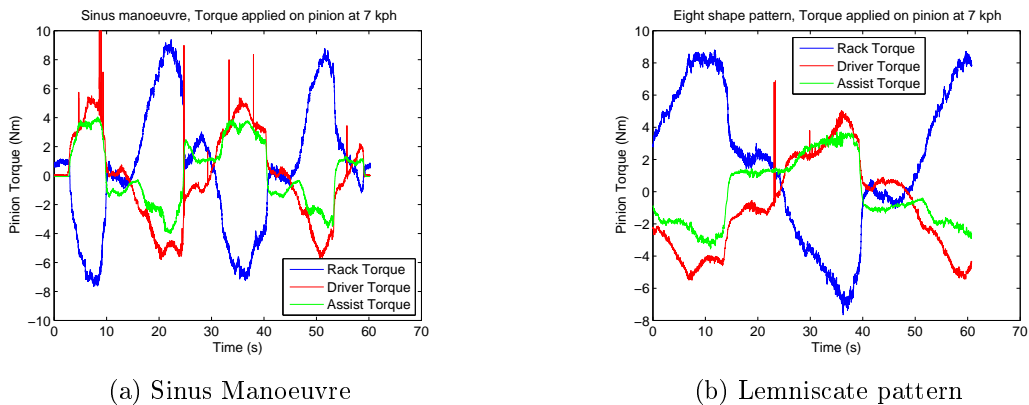


Figure V.46 – PIO+LPV at 7 kph - Evolution of involved torques

In Fig. V.47(a) and V.47(b), the resulting behaviour on the vehicle are presented. In Fig. V.47(a), the evolution of steering wheel angle regarding time is shown respectively for free sinus (blue) and calibrated sinus (purple). A very low frequency manoeuvre is performed in both

cases. In Fig. V.47(b), the steering wheel angle function of rack force is plotted, it is noticed that the same amount of rack force is obtained during both tests, as the tests have been done at same vehicle speed and same steering wheel angle amplitude. Therefore, the steering effort needed in both manoeuvres is similar.

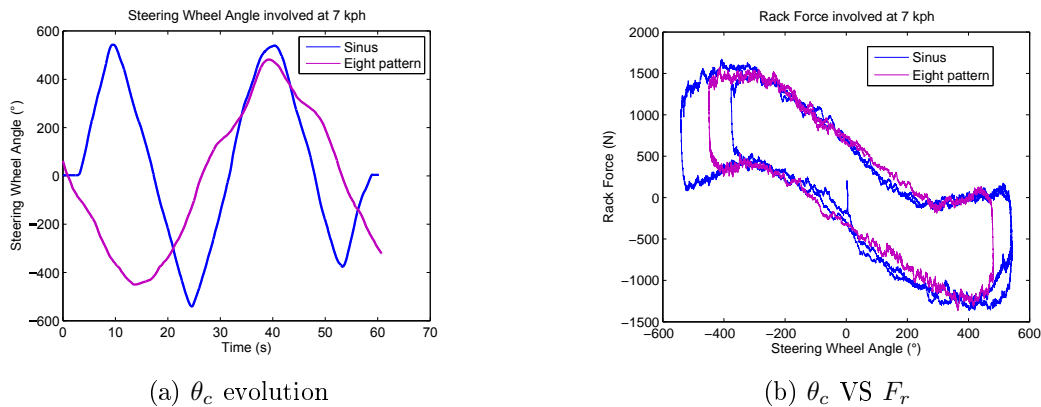


Figure V.47 – PIO+LPV at 7 kph - Resulting behaviour on the vehicle

Vehicle Test at 15kph - Sinus manoeuvre

When started in second gear a corresponding vehicle speed is around 15 kph, so carrying out vehicle test at this velocity is representative of assistance level required at low speed. A calibrated sinus test has been realized on the dynamic pad of JTEKT test ground under two different conditions: with and without assistance.

In Fig V.48, steering wheel angle function of driver torque is plotted. Two results are shown, the test has been driven without assistance (red) and with assistance (blue). The steering torque level is compared in steer out between these two conditions: the steering effort reaches almost 12Nm without assistance, whereas it achieves 6 Nm with assistance. Besides, the hysteresis is smooth and is also shaped well as the steer back remains in the good side. Then, the proposed control strategy provides an acceptable overall performance.

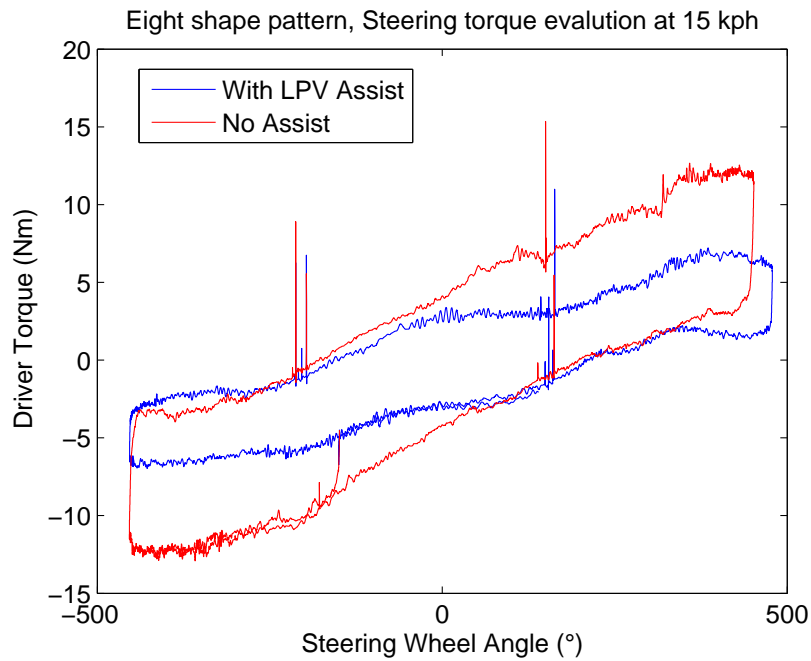


Figure V.48 – PIO+LPV at 15 kph - Hysteresis θ_c VS τ_d

In Fig. V.49, the three EPS inputs (rack force (blue), driver torque (red) and assistance torque (green)) are measured during the previous tests and converted at pinion side such that their evolution according to time is shown. In no assist case, the driver needs to compensate the total force applied on the rack. Thanks to the assistance, the driver and motor torque are almost equivalent which mean that the steering effort is half provided by the assist motor.

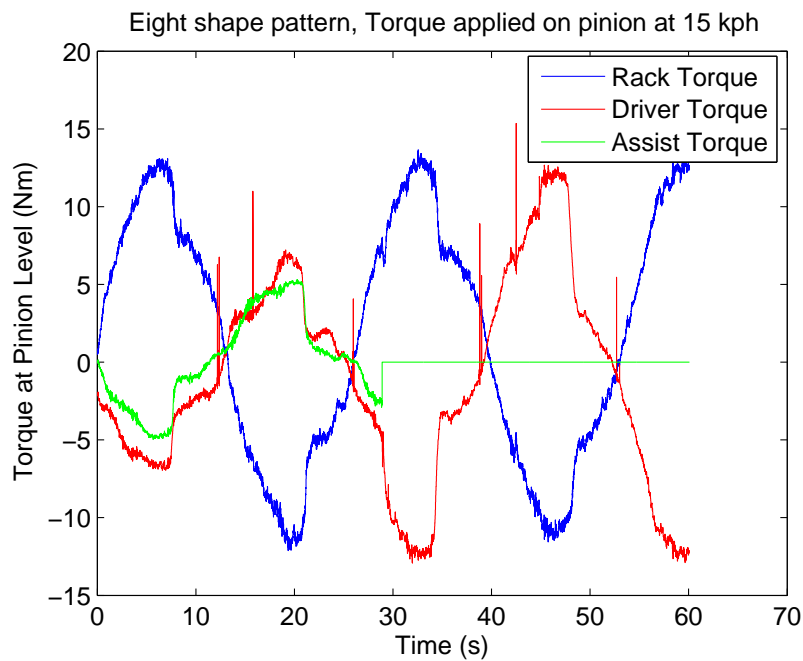


Figure V.49 – PIO+LPV at 15 kph - Evolution of involved torques

The resulting behaviour on the vehicle are presented, in Fig. V.50(a), the evolution of steering wheel angle regarding time is shown, while in Fig. V.50(b), the steering wheel angle function of rack force is plotted, where the rack force and steering wheel amplitude obtained during both cases is the same. Indeed a calibrated sinus is realised, exactly same conditions are obtained either without or with assistance. Besides, compared with previous lemniscate manoeuvre at 7 kph, this case at 15 kph involves a driver input with a higher frequency.

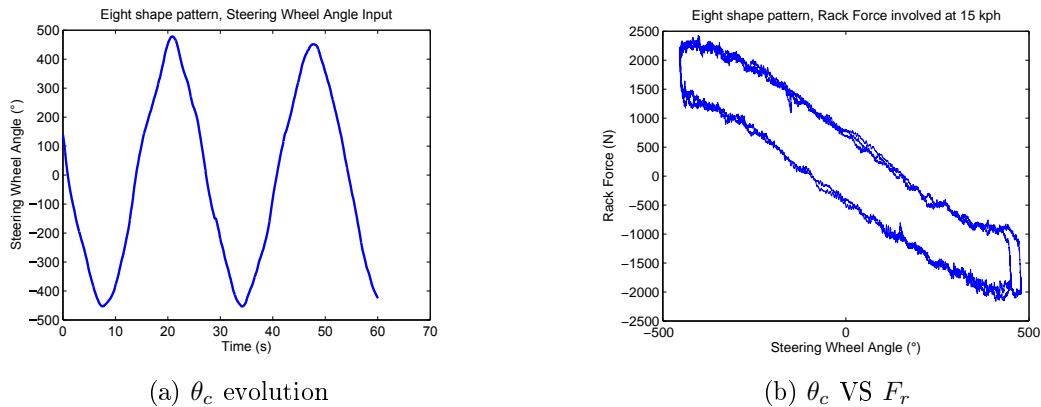


Figure V.50 – PIO+LPV at 15 kph - Resulting behaviour on the vehicle

In Fig. V.51, the two hysteresis obtained for each lemniscate test at 7 kph and 15 kph are compared. The steering effort increases regarding vehicle speed (from 4Nm to 6Nm), this is an expected behaviour considering steering feel, since the rack force to counter also increases (from 1.5kN to more than 2kN) then a correct road information is transmitted.

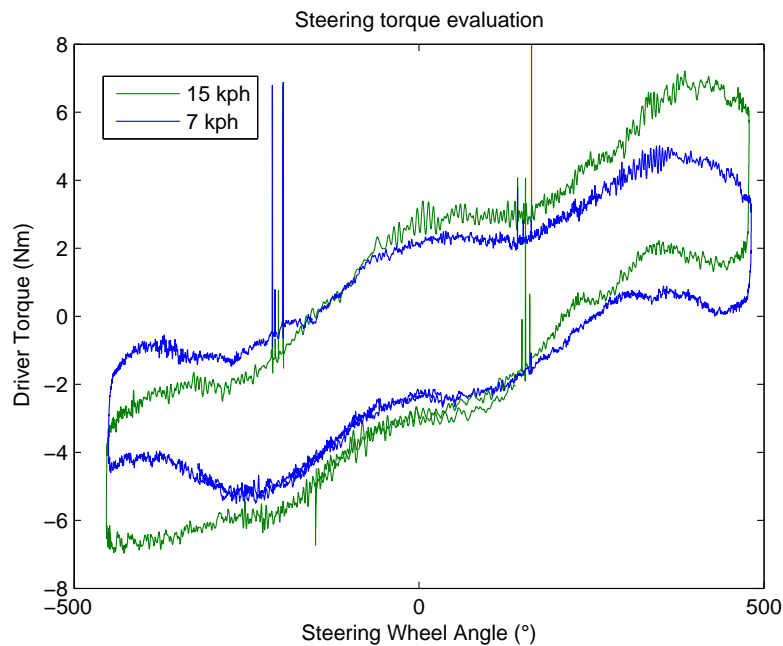


Figure V.51 – PIO and LQR at low speeds - Hysteresis θ_c VS τ_d

Vehicle Test at 30kph - Sinus manoeuvre

When rolling inside a city, a corresponding vehicle speed is around 30 kph, so carrying out vehicle test at this velocity is representative of assistance level required at nominal speed. Moreover, the road reaction force involved between low speed and upper than 30 kph is really different. A free sinus test has been realized on the dynamic pad of JTEKT test ground.

In Fig V.52, steering wheel angle function of driver torque is plotted. Two results are presented, a free sinus test has been carried out with assistance (blue). However, to have an idea on the achieved performance, a comparison with another free sinus test realised without assistance (red) is presented. Considering only the same low steering wheel angle range $[-200^\circ; 200^\circ]$, the proposed strategy in steer out provides a good steering support around 7Nm whereas in no assist case, the steering effort achieves 13Nm. Therefore, on small functional angle, the overall performance obtained is satisfying with smooth and low amplitude hysteresis. Nevertheless, at higher steering wheel amplitude, the driver torque is increasing too widely.

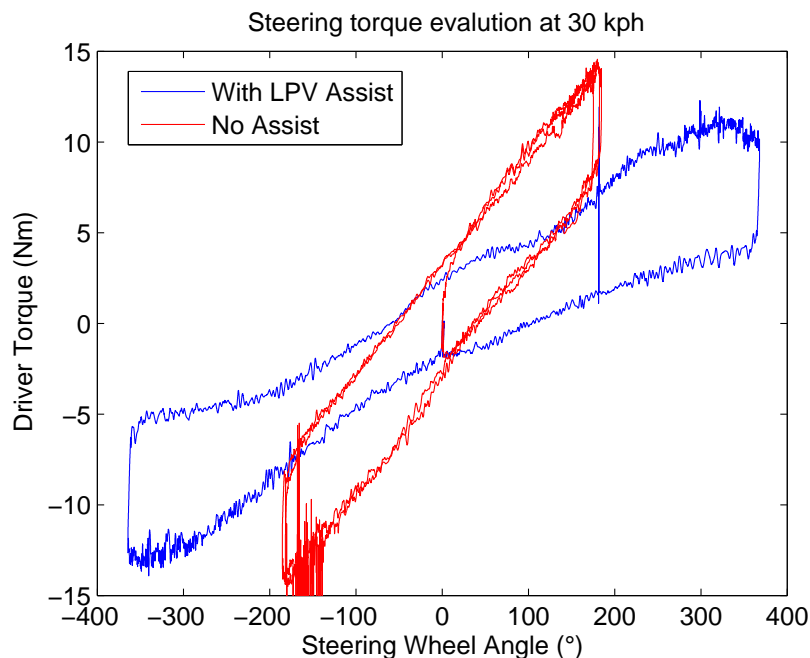


Figure V.52 – PIO+LPV at 30 kph - Hysteresis θ_c VS τ_d

In Fig. V.53, the three EPS inputs (rack force (blue), driver torque (red) and assistance torque (green)) are measured during the previous tests and converted at pinion side such that their evolution according to time is shown. The amount of assistance torque appears to be stabilized from a certain value of driver torque around 6Nm. This explains the increase of driver torque that need to compensate on its own the effect of road reaction force. However at lowest value than 6Nm, the driver torque and the assistance torque are almost equivalent which means that the steering effort is half provided by the assist motor. Therefore, an acceptable steering performance and feeling is provided under this condition (corresponding to a low steering wheel angle range). Thus, this assistance amount could be corrected by changing the slope of $K(\rho)$ in the base assist (refers to V.3.3.3).

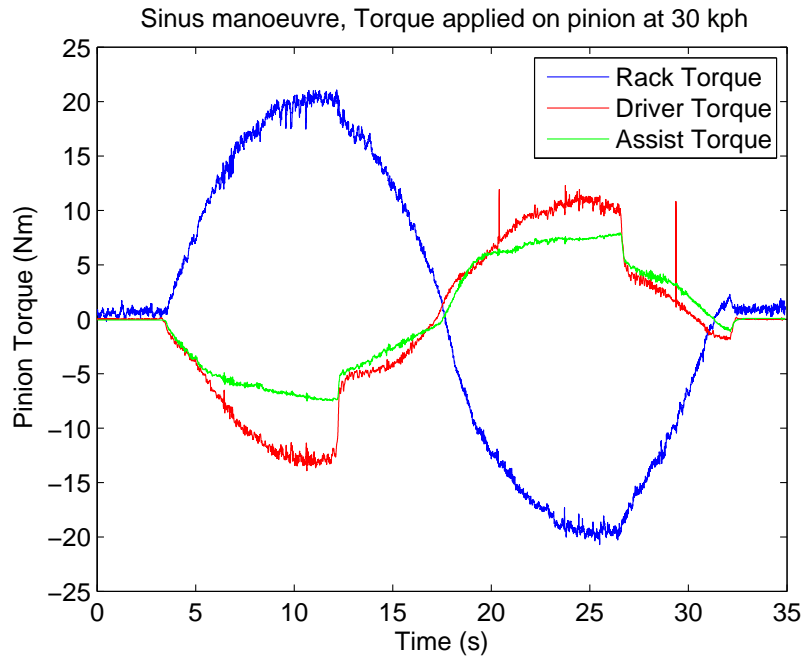


Figure V.53 – PIO+LPV at 30 kph - Evolution of involved torques

In Fig. V.54(a) and V.54(b), the resulting behaviour on the vehicle is presented. In Fig. V.54(a), the evolution of the steering wheel angle regarding time is shown, while in Fig. V.54(b), the steering wheel angle function of rack force is plotted. It is worth noting that the amount of rack force at 30 kph is much more important in this condition (close to 4kN) than at low speed. Then, more assistance torque is required especially at higher steering wheel amplitude (greater than a half steering wheel turn of 180°), as it has been observed on the previous figures V.52 and V.53. Moreover, it confirms that the design characteristics $K(\rho)$ which influences mainly the steering effort, needs to be implemented also as vehicle speed dependent and not only according to the driver torque value (even though less complex solution regarding tuning and implementation issues).

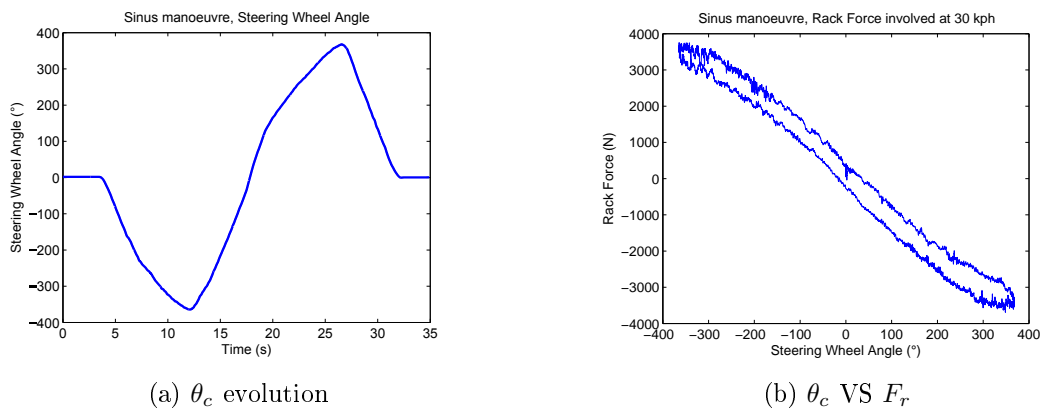


Figure V.54 – PIO+LPV at 30 kph - Resulting behaviour on the vehicle

In what follows, some particular tests regarding driver feeling have been carried out (change in steering wheel dynamic or in road surface).

In depth tests: low friction course

A sinusoidal test at 7 kph have been realised on a low μ track (wet tiles) which is a small straight line. Thus, the amplitude of the steering wheel angle amplitude is smaller than on asphalt in order to remain on the low friction path.

In Fig. V.55, steering wheel angle function of driver torque is plotted. Two results are presented, the same sinus manoeuvre is realised either without assistance (red) or with assistance (blue). The steering torque level is compared in steer out with these two conditions: the steering effort is less than 4 Nm with assistance, whereas it achieves 8 Nm without assistance. Moreover, the hysteresis is smooth, the proposed control strategy provides also an acceptable steering performance. Therefore, it is robust to change in road surface adherence.

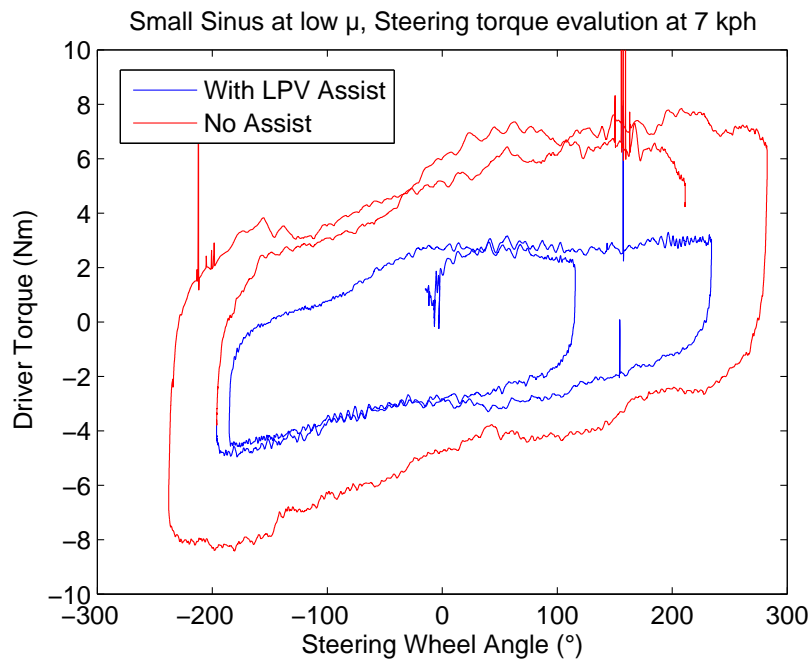


Figure V.55 – PIO and LPV at 7 kph low μ - Hysteresis θ_c VS τ_d

In Fig. V.56, the resulting behaviour on the vehicle is presented. On the top, the evolution of rack force regarding time is shown, while on the bottom, the evolution of steering wheel angle regarding time is shown. The assistance was shut-down after half time (21 s), nevertheless the test conditions remains similar (rack amplitude up to 1kN and steering wheel angle up to 200°). Consequently, the comparison made above on steering torque level hold.

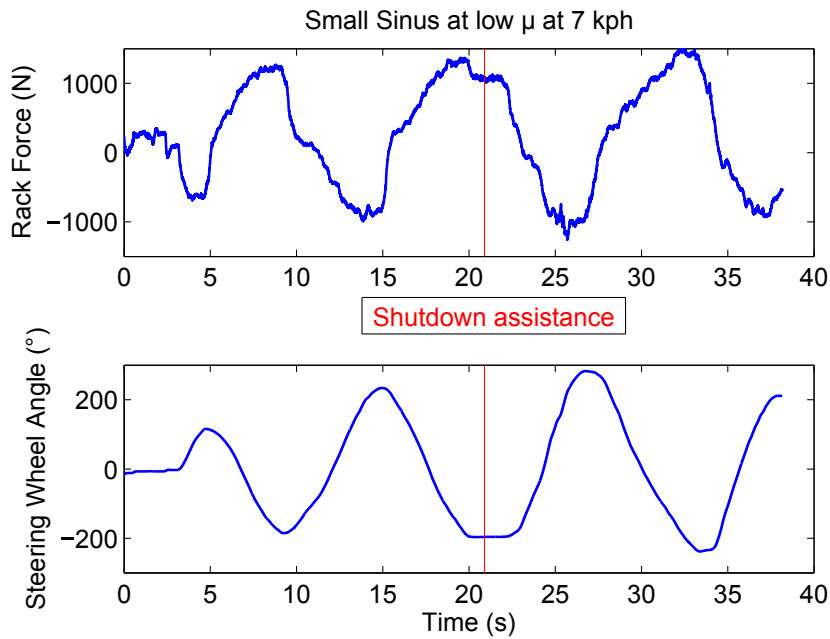
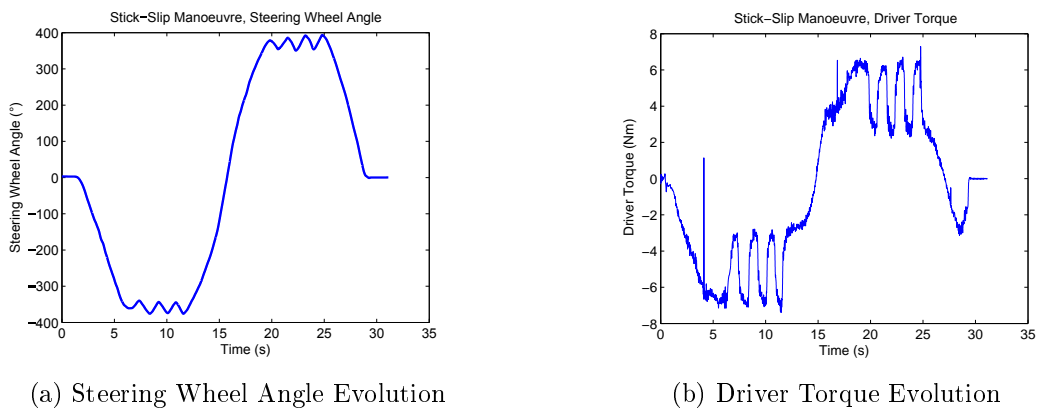


Figure V.56 – Sinus Manoeuvre low μ Rack Force and Steering Wheel Angle evolution

In depth tests: stick-slip manoeuvre

A stick-slip test have been realised at 15 kph on the test track in asphalt. The test consists in verifying that there is no increase in driver torque when manoeuvring around a same operation point.

In Fig. V.57(a) the evolution of steering wheel angle regarding time is shown, whereas in Fig. V.57(b) the evolution of driver torque regarding time is shown. As it could be noticed on the figure at the left, a small steering angular motion is realised repetitively around a same operating point when turning left and right (between 350° to 400°). During this manoeuvre, the driver torque level is kept at the same level as expected (between 4 Nm to 6 Nm). Furthermore, the steering torque level remains acceptable as it remains low around 6 Nm.



(a) Steering Wheel Angle Evolution

(b) Driver Torque Evolution

Figure V.57 – Constant amplitude related to stick-slip test

In depth tests: high steering dynamic manoeuvre

A high steering dynamic test have been realised at 15 kph on the test track in asphalt. The test consists in verifying that there is no increase in driver torque when realising high dynamic manoeuvre.

In Fig. V.58, the resulting behaviour on the vehicle is presented. On the top, the evolution of the steering wheel speed regarding time is shown, while on the bottom, the evolution of steering wheel angle regarding time is shown. At the beginning of the test, a high steering dynamic is applied (fast steering wheel velocity up to $500^{\circ}/s$) then it is followed by a low steering driving (common manoeuvre is around $200^{\circ}/s$). A same manoeuvre (sinusoidal input) is realised in order to compare the obtained results, indeed a same steering wheel angle amplitude (almost more than one steering wheel turn 400°) is achieved.

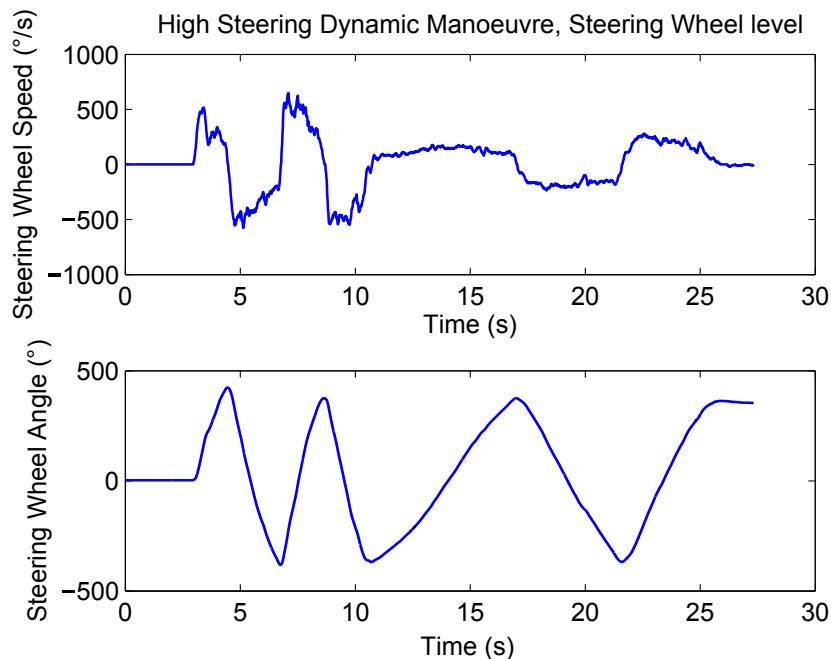


Figure V.58 – Steering Wheel Speed and Angle

In Fig. V.59, the three EPS inputs (rack force (blue), driver torque (red) and assistance torque (green)) are measured during the previous tests and converted at pinion side such that their evolution according to time is shown. The driver torque and the assistance torque are almost equivalent at low steering driving which means that the steering effort is half provided by the assist motor (steering effort around 6 Nm). However, at high steering dynamic, the amount of assistance torque appears to be stabilized, then the driver torque increases to compensate on its own the effect of road reaction force (steering effort around 8 Nm). Moreover, it could be observed that the driver feels more torque ripple at high steering dynamic, then the performance is slightly degraded. Considering this test result, the strategy needs to be improved for high steering velocity manoeuvre.

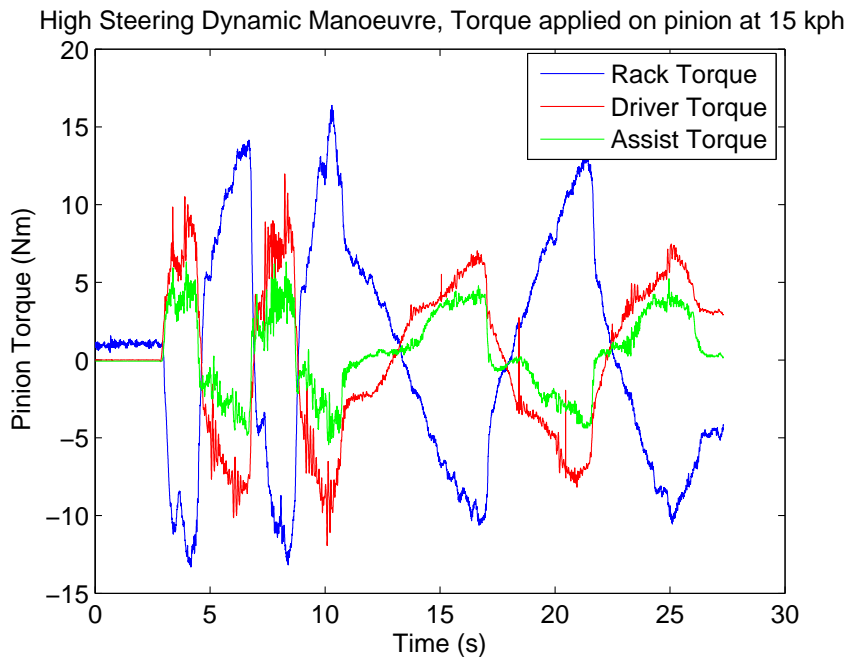


Figure V.59 – PIO and LPV at 15 kph high dynamics - Evolution of involved torque

V.6.3 Torsion Bar Less Control

TBLC have been implemented on the same development vehicle Clio X98 using QP. However this time, it was equipped by a C-EPS prototype with a nominal pinion gear (high pinion/rack ratio) and a mono-bloc pinion shaft (no torsion bar, a very high stiffness element). Indeed, a low cost EPS system without the torque sensor apparatus seems appropriate to a control strategy which does not estimate the driver torque.

Fig. V.60 presents the implementation of TBLC as described in V.4.1. The measurements θ_c (from which the steering wheel velocity is deduced), V_v (vehicle speed) and a_y (the lateral acceleration) are used in TBLC (no θ_m). A dynamometer steering wheel has been mounted on the vehicle which enables to measure the driver torque τ_d and an accurate steering wheel angle for performance analysis purpose.

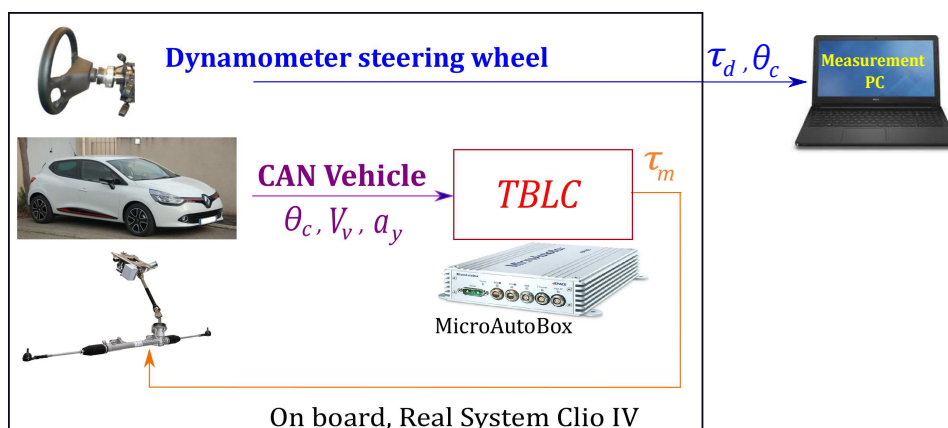


Figure V.60 – TBLC - implementation on real system

In this part, two tests results are presented under a sinusoidal manoeuvre at 30 kph and 50 kph with almost the same steering wheel angle amplitude.

Fig. V.61 (resp. V.62) illustrates the performance of TBLC obtained at 30 kph (resp. 50kph). Indeed, in both figures a comparison between TBLC (blue) and no assistance at all (red) is shown. The steering torque level is compared in steer out between these two conditions: at 30 kph the steering effort achieves 10 Nm with TBLC whereas it achieves 34 Nm without assistance and at 50 kph the steering effort achieves 14 Nm with TBLC whereas it achieves 31 Nm without assistance. Indeed, the driver inputs a lower torque level at both 30 kph and 50 kph compared to a no assistance case. Besides, as explained in II.2.1, *Proto 2* is composed with a nominal pinion gear, therefore the assistance level required is high as in manual condition the driver effort is high (around 30 Nm for half turn the steering wheel 180°). Although the steering effort remains quite high (around 10 Nm), TBLC allows to provide a steering support to the driver in rolling condition without steering torque estimation (and based on a new mechanical type of EPS system with no torsion bar).

Nevertheless, the transition between steer out and steer back needs to be improved at 30 kph, as the driver supplies an opposite torque at the beginning of the changeover (-4 Nm around 180°) which is depicted by the peak at both end in Fig. V.61. Moreover, the hysteresis shape in steer out is expected to continue to increase, such that a correct road information is transmitted to the driver. Therefore, the driver feeling needs to be refined according to steering manoeuvre. Then TBLC strategy shows that at a nominal vehicle speed, a steering support based on a few sensors is achievable, although the steering feel is to be enhanced.

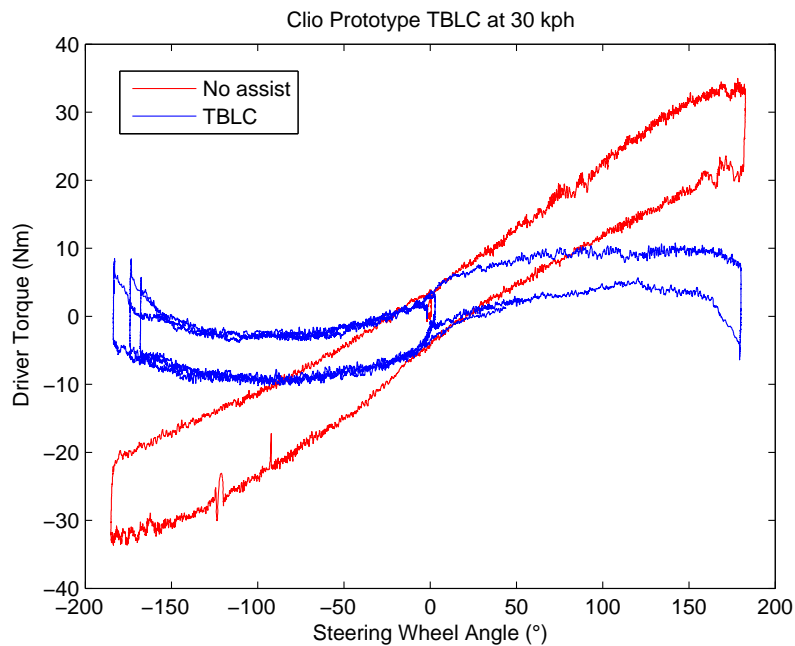


Figure V.61 – TBLC at 30 kph

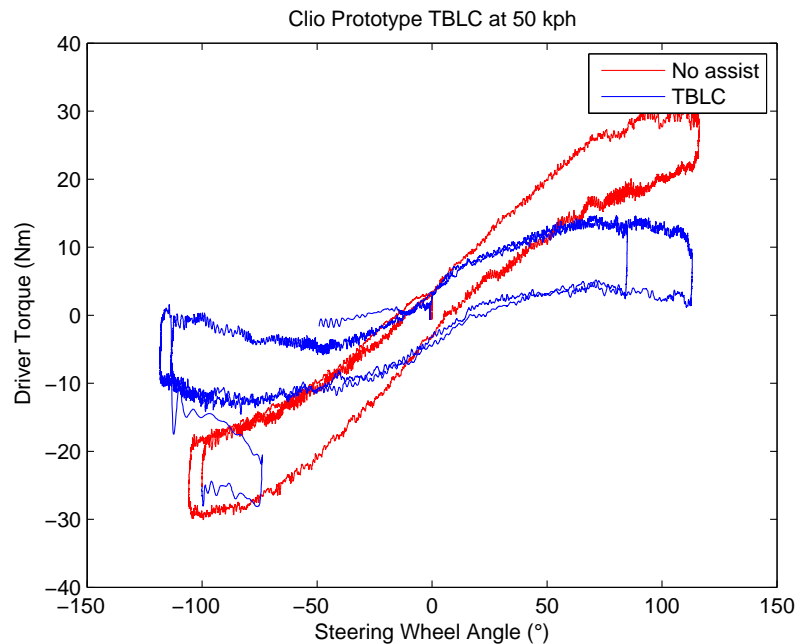


Figure V.62 – TBLC at 50 kph

V.7 Conclusion

In this chapter, different EPS control strategies have been developed subject to two approaches. In the first case, EPS control is based on the driver torque estimation, involving mainly steering wheel angle and motor angle measurements:

- TSLC consists in a torque sensor estimation used in a similar strategy than a conventional EPS controller.
- a LQR control is designed based on the augmented system defined in the previous chapter, where the states including driver torque are estimated using a $\mathcal{H}_\infty/\mathcal{H}_2$ PIO.
- a LPV state feedback control is designed based on a LPV EPS system obtained by including the assistance characteristic curve in the nominal plant, and where some extended states are introduced subject to performance specification. Besides, EPS states are estimated using a $\mathcal{H}_\infty/\mathcal{H}_2$ PIO.

In the second case, EPS control does not require steering torque estimation, then the steering wheel angle and some vehicle data is assumed to be measured:

- TBLC generates a desired assistance torque target based on vehicle (lateral acceleration, vehicle speed) and steering wheel (angle and velocity) data.
- a \mathcal{H}_∞ dynamic output feedback controller is designed with performance specifications on the actuator and synthesized tracking error.

Therefore, the second approach is more advantageous regarding EPS cost reduction as less mechanical component (remove even the torsion bar) and less sensor (no need to measure the motor angle) are required. However, considering EPS performance evaluation (steering effort and driver feeling) the lack of direct steering torque information appears in the presented results. Besides, all these proposed methods could be used as a back-up control in case of torque sensor failure on a nominal EPS systems, since some assistance is provided (better than manual steering). Nevertheless, to reach a lower cost EPS system market, a good steering feel is required in addition to a high assistance level. Then, the strategies based on the driver torque estimation appears more appropriate to meet easily these requirements, also steering torque estimation might benefit to some ADAS.

Several simulations have been realised to evaluate the resulting assistance level. Moreover, driver torque estimation based control strategies (PIO with LQR and LPV) have been implemented on a development vehicle and tested under various driving conditions. Performance have been evaluated through the analysis of steering wheel angle amplitude subject to driver torque level. Although the overall steering effort has been reduced according to the proposed assistance laws, there are ways for improvements on the driver feeling through the assistance characteristic curve. Furthermore, both industrial approaches (TSLC and TBLC) have also been implemented on real vehicles and provide suitable results regarding their respective application objective. In Table V.2, a synthesis of the different configurations is described.

| Methods | Tests : simulation or/and experiment | Comments |
|---------------------------|--|---|
| TSLC | Exp. Class-B, DP-EPS (50kph, 90kph) | better than no assistance (back-up mode) |
| H_∞/H_2 PIO LQR | Exp. Clio IV, C-EPS <i>Proto 1</i> (0kph, 7kph, 15kph) Sim. as Fig. III.12 at 0kph, 15kph, 30kph | high steering support not adapted for all speed |
| H_∞/H_2 PIO LPV | Exp. Clio IV, C-EPS <i>Proto 1</i> (7kph, 15kph, 30kph) Sim. as Fig. III.12 at 15kph, 30kph | good steering support and driver feeling |
| TBLC | Exp. Clio IV, C-EPS <i>Proto 2</i> (30kph, 50kph) | based on vehicle data (reduce EPS cost) |
| H_∞ controller | Sim. as Fig. III.12 at 30 kph | feasibility with steering wheel angle measurement only |

Table V.2 – Synthesis table of the presented results

Conclusions and Future Work

Contents

| | |
|---|------------|
| VI.1 General Conclusions | 143 |
| VI.2 Future Work | 144 |

VI.1 General Conclusions

This thesis deals with various observation and control studies concerning steering performance and safety for EPS systems. Indeed, this work has been carried out under an industrial framework, where JTEKT targets at first to develop a back-up control in EPS systems in case of torque sensor failure, and then to go further through a development of lower production cost EPS systems. This last challenge involves to reconsider the mechanical structure of EPS systems subject to some significant components. Therefore, several control and estimation methods have been proposed to solve those issues using different techniques.

After an overview on steering systems regarding technologies evolutions and growing market trends, specific interest is paid on EPS systems. Thus, EPS systems are required to evolve according to customer expectations. Therefore, EPS structures and their functioning are described to introduce the challenges involved subject to torque sensor.

In the third chapter, dynamic models of EPS systems have been established. A high order P-EPS model for driver torque estimation and a simplified C-EPS model for control design have been described. Furthermore, several rack force models have been developed considering different driving conditions (parking, transition from parking to low speed, nominal or high speed). Indeed, the road reaction force is highly varying according to vehicle speed and presents also a non-linear behaviour. These are important aspects to consider in order to simulate accurately the real environment, i.e EPS system set inside a vehicle. Besides, the experimental tests conditions are presented including description of several manoeuvres on the test track and the characteristics of the development vehicle (the electromechanical system and the specific sensors for measurements purpose). Finally, some experimental results obtained on the real system are compared with models outputs for validation.

In the fourth chapter, a state of the art on different methods to estimate the driver torque is first presented. Then, a driver torque estimation under torque sensor failure is developed to enable steering support, and avoid sudden loss of assist. Therefore, an estimation strategy based on steering wheel angle and motor angle measurements has been developed. Two different methods have been proposed to estimate the driver torque subject to road disturbances

and measurements noise: a proportional integral observer regarding a multi-objective $\mathcal{H}_\infty/\mathcal{H}_2$ performance and H_∞ filtering approach. Then, the estimation performance of both techniques have been compared in simulation. As better results are obtained, the $\mathcal{H}_\infty/\mathcal{H}_2$ PIO has been simulated using real measurements data and has also been implemented on the test car. The efficiency of the proposed observer has been shown through these results under different driving conditions.

In the fifth chapter, a state of the art on different EPS control strategies (developed in the literature as well as in industrial context) has been presented first. This chapter ensures continuity with the previous context, namely torque sensor failure case. Consequently, it is required to develop EPS controller based on the remaining measurements from vehicle and EPS system. Therefore, a back-up mode has been developed within an industrial framework (which means answering customer specifications, with the focus on functional performance and safety concept). TSLC is able to provide some steering support better than no assistance, based on a simplified torsion bar torque estimation and a conventional controller structure. Besides, considering nominal performance objective rather than back-up mode is interested to face the challenge of EPS cost reduction by saving the cost related to torque sensor. Then, a LQR controller and state feedback LPV controller design have been proposed. Since all states are required considering implementation issues, the previously developed $\mathcal{H}_\infty/\mathcal{H}_2$ PIO is used for state estimation. Nevertheless, other EPS control structures have been developed which do not require any observer (this reduces even more the number of sensors needed). Within an industrial R&D framework, the proposed TBLC generates a desired assistance torque target based only on vehicle and steering wheel data. Similarly, a H_∞ dynamic output feedback controller based on steering wheel angle have been designed. Then, EPS controllers performance have been evaluated in simulation. Finally, the efficiency of the proposed observer (PIO) based controller (LQR and LPV) have been shown through experimental results under various driving tests. Furthermore, both industrial approach (TSLC and TBLC) have also been implemented on real system (test car). Moreover, TSLC as described in the patent, will be materialized soon through mass production software.

VI.2 Future Work

As the outcome of the presented works and obtained results, the following perspectives (middle or long terms) could be developed.

- Fault detection and diagnosis concerning torque sensor: as seen in the second chapter, torque sensor calculation is performed through a main and sub cell. In case failure occurs on one of the cells, both are judged deficient (it is difficult to discriminate the faulty cell between the two) and the torque sensor signal is invalid. Therefore, fault detection and diagnosis enable to isolate the faulty cell in order to remain longer under nominal mode with a high steering performance, instead of entering back-up mode with a degraded steering condition.
- Fault tolerant control: as discussed in the introduction, EPS systems are developed under ISO26262, consequently a functional safety concept is required. This means that any sensor or actuator failures upon EPS controller are managed to prevent dangerous situation.

Therefore, a fault tolerant control regarding steering wheel angle sensor is interesting to develop. Besides, a driver torque estimation considering error on measurement following (VI.1) could be proposed:

$$\begin{cases} \dot{x} &= Ax + Bu + Ed + Ww \\ y &= Cx + Nn + Ff \end{cases} \quad (\text{VI.1})$$

with the measurements noise $n \in \mathbb{R}^2$, the sensors fault $f \in \mathbb{R}^2$, the road disturbance $w \in \mathbb{R}$, such that $v = \begin{pmatrix} w & f^T & n^T \end{pmatrix}^T \in \mathbb{R}^5$, and the exogenous inputs $\bar{w} = \begin{pmatrix} v^T & d \end{pmatrix}^T$ where $d \in \mathbb{R}$ is the driver torque.

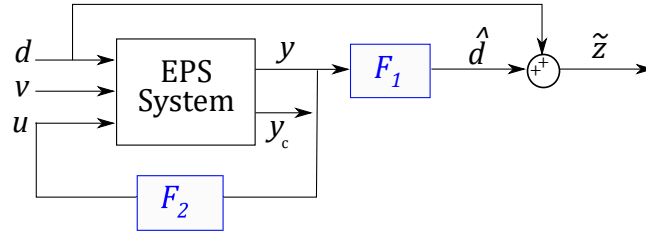


Figure VI.1 – Fault Tolerant Control and Driver Torque Estimation Scheme

Fig. VI.1 shows the integrated design scheme with the estimation error $\tilde{z} = d - \hat{d}$ where \hat{d} is the estimated driver torque, the controlled output $y_c = \dot{\theta}_c$, the driver torque estimator F_1 and the controller F_2 . A transformation in standard H_∞ problem leads to solve $\min_{\gamma_\infty} \|H_{z\bar{w}}\|_\infty < \gamma_\infty$ with $z = \begin{pmatrix} \tilde{z} & y_c \end{pmatrix}^T$.

- Robustness synthesis: as it could be noticed in the third chapter, an uncertain system could be defined considering uncertainties on the mechanical parameters such that

$$\begin{cases} \dot{x} &= (A + \Delta A)x + Bu + Ed + Ww \\ y &= Cx + Nn \end{cases} \quad (\text{VI.2})$$

where the term ΔA is the additional uncertainty on the nominal system, also described as $\Delta A = M_a \Delta_a N_a$ with $\Delta_a^T \Delta_a \leq I$. Then, LMI formulation could be defined through a combination of Majoration lemma (see [Shi 1999]) and Schur complement.

- Implementation: further EPS prototype have to be tested considering different configuration of EPS mechanical structure under cost reduction design target (modify assistance motor, pinion gear ...), while performing the PIO based controller strategy. Furthermore, the state feedback LPV controller of chapter V has to be extended to depend on vehicle speed and shall be implemented on vehicle. Besides, the H_∞ dynamic output feedback controller should also be implemented on vehicle.

Finally, other vehicle tests have to be performed, for instance: avoidance manoeuvre at high speed or public road rolling, to have an overall evaluation of the steering performance.

Implementation Issues

A.1 Discretization

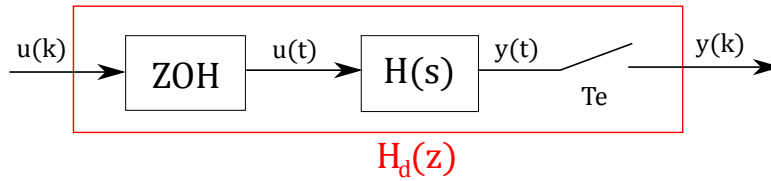


Figure A.1 – Discretization with a Zero-Order Hold

Definition A.1 (*Exact discretization*)

Exact discretization by a ZOH

$$H_d(z) = (1 - z^{-1})Z \left(\frac{H(s)}{s} \right) \quad (\text{A.1})$$

Let consider the state space representation of a continuous time system $H(s)$ such that:

$$\begin{cases} \dot{x}(t) &= Ax(t) + Bu(t) \\ y(t) &= Cx(t) + Du(t) \end{cases} \quad (\text{A.2})$$

where $x(t)$ the state vector, $u(t)$ the input vector and $y(t)$ the output vector.

Then, the discrete time state space representation of system $H_d(z)$ in Fig. A.1, resulting from the exact discretization of $H(s)$ by a ZOH at sample time T_e is such that:

$$\begin{cases} \dot{x}(k) &= A_d x(k) + B_d u(k) \\ y(k) &= C_d x(k) + D_d u(k) \end{cases} \quad (\text{A.3})$$

where $A_d = e^{AT_e}$, $B_d = \int_0^{T_e} e^{A\tau} d\tau B$, $C_d = C$, $D_d = D$.

Definition A.2 (*Tustin's Method*)

Tustin's Method (bilinear transformation), such that $H_d(z) = H(s)$

$$s = \frac{2(z-1)}{T_e(z+1)} \quad (\text{A.4})$$

Tustin discretization method is a finite-difference approximation. It is used to obtain a good frequency domain matching between continuous-time system and the corresponding discretized system.

A.2 Signal characteristics

Regarding steering wheel angle input signals, characteristics have been compared between signals received from CAN Vehicle and CAN SW, see Table A.1.

| | Dynamometer steering wheel | Vehicle angle sensor |
|----------|-----------------------------------|-----------------------------|
| Source | CAN SW | CAN Vehicle |
| Sampling | 1ms | 10ms |
| Accuracy | 0.001° | 0.1° |

Table A.1 – Steering wheel angle characteristics

Therefore, a dynamometer steering wheel have been installed on the development vehicle to recover a higher accuracy and sampling steering wheel angle signal.

Remark A.1

Considering costs and integration with current hardware, this option remains difficult to realise for a mass production objective.

Bibliography

- [Abbas 2014] H.B. Abbas, A. Ali, M. Hashemi et H. Werner. *LPV state-feedback control of a control moment gyroscope*. Control Engineering Practice, pages 129 – 137, 2014. (cited on p. 108.)
- [Ackermann 1996] J. Ackermann et T. Bunte. *Yaw disturbance attenuation by robust decoupling of car steering*. IFAC World Congress, 1996. (cited on p. 30.)
- [Apkarian 1995] P. Apkarian, P. Gahinet et G. Becker. *Self-Scheduled H_∞ Control of Linear Parameter-Varying Systems: A Design Example*. Automatica, pages 1251 – 1261, 1995. (cited on p. 103.)
- [Badawy 1999] A. Badawy, J. Zuraski, F. Bolourchi et A. Chandy. *Modeling and Analysis of an Electric Power Steering System*. SAE Technical Paper, pages 1999–01–0399, 1999. (cited on p. 24 and 93.)
- [Bakhshande 2015] F. Bakhshande et D. Söffker. *Proportional Integral Observer: A brief survey with special attention to the actual methods using ACC Benchmark*. IFAC PapersOn-Line, vol. 48, pages 532 – 537, 2015. (cited on p. 59.)
- [Bakker 1987] E. Bakker, L. Nyborg et H. Pacejka. *Tyre Modelling for Use in Vehicle Dynamics Studies*. SAE Technical paper, 1987. (cited on p. 35.)
- [Blanchini 2000] F. Blanchini. *The Gain Scheduling and the Robust State Feedback Stabilization Problems*. IEEE Transactions on Automatic Control, pages 2061 – 2070, 2000. (cited on p. 104.)
- [Brossard 2006] J-P. Brossard. *Dynamique du véhicule, modélisation des systèmes complexes*. 2006. (cited on p. 35.)
- [Canudas De Wit 2005] C. Canudas De Wit, H. Bechart, X. Claeys, P. Dolcini et J.J Martinez. *Fun-to-Drive by Feedback*. European Journal of Control, pages 353–383, 2005. (cited on p. 95.)
- [Chabaan 2001a] R.C. Chabaan et L.Y. Wang. *Control of Electrical Power Assist systems: \mathcal{H}_∞ design, torque estimation and structural stability*. JSAE Review, pages 435 – 444, 2001. (cited on p. 55 and 56.)
- [Chabaan 2001b] R.C. Chabaan et L.Y. Wang. *Vehicle Electric Power Assist Steering System and Method using Angle based Torque Estimation*, September 2001. US Patent 6293366 B1. (cited on p. 97.)
- [Chabaan 2009] R.C. Chabaan. *Torque Estimation in Electrical Power Steering Systems*. IEEE Vehicle Power and Propulsion Conference, pages 790 – 797, 2009. (cited on p. 56.)

- [Champagne 2014] A. Champagne, T. Kaufmann, K. Pattok et T. Varunjikar. *Providing assist torque without hand wheel torque sensor*, October 2014. US Patent 2014/0324294 A1. (cited on p. 111.)
- [Champagne 2016] A. Champagne, T. Varunjikar et T. Kaufmann. *Method for providing assist in electric power steering system without a torque sensor*. 7th International Munich Chassis Symposium, pages 547 – 560, 2016. (cited on p. 111.)
- [Chen 2005] X. Chen, X. Chen et K. Zhou. *Optimal Control of Electric Power-Assisted Steering System*. IEEE Conference on Control Applications, pages 1403 – 1408, 2005. (cited on p. 113.)
- [Chen 2008a] B. Chen, W. Hsu et D. Huang. *Sliding-Mode Return Control of Electric Power Steering*. SAE 2008 World Congress and Exhibition, SAE Technical Paper, 2008. (cited on p. 96.)
- [Chen 2008b] X. Chen, T. Yang, X. Chen et K. Zhou. *A Generic Model-Based Advanced Control of Electric Power-Assisted Steering Systems*. IEEE Transactions on Control System Technology, pages 1289 – 1300, 2008. (cited on p. 113.)
- [Chilali 1996] M. Chilali et P. Gahinet. *H_∞ Design with Pole Placement Constraints: an LMI Approach*. IEEE Transactions on Automatic Control, vol. 41, pages 358–366, 1996. (cited on p. 63 and 66.)
- [Chitu 2011] C. Chitu, J. Lackner, M. Horn, P.S Pullagura, H. Waser et M. Kohlbock. *A robust and optimal LQR controller design for Electric Power Steering system*. Nonlinear Dynamic and Synchronization, Int’I Symposium on Theoretical Electrical Engineering, 2011. (cited on p. 99.)
- [Chitu 2013] C. Chitu, J. Lackner, M. Horn, H. Waser et M. Kohlbock. *Controller design for an electric power steering system based on LQR techniques*. The international journal for computation and mathematics in electrical and electronic engineering, vol. 32, pages 763 – 775, 2013. (cited on p. 55 and 99.)
- [Cholakal 2009a] S. Cholakkal. Load disturbance torque estimation for motor drive systems with application to electric power steering systems. Master’s thesis, University of Windsor, 2009. (cited on p. 55, 56 and 98.)
- [Cholakal 2009b] S. Cholakkal et X. Chen. *Fault Tolerant Control of Electric Power Steering Using Robust Filter-Simulation Study*. IEEE Vehicle Power and Propulsion Conference, pages 1244 – 1249, 2009. (cited on p. 56 and 98.)
- [Ciarla 2013] V. Ciarla. *Commande d un système de puissance électrique pour des personnes à mobilité réduite*. PhD thesis, Université de Grenoble, 2013. (cited on p. 99.)
- [Coudon 2007] J. Coudon. *Algorithmes de commande pour le pilotage d’une direction découplée*. PhD thesis, Institut National Polytechnique de Grenoble, 2007. (cited on p. 113.)

- [DaedalResearch 2016] DaedalResearch. Global automotive steering market with focus on hydraulic and electric power steering: 2016-2020. 2016. (cited on p. 8.)
- [Dang 2014] Jianmin Dang, Hui Chen, Bolin Gao, Qi Li, Minhao Li, Takeshi Watanabe, Ryouhei Hayama, Liming Lou et Shirou Nakano. *Optimal Design of On-Center Steering Force Characteristic Based on Correlations between Subjective and Objective Evaluations*. SAE International, 2014. (cited on p. 116.)
- [Dang 2015] Jianmin Dang, Hui Chen, Qi Li, Takeshi Watanabe, Ryouhei Hayama et Liming Lou. *A method to set the target on-centre steering force characteristic*. Journal of Automobile Engineering, 2015. (cited on p. 116.)
- [Dong 2010] L. Dong, P. Kandula, Z. Gao et D. Wang. *On a Robust Control System Design for an Electric Power Assist Steering System*. American Control Conference, pages 5356 – 5361, 2010. (cited on p. 96.)
- [Doyle 1992] J.C. Doyle, B.A Francis et A.R Tannenbaum. *Feedback Control Theory*. Macmillan Publishing Company, 1992. (cited on p. 57.)
- [El-Shaer 2008] A.H El-Shaer. *Robust Control Design of Electric Power Steering Systems*. PhD thesis, University of California, Berkeley, 2008. (cited on p. 27, 28 and 96.)
- [El-Shaer 2009] A. El-Shaer, S. Sugita et M. Tomizuka. *Robust Fixed-Structure Controller Design of Electric Power Steering Systems*. American Control Conference, pages 445–450, 2009. Saint-Louis, USA. (cited on p. 97.)
- [El-Shaer 2010] A. El-Shaer et M. Tomizuka. *Robust Multi-Objective Control for Systems Involving Human-in-the-Loop Passivity Constraints with Application to Electric Power Steering*. International Conference on Advanced Intelligent Mechatronics, pages 361–366, 2010. Montreal, Canada. (cited on p. 97.)
- [Endo 2004] S. Endo et H. Kobayashi. *EPS Control Technology*. NSK Technical Journal Motion and Control, vol. 16, pages 51 – 56, 2004. (cited on p. 93.)
- [Farhat 2015] Ahmad Farhat et Damien Koenig. *PI robust fault detection observer for a class of uncertain switched systems using LMIs*. IFAC Symposium on Fault Detection, Supervision and Safety of Technical Processes, 2015. (cited on p. 59.)
- [Farhat 2016] A. Farhat. *Détection et localisation de défaut: Application véhicule*. PhD thesis, Université de Grenoble Alpes, 2016. (cited on p. 70 and 74.)
- [Fu 1991] M. Fu. *Interpolation approach to H_∞ estimation and its interconnection to loop transfer recovery*. Systems and Control Letters, vol. 17, pages 29–36, 1991. (cited on p. 70.)
- [Gahinet 1994] Pascal Gahinet et Pierre Apkarian. *A linear matrix inequality approach to H_∞ control*. International Journal of Robust and Nonlinear Control, vol. 4, pages 421–448, 1994. (cited on p. 74 and 115.)

- [Gillespie 1992] T. D. Gillespie. Fundamentals of vehicle dynamics. 1992. (cited on p. 33.)
- [Grimble 1990] M.J. Grimble et A.E. Sayed. *Solution of the H_∞ Optimal Linear Filtering Problem for Discrete-Time Systems*. IEEE Transactions on Acoustics, Speech, and Signal Processing, vol. 38, pages 1092–1104, 1990. (cited on p. 70.)
- [Hjartarson 2015] A. Hjartarson, P. Seiler et A. Packard. *LPVTools: A Toolbox for Modeling, Analysis, and Synthesis of Parameter Varying Control Systems*. IFAC-PapersOnLine, vol. 48, pages 139 – 145, 2015. (cited on p. 108.)
- [Hu 2008] T.S. Hu, C.J. Yeh, S.R. Ho, T.H. Hsu et M.C. Lin. *Design of Control Logic and Compensation Strategy for Electric Power Steering Systems*. IEEE Vehicle Power and Propulsion Conference, pages 5356 – 5361, 2008. (cited on p. 94.)
- [Hui 2005] S. Hui et S.H. Zak. *Observer Design for Systems With Unknown Inputs*. International Journal of Applied Mathematics and Computer Science, vol. 15, pages 431–446, 2005. (cited on p. 57.)
- [Hung 2003] Y.S. Hung et F. Yang. *Robust H_∞ filtering error variance constraints for discrete time-varying systems with uncertainty*. Automatica, vol. 39, pages 1185 – 1194, 2003. (cited on p. 70.)
- [Illán 2011] J. Tordesillas Illán, V. Ciarla et C. Canudas De Wit. *Oscillation annealing and driver/tire load torque estimation in Electric Power Steering systems*. Proceedings of the IEEE International Conference on Control Applications, pages 1100–1105, 2011. (cited on p. 24 and 55.)
- [JTEKT 2015] JTEKT. <https://www.jtekt.co.jp/e>, 2015. (cited on p. 3, 13 and 95.)
- [Kaczorek 1979] T. Kaczorek. *Proportional-integral observers for linear multivariable time-varying systems*. at - Automatisierungstechnik, pages 359 – 363, 1979. (cited on p. 59.)
- [Kiencke 2005] U. Kiencke et L. Nielsen. Automotive control systems. 2005. (cited on p. 29.)
- [Kim 2002] Ji Hoon Kim et Jae Bok Song. *Control logic for an electric power steering system using assist motor*. Mechatronics, vol. 12, pages 447–459, 2002. (cited on p. 96.)
- [Kim 2006] Young-Man Kim. *Robust and reduced order H_∞ filtering via LMI approach and its applications to fault detection*. Wichita State University, USA, 2006. (cited on p. 70.)
- [Koenig 2002] Damien Koenig et Saïd Mammar. *Design of Proportional-Integral Observer for Unknown Input Descriptor Systems*. IEEE Transactions on Automatic Control, vol. 47, pages 2057 – 2062, 2002. (cited on p. 59.)
- [Koenig 2005] D. Koenig. *Unknown Input Proportional Multiple-Integral Observer Design for Linear Descriptor Systems: Application to State and Fault Estimation*. IEEE Transactions on Automatic Control, vol. 50, pages 212 – 217, 2005. (cited on p. 89.)
- [Kozaki 1999] Y. Kozaki, G. Hirose, S. Sekiya et Y. Miyaura. *Electric Power Steering (EPS)*. NSK Technical Journal Motion and Control, vol. 6, pages 9 – 15, 1999. (cited on p. 94.)

- [Kurishige 2001] M. Kurishige et T. Kifuku. *Static Steering Control System for Electric Power Steering*. Mitsubishi Electric Advance, vol. 94, pages 18 – 20, 2001. (cited on p. 98.)
- [Kurishige 2002a] M. Kurishige, H. Kumamoto et O. Nishihara. *A New Control Strategy to Reduce Steering Torque for Vehicles Equipped with Electric Power Steering*. Transactions of the Japan Society for Mechanical Engineers, vol. 68, pages 3238 – 3245, 2002. (cited on p. 98.)
- [Kurishige 2002b] M. Kurishige, H. Tanaka, N. Inoue, K. Tsutumi et T. Kifuku. *An EPS Control Strategy to Improve Steering Maneuverability on Slippery Roads*. SAE 2002 World Congress and Exhibition, SAE Technical Paper, 2002. (cited on p. 93.)
- [Lawson 2008] M. Lawson et X. Chen. *Controller Design for Electric Power Steering System using T-S Fuzzy Model Approach*. IEEE International Conference on Control Applications, pages 486–491, 2008. Texas, USA. (cited on p. 55 and 98.)
- [Li 1997] H. Li et M. Fu. *A Linear Matrix Inequality Approach to Robust H_∞ Filtering*. IEEE Transaction Signal Processing, vol. 45, pages 2338–2350, 1997. (cited on p. 70.)
- [Li 2009a] Qiang Li, De Song, Feng Cheng, Li Yang et Ren Cai. *A Robust Controller Design for Electric Power Steering System Based on PI Current Loop*. International Conference on Measuring Technology and Mechatronics Automation, pages 753–756, 2009. (cited on p. 113.)
- [Li 2009b] X. Li, X-P. Zaho et J. Chen. *Controller Design for Electric Power Steering System using T-S Fuzzy Model Approach*. International Journal of Automation and Computing, 2009. (cited on p. 96.)
- [Mahmoud 2012] M.S. Mahmoud et M.F. Emzir. *Unknown-input estimator-based controller design of electric power-assisted steering system*. IET Control Theory and Applications, 2012. (cited on p. 56.)
- [Marcos 2000] A. Marcos, S. Ganguli et G.J Balas. *h_∞ fault detection and isolation filter for the boeing 747*. Master's thesis, University of Minnesota, 2000. (cited on p. 70.)
- [Marouf 2010] A. Marouf, M. Djemaï, C. Sentouh et P. Pudlo. *Driver torque and road reaction force estimation of an electric power assisted steering using sliding mode observer with unknown inputs*. IEEE Conference on Intelligent Transportation Systems, Proceedings, ITSC, pages 354–359, 2010. Madeira Island, Portugal. (cited on p. 56.)
- [Marouf 2011] A. Marouf, C. Sentouh, M. Djemaï et P. Pudlo. *Control of an Electric Power Assisted Steering system using reference model*. IEEE Conference on Decision and Control and European Control Conference, pages 6684–6690, 2011. Orlando, USA. (cited on p. 97.)
- [Marouf 2012a] A. Marouf, M. Djemaï, C. Sentouh et P. Pudlo. *A new control strategy of an electric-power-assisted steering system*. IEEE Transactions on Vehicular Technology, vol. 61, no. 8, pages 3574–3589, 2012. (cited on p. 24, 56, 97 and 113.)

- [Marouf 2012b] A. Marouf, M. Djemaï, C. Sentouh et P. Pudlo. *Sensorless control of Electric Power Assisted Steering system*. Mediterranean Conference on Control and Automation, pages 909–914, 2012. Barcelona, Spain. (cited on p. 56 and 97.)
- [Marouf 2013] A. Marouf. *Contribution à la Commande du Système de Direction Assistée Electrique*. PhD thesis, Université de Valenciennes, 2013. (cited on p. 18, 24, 27, 56 and 97.)
- [Matsuoka 2016] H. Matsuoka. *Development and Future Outlook of Steering Systems*. JTEKT Engineering Journal, pages 8 – 13, 2016. (cited on p. 1, 2 and 17.)
- [Mehrabi 2011] N. Mehrabi, N. L. Azad et J. McPhee. *Optimal disturbance rejection control design for Electric Power Steering systems*. IEEE Conference on Decision and Control and European Control Conference, pages 6584–6589, 2011. Orlando, USA. (cited on p. 24 and 99.)
- [Michelis 2011] A. Michelis, P. Pilaz, P. Moulaire et S. Gaudin. *Method for determining a torque set value for a steering wheel for a power steering system of a motor vehicle*, July 2011. US Patent 2012/0203397 A1. (cited on p. 95, 96 and 112.)
- [Miyazaki 2008] H. Miyazaki. *Technical Trends in Steering Systems*. 7th JFPS International Symposium on Fluid Power, pages 133 – 136, 2008. (cited on p. 11 and 17.)
- [Mogi 2011] K Mogi, T Sugai, R Sakurai et N Suzuki. *Development of a New Steer-by-wire System*. NTN Technical Review, no. 79, pages 42 – 50, 2011. (cited on p. 16.)
- [Moreillon 2016] M. Moreillon, T. Tamura, R. Fuchs et P. Mullhaupt. *Detection of the driver's hand on and off the steering wheel for ADAS and autonomous driving*. 7th International Munich Chassis Symposium, pages 505 – 525, 2016. (cited on p. 55.)
- [Morita 2009] Yoshifumi Morita, Akitoshi Yokoi, Makoto Iwasaki, Hiroyuki Ukai, Nobuyuki Matsui, Norihisa Ito, Nobuhiko Uryu et Yasuhiko Mukai. *Controller Design Method for Electric Power Steering System with Variable Gear Transmission System using Decoupling Control*. IEEE Industrial Electronics Conference, 2009. (cited on p. 116.)
- [Noguchi 2001] M. Noguchi. *Trends and Future Prospects Regarding Steering System Technology*. Koyo Engineering Journal, pages 37 – 41, 2001. (cited on p. 1 and 8.)
- [Nouailletas 2008] R. Nouailletas, H.B. Le, E. Mendes et D. Koenig. *New Hybrid model and switched PI observer for dry friction systems*. IFAC World Congress, pages 7504 – 7509, 2008. (cited on p. 59.)
- [Olsson 1998] H. Olsson, Kj K.J. Åström, C. Canudas de Wit, M. Gäfvert et P. Lischinsky. *Friction Models and Friction Compensation*. European Journal of Control, vol. 4, pages 176–195, 1998. (cited on p. 37.)
- [Ono 2016] K. Ono, I. Kushiro, D. Yamada et T. Tomita. *Steering feel design based on the driver's perceived value of steering reaction force*. 7th International Munich Chassis Symposium, pages 595 – 616, 2016. (cited on p. 95.)

- [Parmar 2002] M. Parmar et J.Y. Hung. *Modeling and sensorless optimal controller design for an electric power assist steering system*. IEEE 28th Annual Conference of the Industrial Electronic Society, vol. 3, pages 1784–1789, 2002. (cited on p. 99.)
- [Parmar 2004] M. Parmar et J.Y. Hung. *A Sensorless Optimal Control System for an Automotive Electric Power Assist Steering System*. IEEE Transactions on Industrial Electronics, pages 290 – 298, 2004. (cited on p. 18, 24 and 99.)
- [Poussot-Vassal 2009] C. Poussot-Vassal. *Commande Robuste LPV Multivariable de Chassis Automobile*. PhD thesis, Grenoble INP, 2009. (cited on p. 29.)
- [Qiao 2007] X.J. Qiao, T.X. Qi et C.J. Hong. *A Fuzzy Control in Electric Power Steering System*. Intelligent Systems Design and Applications, pages 240 –245, 2007. (cited on p. 96.)
- [Rajamani 2012] Rajesh Rajamani. *Vehicle dynamics and control*. 2012. (cited on p. 30.)
- [Reichhartinger 2016] M. Reichhartinger, S.K. Spurgeon et M. Weyrer. *Design of an Unknown Input Observer to Enhance Driver Experience of Electric Power Steering Systems*. IEEE European Control Conference, pages 269–274, 2016. Aalborg,Denmark. (cited on p. 55.)
- [Rongyun 2015] Z. Rongyun, Z. Linfeng, C. Wuwei et H. He. *Research on EPS System Based on LPV/ H_∞ Control and its Hardware in Loop Test*. China Mechanical Engineering, vol. 26, pages 545 – 552, 2015. (cited on p. 24 and 103.)
- [Rösth 2007] M. Rösth. *Hydraulic Power Steering System Design in Road Vehicles*. PhD thesis, Linköping University, 2007. (cited on p. 11.)
- [Rothhämel 2010] Malte Rothhämel, Jolle IJkema et Lars Drugge. *On a Method for Generating a Word Pool for the Description of Steering Feel*. International Symposium on Advanced Vehicle Control, 2010. (cited on p. 116.)
- [Rothhämel 2011] Malte Rothhämel, Jolle IJkema et Lars Drugge. *A method to find correlations between steering feel and vehicle handling properties using a moving base driving simulator*. Vehicle Systems Dynamics, 2011. (cited on p. 116.)
- [Saifia 2014] D. Saifia, M. Chadli, H.R. Karimi et S. Labiod. *Fuzzy control for Electric Power Steering System with assist motor current input constraints*. Journal of the Franklin Institute, pages 562 –576, 2014. (cited on p. 24 and 96.)
- [Satake 2003] T. Satake, M. Kurishige, N. Inoue, K. Ikemoto, T. Kifuku et K. Tsutumi. *Evaluation of EPS Control Strategy Using Driving Simulator for EPS*. SAE 2003 World Congress and Exhibition, SAE Technical Paper, 2003. (cited on p. 93.)
- [Scherer 2000] C. Scherer et S. Weiland. *Linear Matrix Inequalities in Control*. Delft University of Technology, 2000. (cited on p. 57 and 65.)
- [Sename 2016] O. Sename. *Robust Control of MIMO Systems*. Master courses, ENSE3 Grenoble INP, 2016. (cited on p. 58.)

- [Sentouh 2011] C. Sentouh, B. Soualmi, J-C. Popieul et S. Debernard. *The H_2 -Optimal Preview Controller for a Shared Lateral Control*. IEEE Conference on Intelligent Transportation Systems, pages 1452 – 1458, 2011. (cited on p. 56 and 59.)
- [Seo 2012] B. Seo, I. Yang et D. Lee. *Robust Control of Electric Power Steering System using PI-type Dynamic Inversion Method*. International Conference on Vehicular Electronics and Safety, pages 84 – 86, 2012. (cited on p. 96.)
- [Shafai 1985] B. Shafai et R.L. Carroll. *Design of Proportional Integral Observer for Linear Time-Varying Multivariable Systems*. IEEE Conference on Decision and Control, pages 597 – 599, 1985. (cited on p. 59.)
- [Shafai 2002] B. Shafai, C.T. Pi, S. Nork et S.P. Linder. *Proportional Integral Adaptive Observer for Parameter and Disturbance Estimations*. IEEE Conference on Decision and Control, pages 4694 – 4699, 2002. (cited on p. 59.)
- [Sheng 2016] D. Sheng. h_∞ filtering based fault detection, estimation and fault tolerant control. Master’s thesis, University of Alberta, 2016. (cited on p. 70.)
- [Shi 1999] P. Shi, E.K. Boukas et R.K. Agarwal. *Control of markovian jump discrete-time systems with norm bounded uncertainty and unknown delay*. IEEE Transactions on Automatic Control, 1999. (cited on p. 145.)
- [Shi 2009] P. Shi, S. Gao, L. Miao et H. Wang. *Optimal Controller Design for Electric Power Steering System Based on LQG*. International Conference on Information Engineering and Computer Science, 2009. (cited on p. 99.)
- [Solomon 1992] D. Solomon. *Helicopter Flight Control System Design Using the Linear Quadratic Regulator for Robust Eigenstructure Assignment*. PhD thesis, Air Force Institute of Technology, 1992. (cited on p. 99.)
- [Soualmi 2014] B. Soualmi, C. Sentouh et J-C. Popieul. *Both Vehicle State and Driver’s Torque Estimation using Unknown Input Proportional Multi-Integral T-S Observer*. IEEE European Control Conference, pages 2957 – 2962, 2014. (cited on p. 56.)
- [Souza 1995] Ce De Souza, Uri Shaked et Minyue Fu. *Robust H_∞ Filtering for Continuous Time Varying Uncertain Systems with Deterministic Input Signals*. IEEE Transaction on Signal Processing, vol. 43, pages 709–719, 1995. (cited on p. 70.)
- [Standard 2011] International Standard. *Road vehicles - Functional safety*, 2011. International Organization for Standardization. (cited on p. 2.)
- [Sugitani 1997] N. Sugitani, Y. Fujiwara, K. Uchida et M. Fujita. *Electric Power Steering with H-infinity Control Designed to Obtain Road Information*. IEEE American Control Conference, pages 2935–2939, 1997. New Mexico, USA. (cited on p. 24 and 96.)
- [Tamura 2012] T. Tamura, A. Maroonian, M. Higashi et R. Fuchs. *Modeling and Simulation for the dynamic analysis of an Electric Power Steering System*. International Chassis Symposium, 2012. (cited on p. 24.)

- [Tanaka 2000] T. Tanaka, A. Daikoku, A. Imagi et Y. Yoshikuwa. *An Advanced Electrical Power Steering Motor*. SAE World Congress, pages 2000–01–0824, 2000. (cited on p. 21.)
- [Tanaka 2003] T. Tanaka. *Motors for Electric Power Steering*. Mitsubishi Electric, Advance, vol. 13, pages 8 – 10, 2003. (cited on p. 20.)
- [Varunjikar 2016] T. Varunjikar, A. Champagne et T. Kaufmann. *Providing assist torque without hand wheel torque sensor for zero to low vehicle speeds*, August 2016. US Patent 9409595 B2. (cited on p. 111.)
- [Wenchang 2011] L. Wenchang et M. Hongqi. *EPS Control Based on State Feedback*. International Conference on Electric Information and Control Engineering, 2011. (cited on p. 99.)
- [Wilhelm 2015] F. Wilhelm, T. Tamura et R. Fuchs. *A Friction Compensation Control for Power Steering*. IEEE Transaction on Control Systems Technology, pages 1354 – 1367, 2015. (cited on p. 96.)
- [Wojciechowski 1978] B. Wojciechowski. *Analysis and Synthesis of Proportional Integral Observers for Single Input Single Output Time-Invariant Continuous Systems*. PhD thesis, Technical University of Gliwice, 1978. (cited on p. 59.)
- [Wong 2001] Tom Wong. *Hydraulic Power Steering System Design and Optimization Simulation*. SAE Technical Paper, 2001. (cited on p. 11.)
- [Wu 1995] F. Wu. *Control of Linear Parameter Varying Systems*. PhD thesis, University of California, Berkeley, 1995. (cited on p. 104 and 108.)
- [Wu 1996] F. Wu, X.H. Yang, A. Packard et G. Becker. *Induced L_2 -norm Control for LPV Systems with bounded parameter variation rates*. International Journal of Robust Nonlinear Control, pages 983 – 998, 1996. (cited on p. 103.)
- [Xue-Ping 2009] Z. Xue-Ping, L. Xin, C. Jie et M. Jin-Lai. *Parametric design and application of steering characteristic curve in control for electric power steering*. Mechatronics, vol. 9, pages 905–911, 2009. (cited on p. 95.)
- [Yamamoto 2011] K. Yamamoto et H. Nishimura. *Control System Design of Electric Power Steering for a Full Vehicle Model with Active Stabilizer*. Journal of System Design and Dynamics, vol. 5, pages 789 – 804, 2011. (cited on p. 103 and 116.)
- [Yang 2005] F. Yang, Z. Wang, Y.S. Hung et H. Shu. *Mixed H_∞/H_2 Filtering for Uncertain Systems with Regional Pole Assignment*. IEEE Transactions on Aerospace and Electronic Systems, vol. 41, pages 438 – 447, 2005. (cited on p. 70.)
- [Yili 2009] Wang Yili, Zhao Yan et Wang Hong. *Development of Steering Simulator System for Evaluation of Electric Power Steering*. International Conference on Computer Science and Education, 2009. (cited on p. 116.)

- [Yu 2017] B. Yu, A. Champagne, T. Varunjikar et T. Kaufmann. *Model based driver torque estimation*, March 2017. US Patent 2017/0066473 A1. (cited on p. 55.)
- [Zaremba 1995] A. Zaremba et R.I Davis. *Dynamic Analysis and Stability of a Power Assist Steering System*. American Control Conference, pages 4253 – 4257, 1995. (cited on p. 24.)
- [Zaremba 1997] AT Zaremba, M K Liubakka et R M Stuntz. *Vibration Control based on Dynamic Compensation in an Electric Power Steering System*. International Conference Control of Oscillations and Chaos, pages 453–456, 1997. (cited on p. 24 and 96.)
- [Zaremba 1998] AT Zaremba, M K Liubakka et R M Stuntz. *Control and steering feel issues in the design of an electric power steering system*. American Control Conference, no. June, pages 36–40, 1998. (cited on p. 96.)
- [Zhang 2007] Hui Zhang, Jing Ren et Yanru Zhong. *Study on assisted performance of electric power steering based on fuzzy control*. IEEE Conference on Electron Devices and Solid-State Circuits, pages 1390–1393, 2007. (cited on p. 96.)
- [Zhang 2009] Hui Zhang, Yuzhi Zhang, Jinhong Liu, Jing Ren et Yongjun Gao. *Modeling and characteristic curves of electric power steering system*. International Conference on Power Electronics and Drive Systems, pages 1390–1393, 2009. (cited on p. 95.)
- [Zhang 2016] L.W. Zhang, R. Du et Y. Cheng. *The Analysis of The Fault of Electrical Power Steering*. International Conference on Electronic, Information and Computer Engineering, vol. 44, 2016. (cited on p. 19.)
- [Zhu 2010] Renxue Zhu, Lanfang Gao et Xuezhi Li. *Research on the energy-saving potentiality of electro-hydraulic power steering system based on energy flow*. International Asia Conference on Informatics in Control, Automation and Robotics, pages 415–418, 2010. (cited on p. 11.)

Résumé

Cette thèse s'inscrit dans le dispositif d'une CIFRE (Conventions Industrielles de Formation par la REcherche). Les travaux de recherches ont été menés au Centre Technique de JTEKT Europe, un équipementier automobile mondial spécialisé notamment dans la conception et la production de systèmes de Directions Assistées Électriques (DAE), en collaboration avec l'équipe SLR (Systèmes Linéaires et Robustesse) du Département Automatique au GIPSA-Lab.

L'étude porte sur le développement de lois de commande de DAEs sans utiliser le signal provenant du capteur de couple (situé en pratique au niveau de la barre de torsion et mesurant une image du couple conducteur, cf. figure A.2) tout en assurant son bon fonctionnement, c'est-à-dire de fournir un couple d'assistance au conducteur.

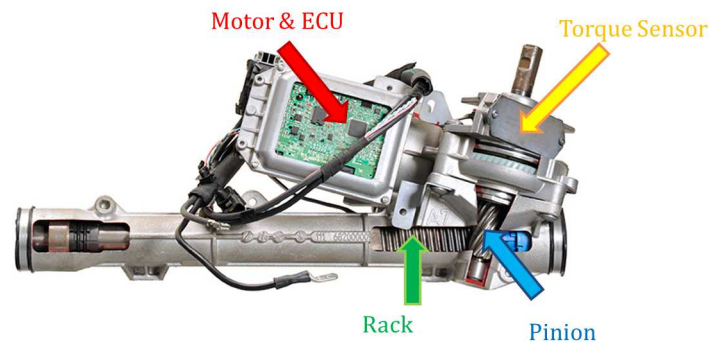


Figure A.2 – DAE de type pignon

En effet, cette problématique majeure découle des demandes des constructeurs automobiles (clients de JTEKT) qui consistent :

- d'une part à améliorer la sécurité fonctionnelle, c'est-à-dire de couvrir la perte soudaine d'assistance liée à un défaut du capteur de couple (i.e la perte du signal). Ainsi, une loi "back-up" (dont les exigences de ressenti sont moindres) permet de continuer à fournir de l'assistance afin que le conducteur puisse aller au garage le plus proche ou rentrer chez lui en toute sécurité.
- d'autre part à abaisser le coût des systèmes de DAE. Ainsi, la modification de la structure mécanique de la DAE en retirant le capteur de couple, mais tout en garantissant des performances nominales correctes (ressenti de conduite, niveau d'assistance...), permet de proposer une solution à bas coût.

Au regard de ces challenges industriels, deux étapes sont à distinguer: tout d'abord le Torque Sensor Less Control (TSLC) qui est un mode de repli (back-up), ensuite une amélioration du concept précédent, le Torsion Bar Less Control (TBLC) qui consistera en une proposition de nouveaux systèmes de DAE moins cher.

Motivation et objectifs

De nos jours, les véhicules automobiles sont de plus en plus équipés de systèmes d'aide à la conduite, axés sur la sécurité telle que l'ABS (système anti-blocage des roues), l'ESP (correcteur électronique de trajectoire) ... ou encore sur le confort du conducteur par exemple le parking automatique, le régulateur de vitesse, la direction assistée ...

La DAE ajuste le niveau de couple nécessaire pour manœuvrer le véhicule tout en procurant une bonne remontée d'information de la route, elle agit donc sur le confort et le ressenti de conduite. Pour cela, la DAE se base principalement sur l'information du capteur de couple qui traduit l'intention du conducteur. Ainsi, une commande en couple est appliquée au moteur électrique d'assistance de la DAE afin qu'un couple additionnel en accord avec le comportement du conducteur et la dynamique du véhicule permette de réduire les efforts que le conducteur doit fournir pour tourner les roues. Il est observé que ce capteur est essentiel au fonctionnement de la DAE.

Afin de pallier à une défaillance du capteur de couple, un estimateur de couple conducteur est développé pour maintenir un certain niveau d'assistance, et donc assurer une maniabilité du véhicule (ce qui diminue le risque d'accident). Les méthodes d'estimation proposées sont basées sur les mesures suivantes: l'angle du moteur d'assistance et l'angle du volant (existants sur véhicule dans cette étude). Par ailleurs, une extension du concept de ce mode dégradé, consiste à proposer une commande de la DAE dont l'objectif est de fournir une prestation nominale (améliorer le ressenti et la maniabilité). Par conséquent, le capteur de couple ne sera plus nécessaire dans la structure de la DAE, ce qui permet d'abaisser le coût du système. Ainsi, des méthodes de commande de la DAE en considérant ces objectifs à la fois de performance et de réduction de coût, sont développées.

Résumé des contributions

Cette thèse est composée de six chapitres qui sont organisés comme suit:

- Le chapitre 1 est une introduction générale qui présente les enjeux portant sur la DAE liés au futur de l'industrie automobile (développement d'ADAS: Advanced Driver Assistance Systems et véhicules autonomes). En effet, la DAE est un élément essentiel comme support de certaines fonctions d'ADAS, par exemple le LKA (système d'aide au maintien dans la file de circulation). De plus, la DAE est un système électromécanique où un fonctionnement sécurisé est requis en cas d'apparition de défaut sur le système et respectant la norme ISO26262 adressant la sécurité fonctionnelle. Une évolution du niveau de couverture des défaillances est ainsi introduite afin d'apporter une visibilité sur le besoin d'un mode refuge.
- Le chapitre 2 présente une vue d'ensemble des différents systèmes de direction existants qui sont séparés en deux catégories distinctes: les directions manuelles et assistées. Au regard de l'évolution du marché automobile, les DAE sont aujourd'hui les systèmes de directions majoritairement demandés par les constructeurs. Effectivement, les DAE présentent certains avantages par rapport à la technologie hydraulique: la réduction de

la consommation de carburant (gain écologique), une adaptation des performances de conduite au travers des courbes d'assistance et une meilleure modularité.

Par la suite, les différents types de DAE sont présentés dont la plupart sont basés sur le système pignon-crémaillère. Afin de compléter cet aperçu, la direction avec démultiplication variable ainsi que le système Steer-By-Wire sont présentés. Enfin, le fonctionnement des principaux composants d'une DAE, le capteur de couple et le moteur électrique d'assistance, est expliqué pour donner une meilleure compréhension du système étudié.

- Le chapitre 3 est consacré à la modélisation du système de DAE. Tout d'abord, des modèles de DAE simplifiés sont décrits par les équations du principe fondamental de la dynamique. Par ailleurs, afin de constituer un environnement de simulation proche de la réalité, un modèle véhicule (modèle bicyclette) et des modèles d'efforts appliqués à la crémaillère (déduits des modèles de contact pneu/sol) sont présentés. Afin de vérifier la pertinence des modèles, une comparaison avec les mesures obtenues sur le système réel (Clio IV) a été réalisée.

Enfin, la structure expérimentale est exposée. L'implémentation sur un véhicule d'essais Clio IV (cf. figure A.3) a été effectuée en utilisant un Prototypage Rapide (QP) avec une MicroAutoBox II. En effet, le logiciel dSpace permet de générer le code du modèle MATLAB/Simulink des stratégies introduites dans les chapitres suivants. La voiture a été équipée de prototypes de DAE - type colonne. Afin d'analyser les résultats expérimentaux, un volant dynamométrique (pour mesurer directement le couple conducteur) et des biellettes instrumentées (pour obtenir les efforts crémaillère) ont été montés sur le véhicule. Les différents tests ont été réalisés avec un essayeur véhicule au volant sur la piste d'essais au sein du site de JTEKT.

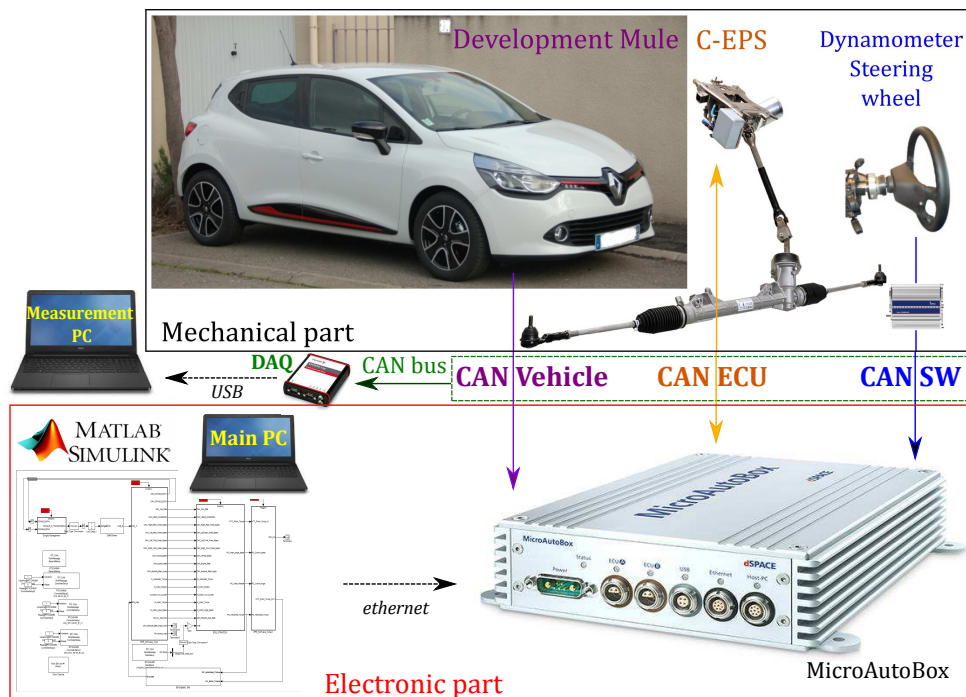


Figure A.3 – Système réel - structure de l'environnement expérimental

- Le chapitre 4 se concentre sur l'estimation du couple conducteur. Tout d'abord, un état de l'art divisé en deux parties, présente les diverses méthodes utilisées pour estimer le couple conducteur. En effet, certaines études se basent sur la mesure du capteur de couple (au niveau de la barre de torsion) alors que d'autres travaux ne s'en servent pas. Au regard du contexte de la thèse, la méthode d'estimation à développer se situe dans les mêmes conditions que ce deuxième cas de figure.

Pour la suite, quelques notions théoriques sont rappelées, puis deux approches d'estimation du couple conducteur sont décrites: d'une part un observateur Proportionnel Intégral (PI) suivant un critère multi-objectif H_∞/H_2 , et d'autre part un filtre H_∞ . Pour chacune des méthodes, un rappel de la définition générale est établi avant de procéder à la formulation de la problématique, puis à l'analyse de la synthèse.

Des résultats de simulation comparent ces deux approches. Par ailleurs, les résultats de l'observateur PI H_∞/H_2 obtenus, d'une part en simulation avec des données d'entrées réelles et d'autre part en implémentation sur le véhicule, montrent la bonne performance de l'estimation proposée.

- Le chapitre 5 est consacré à la partie commande des systèmes de la DAE. Ainsi, la prestation fournie par la DAE (le ressenti de la route, la maniabilité du véhicule) dépend de la commande appliquée. Plusieurs objectifs sont à prendre en considération lors d'un tel design: la capacité à fournir un couple d'assistance adapté au conducteur, la remontée des informations de la route (contact pneu/chaussée) au volant, tout en atténuant les perturbations, la stabilité de la boucle fermée, la robustesse face aux variations paramétriques (dues aux vieillissements des pièces ou aux dispersions de production) et les situations de conduite (la surface d'adhérence de la route ou la charge véhicule). Un état de l'art présente les méthodes de commande de la DAE proposées par les industriels (dont la structure de contrôle dépend des objectifs à atteindre) et académiques. De plus, quelques études portant sur le design des courbes d'assistance viennent compléter cet aperçu.

Par la suite, une première approche de commande de la DAE basée sur une estimation de couple est proposée. Tout d'abord, un mode backup TSLC est développé avec un schéma de commande industriel, où une synthèse, principalement heuristique, est réalisée afin de garantir la stabilité et l'assistance. Le couple au niveau de la barre de torsion est recalculé suivant l'équation liée à la déformation angulaire. Ensuite, un mode nominal (meilleure sensation de conduite requis) est proposé suivant deux méthodes de commande par retour d'état: le LQR (Linear Quadratic Regulator) et le LPV (Linear Parameter Varying). Dans chacune des approches, un rappel théorique est effectué avant de procéder à la synthèse du correcteur de la DAE, puis à l'analyse.

Enfin, une deuxième approche de commande de la DAE ne se basant sur aucune information du couple d'entrée est étudiée. L'objectif étant d'avoir un fonctionnement nominal de la DAE qui utilise très peu de mesures (les informations véhicules et l'angle volant) afin d'obtenir une structure de la DAE à bas coût. Pour cela, le TBLC et la commande par retour de sortie H_∞ ont été développés.

Quelques résultats de simulation sont donnés, pour interpréter les critères d'évaluation de la DAE (du reste subjectifs). Par ailleurs, certaines de ces stratégies ont été implémentés

sur système réel. Le TSLC a été testé à haute vitesse, sur une Mercedes équipée d'une DAE - type double pignon. Puis le TBLC et les commandes LQR et LPV basées sur l'observateur PI H_∞/H_2 , ont été implémentées sur une Clio IV équipée de prototype de DAE - type colonne et testées à basse vitesse. Les conditions de tests dépendent des performances à atteindre. Les résultats des essais indiquent que de bonnes performances sont obtenues avec ces approches qui n'utilisent plus la mesure du capteur de couple.

- Le chapitre 6 est une conclusion générale sur les travaux réalisés dans le cadre de cette thèse, où des perspectives de recherches ultérieures viennent compléter ce récapitulatif.

Perspectives

Certains points abordés dans cette étude semblent intéressants à approfondir.

À court terme

- Amélioration de l'estimation du couple conducteur: introduire un modèle de la dynamique conducteur et un modèle switché de la DAE afin de développer un observateur multi-intégral switché. En effet, cette approche, bien que plus complexe d'un point de vue implémentation, permet d'obtenir une estimation du couple conducteur plus précise (mode parking, mode roulage, mode évitement).
- Amélioration de la partie commande: définir une autre forme de courbe d'assistance utilisée dans le modèle LPV, du fait que les performances de conduite s'y reflètent. Ainsi, une synthèse LPV prenant en compte à la fois le couple conducteur et la vitesse véhicule en paramètres variants serait un moyen d'obtenir de meilleurs résultats en ressenti et maniabilité.

À long terme

- Détection et diagnostic de défauts du capteur de couple: comme mentionné dans le Chapitre II, le couple mesuré au niveau de la barre de torsion est calculé à partir d'une cellule principale et secondaire. Or, lorsqu'un défaut survient dans l'une de ces deux cellules (comportement divergent), les deux sont jugés défaillants et ainsi la mesure du signal capteur devient invalide. Par conséquent, déterminer la cellule défectueuse en corrélant une troisième valeur (par l'estimation présentée dans cette thèse) permettrait de rester dans le mode nominal en utilisant le bon signal (meilleure sensation de conduite), au lieu de basculer dans le mode back-up (conditions de conduite dégradées). Ce qui augmente la disponibilité de la DAE.
- Implémentation: tester divers prototypes de DAE en modifiant les paramètres mécaniques (la raideur de la barre de torsion, le dimensionnement du moteur d'assistance, le rapport de transformation pignon-crémaillère) suivant un objectif de design de la DAE à bas coût, sur une configuration de commande basée sur l'observateur PI. De plus, d'autres types d'essais véhicules seront à réaliser, tel qu'une manœuvre d'évitement ou un roulage sur route ouverte pour affiner l'évaluation de la prestation proposée.

Commande des Systèmes Electromécaniques: Application aux Systèmes de Directions Assistées

Résumé — De nos jours, la plupart des véhicules sont équipés d'une Direction Assistée Electrique (DAE) qui permet de réduire les efforts que le conducteur doit fournir pour tourner le volant. Ainsi, grâce à un moteur électrique, la DAE applique un couple additionnel en accord avec le comportement du conducteur et la dynamique du véhicule. Une commande en couple est majoritairement développée, celle-ci est basée sur le signal provenant d'un capteur mesurant le couple au niveau de la barre de torsion (une image du couple appliqué par le conducteur). Or, une défaillance de ce capteur, essentiel au fonctionnement de la DAE, entraîne le plus souvent une coupure de l'assistance, pouvant mener à un risque d'accidents. Au regard de la sécurité fonctionnelle, un développement d'un mode backup de sécurité est recommandé. Par ailleurs, la baisse des coûts de production de DAE est un challenge constamment recherché dans le secteur très concurrentiel des équipementiers. Cet aspect est abordé comme un prolongement, au travers d'une stratégie qui n'utilisera plus la mesure du capteur de couple. Dans ce cadre, des méthodes d'estimation du couple conducteur sont proposées, ainsi que la conception de commande répondant aux objectifs spécifiques à la DAE. Ces divers approches ont été validées en simulation et mises en oeuvre sur un véhicule prototype où des résultats prometteurs ont été obtenus.

Mots clés : approche LPV, observateurs PI, filtres H_∞ , direction assistée électrique.

Control of Electromechanical Systems: Application on Electric Power Steering Systems

Abstract — Nowadays, most vehicles are equipped with Electric Power Steering (EPS) system, which helps the driver to turn the wheels. Indeed, EPS provides through an electric motor, an additional torque according to the driver's behaviour and the vehicle's dynamics to reduce the amount of effort required by the driver. Therefore, a torque control is commonly developed, based on the torque sensor signal which measures in practice the torsion bar torque (an image of the applied driver torque). However, a failure of this sensor, essential to the functioning of EPS, usually leads to shut-off the assistance. Regarding functional safety, a backup mode is often required by car manufacturers. Besides, reducing EPS production costs remains a major challenge in the competitive OEM sector. This issue is considered as an extension, since the strategy does not use the torque sensor signal anymore. In this framework, some methods to estimate the driver torque are proposed, as well as the design of EPS control subject to specific objectives. These different approaches have been validated in simulation and also implemented on a prototype vehicle, where promising results are obtained.

Keywords: LPV approach, PI observer, H_∞ filtering, Electric Power Steering
